INSTITUTO SUPERIOR TÉCNICO
Universidade Técnica de Lisboa

Lepton Flavour Violation
in the Supersymmetric seesaw type-I

António José Rodrigues Figueiredo

Dissertação para obtenção do Grau de Mestre em

Engenharia Física Tecnológica

Júri

Presidente: Professor Doutor Gustavo Fonseca Castelo-Branco

Orientador: Professor Doutor Jorge Manuel Rodrigues Crispim Romão

Co-orientadora: Doutora Ana Margarida Domingues Teixeira

Vogais: Professor Doutor David Emmanuel-Costa

Setembro de 2009

Abstract

Oscillation experiments demand an avoidable extension to the Standard Model (SM) of particle physics. One of the simplest extensions is to introduce 3 heavy right-handed Majorana neutrinos (seesaw type-I). On the theoretical side, the hierarchy problem constitutes a solid hint for some more fundamental theory emerging at an energy scale $\lesssim 3$ Tev. For this, one of the most well motivated solutions is provided by Supersymmetry. In this thesis we follow these two *a priori* separate extensions to the SM. Since the smallness of neutrino masses is further justified by extremely heavy RH neutrinos, these will decouple from the low energy theory. Unsatisfactorily, all that could be known about their existence is just what we already know: neutrino masses. This general statement is no longer valid when seesaw is embedded in some more fundamental model with which it can communicate. This is exactly what happens in the supersymmetric seesaw.

In this thesis we will study the lepton flavour violation (LFV) processes that originate from the presence of these right-handed neutrinos in the context of the minimal supersymmetric standard model (MSSM) with mSUGRA (minimal supergravity) boundary conditions.

There are already interesting bounds [1] on LFV rates, especially in the radiative decay $\mu \to e\,\gamma$, specifically, $BR(\mu \to e\,\gamma) \leq 1.2 \times 10^{-11}$, constraining simultaneously the MSSM parameter space and the seesaw parameters.

Keywords: Supersymmetry, Minimal Supersymmetric Standard Model, Neutrino Oscillations, Minimal Supergravity, Seesaw Type-I, Lepton Flavour Violation.

Resumo

Experiências de oscilação de neutrinos exigem que o Modelo Padrão (MP) da física de partículas seja estendido. Uma destas extensões consiste em introduzir 3 neutrinos pesados direitos de Majorana (*seesaw* tipo-I). Do ponto de vista teórico, o problema da hierarquia é uma indicação sólida para a existência de um modelo mais fundamental que será observável a uma escala de energia $\lesssim 3$ TeV. Uma das melhores respostas ao problema da hierarquia é fornecida pela Supersimetria. Nesta tese implementamos estas duas extensões *a priori* não relacionadas. Uma vez que a pequenez da massa dos neutrinos é justificada por neutrinos direitos extremamente massivos, estes irão desacoplar da teoria a baixa escala de energia. Insatisfatoriamente, tudo o que se poderia saber sobre a sua existência é apenas o que já se sabe: a massa de neutrinos. Esta afirmação deixa contudo de ser válida quando o *seesaw* é embebido num modelo mais fundamental com o qual poderá comunicar. É exactamente isto que ocorre no *seesaw* supersimétrico.

Nesta tese iremos estudar os processos de violação de sabor leptónico que são provocados pela presença destes neutrinos direitos no contexto do modelo padrão supersimétrico mínimo (MPSM) com condições fronteira mSUGRA (*minimal supergravity*).

Actualmente já existem constrangimentos [1] significativos para processos de violação de sabor leptónico, em especial no decaimento radiativo $\mu \to e\,\gamma$, especificamente, $BR(\mu \to e\,\gamma) \leq 1.2 \times 10^{-11}$, delimitando simultaneamente o espaço de parâmetros do MPSM e os parâmetros do *seesaw*.

Palavras-chave: *Supersimetria*, Modelo Padrão *Supersimétrico* Mínimo, Oscilações de Neutrinos, *Minimal Supergravity*, *Seesaw* Tipo-I, Violação de *Sabor Leptónico*.

Acknowledgements

I would like to thank my supervisor, Professor Jorge C. Romão, and co-supervisor, Doctor Ana M. Teixeira, for the support given and for the opportunity to work on physics in general and supersymmetry in particular.

Other words of recognition are addressed to my mother, Rosa Rodrigues dos Anjos, and my father, António Batista Figueiredo. Their importance is sometimes proportional to my failure in acknowledging it.

A perhaps fuzzy acknowledgment to Bruno Alexandre Eusébio Mendes and Ana Raquel Sequeira Pinto, for their untempered presence.

Uncountable words of an endless gratitude are missing. Thanks, Alda Cristina Antunes Serras.

Table of Contents

Abstract i

Resumo ii

Acknowledgements iii

List of Figures vii

List of Tables viii

List of Acronyms ix

1 Introduction 1

1.1 Standard Model . . . 1

1.1.1 Electroweak symmetry breaking . . . 4

1.1.2 Fermion Masses and Mixings . . . 6

1.2 Evidences and hints for physics beyond the SM . . . 7

1.2.1 Neutrino masses . . . 8

1.2.2 Dark matter . . . 9

1.2.3 Baryon asymmetry of the universe . . . 12

1.2.4 The hierarchy problem . . . 15

2 Supersymmetry 19

2.1 Phenomenological Approach . . . 21

2.2 Superfields: pragmatic notes . . . 22

2.3 The cure of the hierarchy problem . . . 24

2.4 Supersymmetry breaking . . . 26

3 Neutrino physics 27

3.1 Neutrino oscillations: from experiment to flavour mixing . . . 27

3.2 Bounds on the neutrino mass scale . . . 30

3.3 Majorana neutrinos vs Dirac neutrinos . . . 31

3.4 Neutrino mass models and seesaw type-I . . . 32

3.4.1 Seesaw type-I . . . 33

3.4.2 Neutrino Yukawa couplings reconstruction . . . 34

4 The Minimal Supersymmetric Standard Model 35

4.1 Field content . . . 35

4.2 Superpotential . . . 36

4.3 Soft SUSY-breaking sector . . . 37

4.4 Electroweak symmetry breaking . . . 37

4.5 Mass spectrum . . . 39
4.5.1 Neutralinos . . . 40
4.5.2 Charginos . . . 40
4.5.3 Sleptons . . . 41
4.5.4 Squarks . . . 41
4.5.5 Higgses . . . 42
4.6 Constraints . . . 43
4.6.1 Phenomenological . . . 44
4.6.2 The loss of *Motivation* . . . 45
4.7 Constrained MSSM . . . 46
4.8 R-parity and the dark matter candidate . . . 47

5 MSSM extended with seesaw type-I **48**
5.1 Implementation . . . 48
5.2 Slepton flavour mixing in the SUSY seesaw type-I (RGE induced) . . . 49
5.3 Consequences for low energy phenomenology: LFV and EDM . . . 51

6 Lepton Flavour Violation **52**
6.1 Introduction . . . 52
6.2 Model setup: overview . . . 54
6.2.1 Assumptions on $3_{\mathcal{M}} + (3+3)_R$ parameters . . . 54
6.2.2 Assumptions on $(3+3)_{PMNS} + 3_{m_\nu}$ parameters . . . 55
6.3 Numerical procedure . . . 57
6.4 LFV in leading log approximation and the mSUGRA parameters influence . . . 58
6.5 Seesaw parameters impact on LFV processes: a preliminary view . . . 63
6.5.1 On the impact of subdominant RH neutrino masses . . . 66
6.5.2 Organizing note . . . 68
6.6 Reference case: $R = 1$ . . . 69
6.6.1 Degenerate right-handed neutrinos . . . 69
6.6.2 Hierarchical right-handed neutrinos . . . 73
6.7 R-matrix analysis . . . 74
6.7.1 Case 1: real R . . . 74
6.7.2 Case 2: general R . . . 76

7 Conclusions **80**

Bibliography **80**

A Backup figures **86**

B Cosmology basics **87**

B.1 Equilibrium thermodynamics: n, ρ and p . . . 87

B.2 Universe evolution: $R \propto T^{-1}$ . . . 88

B.3 Hubble parameter evolution with T . . . 88

C One-loop calculations **89**

C.1 Feynman's parametrizations . . . 89

C.1.1 Useful results . . . 89

C.2 One-loop integrals in dimensional regularization . . . 90

C.2.1 Useful results . . . 90

D Vertices and propagators **91**

D.1 Notation . . . 91

D.2 Generalities . . . 91

D.3 Standard Model . . . 92

D.3.1 Vertices . . . 93

D.4 The supersymmetric model . . . 94

D.4.1 The MSSM superpotential . . . 94

D.4.2 MSSM gaugino-matter 3-interactions . . . 94

D.4.3 MSSM mass matrices after electroweak symmetry breaking . . . 95

D.4.4 Vertices . . . 97

D.5 Propagators . . . 98

E General formulae in Flavour Violating processes **99**

E.1 FV radiative decays: fermion$_i \to$ fermion$_j + \gamma$ . . . 99

E.1.1 FV radiative decay fermion$_i \to$ fermion$_j + \gamma$ in the SM . . . 100

E.1.2 LFV $\mu \to e\,\gamma$ in the minimal extended SM . . . 103

E.1.3 (L)FV radiative decay fermion$_i \to$ fermion$_j + \gamma$ in the MSSM . . . 104

E.2 FV sparticle decays: sparticle$_X \to$ (gaugino-higgsino)$_A +$ fermion$_i$ . . . 106

E.2.1 LFV charged slepton decays: $\tilde{l}_X \to \tilde{\chi}^0_A + l_i$ . . . 106

List of Figures

1.1 Feynman Diagrams: Dominant 1L contributions to the Higgs boson self-energy in the SM 16

2.1 Feynman Diagrams: Complex scalar self-energy in the toy model 25

3.1 Types of left-handed neutrino hierarchies 30
3.2 Feynman Diagram: LO neutrinoless double beta decay via Majorana neutrinos exchange 31
3.3 Feynman Diagrams: The 3 basic types of seesaw 33

4.1 Feynman Diagrams: Dominant 1L contributions to H_u^0 self-energy in the MSSM 45

5.1 Feynman Diagrams: Dominant 1L mixed slepton self-energy in the seesaw type-I MSSM 49

6.1 Feynman Diagrams: LO radiative LFV decays $l_i \to l_j\,\gamma$ 53
6.2 Low scale U_{PMNS} mixing angles from TBM GUT ansatz 56
6.3 High scale m_ν^0's vs low scale m_ν's 56
6.4 LFV BR's vs $\tan\beta$ for paired values of $\{A_0, \text{sign}(\mu)\}$ 60
6.5 m_0 vs $m_{1/2}$ contour regions for radiative LFV BR's 61
6.6 m_0 vs $m_{1/2}$ contour regions for stau LFV BR's 62
6.7 LFV BR's vs $\mathcal{M}_R$ for degenerate RH neutrinos and SNH 65
6.8 LFV BR's vs $\mathcal{M}_R$ for degenerate RH neutrinos and SIH 66
6.9 LFV BR's vs $\mathcal{M}_R$ for hierarchical RH neutrinos 67
6.10 M_1 vs M_2 contour regions for LFV BR's for hierarchical RH neutrinos 67
6.11 s_{13}^0 influence over the radiative LFV BR's. $R = 1$, DEG RH neutrinos and strict LH 70
6.12 Expected radiative LFV BR's for saturated upper bounds. $R = 1$ and DEG RH neutrinos . 72
6.13 Radiative LFV BR's vs lightest neutrino mass scale. $R = 1$ and DEG RH neutrinos 73
6.14 Expected LFV BR's for saturated experimental upper bounds. $R = 1$ and HIE RH neutrinos 74
6.15 LFV BR's comparison between LH and RH neutrino hierarchies. $R = 1$ 75
6.16 LFV BR's for a general R-matrix with DEG $s_{13}^0 \approx 0$ and HIE $(s_{13}^0)_{max}$ RH neutrinos 77
6.17 LFV BR's for saturated upper bounds vs θ_1. $\theta_2 = 3\,e^{i\pi/2}$, $\arg\theta_1 = \theta_3 = 0$. $s_{13}^0 \approx 0$. HIE RH 79
6.18 LFV BR's for saturated bounds vs θ_1. $\theta_2 = 3\,e^{i\pi/2}$, $\arg\theta_1 = \theta_3 = 0$. $s_{13}^0 = (s_{13}^0)_{max}$. DEG RH 79

A.1 θ_1 vs θ_2 LFV impact with degenerate RH neutrinos 86

List of Tables

1.1 SM gauge structure 2
1.2 SM matter fields and representation assignments 3

3.1 Types of left-handed neutrino hierarchies and mass spectra 30

4.1 MSSM matter fields and representation assignments 36
4.2 Exclusion bounds on mSUGRA-like MSSM mass spectra from LEP2 searches 44
4.3 mSUGRA SPS 47

6.1 Experimental upper bounds on LFV radiative decays $l_i \to l_j\,\gamma$ and $l_i \to l_j\,\bar{l}_j\,l_j$ 52
6.2 Right-handed neutrino hierarchy types and mass spectra 55
6.3 Fitting steps of the solar and atmospheric splittings 58
6.4 Average slopes $\frac{BR(l_i \to l_j\,\gamma)}{BR(l_m \to l_n\,\gamma)}$ for a general R-matrix and choices $\left\{s^0_{13}, \delta^0, \text{RH hierarchy}\right\}$. 77

List of Acronyms

HEP	High Energy Physics
QFT	Quantum Field Theory
RGE	Renormalization Group Equation
RC	Radiative Correction
DREG	Dimensional Regularization
MS	Minimal Subtraction
1L	One-Loop
LO	Leading Order
SM	Standard Model
QCD	Quantum Chromodynamics
BSM	Beyond the SM
EW	Electroweak
EWSB	EW Symmetry Breaking
SB	Symmetry Breaking
VEV	Vaccum Expectation Value
SUSY	Supersymmetry
MSSM	Minimal Supersymmetric Standard Model
cMSSM	Constrained MSSM
NMSSM	Next to MSSM
PMSB	Planck Mediated Supersymmetry Breaking
SUGRA	Supergravity
mSUGRA	Minimal SUGRA
GMSB	Gauge Mediated Supersymmetry Breaking
mGMSB	Minimal GMSB
AMSB	Anomaly Mediated Supersymmetry Breaking
mAMSB	Minimal AMSB
SPA	Supersymmetry Parameter Analysis
SPS	Snowmass Point and Slope
LHA	Les Houches Accord

GUT	Grand Unified Theory
BR	Branching Ratio
CM	Center of Mass
d.o.f	degree of freedom
h.c.	hermitian conjugate
CP	Charge conjugate and Parity
CPV	CP Violation
FV	Flavour Violation
LFV	Lepton Flavour Violation
QFV	Quark Flavour Violation
PMNS	Pontecorvo-Maki-Nakagawa-Sakata
CKM	Cabibbo-Kobayashi-Maskawa
GIM	Glashow-Iliopoulos-Maiani
LH	Left-Handed
RH	Right-Handed
SNH	Strict Normal Hierarchy
SIH	Strict Inverted Hierarchy
QDNH	Quasi-Degenerated Normal Hierarchy
QDIH	Quasi-Degenerated Inverted Hierarchy
TBM	Tri-Bimaximal Mixing
b.f.p.	best fitting point
FLRW	Friedmann-Lemaître-Robertson-Walker
CMB	Cosmic Microwave Background
WMAP	Wilkinson Microwave Anisotropy Probe
BBN	Big Bang Nucleosynthesis
BAU	Baryon Asymmetry of the Universe
DM	Dark Matter
CDM	Cold DM

1 Introduction

In this thesis we will study the lepton flavour violation aspects of the minimal supersymmetric standard model (MSSM) with neutrino masses provided by a type-I seesaw. The thesis is organized as follows: in the introductory chapter we present the standard model of particle physics and discuss its flaws; in the second chapter we motivate supersymmetry (SUSY) as a (spontaneously) broken symmetry of nature; in the third chapter we give an overview on neutrino physics; in the fourth chapter we describe in detail the minimal realisation of SUSY, the MSSM; in the fifth chapter we implement the type-I seesaw to the MSSM and derive its consequences with special focus on lepton flavour violation; in the sixth chapter we study and characterize in great detail the lepton flavour violation processes $l_i \to l_j\,\gamma$ and $\tilde{l}_i \to l_j\,\tilde{\chi}^0_A$ in the seesaw type-I extended MSSM; in the final chapter we outline the main conclusions.

In this chapter we will begin with a brief description of the theoretical paradigm that guides our understanding of particle physics: the Standard Model (SM). We will address the following SM topics in detail: (i) Higgs boson and electroweak symmetry breaking (EWSB); and (ii) fermion masses generation and flavour mixing. Next, we will come to the experimental and theoretical issues which trigger the need for physics beyond the SM (BSM): (i) neutrino oscillations (section 1.2.1); (ii) dark matter (section 1.2.2); (iii) baryon asymmetry of the universe (section 1.2.3); and (iv) the hierarchy problem (section 1.2.4).

1.1 Standard Model

It is modernly assumed that any fundamental theory of nature must be a gauge theory. The root for this assumption comes from Maxwell's electrodynamics (1864 - it was a classical theory but still the first theory of fields) in which the photon (the vector and the scalar potentials of the electromagnetic field) could be redefined without changing the physical description of the theory. To this property we call gauge freedom. It was soon realized by Emmy Noether (1915) that there is a one-to-one correspondence between a continuous symmetry of the action and a conserved charge. Concretely, the gauge freedom of the photon translates into a continuous symmetry of the Lagrangian under U(1)$_Q$ local gauge transformations - the gauge symmetry of the electrodynamics - which in turn implies, by the Noether's theorem, the conservation of the electric charge, Q. Applying this concept to the conservation of the isotopic spin in strong interactions, Yang and Mills (1954) successfully described the strong force resorting to non-abelian gauge symmetries. Finally, In the late 1960s, Glashow, Weinberg and Salam (GWS) created an unified description of the weak and electromagnetic forces in the framework of a gauge theory. The Standard Model is the reunion of these separate achievements.

In a practical sense, to define a gauge theory one needs to specify a gauge group (a group of continuous local transformations under which the theory's action is invariant) and a content of matter fields, each in a chosen representation of the gauge group. To each gauge group G we associate an interaction type, $N[G]$ spin-1 fields (also called gauge fields and which must necessarily be in the adjoint representation of the respective gauge group and be singlets under the others) - the "interaction mediators" - and a coupling strength. The nature of the coupling between matter fields and gauge fields

is set by the representation of the former under the group of the latter.

The Standard Model (SM) of particle physics incorporates three of the four known fundamental forces of nature. It is based on the gauge group U(1)$_y$⊗SU(2)$_L$⊗SU(3)$_c$, where y denotes the hypercharge, the diagonal generator of SU(2)$_L$ - T_3 - is called the weak isospin and c is the quantum chromodynamics (QCD) "color"-charge. The gauge structure of the SM is summarized in Table:1.1.

Gauge group	Interaction type	Coupling strength	Gauge field
U(1)$_y$	electro-weak	g'	B_μ
SU(2)$_L$		g	W_μ^α ($\alpha = 1,2,3$)
SU(3)$_c$	strong	g_s	g_μ^a ($a = 1,...,8$)

Table 1.1: Standard Model gauge structure. $N[U(1)] = 1$ and $N[SU(n)] = n^2 - 1$.

The full Standard Model group can be seen as a full symmetry above a fundamental high energy scale. Below that scale the system undergoes a phase transition from an U(1)$_y$⊗SU(2)$_L$ symmetric vacuum to another vacuum state where U(1)$_y$⊗SU(2)$_L$ has been broken into U(1)$_Q$. This phase transition is called electroweak symmetry breaking (EWSB) and is a fundamental component of the Standard Model, as will be discussed.

In what concerns the matter field content of the SM, there are $2 \times (3 + 2 \times 3 \times 3) + 3 = 45$ fermionic and 4 real scalar degrees of freedom (d.o.f.). Of these 45 fermionic d.o.f. are formed 21 Dirac fermions (particle and anti-particle): 3 are called charged leptons and 18 are called quarks. The remaining 3 fermionic d.o.f. are the neutrinos (neutral leptons), and whether they are Dirac fermions or Majorana fermions remains an open question - we will elaborate on this in chapter 3.

The 18 quarks are arranged in 6 distinct fundamental representations of SU(3)$_c$, called u, c, t, d, s, b:

$$q_i = \begin{pmatrix} q_{(x)} \\ q_{(y)} \\ q_{(z)} \end{pmatrix}_i , \quad \text{for } i = u, c, t, d, s, b; \tag{1.1}$$

where $q_{(x)i}, q_{(y)i}, q_{(z)i}$ denotes the components of q_i in the vector space of the fundamental representation of SU(3)$_c$. The remaining d.o.f. are singlets under SU(3)$_c$.

We note now that the subscript L in SU(2)$_L$ was put there for a reason: the right-handed (RH) components of all the SM Dirac particles are singlets under SU(2)$_L$, that is, the W_μ^α gauge bosons only couple to left-handed (LH) components. For this reason we will adopt the strategy of describing the theory in terms of Weyl spinors instead of Dirac spinors. We note that a Dirac particle p can be decomposed as:

$$P_L \psi_p = \chi_p \,, \quad P_R \psi_p = \overline{\chi}_{\bar{p}} \,, \tag{1.2}$$

where χ_p is the LH component of the Dirac particle p and $\overline{\chi}_{\bar{p}}$ is the RH component of the Dirac particle p which is related to the LH component of the Dirac anti-particle $\bar{p}$ through $\overline{\chi}_{\bar{p}} = i\sigma_2 \chi_{\bar{p}}^{\dagger T}$ (the sign is purely conventional). Thus, for shortness, we fix the convention that when we write p relative to a Dirac particle

p, we are talking about the LH component of the particle - χ_p - and when we write $\bar{p}$ we are talking about the LH component of the anti-particle - $\chi_{\bar{p}}$. For a brief discussion see the appendix D.1.

The 6 LH quarks are arranged in 3 fundamental representations of SU(2)$_L$, and each of the 3 LH charged leptons - l - are accompanied by one of the 3 neutrinos - ν - also in the fundamental representation of SU(2)$_L$:

$$L_i = \begin{pmatrix} \nu \\ l \end{pmatrix}_i \ , \ \ Q_{(a)j} = \begin{pmatrix} u \\ d \end{pmatrix}_{(a)j} \ , \tag{1.3}$$

where $i = e, \mu, \tau$ and $u_{(a)j} = (u, c, t)\,,\ d_{(a)j} = (d, s, b)\,,\ a = (x, y, z)$.

The RH quarks and leptons are singlets under SU(2)$_L$. The four real scalars d.o.f. are arranged as two complex scalars fields in the fundamental representation of SU(2)$_L$:

$$\phi = \begin{pmatrix} \phi^+ \\ \phi^0 \end{pmatrix}, \tag{1.4}$$

called the Higgs doublet.

The hypercharge can be inferred by fixing the electric charge definition $Q = T_3 + \frac{y}{2}$. We present the hypercharge assignments and a summary of the SM matter fields in Table:1.2.

Matter	Representation in			Matter	Representation in		
field	U(1)$_y$	SU(2)$_L$	SU(3)$_c$	field	U(1)$_y$	SU(2)$_L$	SU(3)$_c$
L_i	-1	$\mathbf{2}$	$\mathbf{1}$	Q_i	$\frac{1}{3}$	$\mathbf{2}$	$\mathbf{3}$
$\bar{l}_i$	2	$\mathbf{1}$	$\mathbf{1}$	$\bar{u}_i$	$-\frac{4}{3}$	$\mathbf{1}$	$\bar{\mathbf{3}}$
ϕ	1	$\mathbf{2}$	$\mathbf{1}$	$\bar{d}_i$	$\frac{2}{3}$	$\mathbf{1}$	$\bar{\mathbf{3}}$

Table 1.2: Standard Model matter fields and representation assignments. In the first column the i assumes three different values, one for each family.

As a final note we stress the following:

1. a representation accordingly to SU(2)$_L$ is called a family, namely, there are 3 families of quarks and 3 families of leptons, and to each of these families we associate a different flavour label;
2. if all the SM interactions were purely of gauge-matter type there would be no reason to talk about families, as they would be indistinguishable;
3. the Yukawa type interactions between fermionic d.o.f. and scalar d.o.f., which are a necessary ingredient - to be explained below - of the SM, are the source for the family identification and, equivalently, for the flavour labelling;
4. a gauge symmetry prohibits the gauge bosons of acquiring mass;
5. the different SU(2)$_L$ assignments given to LH and RH components of the Dirac fermions prohibits gauge invariant Dirac mass terms in the unbroken U(1)$_y\otimes$SU(2)$_L$ theory;
6. dropping the U(1)$_y\otimes$SU(2)$_L$ symmetry condition (for instance, as a result of EWSB), Majorana mass terms are prohibited by electric charge conservation for all the SM fermions with the exception of neutrinos, which carry zero electric charge.

1.1.1 Electroweak symmetry breaking

We start from the note that ended the previous section, where we stated that a gauge symmetry prohibits the gauge bosons of acquiring mass. This certainly would pose a problem to any theory trying to describe the weak interaction.

The weak interaction was introduced to explain the nuclear β-decay which was partially explained by a four-fermion point interaction, $-2\sqrt{2}\,G_F\left(p^\dagger\,\bar{\sigma}^\mu n\right)\left(e^\dagger\,\bar{\sigma}_\mu \nu_e\right)$. This was a successful low energy theory that suffered from two drawbacks: certain processes violated unitarity - as the process cross section, σ, indefinitely increased with the center of mass (CM) energy, $\sqrt{s}$, for instance the e-ν_e scattering $\sigma(e\,\nu_e \to e\,\nu_e) = \frac{G_F^2 s}{\pi}$ (at tree-level) - and it was a non-renormalizable interaction (which can be simply seen by noting that the interaction coupling, G_F, has negative mass dimension, specifically, $[M]^{-2}$). A gauge theory for weak interactions replaces the four-fermion point interactions by non-local interactions mediated by gauge bosons. This solves the two referred drawbacks, at the expense of requiring these gauge bosons to be massive - as in the low energy limit one has to recover the effective four-fermion point interactions:

$$\frac{g^2}{2}\left(\frac{g_{\mu\nu}-\frac{k_\mu k_\nu}{M_W^2}}{k^2-M_W^2}\right)\underset{k^2\ll M_W^2}{\longrightarrow} -2\sqrt{2}\,G_F\,g_{\mu\nu} \Rightarrow G_F \equiv \frac{g^2}{4\sqrt{2}M_W^2}. \tag{1.5}$$

To preserve all the advantages of a gauge theory and simultaneously describe the weak interaction one has to spontaneously break the U(1)$_y\otimes$SU(2)$_L$ gauge symmetry. For this, the existence of a (yet to be discovered) particle was postulated: the Higgs boson. Through the Higgs mechanism, the Higgs doublet (introduced earlier) neutral component - ϕ^0 - acquires a non-vanishing vacuum expectation value (VEV), $\langle\phi^0\rangle = v$, triggering EWSB. As a consequence:

1. a non-trivial mass spectra for the U(1)$_y\otimes$SU(2)$_L$ gauge bosons, whose diagonalization allows the identification of a massless gauge boson A_μ - the photon - and three massive gauge bosons, Z_μ and $W_\mu^\pm$ - the weak interaction mediators;
2. the fermion masses (and mixings) through Yukawa type interactions - to be discussed in section 1.1.2.

A scalar field is required to induce spontaneous symmetry breaking (SSB) because to preserve Lorentz covariance every vacuum of the theory must be invariant under transformations of the Lorentz group. This implies that only fields with spin-0 can acquire a non-vanishing VEV. Additionally, the scalar multiplet component that develops the VEV must carry zero electric charge as to conserve electric charge.

Nevertheless, SM mass generation can be put into a broader context than that of a Higgs doublet. We add to our theory a scalar multiplet - Σ - in a certain (for now unspecified) representation of U(1)$_y\otimes$SU(2)$_L$. We assign the hypercharge to the Σ multiplet such that the i-component of the Σ multiplet is neutral. This neutral component will develop a VEV v, triggering EWSB and the U(1)$_y\otimes$SU(2)$_L$ gauge bosons will - through gauge invariant kinetic term $(D^\mu\Sigma)^\dagger D_\mu\Sigma$ - get the following mass terms:

$$g'^2Y^2v^2B_\mu B^\mu + g^2\,(T_3)_{ii}^2\,v^2W_\mu^3W^{3\mu} + 2gg'Y\,(T_3)_{ii}\,v^2B^\mu W_\mu^3 + \frac{1}{2}g^2\,(T_+T_-)_{ii}\,v^2W_\mu^+W^{-\mu}\,, \tag{1.6}$$

where we have defined the covariant derivative as $D_\mu = \partial_\mu + ig'YB_\mu + igT_\alpha W_\mu^\alpha$ (with Y related to the commonly defined hypercharge through $2Y = y$), and the usual combinations for the non-diagonal part of SU(2)$_L$ gauge bosons and group generators $W_\mu^\pm \equiv \frac{W_\mu^1 \mp iW_\mu^2}{\sqrt{2}}$, $T_\pm = T_1 \pm iT_2$.

The diagonalization of the B_μ and W_μ^3 mixture gives automatically rise to a massless mode (A_μ) and a massive mode (Z_μ). It is customary to parametrize this diagonalization by a rotation angle called the weak mixing angle θ_w (with shorthand notation $c_w \equiv \cos\theta_w$, $s_w \equiv \sin\theta_w$ and $t_w \equiv \tan\theta_w$) such that:

$$Z_\mu = c_w W_\mu^3 - s_w B_\mu, \quad A_\mu = c_w B_\mu + s_w W_\mu^3; \quad \text{with } c_w \equiv \frac{g}{\sqrt{g^2 + g'^2}}, \tag{1.7}$$

where we have used $[T_3]_{ii} = -Y$. By requiring that the photon couples with $e\,Q$ strength to particles of electric charge $Q \equiv T_3 + Y$, one determines the relation between the weak coupling constant and the elementary electric charge through the weak mixing angle:

$$g' c_w Y + g s_w T_3 \equiv e\,Q \Rightarrow e \equiv g s_w. \tag{1.8}$$

It is also straightforward to realise that the masses of $W_\mu^\pm$ and Z_μ read:

$$M_W^2 = g^2 v^2 \left[T(T+1) - Y^2\right], \quad M_Z^2 = 2\frac{g^2 v^2}{c_w^2} Y^2, \tag{1.9}$$

where use has been made of $\frac{1}{2}\{T_+, T_-\} + (T_3)^2 = T(T+1)$ and $[T_3]_{ii} = -Y$.

From these we establish a relation between the masses of the weak gauge bosons, the ρ-parameter:

$$\rho \equiv \frac{M_W^2}{c_w^2 M_Z^2} = \frac{T(T+1) - Y^2}{2Y^2}. \tag{1.10}$$

Electroweak precision measurements determined that $\rho = 1$ to an excellent approximation and a deviation from unity can be attributed to radiative corrections (RC) to the $W^\pm$ and Z propagators. Hence, to apply the Higgs mechanism one must resort only to Higgses in representations of U(1)$_y \otimes$SU(2)$_L$ that satisfy:

$$T(T+1) = 3Y^2 = \frac{3}{4} y^2 = 3\,(T_3)_{ii}^2\,. \tag{1.11}$$

From $T = 1/2$ to $T = 10^4$ there are only 8 choices for the SU(2)$_L$ representation and, for each of these, there are 2 possible hypercharge choices: the first of these choices is $T = \frac{1}{2}$ and $y = \pm 1$, the second is $T = 3 \wedge y = \pm 4$, the third and fourth are $T = \frac{25}{2} \wedge y = \pm 15$ and $T = 48 \wedge y = \pm 56$, and the remaining are $T = \frac{361}{2} \wedge y = \pm 209$, $T = 675 \wedge y = \pm 780$, $T = \frac{5041}{2} \wedge y = \pm 2911$ and $T = 9408 \wedge y = \pm 10864$. As stated earlier, in the SM the choice is $T = 1/2$ and $y = 1$, which adds a minimal content of fields. The hypercharge sign has no physical meaning, it is in fact just a matter of convention to whether the VEV will appear in the up or in the down component of the doublet.

Having established the mass spectra of the electroweak gauge bosons we will now give a brief description of the actual mechanism - the Higgs mechanism - that generates the VEV. We consider the most general form of a self-interacting potential for the Higgs doublet that is both gauge-invariant and renormalizable. It reads:

$$V_{Higgs} = \mu^2 |\phi|^2 + \frac{\lambda}{4} |\phi|^4, \tag{1.12}$$

where $\lambda > 0$. At the EWSB energy scale the Higgs doublet mass parameter, μ^2, runs negative and the fields must be redefined in respect to the new global minimum of the potential:

$$\langle \phi^0 \rangle = v, \;\; \phi^0 = v + \frac{H + i\xi}{\sqrt{2}}, \tag{1.13}$$

with tree-level minimization condition $v = \sqrt{-\frac{2\mu^2}{\lambda}}$.

The CP-odd real scalar field ξ and the complex scalar field ϕ^+ are massless fields which are called Goldstone bosons and are non-physical fields which are "eaten" by the Z_μ and $W^\pm_\mu$ longitudinal modes, generating their masses. Moreover, by the Goldstone theorem one knows that the number of unphysical fields that emerge from SSB of a gauge group G into a gauge group G' is equal to the number of broken generators of G. Specifically, EWSB breaks 3 of the 4 generators of U(1)$_y \otimes$SU(2)$_L$, and hence we get 3 real Goldstone bosons: ξ, Re[ϕ^+] and Im[ϕ^+].

In more concrete terms, one can show that there is a gauge choice - the unitary gauge - where the Goldstone bosons disappear, and this corresponds to a specific form for the Z and $W^\pm$ propagators. However, the unitary gauge is not necessarily the more convenient choice for calculations. Hence, one usually includes the Goldstone bosons when describing the theory.

To end this section we summarize the tree-level mass spectra of the theory so far described:

$$M_W^2 = \frac{1}{2} g^2 v^2, \;\; M_Z^2 = \frac{1}{c_w^2} M_W^2, \;\; m_H^2 = -2\mu^2. \tag{1.14}$$

1.1.2 Fermion Masses and Mixings

Since the SU(2)$_L$ gauge symmetry is in fact broken, Dirac mass terms can be accommodated as a result of the EWSB.

Requiring renormalizability[1] one can have interactions of the type:

1. fermion-fermion-scalar;
2. fermion-fermion-(gauge boson);
3. (gauge boson)^2-scalar;
4. (gauge boson)^2-scalar^2;
5. (gauge boson)^3;
6. (gauge-boson)^4.

The second and fourth types are already included in the "covariantized" kinetic term of the matter fields and any additional contribution is excluded because it would explicitly break gauge symmetry. The same applies for the fifth and sixth interaction types but, int this case, for the non-abelian gauge bosons generalized kinetic term. The third type explicitly breaks the gauge symmetry. We are thus left with the first interaction type. As the scalar is the Higgs doublet (the only scalar in the theory) and the fermions are either in doublet or singlet representations of SU(2)$_L$ one realises - by additionally requiring invariance over U(1)$_y$ - that the most general form of non-gauge interactions that we can write is:

$$\mathcal{L}_Y = y^u_{ij} \bar{u}_{(a)j} \phi \, i\sigma_2 \, Q_{(a)i} - y^d_{ij} \bar{d}_{(a)j} \phi^\dagger Q_{(a)i} - y^l_{ij} \bar{l}_j \phi^\dagger L_i + \text{h.c.}\,, \tag{1.15}$$

which are called Yukawa interactions. Sum over i, j families and a colour is implied. The couplings y^u, y^d and y^l are 3×3 (for now general) complex matrices in family space, and are commonly called Yukawa couplings.

[1] We implicitly assume the obvious condition that the Lagrangian must be a Lorentz scalar.

At EWSB, when the Higgs doublet neutral component acquires a non-vanishing VEV, general Dirac mass terms are generated via the Yukawa interactions. Specifically:

$$\mathcal{L}_Y^M = -M_{ij}^l \bar{l}_j l_i - \sum_{q=u,d} M_{ij}^q \bar{q}_{(a)j} q_{(a)i} + \text{h.c.}\ , \quad \text{where}\ \ M^{u,d,l} \equiv v y^{u,d,l}. \tag{1.16}$$

The usual basis to work on is the so called "physical basis", that is, the basis in which the general mass terms are diagonal, allowing one to work with ordinary propagators. Hence, one performs an unitary rotation in family space from the "flavour basis" - the basis in which the SU(2)$_L$ gauge interactions are diagonal among SU(2)$_L$ doublets (or families) - to the mass eigenstate basis (superscript ^{0}) through:

$$l_i = (V_l)_{ij} l_j^0\,,\ \bar{l}_i = (U_l)_{ij}^* \bar{l}_j^0\,,\ q_i = (V_q)_{ij} q_j^0\,,\ \bar{q}_i = (U_q)_{ij}^* \bar{q}_j^0 \quad \text{for}\ \ q = u, d\,, \tag{1.17}$$

so that the diagonalized mass matrices read,

$$\hat{M}^l = V_l^T M^l U_l^*,\ \ \hat{M}^q = V_q^T M^q U_q^* \quad \text{for}\ \ q = u, d\,. \tag{1.18}$$

In turn, the charged SU(2)$_L$ gauge interactions of quarks became of the form[2]:

$$-\frac{g}{\sqrt{2}} W_\mu^+ u_{(a)i}^\dagger \bar{\sigma}^\mu d_{(a)i} + \text{h.c.} = -\frac{g}{\sqrt{2}} W_\mu^+ u_{(a)i}^{0\dagger} (V_{CKM})_{ij} \bar{\sigma}^\mu d_{(a)j}^0 + \text{h.c.}\,, \tag{1.19}$$

where we have defined the Cabibbo-Kobayashi-Maskawa (CKM) matrix,

$$V_{CKM} \equiv V_u^\dagger V_d. \tag{1.20}$$

The neutral SU(2)$_L$ gauge interactions remain diagonal.

Since neutrinos are massless (in the strict sense of the SM) we can arbitrarily change their null-mass eigenstate basis. In particular, it is convenient to rotate them through $\nu_i = (V_l)_{ij} \nu_j^0$ so that all the SU(2)$_L$ gauge interactions among leptons remain diagonal.

We end this section by stating that simultaneous mass terms for the up- and down-type components of the SU(2)$_L$ doublets gives, in a broader sense, rise to flavour violation (FV). In spite of that, one could still have an alignment between up- and down-type rotation matrices so that the mixing matrix is the identity, that is, flavour is still conserved. However, this does not happen in nature. First, because the CKM was envisioned as an extension to the Cabibbo theory, which accommodated the experimentally observed strangeness (the flavour of the quark-s family) violation, for instance in charged kaons decays such as $K^- \to \mu\, \bar{\nu}_\mu$. Secondly, it is well established by now that quark flavour violation (QFV) happens among any two pair of families, being dominant among the first and second families ($\propto \lambda$, where $\lambda \approx 0.22$), then between the second and third families ($\propto \lambda^2$) and finally between the first and third families ($\propto \lambda^3$).

1.2 Evidences and hints for physics beyond the SM

The SM is extremely efficient in accounting for all electroweak precision measurements [2]. The degree of agreement between measurements and the model predictions is known to be better than a few per

[2]For a discussion on the notation used see the appendix D.1.

mille [3]. Nevertheless, the Higgs sector remains untested and only a direct lower bound on the Higgs mass exists, $m_H > 114.4$ GeV (at 95% C.L.) from [4]. Also, an upper bound of $m_H < 212$ GeV (at 95% C.L.) can be extracted [5] from the Higgs radiative contributions to well measured quantities. However, the SM is not the complete theory of nature, even if we discard gravity. In this section we will give an overview of the issues that lead BSM physics. Succinctly, the 4 major issues of the SM are:

1. the currently well established evidence of non-vanishing neutrino masses;
2. it does not contain any particle that fits the profile of the most abundant type of matter in the universe - dark matter;
3. it provides an insufficient baryon asymmetry of the universe (BAU);
4. the Higgs sector is unstable under radiative corrections. Any small-distance (high energy scale) d.o.f. that exists in a prospective full theory dramatically changes the high-distance (electroweak energy scale) scenario we are modelling at the present - the hierarchy problem.

1.2.1 Neutrino masses

In the SM, the neutral lepton in the SU(2)$_L$ doublet has no singlet counterpart which forbids it of acquiring a Dirac mass as a result of the EWSB, in contrast to what happens to the rest of the fermions. Nevertheless, in the spontaneously broken U(1)$_y$⊗SU(2)$_L$ phase, one could think of a hypothetical Majorana mass:

$$\mathcal{L}_\nu^M = -M_{ij}^\nu \, (\nu_i \cdot \nu_j) + \text{h.c.}\,, \tag{1.21}$$

which would arise radiatively. However, it turns out that this Majorana mass term is zero to all orders in perturbation theory because it is protected by an "accidental symmetry" of the SM: the lepton number conservation. Specifically, $L = n_l - n_{\bar{l}}$ - where n_l and $n_{\bar{l}}$ is the number of leptons and anti-leptons, respectively - is a strictly conserved quantity of the SM. The Majorana mass term violates the lepton number by 2 units, $\Delta L = 2$.

An accidental symmetry can occur when we demand renormalizability on top of gauge invariance and, as a result, the full group of symmetry of our model is larger than the gauge group considered. Indeed, the symmetry group of all the renormalizable operators is higher than the SM gauge group. To see this we start by considering the matter-gauge sector of the SM, which is of the form:

$$\sum_p i p^\dagger \bar{\sigma}^\mu D_\mu p\,, \quad \text{where } p = L_i, \bar{l}_i, Q_i, \bar{u}_i, \bar{d}_i\,, \tag{1.22}$$

and i runs over all families, $i = 1, 2, 3$.

These terms are clearly invariant under independent global U(1) transformations for each one of the p's:

$$\begin{cases} L_i \to e^{i\phi_{5i-4}} L_i\,, \quad \bar{l}_i \to e^{i\phi_{5i-3}} \bar{l}_i\,, \\ Q_i \to e^{i\phi_{5i-2}} Q_i\,, \quad \bar{u}_i \to e^{i\phi_{5i-1}} \bar{u}_i\,, \quad \bar{d}_i \to e^{i\phi_{5i}} \bar{d}_i\,, \end{cases} \tag{1.23}$$

where $i = 1, 2, 3$. As there are 15 p's, this sector has the global symmetry group $[\text{U(1)}]^{15}$. However, one of these symmetries is already included in the gauge group specification, that is, U(1)$_y$. To understand

this, consider the 15-dimensional basis of parameters ϕ_i and apply the change of basis from ϕ_i to ϕ'_i:

$$\begin{pmatrix} \phi^0_{5i-4} \\ \phi'_{5i-3} \\ \phi'_{5i-2} \\ \phi'_{5i-1} \\ \phi'_{5i} \end{pmatrix} = \begin{pmatrix} Y_{L_i} & Y_{\bar{l}_i} & Y_{Q_i} & Y_{\bar{u}_i} & Y_{\bar{d}_i} \\ 1 & -1 & 0 & 0 & 0 \\ 0 & 0 & 1/3 & -1/3 & -1/3 \\ 1 & 1 & 0 & 0 & 0 \\ 0 & 0 & -3/4 & -3/4 & -3/4 \end{pmatrix} \begin{pmatrix} \phi_{5i-4} \\ \phi_{5i-3} \\ \phi_{5i-2} \\ \phi_{5i-1} \\ \phi_{5i} \end{pmatrix}, \quad \begin{pmatrix} \phi'_1 \\ \phi'_6 \\ \phi'_{11} \end{pmatrix} = \begin{pmatrix} 1 & 1 & 1 \\ 1/2 & -1/2 & 1/2 \\ 1/2 & 1/2 & -1/2 \end{pmatrix} \begin{pmatrix} \phi^0_1 \\ \phi^0_6 \\ \phi^0_{11} \end{pmatrix}, \tag{1.24}$$

where $i = 1, 2, 3$. Clearly, the parameter ϕ'_1 is the parameter of $\mathrm{U}(1)_y$. So, the accidental symmetry group of the matter-gauge sector is just $[\mathrm{U}(1)]^{14}$.

By including the SM Yukawa sector, which has no mixing in the lepton sector, we break $[\mathrm{U}(1)]^{14}$ into $[\mathrm{U}(1)]^4$. Concretely:

1. the 6 symmetry groups that have as transformation parameters ϕ'_{5i-1} and ϕ'_{5i} (for $i = 1, 2, 3$) are broken due to the fact that LH particle and LH anti-particle carry the same quantum number in each of these groups;
2. the 5 symmetry groups that have as transformation parameters ϕ'_6, ϕ'_{11} and ϕ'_{5i-2} (for $i = 1, 2, 3$) are broken into just one symmetry group of parameter $\phi'' = \phi'_3 + \phi'_8 + \phi'_{13}$, due to the mixing in the quark sector.

Thus, we are left with the symmetry groups of parameters ϕ'_{5i-3} (for i running over each family of leptons, $i = 1, 2, 3$) and ϕ'', which we identify as flavour$_i$ lepton number (L_i) and total baryon number (B), respectively.

Elaborating more on this, we have the flavoured lepton number $L_i = n_{l_i} - n_{\bar{l}_i}$, where n_{l_i} and $n_{\bar{l}_i}$ is the number of leptons and anti-leptons of the family i, respectively. Each of the flavoured lepton numbers is conserved separately. The total baryon number is $B = \frac{1}{3}(n_q - n_{\bar{q}})$, where n_q and $n_{\bar{q}}$ is the number of quarks and anti-quarks, respectively. One would expect that, as the flavoured lepton number is strictly conserved in the SM, the same would happen for the total baryon number. However, this is not the case. To understand why this happens is beyond the scope of this brief exposition. We just note that we have not really quantized our theory. In the fully quantized theory a pseudoparticle called instanton can connect two vacua with different particle definitions, which in turn can originate the creation of particles.

In this section we have shown that, in the SM, neutrinos remain massless to all orders in perturbation theory. To account for the indisputable evidence of massive neutrinos - more on this in chapter 3 - it is mandatory to look for physics BSM. We point towards chapter 3 where we will return to the idea of a Majorana mass term for the neutrinos in the context of the SM extended with RH neutrinos.

1.2.2 Dark matter

The first candidate for dark matter was an already known type of matter: neutral baryonic matter, such as neutron stars and planets. However, this was soon discarded because it could not explain the large scale structure of the universe. Indeed, a non-baryonic type of matter, which interacted weakly with the CMB photons, could have started the density fluctuations before the epoch of recombination and

have the amplitude needed at that time to form structures, without contradicting the CMB data. Also, the amount of baryonic matter predicted by the big bang nucleosynthesis (BBN) was insufficient to account for the amount of DM.

The second candidate was the SM light neutrinos. The problem with the neutrinos is that they move very fast and as such are not able to cluster in small structures of galaxies, as DM do.

Clearly, a weakly interacting massive particle (WIMP) seemed as the ideal DM candidate[3]. As this particle is massive, one usually refers to it as cold dark matter (CDM) in comparison to the neutrino which was a hot dark matter candidate. For a detailed review on its history and concepts see [6].

Currently, it is well established that the matter of the universe amounts to ~ 0.28 of the total energy of the universe. Of this 0.28 the main contribution comes from CDM with ~ 0.23. For definitiveness we list the results taken from the combined data of WMAP (5 years), BAO (Baryonic Acoustic Oscillations) and SN (SuperNovae) from table D1 of [7]:

$$\Omega_{CDM} = 0.233 \pm 0.013\,, \quad \Omega_B = 0.0462 \pm 0.0015\,, \tag{1.25}$$

where Ω is the energy density normalized to the critical density (see (B.3)). Note that we are assuming $\Omega_{total} = 1$ (see the discussion in the appendix B, especially the second footnote).

Next, we will see how to relate cosmology with particle physics.

From cosmology to particle physics: relic densities

Nowadays, the universe is described by the so called standard model of cosmology, which is grounded on the Friedmann-Lemaître-Robertson-Walker (FLRW) metric, being sometimes referred to as: Friedmann cosmology. We start by recalling that in such distance scales it is customary to study the universe as a fluid described by thermodynamics variables such as E, T, S, V, N and p. Moreover, we refer to the appendix B for the important concepts and equations that we will use throughout.

Initially, for sufficiently high temperatures, all the particles were relativistic. As the universe expanded it cooled down and particles of mass m, that were relativistic when $k_B T \gg m$, are now non-relativistic, $k_B T \ll m$, decoupling from the fluid. The number density, energy density and pressure for particles in both the relativistic and non-relativistic regimes are given in the appendix B.1.

At a temperature T_f, in the non-relativistic regime, these particles that were in equilibrium with the fluid, get out of equilibrium and their number freezes in a covolume[4] ($nR^3 =$ constant). This happens because there is not enough energy ($k_B T$) in the fluid to create or destroy any of these particles (note that we are assuming that these particles are stable).

Let us explicitly see what we have just stated qualitatively. For simplicity, we are going to assume that the number of X particles only varies with annihilation processes such as $X\bar{X} \to \phi^\dagger \phi$, and that X is a stable particle.

[3]There is also a null-candidate, which questions whether Newtonian gravity is the whole story at such large scales. These theories, called MOND (modified newtonian dynamics), change the gravitational potential in such a way that the rotation curves can be modelled without the need for any additional mass.

[4]A covolume V_c is a volume whose measure evolves with the scale of the universe: $V_c = R^3 \frac{V_0}{R_0^3}$, where V_0 and R_0 are constant numbers with self-evident meanings.

The evolution of the X particles number density with cosmological time is governed by the Boltzmann equation:

$$\frac{dn_X}{dt} + 3Hn_X = -\langle\sigma v\rangle \left[n_X^2 - n_X^{(eq)2}\right] , \tag{1.26}$$

where n_X is the X particles number density, $n_X^{(eq)}$ is the equilibrium number density, $3Hn_X$ is a sink term due to the expansion of the universe (3 is the volume factor as in R^3) and $\langle\sigma v\rangle$ is the thermal average of the annihilation between X particles (washout term).

In a more realistic scenario, X can take part in various types of processes, such as production processes (for instance, through the inverse process $\phi^\dagger\phi \to X\bar{X}$), co-annihilation processes (like $X\bar{f} \to \phi^\dagger\phi$) and scattering processes ($\phi f \to \phi X$). Thus, one would have to consider, instead of (1.26), a set of coupled equations, balancing the different processes and the number density of each type of particle. Nevertheless, in some cases there are processes which outplay all the others. We will then proceed with our simplified model, considering that we are in a situation where $X\bar{X} \to \phi^\dagger\phi$ is by far the dominant process.

As the temperature of the universe T evolves with R^{-1} (for T sufficiently high - see appendix B.2), we have that $R = T_0\frac{R_0}{T}$ which implies $H \equiv \frac{\dot{R}}{R} = T\frac{d}{dt}\left(\frac{1}{T}\right) = -\frac{\dot{T}}{T}$. We this we can rewrite equation (1.26) as:

$$\frac{d}{dt}\left(\frac{n_X}{T^3}\right) = -\langle\sigma v\rangle T^3 \left[\left(\frac{n_X}{T^3}\right)^2 - \left(\frac{n_X^{(eq)}}{T^3}\right)^2\right] . \tag{1.27}$$

Clearly, if there were no washout of particles X (that is, a null annihilation term), the number of particles would be constant in a covolume even before freeze-out.

Recall that the universe starts with a singularity (infinitely high number density) and expands, dropping both T (increasing R) and the number density n_X. At a temperature T_f, when the expansion rate H becomes of the same size as the annihilation rate ($\Gamma \equiv n_X\langle\sigma v\rangle$, which depends on both n_X and T) the number density in a covolume freezes out: $n_X R^3$ or n_X/T^3 becomes constant. This happens at a temperature T_f (the freezing temperature) approximately given by:

$$n_X(T_f) \sim \left.\frac{H}{\langle\sigma v\rangle}\right|_{T=T_f} . \tag{1.28}$$

Thus, this number density in a covolume, $R^3(T_f)n_X(T_f)$, that was set in the early universe (at a time with $T = T_f$) is the same that we have at the present time:

$$n_X^{(0)} = R^3(T_f)\frac{n_X(T_f)}{R^{(0)3}} = T^{(0)3}\frac{n_X(T_f)}{T_f^3} , \tag{1.29}$$

where $R^{(0)}$, $T^{(0)}$ and $n_X^{(0)}$ is the scale of the universe, the temperature of the universe and the number density of X particles, all at present time, respectively.

From equation (1.28) we can determine the freezing out temperature which depends crucially on the annihilation rate which, in turn, is given by the particle physics model that includes the DM candidate. Inserting the freezing out temperature in (1.29) we can determine the number density of X particles in the universe at the present time and compare to cosmological data.

Concretely, from (1.28) and using both the energy density of a non-relativistic particle $\rho = m\,n$ (with n given in (B.9)) and the universe expansion rate as a function of T (expression (B.15)), we can deduce

an approximate relation between T_f and σ:

$$x_f \equiv \frac{m_X}{k_B T_f}\,, \quad \sqrt{\frac{1}{x_f}} e^{x_f} = \frac{3}{2\pi^2}\sqrt{\frac{5}{\pi}}\frac{g_X}{\sqrt{g_*}}\frac{m_X M_P \langle\sigma v\rangle}{\hbar^2} \Rightarrow x_f \approx \ln\left(\frac{3}{2\pi^2}\sqrt{\frac{5}{\pi}}\frac{g_X}{\sqrt{g_*}}\frac{m_X M_P \langle\sigma v\rangle}{\hbar^2}\right)\,, \quad (1.30)$$

where $M_P \equiv \sqrt{\frac{\hbar c}{8\pi G_N}}$ is the Planck mass, g_X is the number of d.o.f. of the X particles, m_X is the X particles mass and g_* - defined in (B.14) - is the total number of relativistic d.o.f. in the universe at the time of X particles decoupling.

Next, from (1.29) combined with (1.28) (substituting in favour of n_X) and (1.30) (substituting in favour of T_f in $H(T_f)$ given by (B.15)) we can further deduce:

$$\Omega_X^{(0)} = \frac{m_X n_X^{(0)}}{\rho_c^{(0)}} = \frac{1}{3\pi}\sqrt{\frac{5}{2}}\frac{a_R}{k_B}\frac{T^{(0)3}}{H^{(0)2}}\frac{\hbar^3}{M_P^3}\frac{x_f\sqrt{g_*}}{\langle\sigma v\rangle}\,, \quad (1.31)$$

where a_R is the radiation constant given in (B.8). Plugging all the numbers, such as $T^{(0)} = T_\gamma^{(0)} = 2.725$ K, we arrive at:

$$h^{(0)2}\,\Omega_X^{(0)} \approx 8.45\, x_f\sqrt{g_*}\left[\frac{1\text{ fb}}{\langle\sigma v\rangle}\right]\,, \quad (1.32)$$

where h is the reduced Hubble parameter, defined by (B.2) in the appendix B.

From the previous equation we conclude that energy density of DM decreases with increasing annihilation rate. As the annihilation rate is, in general, proportional to the inverse of the mass squared and x_f depends very smoothly on m_X (x_f is of order 10 to 30 for m_X of 1 MeV to 10^3 TeV), we see that the DM energy density increases parabolically with increasing mass of the DM candidate.

To have an idea of the mass of the DM candidate that reproduces the DM parameter density:

$$h^{(0)2}\,\Omega_{CDM}^{(0)} = 0.1143 \pm 0.0034\,, \quad (1.33)$$

obtained from the combined results of WMAP + BAO + SN (table D1 of [7]); let us assume that the annihilation process has a typical size of an electroweak process $\langle\sigma v\rangle \sim \frac{\alpha^2}{m_X^2}$. Hence:

$$m_{DM} \sim 100\text{ GeV}\,, \quad (1.34)$$

where we have considered g_* of order 1.

1.2.3 Baryon asymmetry of the universe

Observational data confirms categorically that matter dominates over anti-matter and that this matter anti-matter asymmetry is the same throughout the entire universe.

We express this matter anti-matter asymmetry through the introduction of the difference between the number density of baryons and anti-baryons normalized to the number density of photons:

$$\eta_B = \frac{n_B - n_{\bar{B}}}{n_\gamma}\,, \quad (1.35)$$

which we call the baryon asymmetry of the universe (BAU). Moreover, and because at the present $n_{\bar{B}}^{(0)} \simeq 0$ in comparison to $n_B^{(0)}$, we use the baryon-to-photon ratio,

$$\eta_B^{(0)} \simeq \frac{n_B^{(0)}}{n_\gamma^{(0)}}\,, \quad (1.36)$$

when we talk of the present BAU.

From the temperature of the photons at the present $T_\gamma^{(0)} = 2.725$ K and using the relation (B.7), between the number density of photons $n_\gamma^{(0)}$ and their temperature, we can deduce:

$$\eta_{10} \equiv 10^{10}\eta_B^{(0)} = 10^{10}\left(\frac{n_B^{(0)}}{n_\gamma^{(0)}}\right) = 10^{10}\Omega_B^{(0)}\left(\frac{\rho_c^{(0)}}{m_B}\right)\left[g\frac{\zeta(3)}{\pi^2}\left(\frac{k_B T_\gamma^{(0)}}{c\hbar}\right)^3\right]^{-1} \simeq 273.6\times\Omega_B^{(0)}h^{(0)2}\,, \quad (1.37)$$

where we have restored the c factors by dimensional analysis, $\rho_B^{(0)} = m_B\, n_B^{(0)}$ and for m_B we have taken the proton's ($\simeq$ neutron's) mass.

Determination

There are essentially two independent ways to determine the present BAU. The first one is from the comparison of the observed light nuclei mass fractions with the BBN predictions. The other is from the measurement of the anisotropies in the CMB power spectra that depend on the baryon density parameter which, in turn, is related to the present BAU through (1.37).

BBN determines the abundance of light elements, such as ^{1}H, D, ^{3}He, ^{4}He and ^{7}He relying on SM physics. It turns out that the most abundant elements (^{1}H and ^{4}He represent roughly 75% and 25% of the total baryonic matter in the universe) are almost insensitive to the BAU. We will outline the main stages of the BBN with some qualitative assessments and quote results from detailed analysis.

The nuclei are synthesized from neutrons and protons that remained after the baryon/anti-baryon annihilation period, which ended at ~ 20 MeV (see below, equation (1.47)) when the annihilation rate was of the same size as the expansion rate. After this period, the protons and neutrons undergone weak interaction processes with the rest of the particles of the thermal bath ($l_i^\pm$ and ν_i):

$$n + \nu_i \leftrightarrow p + l_i\,, \quad p + \bar{\nu}_i \leftrightarrow n + \bar{l}_i\,, \quad n \leftrightarrow p + l_i + \bar{\nu}_i\,, \quad (1.38)$$

with which they maintained a thermal equilibrium. At a temperature T_f when the typical $n \leftrightarrow p$ interconversion rate ($\Gamma_{n\leftrightarrow p} \simeq N_{int}G_F^2T^5$, where $N_{int} = 3N$ with N the number of families and the factor 3 in $3N$ comes from the 3 types of $n \leftrightarrow p$ interactions as shown in (1.38)) was of the same size of the expansion rate, whose T-dependence is derived in (B.15), the number of neutrons and protons froze out. Plugging the numbers one determines this temperature as:

$$T_f = \left(\frac{\sqrt{g_*}\pi}{3\sqrt{10}N_{int}M_PG_F^2}\right)^{1/3} \simeq 0.71\ \text{MeV}\,, \quad (1.39)$$

where $g_* = 79/8$ (as calculated via (B.14) with the photon + 3 charged leptons + 3 neutrinos) and $N_{int} = 9$. Hence, the ratio between the number of neutrons and protons after the freezing out of the weak interactions is:

$$\frac{n_n}{n_p} = \exp\left\{-\frac{m_n - m_p}{T_f}\right\} \simeq 0.16 \quad (1.40)$$

After this period the temperature continues to drop, going below the different binding energies of the light nuclei, favouring their formation. The most stable light nuclei, ^{4}He, is the most likely to be formed.

Assuming ^{4}He are quickly formed from all the neutrons available and that there are roughly 0.16 neutrons for every proton (see (1.40)), one computes the mass fraction of deuterium as:

$$Y_p = \frac{2n_n}{n_n + n_p} \simeq 0.27\,. \tag{1.41}$$

However, direct production $2p + 2n \to {}^4\text{He} + \gamma$ turns out to be inefficient due to a very small cross-section. Thus, ^{4}He is synthesized in a chain reaction whose first step is the formation of deuterium, $p + n \to D + \gamma$, with a very small binding energy of $\simeq 2.2$ MeV. Due to this small binding energy, the inverse process (deuterium photodissociation) has an energy threshold that is below the temperature of the photons in the thermal bath, dissociating any deuterium that is formed. Hence, the synthesization of ^{4}He is postponed until the temperature drops below ~ 0.06 MeV. Hence, our crude estimate (1.41) is inaccurate. A detailed calculation that accounts for this "deuterium bottleneck", renders [8]:

$$Y_p \simeq 0.2485 + 0.0006 + 0.0016\,(\eta_{10} - 6)\ , \tag{1.42}$$

for $\eta_{10} \simeq 6$. Clearly, from the time $T \simeq 2.2$ MeV to $T \simeq 0.06$ MeV some neutrons have decayed into protons, reducing the deuterium mass fraction from 0.27 to 0.2485. A stronger dependence on the baryon-to-photon ratio is obtained through the D-to-^{1}H ratio [8]:

$$y_D = 2.64\,(1 \pm 0.03)\left(\frac{6}{\eta_1}\right)^{1.6}\ ,\quad y_D \equiv 10^5 (D/H)\,. \tag{1.43}$$

Being the primordial abundance of deuterium $y_D = 2.68^{+0.27}_{-0.25}$ and the mass fraction of helium $Y_p = 0.240 \pm 0.006$, one determines the baryon-to-photon ratio [8]:

$$\eta = (5.7 \pm 0.4)\,10^{-10}\,. \tag{1.44}$$

After BBN, the universe was mainly composed of protons, electrons, helium nuclei and photons. At a temperature below $\simeq 13.6$ eV the hydrogen photodissociation stopped and the protons decoupled from the thermal bath as hydrogen formed. At a temperature below 1 eV the electrons decoupled from the photons which could now free stream throughout the universe.

The **CMB** photons come from this epoch, which is called the recombination epoch, appearing to us as a quasi-isotropic distribution of radiation with a mean temperature of $T_{mean} = T_\gamma^{(0)} = 2.725$ K. However, photons and baryons were coupled through competitive processes: the attractiveness of matter and the repulsion of the radiation pressure. This originated acoustic oscillations which were imprinted as anisotropies in the CMB power spectra, and are usually decomposed in spherical harmonics:

$$\frac{\Delta T(\theta,\phi)}{T_{mean}} = \sum_{l=1}^{\infty} \sum_{m=-l}^{l} a_{lm} Y_{lm}(\theta,\phi)\,, \tag{1.45}$$

where $\Delta T \equiv T(\theta,\phi) - T_{mean}$. The first acoustic peak appears around $l \simeq 200$, being sensitive to the density of baryons which can be related to η_B through (1.37). We quote the value from [8]:

$$\eta_B = 6.1^{+0.26}_{-0.27} \times 10^{-10}\,. \tag{1.46}$$

Sakharov's conditions and baryogenesis in the SM

We have just seen how the baryon asymmetry is determined and to complete the picture we need to understand how it is generated.

The freezing out of baryon/anti-baryon annihilations occurred at a temperature $T_{b\bar{b}}$, when the baryon annihilation rate $\langle \sigma v \rangle \sim \frac{1}{m_\pi^2}$ become of the order of the universe expansion rate. Specifically, from (B.15) and (B.9), we find:

$$\frac{2}{m_\pi^2}\left(\frac{m_B T_{b\bar{b}}}{2\pi}\right)^{3/2} \exp\left\{-\frac{m_B}{T_{b\bar{b}}}\right\} = \frac{\pi\sqrt{g_*}}{3\sqrt{10}}\left(\frac{T_{b\bar{b}}^2}{M_P}\right) \Rightarrow T_{b\bar{b}} \simeq 20 \text{ MeV}, \tag{1.47}$$

where $g_* = 79/8$ as in (1.39). Thus, the baryon-to-photon ratio at this temperature was:

$$\frac{n_B}{n_\gamma} \simeq \frac{n_{\bar{B}}}{n_\gamma} \simeq \left(\frac{m_B}{T_{b\bar{b}}}\right)^{3/2} \exp\left\{-\frac{m_B}{T_{b\bar{b}}}\right\} \simeq 1.3 \times 10^{-18} \ll 6 \times 10^{-10}\,, \tag{1.48}$$

which is manifestly below the experimentally determined baryon-to-photon ratio. Solely from cosmology arguments one cannot explain how the asymmetry is generated. Additionally, cosmology by itself does not even reproduce the correct baryon-to-photon ratio.

The first idea is to consider the asymmetry as an initial condition of the big bang. However, besides being an unnatural hypothesis, that asymmetry would hardly survive the homogenization that took place during the inflation period [9], diluting any asymmetry by a factor of $\sim 10^{-30}$.

A. D. Sakharov has shown [10] that to generate a baryon asymmetry from an initial symmetric state three conditions must be fulfilled: (i) baryon number violation; (ii) charge conjugation (C) violation and CP (C + parity) violation; and (iii) an out of equilibrium period.

In the SM, baryogenesis is accommodated in the strong departure from equilibrium occurring at the EWSB phase transition, [11]. The first of the Sakharov's conditions is obvious and, as already noted in section 1.2.1, the baryon number is violated in the SM. The second condition is also satisfied in the SM. This happens in the quark sector by means of the (only) physical phase $\delta \neq 0$ of the CKM mixing matrix.

However, it turns out that the SM is unable to generate the amount of desired asymmetry [12], [13], [14]. This happens for two main reasons (i) the source of CP violation is insufficient and (ii) the Higgs mass should be below ~ 40 GeV.

1.2.4 The hierarchy problem

Concept: In general terms, we say that we face a hierarchy problem when a model formulated at an energy scale M, with a certain number of active d.o.f., is highly **sensitive** to the presence of any d.o.f. at a higher energy scale Λ. Especially, when one has plenty of reasons to think that some new physics must necessarily appear at the scale Λ.

Related to this **sensitiveness** is the concept of fine-tuning, which qualitatively evaluates whether a model, whose parameters are defined at an energy scale M, is unstable under small variations of its parameters defined at another energy scale Λ. We will see that this happens whenever a model contains at least a scalar field that is not protected by a "special type" of symmetry. The reason for this can be simply put as the quadratically divergent self-energy of the scalar fields.

Domain of applicability of the SM

The SM is, by construction, unable to account for gravity. Nevertheless, being gravity a known force of nature, the SM can only remain as a valid theory if one assumes that the quantum gravitational effects decouple from the low energy phenomena that the SM aims to describe. Thus, the SM should remain applicable until the Planck scale, $M_P \equiv \sqrt{\frac{\hbar c}{8\pi G_N}} \approx 2.4 \times 10^{18}$ GeV, at which the quantum gravitational effects become relevant. To the scale at which a theory stops to be applicable we call the cutoff.

It turns out that the Higgs boson mass is highly sensitive to this cutoff scale, which sets the hierarchy problem of the SM. If we require the SM to remain valid at an energy scale much higher than the natural scale at which the SM is constructed (the electroweak scale), we encounter a fine-tuning problem in the Higgs boson mass. To see this, let us compute the 1-loop (!L) corrections to the Higgs boson propagator.

The Higgs propagator receives dominant contributions from quadratically divergent - in the superficial degree of divergence sense - loops with the top-quark, the $W^{\pm}_{\mu}$ and Z_{μ} gauge bosons and the Higgs itself through the λ four-interaction. We will work in the 't-Hooft-Feynman gauge ($\xi = 1$, where ξ is the Lagrangian multiplier of the gauge fixing term. See the appendix D.5). Thus, by simply analysing the superficial degree of divergence, we determine that the relevant vertices are of the type H-fermion-fermion, H^2-(gauge-boson)^2, H^4, H^2-ξ^2, H^2-ϕ^+-ϕ^-, $W^{\pm}_{\mu}$-∂^{μ} (H-$\phi^{\mp}$) and Z_{μ}-∂^{μ} (H-ξ).

The Higgs-(gauge bosons) interactions can be easily inferred from the gauge bosons mass terms with the replacement $v \to \frac{1}{\sqrt{2}}H$ and the Higgs-(top-quark) vertex from the mass term of the quark-t. Specifically, one finds:

$$H^4\text{:}\ \ -\frac{g^2 m_H^2}{32 M_W^2}H^4\,;\ \ H^2\text{-}\xi^2\text{:}\ \ -\frac{g^2 m_H^2}{16 M_W^2}H^2\xi^2\,;\ \ H^2\text{-}\phi^+\text{-}\phi^-\text{:}\ \ -\frac{g^2 m_H^2}{8 M_W^2}H^2\phi^+\phi^-\,; \tag{1.49}$$

$$H^2\text{-}Z^2\text{:}\ \ \frac{g^2}{8c_w^2}H^2 Z_\mu Z^\mu\,;\ \ H^2\text{-}W^+\text{-}W^-\text{:}\ \ \frac{g^2}{4}H^2 W^+_\mu W^{-\mu}\,; \tag{1.50}$$

$$Z_\mu\text{-}\partial^\mu\,(H\text{-}\xi)\text{:}\ \ \frac{g}{2c_w}Z_\mu\left(\xi\partial^\mu H - H\partial^\mu\xi\right)\,;\ \ H\text{-}t\text{-}\bar{t}\text{:}\ \ -\frac{g m_t}{2M_W}H\left(\bar{t}_{(a)}\cdot t_{(a)}\right) + \text{h.c.}\,; \tag{1.51}$$

$$W^{\pm}_\mu\text{-}\partial^\mu\left(H\text{-}\phi^{\mp}\right)\text{:}\ \ \frac{ig}{2}W^+_\mu\left(H\partial^\mu\phi^- - \phi^-\partial^\mu H\right) + \text{h.c.}\,; \tag{1.52}$$

where no symmetry factor has been added and we used $v = \frac{1}{g}\sqrt{2}M_W$ and $\lambda = \frac{g^2 m_H^2}{2M_W^2}$.

The dominant quadratically divergent Feynman diagrams contributing to the Higgs boson self-energy are depicted below, in Fig:1.1.

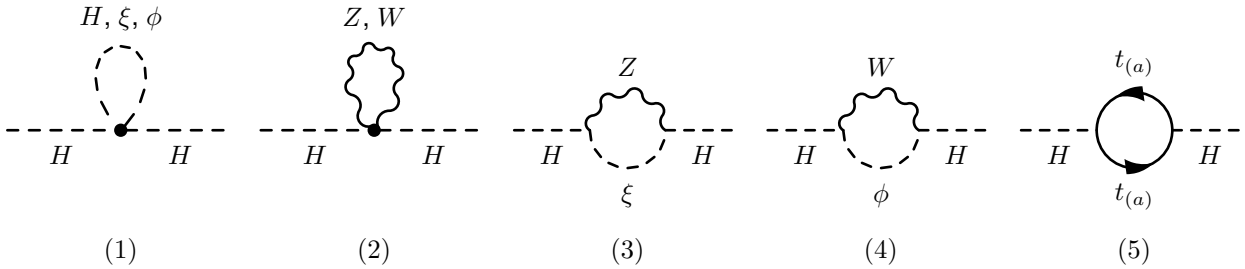

Figure 1.1: Dominant 1L diagrams contributing to the Higgs boson self-energy in the SM. For compactness, we have not displayed the arrows in the ϕ and W propagators

The symmetry factors for each of these diagrams are: for (1) 4×3, 2 and 2 (H, ξ and ϕ loops, respectively); for (2) 2 and 2 (Z and W loops, respectively); for (3) $\frac{2}{2}$; for (4) $\frac{2\times 2}{2}$; and for (5) $\frac{2}{2}$. Moreover,

for the fifth diagram there is the typical (-1) fermion loop sign and an additional factor of 3 due to the 3 QCD-colours of quark-t.

We compute the contribution of each of these diagrams in dimensional regularization ($d = 4 - \epsilon$). For the third, fourth and fifth diagrams we use the Feynman parametrization (C.7)-(C.9) (see appendix C.1) with the change of variables $k \to k + p\,x$ (k is the 1L integration variable, p is the external momentum and x is the Feynman parametrization variable) and integrating to zero the k-odd terms in the numerator. For the 1L integration over k we use the notation (C.10) (see appendix C.2). Putting all together, we find:

$$(1) = \frac{3g^2 m_H^2}{8M_W^2} I_{0,1}(m_H^2) + \frac{g^2 m_H^2}{8M_W^2} I_{0,1}(m_\xi^2 = M_Z^2) + \frac{g^2 m_H^2}{4M_W^2} I_{0,1}(m_\phi^2 = M_W^2)\,; \tag{1.53}$$

$$(2) = \frac{g^2 d}{4c_w^2} I_{0,1}(M_Z^2) + \frac{d}{2} g^2 I_{0,1}(M_W^2)\,; \tag{1.54}$$

$$(3) = -\frac{g^2}{4c_w^2} \int_0^1 dx \left[p^2(x-1)^2 I_{0,2}(\Delta_1) + I_{1,2}(\Delta_1)\right]\,, \quad \text{where } \Delta_1 \equiv p^2 x(x-1) + M_Z^2\,; \tag{1.55}$$

$$(4) = -\frac{g^2}{2} \int_0^1 dx \left[p^2(x-1)^2 I_{0,2}(\Delta_2) + I_{1,2}(\Delta_2)\right]\,, \quad \text{where } \Delta_2 \equiv p^2 x(x-1) + M_W^2\,; \tag{1.56}$$

$$(5) = -\frac{3g^2 m_t^2}{M_W^2} \int_0^1 dx \left\{\left[p^2 x(x-1) + m_t^2\right] I_{0,2}(\Delta_3) + I_{1,2}(\Delta_3)\right\}\,, \quad \text{where } \Delta_3 \equiv p^2 x(x-1) + m_t^2\,. \tag{1.57}$$

As we are interested in analysing our theory as an effective theory with a limiting domain of applicability given by the cutoff, Λ, we convert our results obtained in dimensional regularization to regularization by cutoff, focusing on the dominant contributions, which are of power 2 in the cutoff. To do this we use $d \to 4$, $I_{0,1} \to -i\frac{\Lambda^2}{8\pi^2}$ (derived in [15]) and $I_{1,2}(\Delta_3) = \Delta_3 I_{0,2}(\Delta_3) + I_{0,1}(\Delta_3)$, with which we obtain:

$$m_{H\,(1\mathsf{L})}^2 = m_{H(0)}^2 - \frac{3g^2\Lambda^2}{32\pi^2 M_W^2}\left[m_H^2 + M_Z^2 + 2M_W^2 - 4m_t^2\right]\,, \tag{1.58}$$

where m_H^2 is the 1L renormalized mass squared and $m_{H(0)}^2$ is the bare mass squared.

Taking v from the W boson mass by giving as input the Fermi constant $G_F \simeq 1.17 \times 10^{-5}$ GeV^{-2}, we find $v \simeq 174$ GeV. Additionally, if we require λ to be perturbative, one finds:

$$m_H = v\sqrt{\lambda} \lesssim 174 \text{ GeV}\,, \tag{1.59}$$

being ~ 174 GeV the "natural" tree-level mass for the Higgs boson, which is "naturally" ($\hat{y}_{33}^u \approx 1$) set by the heaviest fermion of the theory, the t-quark.

Stringent Λ-dependent bounds on the Higgs mass can be determined by requiring that the theory is free from infrared and ultraviolet singularities in the Higgs self-interaction coupling, λ. See, for instance, the Figure 6 of [16]. The infrared singularity causes λ to turn negative and the Higgs potential stops to be unbounded from below (vacuum stability), and a lower bound on the Higgs mass can be determined. In turn, the ultraviolet singularity causes λ to explode at $\Lambda = \Lambda_{pole}$ (the Landau pole), at which the theory breaks down, allowing one to put an upper bound on the Higgs mass.

Plugging all the numbers, we arrive at:

$$174^2 \text{ GeV}^2 \simeq m_{H(0)}^2 + 0.044 \times \Lambda^2\,. \tag{1.60}$$

Thus, if we want the SM to be applicable until $\Lambda = M_P$, one has to accurately set $m_{H(0)}$ with a precision

of 15 to 16 decimal places [5] . This is an intolerable fine-tuning. The exact amount of tolerable fine-tuning is a qualitative assessment, but it is rather consensual that 1 decimal place is a reasonable tolerability. Hence, for the SM to be purged from fine-tuning problems, some new physics must appear at the scale $\Lambda \lesssim 3$ TeV.

General remarks

From the previous treatment it is clear that any theory which contains scalar fields will be plagued with fine-tuning problems[6] in the bilinear parameters of the scalars. Moreover, solely by dimensional analysis one would generally expect the self-energy to have terms that are proportional to Λ^2.

The questions one might pose are: (i) what would prevent the scalar self-energy to develop a Λ^2 dependence? (ii) by analogy, does the self-energy of the fermions develop a Λ proportionality factor?

If we compute the self-energy contribution to any of the fermions we see that these are only logarithmically dependent on the cutoff. Indeed, the fermion masses are "naturally" small. To understand why this happens let us recall the naturalness definition given by 't-Hooft [17]:

> "A theory is natural if, for all its parameters p which are small with respect to the fundamental scale Λ, the limit $p \to 0$ corresponds to an enhancement of the symmetry of the system."

Applying this to the fermion masses one sees that they are naturally small because in the limit $m \to 0$ the theory acquires a chiral symmetry. Under a chiral transformation the LH fermions transform with U(1) chiral charge -1 and the RH fermions with charge $+1$. Concretely:

$$f_L \equiv f \to e^{-i\phi} f\,, \quad f_R \equiv i\sigma_2 \bar{f}^{\dagger T} \to e^{i\phi} f_R\,, \tag{1.61}$$

where f_L and f_R are the LH and RH components of the Dirac particle f, respectively, and $\bar{f}$ is the LH component of the Dirac anti-particle. The same obviously applies when f is not a component of a Dirac fermion but rather of a Majorana fermion. Explicitly, one has for both type of mass terms transforming under the chiral transformation:

$$\begin{cases} \text{Dirac mass:} & m\left(\bar{f}\cdot f\right) + \text{h.c.} \to m\, e^{-2i\phi}\left(\bar{f}\cdot f\right) + \text{h.c.}\,; \\ \text{Majorana mass:} & m\left(f\cdot f\right) + \text{h.c.} \to m\, e^{-2i\phi}\left(f\cdot f\right) + \text{h.c.}\,; \end{cases} \tag{1.62}$$

and for the "covariantized" kinetic terms: $i f^\dagger \bar{\sigma}^\mu D_\mu f \to i f^\dagger \bar{\sigma}^\mu D_\mu f$.

We will reconvene the idea of symmetry-protected "naturally" small scalar mass in the context of Supersymmetry, chapter 2.

Some models beyond the SM have been proposed that, intentionally or not, are free from the hierarchy problem. As we have seen the scale of new physics of such models must be of $\Lambda \lesssim 3$ TeV. The most popular models are: (i) Supersymmetry; (ii) Little Higgs; (iii) Technicolor; and (iv) Extra-dimensions. A full chapter, 2, will be dedicated to talk about Supersymmetry (SUSY) and in section 2.3 how SUSY cures the hierarchy problem.

[5] Let $x = y + z^n$ with $|x| < |y|$ and $n > 0$. We define that the amount of fine-tuning in z, measured in decimal places, is given by $ft_z \equiv -\log_{10}\left|\sqrt[n]{\frac{|y|}{|x|}}\left(1 - \sqrt[n]{1-\frac{x}{y}}\right)\right|$. In the limit $|y| \gg |x|$ one has $ft_z \simeq -\log_{10}\left[\frac{1}{n}\left|\frac{x}{y}\right|^{\frac{n-1}{n}}\right]$.

[6] Unless some miraculous cancellation happens between formerly unrelated parameters, such as $4m_t^2 = m_H^2 + M_Z^2 + 2M_W^2$. However, if this is just a fortuitous relation (that is, not symmetry related) it will not hold at higher orders in perturbation theory.

2 Supersymmetry

Supersymmetry (SUSY) is an extension to the ordinary spacetime symmetries obtained by defining N spinorial generators Q whose commutator yields the spacetime translation operator:

$$\left\{Q_a^A, \overline{Q}_{\dot{b}}^B\right\} = \delta_{AB}\sigma^{\mu}_{a\dot{b}}P_{\mu} \text{ with } A, B = 1, ..., N\,. \tag{2.1}$$

Thus, concretely speaking, supersymmetry is a symmetry realised over an extended 8-dimensional space which includes the spacetime, x^{μ}, together with the spinorial space, θ_a and $\overline{\theta}^{\dot{a}}$ (where $a = 1, 2$). In here, θ_a and $\overline{\theta}^{\dot{a}}$ are the two-component Weyl spinors that decompose the 4-component Dirac spinors and are Grassmann variables, as the anti-commuting nature of fermions demands.

We will exclusively talk about the minimal $N = 1$ supersymmetry. However, a brief note about why $N \neq 1$ supersymmetry seems to be disfavoured by nature will be given later.

The algebra of the $N = 1$ supersymmetry reads:

$$\left\{Q_a, \overline{Q}_{\dot{b}}\right\} = \sigma^{\mu}_{a\dot{b}}P_{\mu}\,, \quad \{Q_a, Q_b\} = \left\{\overline{Q}_{\dot{a}}, \overline{Q}_{\dot{b}}\right\} = 0\,, \tag{2.2}$$

and is closed over Q_a, $\overline{Q}_b$ and P_{μ}, since P_{μ} commutes with itself and with the Q's. Moreover, this means that every state of a set of states that transform into one another by the action of the Q's - we call such a set of states a supermultiplet - has the same P^2 eigenvalue and, thus, the same mass.

We take our SUSY algebra generators in the Lorentz group representation of two-component Weyl spinors: Q_a and $\overline{Q}^{\dot{a}}$, which transform under infinitesimal Lorentz transformations as

$$Q \to \left(1 + \frac{i}{2}\vec{\epsilon}\cdot\vec{\sigma} + \frac{1}{2}\vec{\eta}\cdot\vec{\sigma}\right)Q\,, \quad \overline{Q} \to \left(1 + \frac{i}{2}\vec{\epsilon}\cdot\vec{\sigma} - \frac{1}{2}\vec{\eta}\cdot\vec{\sigma}\right)\overline{Q}\,, \tag{2.3}$$

where $\vec{\epsilon}$ and $\vec{\eta}$ are the infinitesimal rotation and boost parameters, respectively. Clearly, $-i(\sigma_2)_{\dot{a}\dot{b}}\overline{Q}^{\dot{b}}$ transforms as $(Q_a)^{\dagger}$, thus we define $\bar{Q}_{\dot{a}} \equiv Q_a^{\dagger} \equiv -i(\sigma_2)_{\dot{a}\dot{b}}\overline{Q}^{\dot{b}}$. In the same manner, $i(\sigma_2)_{ab}Q_b$ transforms as $(\overline{Q}^{\dot{a}})^{\dagger}$, and we define $Q^a \equiv \overline{Q}^{\dot{a}\dagger} \equiv i(\sigma_2)_{ab}Q_b$. This is the dotted-undotted notation, for further considerations see [18] and also the appendix D.1.

The key concept that we will talk about next is that SUSY generators link bosonic and fermionic states,

$$Q|fermion\rangle \propto |boson\rangle\,, \quad Q|boson\rangle \propto |fermion\rangle\,. \tag{2.4}$$

Furthermore, for the Lagrangian density to transform as a total derivative under the transformation of fermions into bosons and vice-versa, certain relations among the parameters with which we write our theory are required. This is a fundamental aspect that will be explored later.

To see how fermions and bosons are related, let us study how the SUSY generators transform under spatial rotations. From (2.3) we have that under spatial rotations, whose generators are the "angular-momentum" operators J_i,

$$-\frac{1}{2}(\sigma_i)_{ab}Q_b = [J_i, Q_a] \Rightarrow [J_3, Q_1] = -\frac{1}{2}Q_1\,, \quad [J_3, Q_2] = \frac{1}{2}Q_2, \tag{2.5}$$

hence,

$$J_3Q_1|j, m\rangle = \left(m - \frac{1}{2}\right)Q_1|j, m\rangle \Rightarrow Q_1|jm\rangle \propto |j, m - \frac{1}{2}\rangle\,. \tag{2.6}$$

Additionally, following an analogous procedure, one finds:

$$Q_2|j,m\rangle \propto |j,m+\frac{1}{2}\rangle\,,\quad \overline{Q}_{\dot{1}}|j,m\rangle \propto |j,m+\frac{1}{2}\rangle\,,\quad \overline{Q}_{\dot{2}}|j,m\rangle \propto |j,m-\frac{1}{2}\rangle\,. \tag{2.7}$$

Notoriously, the SUSY generators connect states that differ by one-half spin projections.

Consider a massive initial state of spin 0, with 4-momentum $p^\mu \equiv (E,0,0,|\vec{p}|)$, and define it as

$$|0,0\rangle \equiv Q_1 Q_2 |j,m\rangle\,, \tag{2.8}$$

which satisfies $Q_1|0,0\rangle = Q_2|0,0\rangle = 0$ from $Q_1Q_2 = -Q_2Q_1$ and $Q_1Q_1 = Q_2Q_2 = 0$. The action of $\overline{Q}_{\dot{1}}$ and $\overline{Q}_{\dot{2}}$ gives another two states:

$$|j_1,\frac{1}{2}\rangle \equiv \overline{Q}_{\dot{1}}|0,0\rangle\,,\quad |j_2,-\frac{1}{2}\rangle \equiv \overline{Q}_{\dot{2}}|0,0\rangle\,, \tag{2.9}$$

respectively. From (2.5) we can deduce:

$$[J_+,Q_2] = [J_-,Q_1] = 0 \quad \text{and applying the } ^\dagger \quad \left[J_-,\overline{Q}_{\dot{2}}\right] = \left[J_+,\overline{Q}_{\dot{1}}\right] = 0\,, \tag{2.10}$$

where $J_\pm = J_1 \pm iJ_2$, are the usual "ladder" operators. Applying them to $|j_1,\frac{1}{2}\rangle$ and $|j_2,-\frac{1}{2}\rangle$, and using the commutation relations just written, we determine the spin j_1 and j_2 of each of these states:

$$J_+|j_1,\frac{1}{2}\rangle = \overline{Q}_{\dot{1}}J_+|0,0\rangle = 0 \Rightarrow j_1 = \frac{1}{2}\,,\quad J_-|j_2,-\frac{1}{2}\rangle = \overline{Q}_{\dot{2}}J_-|0,0\rangle = 0 \Rightarrow j_2 = \frac{1}{2}. \tag{2.11}$$

Moreover, from $\left\{\overline{Q}_{\dot{1}},Q_2\right\} = \left\{\overline{Q}_{\dot{2}},Q_1\right\} = 0$ we have $Q_2|\frac{1}{2},\frac{1}{2}\rangle = Q_1|\frac{1}{2},-\frac{1}{2}\rangle = 0$. Furthermore:

$$Q_1|\frac{1}{2},\frac{1}{2}\rangle = (E-|\vec{p}|)\,|0,0\rangle\,,\quad Q_2|\frac{1}{2},-\frac{1}{2}\rangle = (E+|\vec{p}|)\,|0,0\rangle\,, \tag{2.12}$$

and $\overline{Q}_{\dot{1}}|\frac{1}{2},\frac{1}{2}\rangle = \overline{Q}_{\dot{2}}|\frac{1}{2},-\frac{1}{2}\rangle = 0$. We are then left with determining the action of $\overline{Q}_{\dot{1}}$ and $\overline{Q}_{\dot{2}}$ over $|\frac{1}{2},-\frac{1}{2}\rangle$ and $|\frac{1}{2},\frac{1}{2}\rangle$, respectively. We find one last state:

$$|j_3,0\rangle' \equiv \overline{Q}_{\dot{2}}|\frac{1}{2},\frac{1}{2}\rangle \Rightarrow J_-|j_3,0\rangle = \overline{Q}_{\dot{2}}|\frac{1}{2},-\frac{1}{2}\rangle = 0 \Rightarrow j_3 = 0\,, \tag{2.13}$$

which has the same quantum numbers of the initial state. To prove that $|0,0\rangle'$ is a new state, just note: $Q_2|0,0\rangle = 0 \neq Q_2|0,0\rangle' = (E+|\vec{p}|)\,|\frac{1}{2},\frac{1}{2}\rangle$.

Indeed, by successive operations of Q's in each of these states, one concludes that there are just 4 different states connected by the Q's. Summarizing them:

$$|\frac{1}{2},\frac{1}{2}\rangle\,,\quad |\frac{1}{2},-\frac{1}{2}\rangle\,,\quad |0,0\rangle\,,\quad |0,0\rangle'\,, \tag{2.14}$$

and we call to this representation a massive chiral supermultiplet.

Now, if we take the limit $m \to 0 \Rightarrow p^\mu = (E,0,0,E)$, we obtain two interesting relations from (2.2):

$$\left\{Q_1,\overline{Q}_{\dot{1}}\right\} = E - E = 0 \Rightarrow \overline{Q}_{\dot{1}}|0,0\rangle = 0\,, \tag{2.15}$$

$$\left\{Q_2,\overline{Q}_{\dot{2}}\right\} = 2E\,, \tag{2.16}$$

where we have used $Q_1|0,0\rangle = 0$. Besides that, recall also $Q_2|0,0\rangle = 0$. Thus, all that is left to analyse is $|j_4,-\frac{1}{2}\rangle \equiv \overline{Q}_{\dot{2}}|0,0\rangle$:

$$J_-|j_4,-\frac{1}{2}\rangle = \overline{Q}_{\dot{2}}J_-|0,0\rangle = 0 \Rightarrow j_4 = \frac{1}{2}\,. \tag{2.17}$$

Additionally, $\overline{Q}_{\dot{2}}|\frac{1}{2},-\frac{1}{2}\rangle = 0$ and $Q_2|\frac{1}{2},-\frac{1}{2}\rangle = 2E|0,0\rangle$ (using (2.16)). Hence, we see that in the limit of massless states the chiral supermultiplet is composed of just two states, 1 Weyl fermion + 1 real scalar boson, that is, half of d.o.f. of the massive case. Clearly, the two pairs of fermion/boson states of the massive chiral supermultiplet decouple from one another as the mass goes to zero, and we get two massless chiral supermultiplets.

More generally, we can use (2.15) and (2.16) to prove that starting from a state $|j,\pm j\rangle$ (with $j>0$) of a massless supermultiplet, there is only another state in that supermultiplet, $|j-\frac{1}{2},\pm j\mp\frac{1}{2}\rangle$. For e.g., there is a supermultiplet that groups together a massless spin-1 vector boson with a particular spin projection j and a spin-1/2 Weyl fermion with spin projection $j/2$. Recall that to guarantee TCP invariance we have to include in the model the TCP-conjugate fields, that is, the supermultiplet of the TCP-conjugate fields. Returning to the e.g. and demanding TCP invariance, we end up with two massless vector supermultiplets that combined give 2 d.o.f. of a massless spin-1 vector boson (with $\pm j$ spin projections) and 2 d.o.f. of a Majorana fermion (with $\pm j/2$ spin projections).

As SUSY transformations send a bosonic d.o.f. into a fermionic d.o.f., this matching implies that there is always the same number of fermionic d.o.f. and bosonic d.o.f. in any supermultiplet. Concretely, the action of a generator Q over a state $|k\rangle$ changes the fermion number N_F by one unit, then $(-1)^{N_F}Q = -Q(-1)^{N_F}$. From here we can deduce via the cyclic property of the trace together with (2.2), that $\sum_k \langle k|(-1)^{N_F}|k\rangle = 0$. Hence, as $(-1)^{N_F}|boson\rangle = |boson\rangle$ and $(-1)^{N_F}|fermion\rangle = -|fermion\rangle$ we conclude that the number of fermion states and of boson states in the supermultiplet must be equal.

Now we quote a general result for massive supermultiplets [19]. If we begin from an initial state of spin $(2j+1)$, with $j>0$, we can generate a spin-$(j+\frac{1}{2})$ supermultiplet, a spin-$(j-\frac{1}{2})$ supermultiplet and spin-j supermultiplet. The number of bosons and fermions will then be $n_B = n_F = 2(2j+1)$.

Before ending this brief introduction let us comment on $N \neq 1$ supersymmetry. In $N=2$ SUSY a massless chiral supermultiplet contains 4 states with spins $+\frac{1}{2}$, $-\frac{1}{2}$, 0 and 0, see [19]. If we try to extend the SM we face serious problems because LH and RH fermions transform differently under SU(2)$_L$. Indeed, all the states belonging to the same supermultiplet must have the same quantum numbers because the SUSY generators commute with all gauge group generators. Thus, if we require gauge invariance we break explicitly SUSY invariance and if we require SUSY we break explicitly the SU(2)$_L$ gauge symmetry. Clearly, $N>1$ supersymmetry is disfavoured by the SM.

2.1 Phenomenological Approach

If nature has a supersymmetric character it must be broken. Indeed, if SUSY was an exact symmetry the known particles of the SM would have supermultiplet partners with the same mass. No mass degenerated states have been observed in the energy range of the SM. Moreover, there would be the same number of bosons as there are of fermions: in the SM there is only one doublet of bosons.

We are interested in supermultiplet representations that contain spin-1/2 states (the SM fermions), spin-0 states (the Higgs) and spin-1 states (the gauge bosons).

We have seen above that the minimal choice for spin-1/2 and spin-0 states is a chiral supermultiplet. For instance, take the LH component of the Dirac fermion f of the SM, we consider it as a state of the massive chiral supermultiplet with the identification:

$$\left\{\begin{array}{l} |\frac{1}{2},-\frac{1}{2}\rangle \to (\chi_f)_a\,, \\ |\frac{1}{2},\frac{1}{2}\rangle \to (\overline{\chi}_f)^{\dot{a}} \end{array}\right. , \quad \left\{\begin{array}{l} |0,0\rangle \to \phi_f \\ |0,0\rangle' \to \phi_f^\dagger\,, \end{array}\right. , \tag{2.18}$$

where $(\overline{f}_f)_{\dot{a}} \equiv (\chi_f)^\dagger_a$ and $\phi_f^\dagger = (\phi_f)^\dagger$. Clearly, this massive chiral supermultiplet is formed by 1 Majorana-like fermion (the LH Dirac fermion and its hermitian conjugate) and 1 complex boson. The choice made for the massive chiral supermultiplet is equivalent to choose two massless chiral supermultiplets that are TCP-conjugates of one another. Applying the same construction for the LH component of the Dirac anti-fermion $\bar{f}$, one has:

$$\left\{\begin{array}{l} |\frac{1}{2},-\frac{1}{2}\rangle \to (\chi_{\bar{f}})_a\,, \\ |\frac{1}{2},\frac{1}{2}\rangle \to (\overline{\chi}_{\bar{f}})^{\dot{a}} \end{array}\right. , \quad \left\{\begin{array}{l} |0,0\rangle \to \phi_{\bar{f}} \\ |0,0\rangle' \to \phi_{\bar{f}}^\dagger\,, \end{array}\right. . \tag{2.19}$$

Thus, for every Dirac fermion we have 2 massive chiral supermultiplets, one for each chirality of the Dirac fermion. On the other hand, to extend a SM neutrino to SUSY we need just two, TCP-conjugates of each other, massless chiral supermultiplets, since there is no RH neutrino. Analogously, each complex scalar boson of the SM will fit into a massive chiral supermultiplet. For instance, the SM Higgs doublet (a doublet of complex scalars) are partnered with a doublet of Majorana fermions.

A massless spin-1 gauge boson is partnered together with a Majorana fermion in two massless vector supermultiplets (TCP-conjugates of one another):

$$|1,\pm 1\rangle \to W_\mu\,, \quad |1,-\frac{1}{2}\rangle = (\chi_W)_a\,, \quad |\frac{1}{2},\frac{1}{2}\rangle \to (\overline{\chi}_W)^{\dot{a}}\,. \tag{2.20}$$

Labelling conventions: Each particle of a supermultiplet state that is not contained in the SM is called a sparticle. Consider that a SM fermion X is a state of a supermultiplet with a sparticle Y, we label the name of the sparticle as $Y = sX$, that is, by appending a prefix "s". On the other hand, the partner Y of an SM boson X is called a $Y = Xino$, that is, we append the suffix "ino". Moreover, as we work with Dirac fermions decomposed in LH and RH chiralities, the spartner of a LH (RH) fermion X is also called a LH (RH) sX.

2.2 Superfields: pragmatic notes

To work with a supersymmetric QFT it is more convenient to use the superfield formalism. Indeed, the superfield formalism provides a direct and automatic way to write supersymmetric interactions by means of the product of superfields. Using a set of "rules", we can then expand these products in terms of ordinary fields and a contact to ordinary QFT can easily be made. As we have noted above, SUSY requires a relation among the interaction parameters that would, in the absence of SUSY, be independent (unrelated). This is automatically encoded in the superfield language of writing interactions.

No derivation will be given here. For a pedagogical introduction to superfields see [18], [20] and for a more technical comprehensive discussion see [19].

A superfield is in essence a representation of the SUSY algebra in the "coordinate" 8-dimensional superspace. For instance, a chiral supermultiplet is realised in the superspace as a chiral superfield.

We begin by writing the massless chiral superfield by expanding it in Taylor series of the superspace variables $x^\mu, \theta_a, \overline{\theta}^{\dot{a}}$:

$$\widehat{\Phi}(x,\theta,\overline{\theta}) = \phi(x) + \theta\cdot\chi(x) + \frac{1}{2}\,(\theta\cdot\theta)\,F(x)\,. \tag{2.21}$$

where no dependence over $\overline{\theta}$ exists. Indeed, as θ_a are Grassmann variables ($\theta_1\theta_1 = \theta_2\theta_2 = 0$) the Taylor series in the "fermionic" space stops at $\theta\cdot\theta$. Furthermore, ϕ, χ and F can be seen as components in the $\theta^0, \theta^1, \theta^2$ fermionic space. Moreover, $\phi(x)$, $\chi(x)$ and $F(x)$ contain in themselves the sum of the spacetime Taylor series.

The TCP-conjugate of that superfield, also called the conjugate chiral superfield, reads:

$$\widehat{\Phi}^\dagger(x,\theta,\overline{\theta}) = \phi^\dagger(x) + \overline{\theta}\cdot\overline{\chi}(x) + \frac{1}{2}\left(\overline{\theta}\cdot\overline{\theta}\right)F^\dagger(x)\,, \tag{2.22}$$

which in turn does not depend on θ.

Both the chiral superfield and its conjugate possess 1 scalar boson, 1 Weyl fermion and 1 extra field F of mass dimension $[M]^2$. One can show that the F fields do not propagate, having as kinetic terms: $F^\dagger F$.

It turns out that these F fields are mandatory to have off-shell SUSY. Indeed, when we are off-shell, the Weyl fermion χ has 2 d.o.f., and there is only 1 scalar d.o.f. from the ϕ. Hence, to restore the balance between fermionic and bosonic d.o.f., another d.o.f. must be supplied: the auxiliary field F.

By definition, a product of superfields must also be a superfield. Moreover, one could show that under SUSY transformations of parameter ξ_a the chiral superfield is changed by an amount:

$$\delta_\xi\widehat{\Phi} = \delta_\xi\phi + \theta^a\delta_\xi\chi_a + \frac{1}{2}\,(\theta\cdot\theta)\,\delta_\xi F\,, \tag{2.23}$$

where[1]

$$\delta_\xi\phi = \xi\cdot\chi\,,\quad \delta_\xi\chi_a = -i(\sigma^\mu\overline{\xi})_a\partial_\mu\phi\,,\quad \delta_\xi F = -i\overline{\chi}\bar{\sigma}^\mu\partial_\mu\chi\,. \tag{2.24}$$

The hermitian conjugate of these transformation rules apply as the transformations rules for the conjugate chiral superfield.

Notoriously, from (2.24) we clearly see that the F component of a chiral superfield transforms as a total derivative under SUSY transformations. This is exactly what is required to have a theory whose action is SUSY invariant, that is, whose Lagrangian density transforms as a total derivative under SUSY.

Thus, if a product of chiral superfields is a chiral superfield, the F component of a product of chiral superfields is a SUSY invariant term of the Lagrangian density. Note that being θ Grassmann variables, integrating a product of superfields over $d^2\theta \equiv -\frac{1}{2}d\theta\cdot d\theta = d\theta_1 d\theta_2$ yields the F component. Hence, we write bilinear and trilinear supersymmetric interactions among chiral superfields as:

$$\mathcal{L}_{bilinear} = \int d^2\theta\, M_{ij}\widehat{\Phi}_i\widehat{\Phi}_j + \int d^2\overline{\theta}\, M^*_{ij}\widehat{\Phi}^\dagger_i\widehat{\Phi}^\dagger_j \equiv \int d^2\theta\, M_{ij}\widehat{\Phi}_i\widehat{\Phi}_j + \text{h.c.}\,, \tag{2.25}$$

$$\mathcal{L}_{trilinear} = \int d^2\theta\, y_{ijk}\widehat{\Phi}_i\widehat{\Phi}_j\widehat{\Phi}_k + \int d^2\overline{\theta}\, y^*_{ijk}\widehat{\Phi}^\dagger_i\widehat{\Phi}^\dagger_j\widehat{\Phi}^\dagger_k \equiv \int d^2\theta\, y_{ijk}\widehat{\Phi}_i\widehat{\Phi}_j\widehat{\Phi}_k + \text{h.c.}\,, \tag{2.26}$$

[1] The index position of $\overline{\xi}$, $\overline{\chi}$ and χ is implied by $\sigma^\mu \equiv (\sigma^\mu)_{a\dot{b}}$ and $\bar{\sigma}^\mu \equiv (\bar{\sigma}^\mu)^{\dot{a}b}$.

where M_{ij} and y_{ijk} are the bilinear and trilinear couplings and h.c. denotes the hermitian conjugate of the preceding term. This is mandatory for TCP invariance.

Finally, all that is left to do is to determine the F component of a product of chiral superfields. We quote the results:

$$\int d^2\theta\, \widehat{\Phi}_i \widehat{\Phi}_j = -\left(\chi_i \cdot \chi_j\right) + F_i \phi_j + \phi_i F_j \,, \tag{2.27}$$

$$\int d^2\theta\, \widehat{\Phi}_i \widehat{\Phi}_j \widehat{\Phi}_k = -\left(\chi_i \cdot \chi_j\right) \phi_k - \left(\chi_j \cdot \chi_k\right) \phi_i - \left(\chi_k \cdot \chi_i\right) \phi_j + \phi_i \phi_j F_k + \phi_j \phi_k F_i + \phi_k \phi_i F_j \,. \tag{2.28}$$

We have not yet addressed the vector superfield which is an important element if we want to construct a supersymmetric SM, that is, a supersymmetric gauge theory. However, we will not go formal on this.

In here, we just state that we can transform a gauge theory into a supersymmetric gauge theory at the expense of considering additional interactions. These additional interactions are of two types: (i) trilinear - between the spartners of the gauge bosons (gauginos), the fermions and their scalar partners; and (ii) trilinear - between the auxiliary fields (D) of the vector superfield and the scalar bosons.

For example, assume that $\widehat{\Phi}$ transforms in the representation R of SU(2)$_L$, with components $\widehat{\Phi}^a$ in the vector space of the representation R of SU(2)$_L$. The SU(2)$_L$ vector superfield contains the SU(2)$_L$ gauge bosons W_μ^α, the gauginos λ^α and the auxiliary fields[2] D^α, where $\alpha = 1, 2, 3$. We define the SU(2)$_L$ gauge coupling as g. Hence, besides the usual (non-supersymmetric) gauge interactions, the additional interactions we have to consider are:

$$\mathcal{L}_{gauginos} = -\sqrt{2} g \left[\phi^{a\dagger} T^\alpha_{ab} \left(\chi^b \cdot \lambda^\alpha\right) + \text{h.c.}\right] - g D^\alpha \left(\phi^{a\dagger} T^\alpha_{ab} \phi^b\right) \,, \tag{2.29}$$

with a covariant derivative defined as $D_\mu = \partial_\mu + i g T^\alpha W_\mu^\alpha$.

To end this section we note that, as F and D have no derivative terms and their kinetic term is just a bilinear, it is customary to remove the F and D auxiliary fields from the theory by using their equations of motion. Specifically:

$$F_i^\dagger = -\frac{\partial \mathcal{L}}{\partial F_i} \,, \quad F_i = -\frac{\partial \mathcal{L}}{\partial F_i^\dagger} \,, \quad D^\alpha = -\frac{\partial \mathcal{L}}{\partial D^\alpha} \,, \tag{2.30}$$

and the interactions that were mediated by the auxiliary fields are now given by:

$$\mathcal{L}_F^{int} = -\sum_i \left|\frac{\partial \mathcal{L}}{\partial F_i}\right|^2 \,, \quad \mathcal{L}_D^{int} = -\frac{1}{2} \sum_\alpha \left(\frac{\partial \mathcal{L}}{\partial D^\alpha}\right)^2 \,. \tag{2.31}$$

2.3 The cure of the hierarchy problem

We have seen in section 1.2.4 that the hierarchy problem can be formulated as the problem of the quadratically divergent contributions to the self-energy of a scalar field. We have also discussed how the self-energy of fermions are protected against such radiative contributions.

In this section we will show that the self-energy of a scalar field that belongs to a supermultiplet receives no quadratically divergent contribution to its self-energy. Moreover, we will clearly see that this is a property that is insured by two “coincidences”:

[2] D^α are real fields, have mass dimension $[M]^2$ and kinetic term $\frac{1}{2} D^\alpha D^\alpha$.

1. for every loop contribution from a boson X there is a cancelling contribution (relative minus sign) from loops with a fermion Y, where X and Y belong to the same supermultiplet.
2. the interaction coupling of the contribution given by the boson X is related to the interaction coupling of the contribution given by the fermion Y, where X and Y belong to the same supermultiplet.

Indeed, even in the expression that we obtained for the 1L self-energy of the SM Higgs (1.58), we have noted that the quark-t loop contributes to reduce the W, Z and H contributions. They would magically cancel one another if a symmetry relating the masses and the interaction couplings would be at work. This is exactly what happens in SUSY.

Consider a model composed by 1 complex scalar and 1 Majorana fermion. The most general Lagrangian we can write which is renormalizable and holomorphic reads,

$$\mathcal{L}_m^{(\text{toy})} = -\frac{1}{2}\left[m_\chi\,(\chi\cdot\chi) + \text{h.c.}\right] - m_\phi^2\phi^\dagger\phi \quad \text{and} \quad \mathcal{L}_{int}^{(\text{toy})} = -\left[y\,(\chi\cdot\chi)\,\phi + \text{h.c.}\right] - \frac{\lambda}{4}\left(\phi^\dagger\phi\right)^2 , \tag{2.32}$$

for the mass and interaction sectors, respectively.

The complex scalar field ϕ self-energy receives 1L contributions from the Feynman diagrams in Fig:2.1.

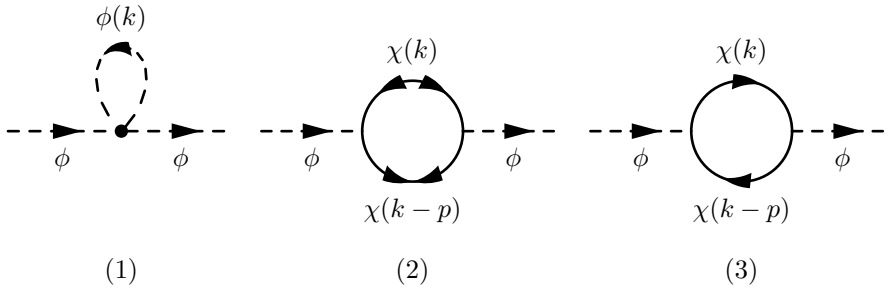

Figure 2.1: Dominant 1L diagrams contributing to the complex scalar self-energy in the toy model.

We have considered the Majorana nature of the fermion (see the appendix D.5 for the 3 types of Majorana propagators, expressions (D.48)). Calculating in dimensional regularization ($d = 4-\epsilon$) the sum of the three diagrams, we find:

$$\text{Div}\left[-4|y|^2\int_0^1 dx\,\left\{p^2x(x-1)I_{0,2}(\Delta) + I_{1,2}(\Delta)\right\} + \lambda I_{0,1}(m_\phi^2)\right] = \frac{i}{8\pi^2\epsilon}\left\{-8|y|^2\left(-\frac{1}{4}p^2 + m_\chi^2\right) + \lambda m_\phi^2\right\}, \tag{2.33}$$

where we have defined the generalized 1L mass-squared $\Delta \equiv p^2x(x-1) + m_\chi^2$, and the $I_{m,n}$ are the 1L integrals over d^4k defined in the appendix C.2. In cutoff regularization one has[3] $\frac{i\Lambda^2}{8\pi^2}\left\{4|y|^2 - \lambda\right\}$, and hence:

$$m^2_{\phi\,(1\text{L})} = m^2_{\phi\,(0)} + \frac{\Lambda^2}{8\pi^2}\left\{4|y|^2 - \lambda\right\} . \tag{2.34}$$

Thus, to purge the quadratic divergence we postulate the following relation between the couplings:

$$\frac{1}{4}\lambda = |y|^2. \tag{2.35}$$

[3]See the relevant correspondence between dimensional regularization and regularization by cutoff in the discussion preceding equations (1.53)-(1.57).

Clearly, to remove the quadratic divergences all that is needed is a relation between the dimensionless interaction couplings. This is obvious by dimensional analysis. Thus, there is no *a priori* need to take any particular relation between m_ϕ and m_χ.

Let us now see that taking ϕ and χ as states of a chiral supermultiplet, we do indeed satisfy (2.35) automatically. We begin by writing the bilinear and trilinear supersymmetric interactions using the superfield formalism:

$$\mathcal{L}^{(\text{stoy})}_{m+int} = \int d^2\theta \left[\frac{m}{2}\widehat{\Phi}^2 + \frac{y}{3}\widehat{\Phi}^3\right] + \text{h.c.}\,, \tag{2.36}$$

from which we determine,

$$\mathcal{L}^{(\text{stoy})}_{m+int} = -\left|m\,\phi + y\phi^2\right|^2 - \left[y\,(\chi\cdot\chi)\,\phi + \frac{m}{2}\,(\chi\cdot\chi) + \text{h.c.}\right]\,, \tag{2.37}$$

having replaced F by its equation of motion.

In due time, we will see that, in spite of a SUSY model (even a softly broken one) protects the scalars of getting quadratically divergent contributions, solving the tough fine-tuning problem, another refined (smooth) type of fine-tuning can take place in softly broken SUSY when there is a sizable mass difference between two states of the same supermultiplet.

2.4 Supersymmetry breaking

We have already noted that if SUSY is manifest in nature, it is in a broken manner. In here we will briefly report on the archetypes of spontaneous SUSY breaking.

Of the superfields we have considered (chiral and vector) the only components that can acquire a non-vanishing VEV which breaks SUSY are the auxiliary fields. Indeed, we already knew by requiring Lorentz invariance that the field must be a scalar but why not the component ϕ of the chiral superfield? The reason is as follows. Looking at (2.24) we see that ϕ appears on the right hand side of SUSY transformations together with a derivative, thus, the VEV of ϕ has no impact on breaking SUSY.

Hence, the two archetypes to spontaneously break SUSY are [21]:

1. F-type SUSY breaking (e.g. [22]);
2. D-type SUSY breaking (e.g. [23]).

However, how this mechanism of SUSY breaking happens (if SUSY ever happens) is still hard to perceive. Thus, it is customary to follow a more pragmatic approach and parametrize our ignorance by introducing by hand a set of terms that explicitly break SUSY in a "softly manner". To break SUSY and simultaneously preserve its distinct characteristic (otherwise we would lose the motivation for SUSY in the first place), namely, the cancellation of the quadratic divergences, SUSY must be "softly broken".

There are three popular frameworks of SUSY breaking [20, 21]: (i) Planck Mediated: Supergravity; (ii) Gauge Mediated; and (iii) Anomaly Mediated. These are characterized by the hidden sector that operates the breaking, the energy scale at which it occurs and how that is communicated to the visible sector via the soft breaking parameters.

3 Neutrino physics

The idea of a very light neutral particle (a "neutrino") was first proposed by Pauli (1930) as a way to rescue conservation of 4-momentum and angular momentum in the nuclear β-decay. Its weakly interacting nature explained why it escaped the detector carrying the 4-momentum difference that restored its conservation. The very small mass was crucial to account for the observed end-point in the energy spectrum. At the time, a vanishing mass was consistent with all data.

Experiments involving the flux of solar neutrinos (since 1968 [24]) as well as atmospheric neutrinos (since 1992 [25]) have pointed towards the now established knowledge that neutrinos do possess mass. Nevertheless, as neutrino masses are at least ~ 6 orders of magnitude lower than any other fermion and ~ 12 orders of magnitude lower than the scale of the EWSB, for the SM physics probed at colliders neutrinos can be taken, at an excellent approximation, as massless states.

These experiments undergo under the label of what we now call "oscillations experiments", a label which we easily understand today but it was not so in the past. We will see in section 3.1 how oscillation experiments are interpreted and how they imply massive neutrinos. We anticipate that this type of experiments are not able to determine the absolute mass scale of neutrinos, a determination which requires another type of experiment that we will see on 3.2. In section 3.3 we will show how some light can be shed into the Majorana vs Dirac nature of the neutrinos (a subject that we have talked about earlier). In section 3.4.1 we will discuss how a neutrino mass term can be accommodated in the SM and a general framework for neutrino mass generation: the seesaw mechanism.

3.1 Neutrino oscillations: from experiment to flavour mixing

Neutrino oscillation experiments are based on the measurement of neutrino fluxes coming from distant sources. Historically, the first studied source was the Sun. Electron-neutrinos are produced at the Sun's core by the fusion reaction,

$$4p \rightarrow {}^4\mathrm{He}^{2+} + 2\bar{e} + 2\nu_e + 28\ \mathrm{MeV}\,. \tag{3.1}$$

Due to their weakly interacting nature, electron-neutrinos produced in this way will escape from the core of the Sun and some of them will be measured on Earth.

The flux measured is known to be $1/3$ below the predicted by the solar model. One hypothesis was to consider that the solar model had problems. The SNO experiment [26] measured all the neutrino flavours and concluded that their sum accounted for the number of electron-neutrinos produced at the Sun's core. This confirmed that the solar model was correct and that the deficit was due to electron-neutrinos disappearance and $\nu_{\mu,\tau}$ appearance.

Another studied source for neutrino production was the high atmosphere. In the high atmosphere, cosmic rays interacting with nuclei produce pions which in turn decay into a (charged lepton)-neutrino pair: $\pi^- \rightarrow \mu + \nu_\mu$, thus producing a high energy muon. Subsequently, this muon decays ($\approx 100\%$) via $\mu \rightarrow e + \bar{\nu}_e + \nu_\mu$. Thus, the ratio of muon-neutrinos to electron-neutrinos that we expect to measure is roughly 2. The Kamiokande experience [25] measured this ratio and compared to the expected,

reporting

$$R \equiv \frac{N^{obs}_{\nu_\mu}}{N^{th}_{\nu_\mu}} \frac{N^{th}_{\nu_e}}{N^{obs}_{\nu_e}} = 0.60^{+0.07}_{-0.06}(\text{stat.}) \pm 0.05(\text{syst.}). \tag{3.2}$$

At the time it was not known if the deviation from the expected value of $R = 1$ was due to ν_e appearance or ν_μ disappearance, or even a little of both. Later on, Super-Kamiokande confirmed that the deficit is due to ν_μ disappearance.

Flavour mixing

To understand what caused the deficits in the neutrino fluxes several hypothesis were given, such as neutrino oscillations, neutrino decays and decoherence in the ν propagation. Currently, the no-oscillation hypothesis are clearly disfavoured and there are well established evidences for neutrino oscillations.

A neutrino oscillates in the following sense. A neutrino is produced by a certain source via weak interaction processes and, as such, it is a state of the gauge interaction basis, where neutrino-(charged lepton)-W is diagonal. The charged lepton is, by definition, a mass eigenstate in this basis. This is the basis where the flavour labelling is made. Indeed, we say that a neutrino is, for instance, an electron-neutrino because somewhere an electron was involved in the production of the neutrino. Having stated this, we can now understand that if the neutrino interacts in a basis that differs from the neutrino mass eigenstate basis, it will be changing flavour while propagating from one interaction point (the source) to the other interaction point (the detector).

Let us make a formal explanation. A neutrino X propagates in the mass eigenstate basis labeled by $X = 1, 2, 3$, which is related to the flavour basis through the unitary transformation:

$$|\nu_i\rangle = \sum_X (U_{PMNS})_{iX} |\nu_X\rangle \,. \tag{3.3}$$

This matrix is called the Pontecorvo-Maki-Nakagawa-Sakata matrix, and it is commonly parametrized as the Chau-Keung proposed parametrization for the CKM matrix with an additional "phase matrix" ($V_{Maj.}$):

$$U_{PMNS} = \begin{pmatrix} c_{12}c_{13} & s_{12}c_{13} & s_{13}e^{-i\delta} \\ -s_{12}c_{23} - c_{12}s_{23}s_{13}e^{i\delta} & c_{12}c_{23} - s_{12}s_{23}s_{13}e^{i\delta} & s_{23}c_{13} \\ s_{12}s_{23} - c_{12}c_{23}s_{13}e^{i\delta} & -c_{12}s_{23} - s_{12}c_{23}s_{13}e^{i\delta} & c_{23}c_{13} \end{pmatrix} \cdot V_{Maj.}\,, \tag{3.4}$$

$$V_{Maj.} = diagonal\left(-i\frac{\phi_1}{2}, -i\frac{\phi_2}{2}, 1\right)\,, \tag{3.5}$$

characterized by 3 real angles of rotation and 3 physical phases. We have defined for shortness $c_{ij} \equiv \cos\theta_{ij}$ and $s_{ij} \equiv \sin\theta_{ij}$. The remaining 3 phases that an unitary matrix possesses were absorbed by a redefinition of the fields. δ is a CP violating Dirac phase and ϕ_i, ϕ_2 are Majorana phases that are physical only if the neutrinos are Majorana-type particles, otherwise can also be rotated away as it happens for the CKM matrix. Note: when writing long equations we use U instead of U_{PMNS}.

A neutrino of flavour i produced at time $t = x = 0$ with state $|\nu_i(0)\rangle$, propagates a distance L in a time t_L and is now described by $|\nu_i(L)\rangle$:

$$\begin{aligned} |\nu_i(L)\rangle &= \sum_X U_{iX} |\nu_X(L)\rangle = \sum_X U_{iX} \exp\{-iE_X t_L + ip_X L\} |\nu_X(0)\rangle \\ &= \sum_j \sum_X U_{iX} \exp\{-iE_X t_L + ip_X L\} U^*_{jX} |\nu_j(0)\rangle \simeq \sum_j \sum_X U_{iX} \exp\left\{-i\frac{m^2_X L}{2E}\right\} U^*_{jX} |\nu_j(0)\rangle\,, \end{aligned} \tag{3.6}$$

where we have used (3.3) to rotate from the flavour basis to the mass basis, where the energy and the 3-momentum is defined, then rotate from the mass basis at $t = x = 0$ to the flavour basis. Now we can relate the final flavour state with the initial. In these steps we have used the approximations $t_L \simeq L$ and $E_X - p_X \simeq \frac{m_X^2}{2E_X} \simeq \frac{m_X^2}{2E}$, because the neutrino is ultrarelativistic and we have taken the energy of each of the mass eigenstates as being approximately described by a mean energy E. Hence, the probability that we will detect a neutrino of flavour j after a travelling distance of L is given by:

$$\begin{aligned} P(\nu_i \to \nu_j) &= |\langle \nu_j | \nu_i(L) \rangle|^2 \\ &= \delta_{ij} - 4 \sum_{X>X'} \mathsf{Re}\left[U_{iX} U_{iX'}^* U_{jX}^* U_{jX'}\right] \sin^2\left(\frac{\Delta m_{XX'}^2 L}{4E}\right) \\ &\quad +2 \sum_{X>X'} \mathsf{Im}\left[U_{iX} U_{iX'}^* U_{jX}^* U_{jX'}\right] \sin\left(\frac{\Delta m_{XX'}^2 L}{2E}\right), \end{aligned} \tag{3.7}$$

where $\Delta m_{XX'}^2 \equiv m_X^2 - m_{X'}^2$.

The U_{PMNS} mixing parameters are determined from the measurement of neutrino fluxes coming from different sources and at different distances.

The muon-neutrino disappearance, in the atmospheric neutrinos experiments, is explained by $\nu_\mu \leftrightarrow \nu_\tau$ transitions which constrain θ_{23} and $\Delta m_{atm}^2 \equiv |\Delta m_{32}^2|$, that are commonly called the atmospheric mixing angle and the atmospheric mass splitting, respectively. The solar neutrinos phenomena is explained by $\nu_e \leftrightarrow \nu_\mu$ oscillations which constrain the so called solar mixing angle, θ_{12}, and the solar mass splitting $\Delta m_{sol}^2 \equiv \Delta m_{21}^2$. Finally, the remaining parameters θ_{13} and Δm_{31}^2 are involved in the solar and atmospheric phenomena but are directly constrained by the CHOOZ reactor experiment [27]. For this reason, θ_{13} is also called the Chooz mixing angle (or the reactor angle). Note that if there are just 3 neutrino mass eigenstates, as it has been assumed, then Δm_{31}^2 is fixed by $\Delta m_{31}^2 = \Delta m_{32}^2 + \Delta m_{21}^2$.

At the present time the measured U_{PMNS} angles [1]

$$\sin^2(2\theta_{12}) = 0.87 \pm 0.03\,, \quad \sin^2(2\theta_{23}) > 0.92\,, \quad \sin^2(\theta_{13}) < 0.05\,, \tag{3.8}$$

are consistent with tri-bimaximal mixing (TBM):

$$s_{12}^2 = \frac{1}{3}\,, \quad s_{23}^2 = \frac{1}{2}\,, \quad s_{13}^2 = 0. \tag{3.9}$$

The measured mass splittings are [1]:

$$\Delta m_{sol}^2 = \Delta m_{21}^2 \equiv m_2^2 - m_1^2 = (8.0 \pm 0.3) \times 10^{-5}\ \mathsf{eV}^2\,, \tag{3.10}$$

$$\Delta m_{atm}^2 = |\Delta m_{32}^2| \equiv |m_3^2 - m_2^2| = (1.9 - 3.0) \times 10^{-3}\ \mathsf{eV}^2\,. \tag{3.11}$$

Moreover, neutrino data is consistent with two types of mass spectrum, which are classified according to the mass scale of the solar pair (ν_e-ν_μ): normal hierarchy (NH), where the masses of the solar pair are at the bottom; and inverted hierarchy (IH), where the masses of the solar pair are at the top. See an illustration in Fig:3.1.

In this thesis we will consider both normal and inverted hierarchies, and for each of them take two representative limits. This is shown in Table:3.1. The lightest neutrino mass, m_ν, and the sign of Δm_{32}^2

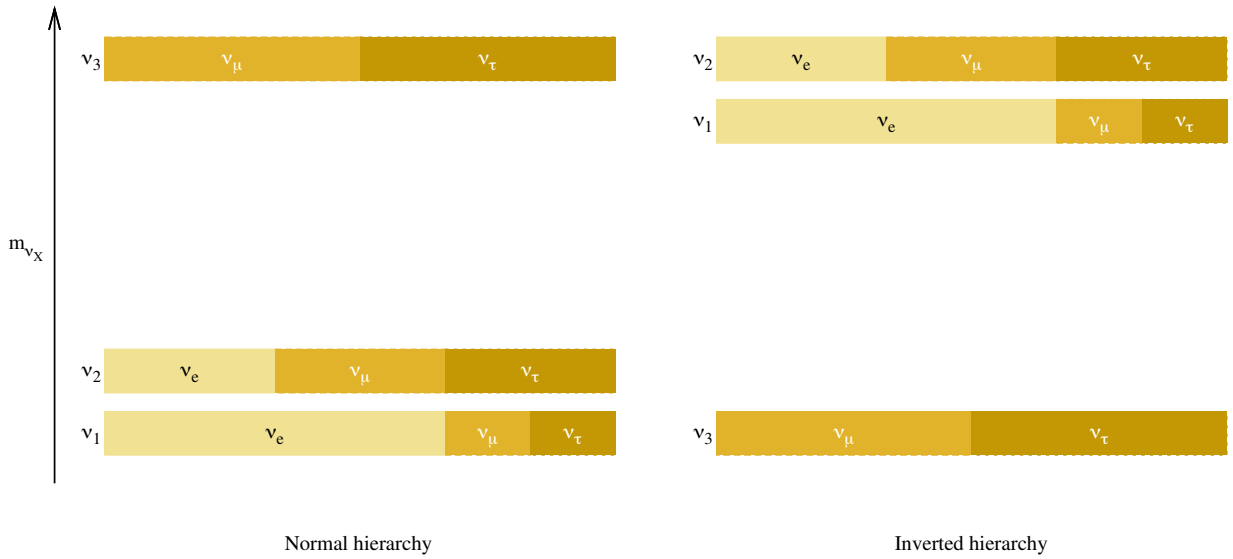

Figure 3.1: Types of left-handed neutrino hierarchies. The content shown for each of the mass eigenstates corresponds to TBM mixing angles.

(which sets the hierarchy type) completely determine the mass spectrum. We will focus on the choice $m_\nu \approx 10^{-6}$ eV for the strict hierarchies and $m_\nu = 10^{-1}$ eV for the QD-type hierarchies.

Hierarchy type	Mass spectrum
SNH	$m_\nu \equiv m_1 \ll m_2^2 = m_1^2 + \Delta m^2_{sol} < m_3^2 = m_2^2 + \Delta m^2_{atm}$
SIH	$m_\nu \equiv m_3 \ll m_1^2 = m_2^2 - \Delta m^2_{sol} < m_2^2 = m_3^2 + \Delta m^2_{atm}$
QDNH	$m_\nu \equiv m_1 < m_2 \simeq m_1 + \frac{\Delta m^2_{sol}}{2m_1} < m_3 \simeq m_2 + \frac{\Delta m^2_{atm}}{2m_2}$
QDIH	$m_\nu \equiv m_3 < m_1 \simeq m_2 - \frac{\Delta m^2_{sol}}{2m_2} < m_2 \simeq m_3 + \frac{\Delta m^2_{atm}}{2m_3}$

Table 3.1: Types of left-handed neutrino hierarchies and mass spectra. The acronyms are formed by: S = Strict, N = Normal, I = Inverted, QD = quasi-degenerated

3.2 Bounds on the neutrino mass scale

As previously seen, oscillation experiments give no information about the overall neutrino mass scale. In here, we briefly state the two methods that provide a bound on the neutrino mass scale.

β-decay

The neutrino mass scale manifests itself in the distortion of the energy spectrum end-point of the final states of a nuclear β-decay. For instance, take the tritium β-decay:

$$^3\mathrm{H} \rightarrow {}^3\mathrm{He} + e + \bar{\nu}_e \,. \tag{3.12}$$

In here the tritium decays into ^{3}He releasing an energy of $Q \equiv m_{^3\mathsf{He}} - m_{^3\mathsf{H}} \simeq 18.6$ keV. The electron will then be emitted with an energy $E_e = Q - E_\nu$, where ν is the energy of the emitted neutrino.

The most stringent constraint to time is given by the MAINZ [28] and TROITSK [29] experiments:

$$m_{\nu_e} \lesssim 2.2 \text{ eV} . \tag{3.13}$$

Cosmological

In section 1.2.2 of the introductory chapter, when talking about how neutrinos were ruled out as valid DM candidates, we pointed out that due to very tiny neutrino masses these are not capable of clustering as soon as ordinary matter, postponing their participation in large structure formation for a later time, when the universe is cool enough. Thus, large structure formation is related to the clustering properties of the neutrinos which, in turn, is related to the neutrino mass scale. We quote the more stringent (CMB) and the more relaxed (WMAP) upper bounds from table 11 of [30],

$$\sum_\nu m_\nu < 0.66 \text{ eV} \;\; \text{(at 95\% C.L.)} , \quad \sum_\nu m_\nu < 1.8 \text{ eV} \;\; \text{(at 95\% C.L.)} . \tag{3.14}$$

3.3 Majorana neutrinos vs Dirac neutrinos

If the neutrinos are massive Majorana fermions, they give rise to processes that violate by 2 units the lepton number, $\Delta L = 2$ (recall the discussion in section 1.2.1 of the introductory chapter). One of these processes is the double beta nuclear decay with no neutrinos in the final state, for shortness $0\nu\beta\beta$,

$$^A_Z\mathsf{X} \to {}^A_{Z+2}\mathsf{X'} + 2e . \tag{3.15}$$

We show the Feynman diagram for the $0\nu\beta\beta$ process via Majorana neutrinos exchange in Fig:3.2. Clearly, only a Majorana fermion can have such a propagator $\langle 0|\psi_a\psi_b|0\rangle \neq 0$ (see the appendix D.5).

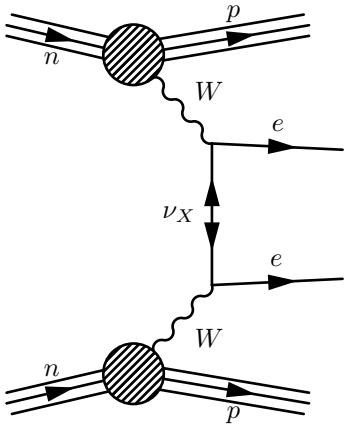

Figure 3.2: Leading order diagram for the neutrinoless double beta decay process via Majorana neutrinos exchange.

The width for this process depends on the nuclear transition amplitude, $\mathcal{M}$, and on m_{ee} which is the "total mass" of an electron-neutrino. Concretely,

$$\Gamma_{0\nu\beta\beta} \propto |\mathcal{M}|^2 |m_{ee}|^2 \quad \text{with} \quad m_{ee} \equiv \sum_X (U_{PMNS})^2_{eX} m_{\nu_X} . \tag{3.16}$$

However, there is a substantial uncertainty on how to calculate correctly the nuclear transition amplitude. Moreover, we would like to add that even if there is a confirmed positive signal for $0\nu\beta\beta$ it does not imply automatically that neutrinos are Majorana particles. In turn, it assures that lepton number is violated but that can happen with a Majorana mass term and/or with lepton number violating interactions.

3.4 Neutrino mass models and seesaw type-I

Having set that neutrinos are massive we now face the task of understanding how that mass is generated. The trivial extension to the Standard Model to accommodate this, is to introduce by hand three fermionic U(1)$_y\otimes$SU(2)$_L\otimes$SU(3)$_c$ singlets (which can be identified as the "missing" RH neutrinos) and write down the neutrino Yukawa couplings which, analogously to the rest of the SM fermions, generate, via EWSB, the neutrino masses. This automatically gives rise to neutrino physical states which are not, in general, flavour aligned with the charged leptons physical states and, consequently, generate flavour changing currents.

However, this extension to the SM (νMSM, [31]) suffers from two prejudices: (i) it requires extremely small neutrino Yukawa couplings ($y^\nu \sim 10^{-12}$); (ii) violates lepton number at a low energy scale.

To justify the (i) smallness of the neutrino masses, (ii) link the lepton number violation with some high energy scale and (iii) the non-observation of light RH neutrinos, one usually considers a more sound mechanism for generating the effective low energy mass matrix, [32, 33]. These mechanisms, called seesaw, assume that (i) neutrinos are Majorana particles and (ii) the existence of very massive particles that couple to the neutrinos in a Yukawa-type analogue. The neutrino masses are then generated by an effective dimension-5 operator:

$$\mathcal{L}^\nu_{\text{dim5}} = \frac{1}{2}\left(\frac{f}{\Lambda}\right)_{ij}(\phi\, i\sigma_2 L_i)\cdot(\phi\, i\sigma_2 L_j)\ , \tag{3.17}$$

(the dot denotes the Lorentz invariant contraction in fermionic space) which arises after integrating out those heavy ($\Lambda \gg M_Z$) d.o.f. [34]. After EWSB the neutrino mass term arises from the ϕ^0 VEV,

$$\frac{1}{2}v^2\left(\frac{f}{\Lambda}\right)_{ij}(\nu_i\cdot\nu_j) + \text{h.c.} \tag{3.18}$$

and the neutrino mass matrix reads:

$$M^\nu_{ij} = -v^2\left(\frac{f}{\Lambda}\right)_{ij}. \tag{3.19}$$

Working in a basis of diagonalized charged lepton Yukawa couplings and simultaneously rotating the neutrinos so that the charged W weak interaction neutrino-(charged lepton)-$W^\pm$ is diagonal, one has by definition that the neutrino mass matrix is diagonalized by the unitary mixing matrix U_{PMNS}.

Seesaw types

There are three basic seesaw realisations, being characterized by the type of heavy d.o.f. and their SU(2)$_L$ representations: fermionic singlets N_i (type-I), scalar triplets $\vec{\Delta}$ (type-II) and fermionic triplets $\vec{\Sigma}$ (type-III). The effective dimension-5 operator generating neutrino masses are then obtained by integrating out the heavy d.o.f. in the diagrams depicted in Fig:3.3.

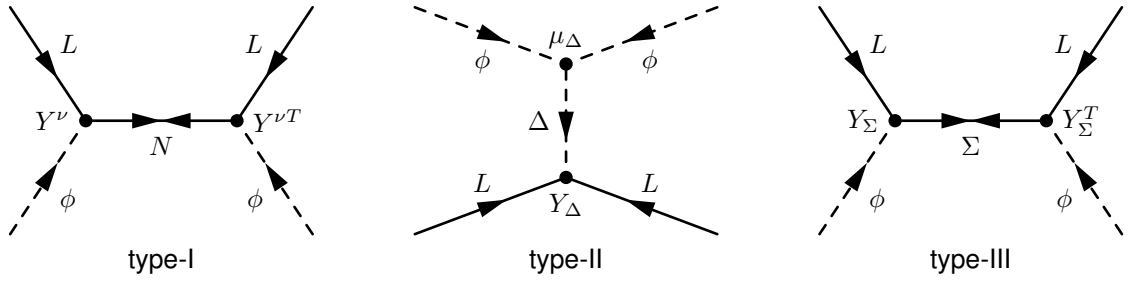

Figure 3.3: The 3 basic types of seesaw and the diagrams behind their dimension-5 operators.

Although an interplay between different seesaw types can be considered [35], in here we focus on the pure type-I seesaw and its extension to the SM and, later on, to the MSSM.

3.4.1 Seesaw type-I

The seesaw type-I adds to SM particle content 3 heavy RH neutrinos, N_i, which are singlets under U(1)$_y$⊗SU(2)$_L$⊗SU(3)$_c$. With these extra fields we can add to the SM additional gauge-invariant renormalizable terms. Indeed, a singlet can have a gauge-invariant Majorana mass term and, moreover, has the correct quantum numbers to have a Higgs-mediated Yukawa couplings with the SM lepton doublets,

$$\mathcal{L}_{\text{seesaw-I}} = -\frac{1}{2}\mathcal{M}_{ij}\left(N_i \cdot N_j\right) + y^\nu_{ij} N_j \phi\, i\sigma_2 L_i + \text{h.c.}\,, \tag{3.20}$$

where $\mathcal{M}$ is a 3×3 complex symmetric mass matrix and y^ν is a 3×3 complex matrix. As the RH neutrinos have no additional couplings we can rotate them to the Majorana mass basis by just redefining the neutrino Yukawa couplings. Therefore, we will consider in what follows that $\mathcal{M}$ is a diagonal real matrix.

At EWSB the neutrino Yukawa couplings will generate a Dirac mass term, $m_D \equiv v y^\nu$, mixing RH neutrinos with LH neutrinos, giving:

$$\mathcal{L}_{\text{seesaw-I}} = -\frac{1}{2}\mathcal{M}^\nu_{ij}\left(N^0_i \cdot N^0_j\right) + \text{h.c.}\,, \quad \mathcal{M}^\nu \equiv \begin{pmatrix} 0 & m_D \\ m_D^T & \mathcal{M} \end{pmatrix}\,, \tag{3.21}$$

where we have defined $N^0 \equiv \{\nu, N\}$. Since $\mathcal{M}^\nu$ is complex symmetric it can be diagonalized by an unitary matrix U^ν, such that,

$$\hat{\mathcal{M}^\nu} = U^{\nu T}\mathcal{M}^\nu U^\nu\,, \quad N' = U^{\nu\dagger} N^0\,, \tag{3.22}$$

where N' are the mass eigenstates.

In the limit where $\mathcal{M} \gg m_D$ we can diagonalize $\mathcal{M}^\nu$ by an expansion on the small parameter $\eta = m_D\mathcal{M}^{-1}$. Indeed, $\mathcal{M}^\nu$ can be first diagonalized into 2 blocks of 3×3 matrices given by:

$$M^\nu = -m_D\eta^T + \mathcal{O}(m_D\eta^3) \simeq -m_D\mathcal{M}^{-1}m_D^T\,, \quad M_N = \mathcal{M} + \mathcal{O}(m_D\eta) \simeq \mathcal{M}\,, \tag{3.23}$$

where M^ν is the upper block and we kept only the first order term in the small parameter expansion. Thus, one would find that the rotation matrix U^ν is:

$$U^\nu = \begin{pmatrix} (1-\frac{1}{2}\eta^*\eta^T)U_{PMNS} & \eta^*(1-\frac{1}{2}\eta^T\eta^*) \\ -\eta^T(1-\frac{1}{2}\eta^*\eta^T)U_{PMNS} & (1-\frac{1}{2}\eta^T\eta^*) \end{pmatrix} + \mathcal{O}(\eta^4)\,, \tag{3.24}$$

where U_{PMNS} is the unitary matrix that diagonalizes M^ν:

$$\hat{M}^\nu = U_{PMNS}^T M^\nu U_{PMNS}\,, \tag{3.25}$$

being identified with (3.4).

We see that for very massive RH neutrinos they completely decouple from the low energy theory because the content of RH neutrino that a neutrino mass eigenstate will have is of order $\eta \simeq 0$. Additionally, in this limit the neutrino mass matrix will be naturally small $\propto v^2\mathcal{M}^{-1}$.

3.4.2 Neutrino Yukawa couplings reconstruction

To reconstruct the high energy Yukawa couplings which satisfy the low energy constraints, namely, the light neutrino mass splittings and mixing angles, we apply the procedure outlined in [36]. Multiplying the left and the right sides of the mass matrix (3.19) by $\sqrt{\hat{M}^{\nu-1}} \equiv diagonal\left(\sqrt{m_1^{-1}}, \sqrt{m_2^{-1}}, \sqrt{m_3^{-1}}\right)$, we have:

$$\begin{aligned} 1 &= \sqrt{\hat{M}^{\nu-1}} U_{PMNS}^T M^\nu U_{PMNS} \sqrt{\hat{M}^{\nu-1}} = -v^2 \sqrt{\hat{M}^{\nu-1}} U_{PMNS}^T Y^\nu \sqrt{\mathcal{M}^{-1}} \sqrt{\mathcal{M}^{-1}} Y^{\nu T} U_{PMNS} \sqrt{\hat{M}^{\nu-1}} \\ &= \bar{R}^T \bar{R} \Rightarrow \bar{R} \equiv iv \sqrt{\mathcal{M}^{-1}} Y^{\nu T} U_{PMNS} \sqrt{\hat{M}^{\nu-1}}\,, \end{aligned} \tag{3.26}$$

where $\bar{R}$ is an orthogonal complex matrix. We follow the convention of factorizing $\bar{R} = iR$ and construct R by applying 3 successive independent rotations: around x an angle θ_1, around y an angle θ_2 and, finally, around z an angle θ_3:

$$\bar{R} = iR\,, \quad R = \begin{pmatrix} c_2c_3 & -c_1s_3 - s_1s_2c_3 & s_1s_3 - c_1s_2c_3 \\ c_2s_3 & c_1c_3 - s_1s_2s_3 & -s_1c_3 - c_1s_2s_3 \\ s_2 & s_1c_2 & c_1c_2 \end{pmatrix}, \tag{3.27}$$

where $\theta_{i=1,2,3}$ are complex numbers and so R is parametrized by 6 independent real numbers.

Therefore, the neutrino Yukawa couplings can be written as:

$$Y^{\nu T} = \frac{1}{v}\sqrt{\mathcal{M}}\, R \sqrt{\hat{M}^\nu} U_{PMNS}^\dagger\,, \tag{3.28}$$

being determined by $(3\times 2)_R + (3+3)_{PMNS} + 3_{m_\nu} + 3_{\mathcal{M}} = 18$ continuous parameters.

4 The Minimal Supersymmetric Standard Model

In spite of a handful of theoretical reasons to look for supersymmetry, at the time of this writing there is no experimental evidence favouring or disfavouring SUSY.

Hence, to look for supersymmetry we follow the conservative approach of considering the minimal extension to the SM that renders a SUSY invariant model: the minimal supersymmetric standard model (MSSM).

4.1 Field content

Recall the discussion about the different supermultiplet representations of the SUSY algebra and the "phenomenological" remarks given in section 2.

Each chiral component of a SM Dirac fermion will fit into a chiral supermultiplet together with a complex scalar (sfermion). We decide to work only with LH chiralities, namely, with the LH Dirac fermion and the LH Dirac anti-fermion. Moreover, each SM gauge boson will fit into a vector supermultiplet together with a Majorana fermion and each SM complex scalar will fit into a chiral supermultiplet together with a Majorana fermion,

SM	MSSM	
spin-1/2	spin-1/2	spin-0
$P_L\psi_{f_i} = f_i$	f_i	$\tilde{f}_{i,L}$, F_{f_i}
$P_L\psi_{\bar{f}_i} = \bar{f}_i$	$\bar{f}_i$	$\tilde{f}^\dagger_{i,R}$, $F_{\bar{f}_i}$

SM	MSSM		
spin-1	spin-1	spin-1/2	spin-0
B_μ	B_μ	$\tilde{B}$	D_B
W^α_μ	W^α_μ	$\tilde{W}^\alpha$	D^α_W
g^a_μ	g^a_μ	$\tilde{g}^a$	D^a_g

SM	MSSM	
spin-1/2	spin-1/2	spin-0
$P_L\psi_{\nu_i} = \nu_i$	ν_i	$\tilde{\nu}_i, F_{\nu_i}$

where ψ_{f_i} is the Dirac spinor of the fermion f_i and $\psi_{\bar{f}_i} \equiv (\psi_{f_i})^c \equiv C\bar{\psi}^T_{f_i}$ is the Dirac spinor of the anti-fermion of f_i. In the case of the neutrino ψ_{ν_i} may be a Majorana or a Dirac spinor.

For the "SM Higgs doublet" (hypercharge assignment $y = 1$) we introduce the superfield $\widehat{H}_u$,

SM	MSSM	
spin-0	spin-1/2	spin-0
ϕ^+	$\tilde{H}^+_u$	$H^+_u, F_{H^+_u}$
ϕ^0	$\tilde{H}^0_u$	$H^0_u, F_{H^0_u}$

where ^+_u and ^0_u label the up and down components of the SU(2)$_L$ doublet, respectively.

We will see that the supersymmetrization of the Yukawa sector requires the introduction of an extra Higgs-like doublet with opposite hypercharge of that of the SM Higgs doublet. Thus, we introduce the superfield $\widehat{H}_d$,

SM	MSSM	
spin-0	spin-1/2	spin-0
-	$\tilde{H}^0_d$	$H^0_d, F_{H^0_d}$
-	$\tilde{H}^-_d$	$H^-_d, F_{H^-_d}$

where ^0_d and ^-_d label the up and down components of the SU(2)$_L$ doublet, respectively.

Clearly, naming the first as the "SM Higgs doublet" and the second as the extra doublet has no fundamental meaning. Indeed, none of them will couple to SM particles as the SM Higgs doublet does in the SM. In practice. the lightest massive state will be a mixed state between Re[H^0_d] and Re[H^0_u]. To this lightest physical state we call the Higgs boson.

In Table:4.1 we summarize the arrangement of the supermultiplets in gauge group representations, which of course were set by SM.

Chiral superfield	spin-1/2	spin-0	Representation in		
			U(1)$_y$	SU(2)$_L$	SU(3)$_c$
$\widehat{Q}_i$	Q_i	$\tilde{Q}_i$	$\frac{1}{3}$	$\mathbf{2}$	$\mathbf{3}$
$\widehat{L}_i$	L_i	$\tilde{L}_i$	-1	$\mathbf{2}$	$\mathbf{1}$
$\widehat{\overline{u}}_i$	$\overline{u}_i$	$\tilde{u}^\dagger_{i,R}$	$-\frac{4}{3}$	$\mathbf{1}$	$\bar{\mathbf{3}}$
$\widehat{\overline{d}}_i$	$\overline{d}_i$	$\tilde{d}^\dagger_{i,R}$	$\frac{2}{3}$	$\mathbf{1}$	$\bar{\mathbf{3}}$
$\widehat{\overline{l}}_i$	$\overline{l}_i$	$\tilde{l}^\dagger_{i,R}$	2	$\mathbf{1}$	$\mathbf{1}$
$\widehat{H}_u$	$\tilde{H}_u$	H_u	1	$\mathbf{2}$	$\mathbf{1}$
$\widehat{H}_d$	$\tilde{H}_d$	H_d	-1	$\mathbf{2}$	$\mathbf{1}$

Table 4.1: Minimal Supersymmetric Standard Model matter fields and representation assignments. The i assumes three different values, one for each family. For shortness we have not displayed the auxiliary fields.

4.2 Superpotential

The superpotential is the supersymmetrized version of the SM Yukawa sector (1.15) with an additional bilinear. However, in the SM the Yukawa sector is not holomorphic in the fields. Indeed, both the Higgs doublet ϕ and its hermitian conjugate $\phi^\dagger$ couple to the same quark doublets Q_i. Recall that SUSY requires the sum of products of superfields to be holomorphic. This is the reason why we need an additional Higgs-like doublet.

Thus, we make the replacement $\phi \to H_u$ and $\phi^\dagger \to H_d i\sigma_2$ in (1.15) and cast the ordinary fields to superfields.

Recall that the SM Yukawa sector was founded on the principle of the most general renormalizable interactions that one could write without explicitly breaking gauge symmetry. Indeed, because in SUSY we have an extra Higgs-like doublet, there is an additional term that is renormalizable and gauge invariant. There are however additional 4 types of terms that could be introduced solely on the principle of renormalizability and gauge invariance. Three of these terms violate lepton number and the other violates the baryon number. All of them are absent in the SM just on renormalizability grounds, but in the MSSM each fermion has a boson partner, thus, terms of the form $\tilde{l}_i$-$\overline{\text{fermion}}_j$-fermion$_k$ and $\tilde{q}_i$-$\overline{\text{fermion}}_j$-fermion$_k$ are indeed renormalizable. We will talk about this in section 4.8.

Putting all together, we write the MSSM superpotential as:

$$\mathcal{L}_Y = \int d^2\theta \left\{ -y^u_{ij}\widehat{\overline{u}}_{(a)j}\widehat{H}_u i\sigma_2 \widehat{Q}_{(a)i} + y^d_{ij}\widehat{\overline{d}}_{(a)j}\widehat{H}_d i\sigma_2\widehat{Q}_{(a)i} + y^l_{ij}\widehat{\overline{l}}_j\widehat{H}_d i\sigma_2\widehat{L}_i + \mu\,\widehat{H}_u i\sigma_2\widehat{H}_d \right\} + \text{h.c.}\,, \quad (4.1)$$

where the Yukawa couplings and the sign of the mass parameter μ are defined following the Les Houches Accord (LHA) convention, [37, 38].

4.3 Soft SUSY-breaking sector

As noted in section 2.4, we will not tackle the question of how SUSY is broken, but rather assume that it was broken by a "mysterious" mechanism at a high energy scale that we will not be able to probe, directly, in any near future. Thus, for phenomenology, all that it is important to know is what type of soft breaking parameters can we expect to be present in the low energy theory.

Recall that SUSY has to be broken in the first place to avoid mass degeneracy between particles and partner sparticles. Thus, we start by this motivation and admit that the hidden sector communicated to the low energy theory general bilinear terms for the sparticles:

$$\begin{aligned}\mathcal{L}_{\tilde{M}}^{soft} &= -\frac{1}{2}M_3\left(\tilde{g}^a\cdot\tilde{g}^a\right)-\frac{1}{2}M_2\left(\tilde{W}^\alpha\cdot\tilde{W}^\alpha\right)-\frac{1}{2}M_1\left(\tilde{B}\cdot\tilde{B}\right)+\text{h.c.}\\ &\quad -(m^2_{\tilde{Q}})_{ij}\tilde{Q}^\dagger_{(a)i}\tilde{Q}_{(a)j}-(m^2_{\tilde{u}_R})_{ij}\tilde{u}^\dagger_{(a)i,R}\tilde{u}_{(a)j,R}-(m^2_{\tilde{d}_R})_{ij}\tilde{d}^\dagger_{(a)i,R}\tilde{d}_{(a)j,R}\\ &\quad -(m^2_{\tilde{L}})_{ij}\tilde{L}^\dagger_i\tilde{L}_j-(m^2_{\tilde{l}_R})_{ij}\tilde{l}^\dagger_{i,R}\tilde{l}_{j,R}\\ &\quad -m^2_{H_u}H_u^\dagger H_u-m^2_{H_d}H_d^\dagger H_d-(bH_u i\sigma_2 H_d+\text{h.c.})\ .\end{aligned}\tag{4.2}$$

Moreover, SUSY can also be softly broken via dimensionful trilinear couplings, namely, by an Yukawa-type sector involving only sparticles:

$$\mathcal{L}_Y^{soft}=A^u_{ij}\tilde{u}^\dagger_{(a)j,R}H_u i\sigma_2\tilde{Q}_{(a)i}-A^d_{ij}\tilde{d}^\dagger_{(a)j,R}H_d i\sigma_2\tilde{Q}_{(a)i}-A^l_{ij}\tilde{l}^\dagger_{j,R}H_d i\sigma_2\tilde{L}_i+\text{h.c.}\,.\tag{4.3}$$

The proof that none of these terms introduce quadratic divergence in the self-energy of scalar fields was given in [39].

Besides those soft-breaking terms we could also have [18]:

$$\mathcal{L}^{soft}_{negligible}=C^u_{ij}\tilde{u}^\dagger_{(a)j,R}H_d^\dagger\tilde{Q}_{(a)i}-C^d_{ij}\tilde{d}^\dagger_{(a)j,R}H_u^\dagger\tilde{Q}_{(a)i}-C^l_{ij}\tilde{l}^\dagger_{j,R}H_u^\dagger\tilde{L}_i+\text{h.c.}\,.\tag{4.4}$$

However, it turns out that these non-holomorphic terms are hard to generate via any SUSY breaking mechanism and, when generated, are typically very small. We will discard them.

4.4 Electroweak symmetry breaking

Just like in the SM, the MSSM undergoes a spontaneous symmetry breaking from U(1)$_y\otimes$SU(2)$_L$ into U(1)$_Q$. The mechanism is a generalization of the 1-doublet EWSB of the SM to the 2-doublets EWSB of the MSSM.

Collecting the interaction terms involving just both Higgs doublets (as all other fields will have vanishing VEVs, having no contribution to the minimization), one determines the following potential:

$$\begin{aligned}\mathcal{V}_{EWSB} &= \left(|\mu|^2+m^2_{H_u}\right)\left(|H_u^+|^2+|H_u^0|^2\right)+\left(|\mu|^2+m^2_{H_d}\right)\left(|H_d^0|^2+|H_d^-|^2\right)\\ &\quad +\left[b\left(H_u^+H_d^--H_u^0H_d^0\right)+\text{h.c.}\right]\\ &\quad +\frac{1}{8}\left(g^2+g'^2\right)\left\{|H_u^+|^2+|H_u^0|^2-|H_d^0|^2-|H_d^-|^2\right\}^2+\frac{g^2}{2}\left|H_u^+H_d^{0\dagger}+H_u^0H_d^{-\dagger}\right|^2\ ,\end{aligned}\tag{4.5}$$

where the last line comes from the D^α_W-terms (for g) and D_B-terms (for g'), the $|\mu|^2$ terms come from the superpotential F-term involving μ and the other terms come from the soft breaking sector.

Recall that we can freely use the SU(2)$_L$ gauge symmetry to redefine the components of a doublet, which means that we can rotate a VEV from one component of a doublet to another component of the same doublet. We choose to put $H_u^+ = 0$ at the minimum of the potential. Hence, by the minimum condition we have $\partial \mathcal{V}_{EWSB}/\partial H_u^+ = 0$ which in turns implies $H_d^- = 0$ (there is another choice to make $H_u^+ = 0$ a minimum, but that choice would lead to the trivial minimum $H_u^+ = H_u^0 = H_d^- = H_d^0 = 0$, which does not break the gauge symmetry).

We are thus left with,

$$\begin{aligned} \mathcal{V}_{EWSB}^{(0)} &= \left(|\mu|^2 + m_{H_u}^2\right)|H_u^0|^2 + \left(|\mu|^2 + m_{H_d}^2\right)|H_d^0|^2 \\ &\quad - \left[bH_u^0 H_d^0 + \text{h.c.}\right] + \frac{1}{8}\left(g^2 + g'^2\right)\left\{|H_u^0|^2 - |H_d^0|^2\right\}^2 . \end{aligned} \tag{4.6}$$

Notoriously, the 4-interaction of the MSSM Higgs potential is a known parameter which is rather small $\frac{1}{2}\left(g^2 + g'^2\right) \simeq 0.26$, in manifest opposition to the unknown λ coupling of the SM Higgs potential (1.12). Moreover, we have also seen that the SM Higgs mass would be proportional to $\sqrt{\lambda}$, which motivates us to think that in the MSSM we will have a rather light Higgs.

In (4.6) the only parameter whose phase is relevant is b. However, we can rotate the phase away and make $b > 0$ by redefining H_u^0 and H_d^0. Additionally, and by looking at (4.6), a non-trivial minimum implies that both H_u^0 and H_d^0 acquire a VEV. Thus, as every other term, except the b-term (and $b > 0$), is real and positive the minimum implies that both VEVs have opposite phases so that $bH_u^0 H_d^0$ is real and positive. As H_u^0 and H_d^0 have opposite hypercharges, we can further make use of the U(1)$_y$ gauge symmetry to absorb the phase of both VEVs. In conclusion, all parameters in (4.6) and the VEVs can be made real and positive.

For a non-trivial minimum of $\mathcal{V}_{EWSB}$ two conditions must be verified: (i) the potential is bounded from below,

$$2|\mu|^2 + m_{H_u}^2 + m_{H_d}^2 > 2b > 0\,, \tag{4.7}$$

implying that at least $(|\mu|^2 + m_{H_u}^2)^2$ or $(|\mu|^2 + m_{H_d}^2)^2$ is positive (when both are positive the second condition must be verified to prevent the trivial minimum); and (ii) the origin must be a saddle point,

$$\left(|\mu|^2 + m_{H_u}^2\right)\left(|\mu|^2 + m_{H_d}^2\right) < b^2\,. \tag{4.8}$$

From now on we assume that the parameters are such that there is indeed a non-trivial minimum. This minimum occurs at:

$$\langle H_u^0 \rangle \equiv v_u\,,\ \langle H_d^0 \rangle \equiv v_d\,. \tag{4.9}$$

The gauge boson masses will have the same form as those generated in the SM EWSB with the following identification:

$$v \equiv \sqrt{v_u^2 + v_d^2}. \tag{4.10}$$

Finally, the two conditions for the minimum of the potential can be written as (which obviously satisfy (4.7) and (4.8)):

$$\begin{cases} \left.\frac{\partial \mathcal{V}_{EWSB}^{(0)}}{\partial H_u^0}\right|_{H_u^0 = v_u, H_d^0 = v_d} = 0 \Rightarrow \left(|\mu|^2 + m_{H_u}^2\right) = b\cot\beta + \frac{1}{2}M_Z^2\cos 2\beta\,, \\ \left.\frac{\partial \mathcal{V}_{EWSB}^{(0)}}{\partial H_d^0}\right|_{H_u^0 = v_u, H_d^0 = v_d} = 0 \Rightarrow \left(|\mu|^2 + m_{H_d}^2\right) = b\tan\beta - \frac{1}{2}M_Z^2\cos 2\beta\,, \end{cases} \tag{4.11}$$

where,

$$\tan\beta \equiv \frac{v_u}{v_d}\,. \tag{4.12}$$

Using (4.11), of the initial 3 free parameters μ, b and $\tan\beta$, we end up with 1 continuous free parameter, $\tan\beta$, plus 1 discrete free parameter, sign(μ). Summing the two equations in (4.11), we determine μ,

$$|\mu|^2 = \frac{m_{H_d}^2 - m_{H_u}^2\tan^2\beta}{\tan^2\beta - 1} - \frac{1}{2}M_Z^2\,. \tag{4.13}$$

Here we see that, by requiring no exceptional fine-tuning between parameters, the Higgs soft-breaking masses and the $|\mu|$-parameter should be at most one or two orders of magnitude from the electroweak energy scale. However, the $|\mu|$-parameter is SUSY-preserving on contrary of the soft-breaking masses. Thus, it seems unnatural that parameters which come from different sources have a similar mass. This is the so called μ-problem. For some proposed solutions see [40, 41]. A MSSM extension exists, called Next-to-MSSM (NMSSM), whose principal motivation is indeed to answer to the μ-problem, [42].

4.5 Mass spectrum

After EWSB the SM particles will have the same mass spectrum as they have in the SM. In turn, the sparticles will mix and form the mass eigenstates identified in the following table,

Mass eigenstates	Mixture of
Neutralinos $\tilde{\chi}^0_{A=1,2,3,4}$	neutral Higgsinos ($\tilde{H}_u^0$ and $\tilde{H}_d^0$), neutral Wino ($\tilde{W}^3$) and Bino ($\tilde{B}$)
Charginos $\tilde{\chi}^\pm_{A=1,2}$	charged Higgsinos ($\tilde{H}_u^+$ and $\tilde{H}_d^-$) and charged Winos ($\tilde{W}^\pm \equiv \frac{\tilde{W}^1 \mp i\tilde{W}^2}{2}$)
Sneutrinos X, $\tilde{\nu}_{X=1,\ldots,3}$	LH sneutrinos ($\tilde{\nu}_{i=e,\mu,\tau}$)
Charged-sleptons X, $\tilde{l}_{X=1,\ldots,6}$	LH and RH charged sleptons ($\tilde{l}_{i=e,\mu,\tau;L}$ and $\tilde{l}_{i=e,\mu,\tau;R}$)
up-squarks X, $\tilde{u}_{(a)X=1,\ldots,6}$	LH and RH up-squarks ($\tilde{u}_{(a)i=u,c,t;L}$ and $\tilde{u}_{(a)i=u,c,t;R}$)
down-squarks X, $\tilde{d}_{(a)X=1,\ldots,6}$	LH and RH down-squarks ($\tilde{d}_{(a)i=d,s,b;L}$ and $\tilde{d}_{(a)i=d,s,b;R}$)
CP-even neutral Higgses h and H	Re[H_u^0] and Re[H_d^0]
CP-odd neutral Higgs A^0	Im[H_u^0] and Im[H_d^0]
Charged Higgses $H^\pm$	H_u^+ and H_d^-

the other 3 d.o.f. that remain in the two Higgs doublets are Goldstone bosons, specifically: $G^\pm$ (mixture of H_u^+ and H_d^-) will be the longitudinal component of $W_\mu^\pm$; and Z^0 (mixture of Im[H_u^0] and Im[H_d^0]), the longitudinal component of Z_μ.

Work basis

We choose to work in the so called super-CKM basis, which rotates both the SM particles and respective spartners just as in (1.18). Concretely, in this basis the Yukawa interactions sfermion-fermion-(neutral Higgsino) are diagonal (in family space) just as fermion-fermion-(neutral Higgs).

Take the superfields with superscript ^{0} as being in the gauge-interaction basis (or the flavour basis).

After EWSB the Yukawa couplings are diagonalized by:

$$\hat{y}^l = V_l^T y^l U_l^* \,, \quad \hat{y}^q = V_q^T y^q U_q^* \quad \text{for } \; q = u, d \,, \tag{4.14}$$

where we rotate the superfields (particle and respective spartner) to the super-CKM basis (no superscript ^{0}) by:

$$\widehat{l}_i^0 = (V_l)_{ij} \widehat{l}_j \,, \; \widehat{\tilde{l}}_i^{\,0} = (U_l)_{ij}^* \widehat{\tilde{l}}_j \,, \; \widehat{q}_i^0 = (V_q)_{ij} \widehat{q}_j \,, \; \widehat{\tilde{q}}_i^{\,0} = (U_q)_{ij}^* \widehat{\tilde{q}}_j \quad \text{for } \; q = u, d \,, \tag{4.15}$$

with a CKM matrix defined just as in (1.20): $V_{CKM} \equiv V_u^\dagger V_d$. Thus, the Yukawa couplings are identified with the fermion masses through:

$$\hat{y}^u_{ii} = \frac{m_{u_i}}{\sqrt{2} M_W \sin\beta} \,, \quad \hat{y}^d_{ii} = \frac{m_{d_i}}{\sqrt{2} M_W \cos\beta} \,, \quad \hat{y}^l_{ii} = \frac{m_{l_i}}{\sqrt{2} M_W \cos\beta} \,. \tag{4.16}$$

Moreover, in the absence of neutrino masses, we can choose to work in the basis where also the lepton-neutrino gauge interactions are diagonal by applying to the neutrino superfields the same rotation that we applied to the LH charged (s)lepton superfields: $\widehat{\nu}_i^0 = (V_l)_{ij} \widehat{\nu}_j$.

In what follows, the sparticle mass matrices are written in the super-CKM basis.

4.5.1 Neutralinos

Neutralinos $\tilde{\chi}_A^0$ are the set of linear combinations of $\tilde{G}^0 \equiv \left\{ \tilde{B}, \tilde{W}^3, \tilde{H}_d^0, \tilde{H}_u^0 \right\}$ that diagonalize the mass matrix (D.27). As this mass matrix is complex symmetric, it can be diagonalized by one unitary matrix N such that:

$$\hat{M}^N = N^* M^N N^{-1} \,, \quad \tilde{\chi}_A^0 = N_{Ai} \tilde{G}_i^0 \,, \tag{4.17}$$

where $A = 1, .., 4$. These are Majorana fermions that can be cast to 4-component Majorana spinors:

$$\psi^M_{\tilde{\chi}_A^0} \equiv \begin{pmatrix} i\sigma_2 (\tilde{\chi}_A^0)^{\dagger T} \\ \tilde{\chi}_A^0 \end{pmatrix} . \tag{4.18}$$

4.5.2 Charginos

Charginos $\tilde{\chi}_A^+$ and $\tilde{\chi}_A^-$ are the set of linear combinations of $\tilde{G}^+ \equiv \left\{ \tilde{W}^+, \tilde{H}_u^+ \right\}$ and $\tilde{G}^- \equiv \left\{ \tilde{W}^-, \tilde{H}_d^- \right\}$, respectively, which bidiagonalize the mass matrix (D.29). Following the Les Houches Accord:

$$\tilde{\chi}_A^+ = V_{Ai} \tilde{G}_i^+ \,, \quad \tilde{\chi}_A^- = U_{Ai} \tilde{G}_i^- \,, \tag{4.19}$$

where V, U are two unitary matrices and $A = 1, 2$. Concretely, the diagonalized mass terms will be:

$$- \sum_{A=1,2} m_{\tilde{\chi}_A^\pm} \left(\tilde{\chi}_A^+ \cdot \tilde{\chi}_A^- \right) + \text{h.c.} \,, \tag{4.20}$$

hence, $\tilde{\chi}_A^+$ and $\tilde{\chi}_A^-$ are the two components of a physical Dirac-like fermion $\tilde{C}_A$:

$$\tilde{C}_A \equiv \begin{pmatrix} i\sigma_2 \tilde{\chi}_A^{+\dagger T} \\ \tilde{\chi}_A^- \end{pmatrix} . \tag{4.21}$$

4.5.3 Sleptons

We label each entry of the charged slepton mass matrix by the "chiralities" and flavours involved. The mass matrix reads,

$$m_{\tilde{l}}^2 \equiv \begin{pmatrix} (m^2_{\tilde{l},LL})_{ee} & (m^2_{\tilde{l},LL})_{e\mu} & (m^2_{\tilde{l},LL})_{e\tau} & (m^2_{\tilde{l},LR})_{ee} & (m^2_{\tilde{l},LR})_{e\mu} & (m^2_{\tilde{l},LR})_{e\tau} \\ (m^2_{\tilde{l},LL})_{\mu e} & (m^2_{\tilde{l},LL})_{\mu\mu} & (m^2_{\tilde{l},LL})_{\mu\tau} & (m^2_{\tilde{l},LR})_{\mu e} & (m^2_{\tilde{l},LR})_{\mu\mu} & (m^2_{\tilde{l},LR})_{\mu\tau} \\ (m^2_{\tilde{l},LL})_{\tau e} & (m^2_{\tilde{l},LL})_{\tau\mu} & (m^2_{\tilde{l},LL})_{\tau\tau} & (m^2_{\tilde{l},LR})_{\tau e} & (m^2_{\tilde{l},LR})_{\tau\mu} & (m^2_{\tilde{l},LR})_{\tau\tau} \\ (m^2_{\tilde{l},RL})_{ee} & (m^2_{\tilde{l},RL})_{e\mu} & (m^2_{\tilde{l},RL})_{e\tau} & (m^2_{\tilde{l},RR})_{ee} & (m^2_{\tilde{l},RR})_{e\mu} & (m^2_{\tilde{l},RR})_{e\tau} \\ (m^2_{\tilde{l},RL})_{\mu e} & (m^2_{\tilde{l},RL})_{\mu\mu} & (m^2_{\tilde{l},RL})_{\mu\tau} & (m^2_{\tilde{l},RR})_{\mu e} & (m^2_{\tilde{l},RR})_{\mu\mu} & (m^2_{\tilde{l},RR})_{\mu\tau} \\ (m^2_{\tilde{l},RL})_{\tau e} & (m^2_{\tilde{l},RL})_{\tau\mu} & (m^2_{\tilde{l},RL})_{\tau\tau} & (m^2_{\tilde{l},RR})_{\tau e} & (m^2_{\tilde{l},RR})_{\tau\mu} & (m^2_{\tilde{l},RR})_{\tau\tau} \end{pmatrix}, \tag{4.22}$$

in the basis $\tilde{l}^0 \equiv \{\tilde{e}^0_L, \tilde{\mu}^0_L, \tilde{\tau}^0_L, \tilde{e}^0_R, \tilde{\mu}^0_R, \tilde{\tau}^0_R\}$ (the superscript ^{0} denotes the super-CKM family basis), and the corresponding Lagrangian density mass term $-(m^2_{\tilde{l}})_{ij}\tilde{l}^{0\dagger}_i\tilde{l}^0_j$.

Each of these entries is calculated to be given by[1]:

$$(m^2_{\tilde{l},LL})_{ij} = (m^2_{\tilde{L}})_{ij} + \delta_{ij}\left[m^2_{l_j} + \Delta_{\tilde{l}_{j,L}}\right], \quad (m^2_{\tilde{l},RR})_{ij} = (m^2_{\tilde{l}_R})_{ij} + \delta_{ij}\left[m^2_{l_j} + \Delta_{\tilde{l}_{j,R}}\right], \tag{4.23}$$

$$(m^2_{\tilde{l},RL})_{ij} = (m^2_{\tilde{l},LR})^*_{ji} = v_d(A^l)_{ji} - \delta_{ij}\,\mu\, m_{l_j}\tan\beta\,, \tag{4.24}$$

where $\Delta_f \equiv M_Z^2\left(T_3|_f - s_w^2\, Q|_f\right)\cos 2\beta$, comes from the 4-interactions with the neutral Higgses mediated by D_B and D^3_W (see the appendix D.4.3.3). The term $\propto \mu$ comes from the 3-interactions with the neutral Higgs H^0_u mediated by $F_{H^0_d}$ auxiliary field. The $m^2_{l_j}$ term of the first and of the second equations come from the 4-interactions with neutral Higgses mediated by the the $F_{\tilde{l}_{j,R}}$ and $F_{\tilde{l}_{j,L}}$ fields, respectively. The terms we have described so far are all flavour conserving. However, as the soft-breaking parameters $(m^2_{\tilde{L}})_{ij}$ and $v_d(A^l)_{ji}$ are general, they can be non-vanishing for $i \neq j$, thus violating flavour.

For the sneutrinos the treatment is simplified due to the absence of the RH component. One finds,

$$(m^2_{\tilde{\nu}})_{ij} = (m^2_{\tilde{\nu},LL})_{ij} = (m^2_{\tilde{L}})_{ij} + \delta_{ij}\,\Delta_{\tilde{\nu}_{j,L}}\,, \tag{4.25}$$

were we have taken $m^2_{\nu_j} = 0$ when compared to the other terms.

The slepton mass eigenstates $\tilde{l}_X$ and $\tilde{\nu}_X$ are obtained via the rotation matrices R^l_{Xi} and R^ν_{Xi}, which diagonalize $(m^2_{\tilde{\nu}})_{ij}$ and $(m^2_{\tilde{l}})_{ij}$, respectively. Thus,

$$\tilde{l}_X = R^l_{Xi}\tilde{l}^0_i\,, \quad \tilde{\nu}_{X'} = R^\nu_{X'i}\tilde{\nu}^0_i, \quad \text{where } X = 1,...,6 \text{ and } X' = 1,...,3. \tag{4.26}$$

4.5.4 Squarks

For the squarks we follow the same labelling as for the sleptons, and find[2]:

$$(m^2_{\tilde{q},LL})_{ij} = (m^2_{\tilde{Q},\tilde{q}})_{ij} + \delta_{ij}\left[m^2_{q_j} + \Delta_{\tilde{q}_{j,L}}\right], \quad (m^2_{\tilde{q},RR})_{ij} = (m^2_{\tilde{q}_R})_{ij} + \delta_{ij}\left[m^2_{q_j} + \Delta_{\tilde{q}_{j,R}}\right], \tag{4.27}$$

$$(m^2_{\tilde{q},RL})_{ij} = (m^2_{\tilde{q},LR})^*_{ji} = v_d(A^q)_{ji} - \delta_{ij}\,\mu\, m_{q_j}\begin{cases} \cot\beta\,, \text{ if } q = u \\ \tan\beta\,, \text{ if } q = d \end{cases}, \tag{4.28}$$

[1] The soft-breaking parameters are already in the super-CKM basis. An explicit discussion is postponed to the squark sector (see the next footnote) whose correspondence to the lepton sector can be easily established.

[2] Note that in the super-CKM basis the $(A^q)_{ji}$ couplings in (4.3) and the soft-breaking mass matrices $m^2_{\tilde{Q}}$ and $m^2_{\tilde{q}_R}$ in (4.2) are transformed to $(V_q^T A^q U_q^*)_{ji}$, $V_q^\dagger m^2_{\tilde{Q}} V_q$ (q is the involved component of the LH squark doublet $\tilde{Q}$) and $U_q^\dagger m^2_{\tilde{q}_R} U_q$, respectively. For shortness, we maintain the original letters when referring to the soft-breaking parameters in the super-CKM basis.

for $q = u, d$. The bases are $\tilde{u}^0 \equiv \{\tilde{u}^0_L, \tilde{c}^0_L, \tilde{t}^0_L, \tilde{u}^0_R, \tilde{c}^0_R, \tilde{t}^0_R\}$ and $\tilde{d}^0 \equiv \left\{\tilde{d}^0_L, \tilde{s}^0_L, \tilde{b}^0_L, \tilde{d}^0_R, \tilde{s}^0_R, \tilde{b}^0_R\right\}$. Note that the $\propto \mu$ term has a $\cot\beta$ ($\tan\beta$) dependence because the up-component (down-component) of the SU(2)$_L$ doublet will have 3-interactions with the neutral Higgs H^0_d (H^0_u) mediated by $F_{H^0_u}$ ($F_{H^0_d}$) and $m_{u_j} = \hat{y}^u_{jj} v_u$ ($m_{d_j} = \hat{y}^d_{jj} v_d$). The mass eigenstates $\tilde{u}_X$ and $\tilde{d}_X$ are obtained via:

$$\tilde{u}_X = R^u_{Xi}\tilde{u}^0_i\,, \quad \tilde{d}_X = R^d_{Xi}\tilde{d}^0_i, \quad \text{where } X = 1, ..., 6. \tag{4.29}$$

4.5.5 Higgses

We divide the analysis of the Higgs sector mass spectrum in three components.

The first is the imaginary part of the neutral Higgses, which originate one massless state Z^0 (the Goldstone boson that is "eaten" up by the longitudinal component of the Z_μ gauge boson) and a massive state A^0, a pseudo-scalar (CP-odd) with mass $m^2_{A^0} = \frac{2b}{\sin 2\beta}$. The rotation matrix is the following:

$$\begin{pmatrix} A^0 \\ Z^0 \end{pmatrix} = \sqrt{2} \begin{pmatrix} \cos\beta & \sin\beta \\ -\sin\beta & \cos\beta \end{pmatrix} \begin{pmatrix} \text{Im}\left[H^0_u\right] \\ \text{Im}\left[H^0_d\right] \end{pmatrix}, \tag{4.30}$$

which diagonalizes (D.24).

The second component comprehends the charged Higgses which give rise to a complex Goldstone boson G^- ($= G^{+\dagger}$), making the longitudinal component of the $W^\pm_\mu$ gauge boson, and a massive complex scalar H^- ($= H^{+\dagger}$) with mass $m^2_{H^\pm} = M^2_W + m^2_{A^0}$. The rotation matrix is given by:

$$\begin{pmatrix} H^+ \\ G^+ \end{pmatrix} = \begin{pmatrix} \cos\beta & \sin\beta \\ -\sin\beta & \cos\beta \end{pmatrix} \begin{pmatrix} H^+_u \\ H^{-\dagger}_d \end{pmatrix}, \tag{4.31}$$

diagonalizing (D.25).

Finally, the real part of the neutral Higgses, which give rise to two massive states: the lightest state of all the physical Higgses, h, and a heavier state H. The rotation matrix is defined as:

$$\begin{pmatrix} h \\ H \end{pmatrix} = \sqrt{2} \begin{pmatrix} \cos\alpha & -\sin\alpha \\ \sin\beta & \cos\alpha \end{pmatrix} \begin{pmatrix} \text{Re}[H^0_u] - v_u \\ \text{Re}[H^0_d] - v_d \end{pmatrix}, \tag{4.32}$$

where α is a parameter fixed by the diagonalization of the mass matrix (D.26), depending on $\tan\beta$ and $m^2_{A^0}$. One could find:

$$\sin 2\alpha = -\frac{m^2_{A^0} + M^2_Z}{m^2_H - m^2_h}\sin 2\beta\,, \quad \cos 2\alpha = -\frac{m^2_{A^0} - M^2_Z}{m^2_H - m^2_h}\sin 2\beta\,. \tag{4.33}$$

The masses of these CP-even Higgses are give by:

$$m^2_h = \frac{1}{2}\left[x + a - \sqrt{(x+a)^2 - 4a\,x\cos^2 2\beta}\right], \tag{4.34}$$

$$m^2_H = \frac{1}{2}\left[x + a + \sqrt{(x+a)^2 - 4a\,x\cos^2 2\beta}\right], \tag{4.35}$$

where we have defined for shortness $a \equiv M^2_Z$ and $x \equiv m^2_{A^0}$.

Clearly, the minus sign that distinguishes the h mass of the H mass is crucial to realise that h is indeed the lightest of the physical Higgses. Concretely, we see that its tree-level mass is bounded from

above by studying the two limits of the free parameter $m^2_{A^0}$. We have: $m^2_{A^0} \to \infty \Rightarrow m^2_h = M^2_Z \cos^2 2\beta$, $m^2_{A^0} \ll 1 \Rightarrow m^2_h \approx m^2_{A^0} \cos^2 2\beta$. Hence,

$$m^2_h \leq M^2_Z \cos^2 2\beta \leq M^2_Z \,. \tag{4.36}$$

This upper bound is dangerously below the LEP2 exclusion bound of $m_H > 114.4$ GeV (at 95% C.L.), [4]. However, m^2_h is positively enhanced by RC from quarks and squarks loops relaxing the upper bound so that it is able to exceed the LEP2 exclusion bound. For instance, in a naive first approximation neglecting the mixing of squarks we find:

$$m^2_h \leq M^2_Z + \frac{3m^4_t}{2\pi^2 v^2} \cos^2\alpha \ln\left(\frac{m_s}{m_t}\right) \leq (115 \text{ GeV})^2 \,, \tag{4.37}$$

where m_s is an average stop mass and we have taken $m_s \equiv \frac{m^2_{\tilde{t}_1}+m^2_{\tilde{t}_2}}{2} \approx 500$ GeV. Note that the new upper limit corresponds to a h entirely made of Re$[H^0_u]$, maximizing the coupling with the (s)tops. Even more relaxed upper bounds can be achieved when one includes the mixing of squarks, $m_h \lesssim 135$ GeV, quoted from [20].

4.6 Constraints

In the MSSM soft-breaking sector (4.2)-(4.3) there are 109 parameters: each sfermion soft-breaking mass matrix is hermitian, adding a total of $5 \times 9 = 45$ parameters; the gaugino masses are complex parameters $2 \times 3 = 6$; the soft-breaking Yukawa sector is composed of 3 general complex 3×3 matrices, adding $3 \times 18 = 54$ parameters; the masses of the two doublets of Higgses are real, adding 2; and finally b is a complex number. However, we have shown that we can redefine the Higgses so that b is real, subtracting 1 parameter. Additionally, by a non-trivial change of basis, 4 of these parameters can be rotated away [43]. We end up with only $109 - 1 - 4 = 104$ parameters.

Besides the soft-breaking parameters the MSSM has 3 other parameters: the absolute value of the SUSY-preserving parameter $|\mu|$, its sign sign(μ) and the ratio of the VEVs, $\tan\beta$. However, we can determine $|\mu|$ and $\tan\beta$ through EWSB conditions (4.11), and only sign(μ) remains free. Hence, there are 105 free parameters in the MSSM.

A model with such a plethora of free parameters is phenomenologically arbitrary, leading to an extremely weak predictive power which simultaneously means that it is hard do identify and/or to exclude through observations. However, there are already strong experimental evidences that constrain much of this arbitrariness. These evidences come from the fact that completely general soft-breaking terms have phases and are flavour mixing, giving rise to sizable CP violating processes, flavour violating processes and severely constrained flavour changing neutral currents (FCNC), such as $b \to s\,\gamma$ and $\mu \to e\,\gamma$, [44–50].

Besides the experimental constraints, there is also the "motivation constraint". We will see that one of the simplest assumptions to avoid most of the experimental constraints is to admit very massive sparticles. However, this leads to two unwanted situations: (i) it reintroduces the fine-tuning problem; and (ii) as it decouples the model from the low energy domain, it may not be observable/testable at near future experiments.

In what follows we will qualitatively assess these constraints.

4.6.1 Phenomenological

Transitions f_i-to-f_j, where $i \neq j$ and f is a SM charged fermion, are completely absent at tree-level but can appear radiatively from loops involving sfermions, besides the usual SM contribution.

A non-vanishing off-diagonal (in flavour space) entry in any of the sfermion soft-breaking mass matrices can lead to indeed sizable flavour changing currents. This is because a mixed-state mass matrix gives rise to transitions sfermion$_i$-sfermion$_j$ (where $i \neq j$ denote flavour) during the propagation with an amplitude proportional to $(m^2_{\tilde{f}})_{ij}$. Thus, a SM fermion$_i$ which has dominant flavour conserving couplings to a sfermion$_i$, via the Yukawa and the gaugino sectors, can change flavour "internally" through fermion$_i$-sfermion$_i$-sfermion$_j$-fermion$_j$, which translates into effective flavour violating currents.

Lepton Flavour Violation

Radiative decays $l_i \to l_j\,\gamma$, such as $\mu \to e\,\gamma$, are known to be severely constrained by experiment $BR(\mu \to e\,\gamma) \leq 1.2 \times 10^{-11}$, [1]. In the MSSM with general soft-breaking mass matrices this process is of the order of [20]:

$$BR(\mu \to e\,\gamma) \approx \left(\frac{|(m^2_{\tilde{l}})_{\mu e}|^2}{m^2_{\tilde{l}}}\right)\left(\frac{100\text{ GeV}}{m_{\tilde{l}}}\right)^4 10^{-6}\,. \tag{4.38}$$

If the slepton soft-breaking mass matrix is arbitrary, the off-diagonal elements should be roughly of the order of the diagonal elements, thus, $\left(\frac{|(m^2_{\tilde{l}})_{\mu e}|^2}{m^2_{\tilde{l}}}\right) \approx 1$. Hence, to satisfy the experimental upper bound we would have to admit extremely massive sleptons, $m_{\tilde{l}} \gtrsim 1.5$ TeV.

The trilinear couplings A^l_{ij} of the soft-breaking Yukawa sector are also constrained for the same reason. Indeed, after EWSB, the LR-sector of the slepton mass matrix develops a term that is proportional to $v_d A^l$, see (4.24).

Colliders: LEP2 searches

In here we present the current experimental bounds on SUSY particle masses. These bounds are based on the direct searches at high energy colliders, specifically, LEP2, [1].

$m_{\tilde{\chi}^0_{i=1,2,3,4}}$	$m_{\tilde{\chi}^\pm_1}$	$m_{\tilde{l}_R=\tilde{e}_R,\tilde{\mu}_R,\tilde{\tau}_R}$	$m_{\tilde{t},\tilde{b},others}$	$m_{\tilde{g}}$
$46, 62.4, 99.9, 116$ GeV	94 GeV	$73, 94, 81.9$ GeV	$95.7, 89, 379$ GeV	308 GeV

Table 4.2: Exclusion bounds on mSUGRA-like MSSM mass spectra from LEP2 searches at 95% CL, [1]. Assumptions include: R-parity is conserved, the LSP is the lightest neutralino, degenerate squark masses except $\tilde{t}$ and $\tilde{b}$, the lightest sleptons are RH and gaugino mass unification at GUT. Bounds on the LSP-sparticle mass differences are also available in [1].

Others

The mixing in the neutral kaon system receives potentially sizable contributions of box diagrams with internal gluinos and s- and d-squarks. The mass splitting Δm_K, which is related to the real part of the box diagrams, and the amount of CP violation in the kaon system, which is proportional to the imaginary

part, result in strong constraints on the phases and mixing of the squark soft-breaking masses and trilinear couplings [51].

Moreover, the phases in the soft-breaking masses, gaugino masses and trilinear couplings are also severely constrained by the electric dipole moment of the proton and electron [52, 53].

For a more comprehensive review see, for instance, [20].

4.6.2 The loss of *Motivation*

We have stated before that the main motivation behind SUSY is to provide a solution to the hierarchy problem. Additionally, we have seen that to simultaneously preserve this solution with a broken SUSY the break has to be soft in the sense that SUSY is still realised in the relation among dimensionless coupling constants which guarantee that the quadratically divergent contributions to any scalar self-energy vanish to all orders in perturbation theory. Nevertheless, logarithmic contributions which are proportional to broken relations such as $\delta m = m_b - m_f \neq 0$, where m_f is the mass of a fermion and m_b is the mass of its bosonic spartner, can reintroduce the fine-tuning problem whenever δm is large.

In the MSSM, spartners with sizable couplings to a scalar field, as it happens between the stops and H_u^0 (the Yukawa coupling is $y_{33}^u \approx 1$), can indeed reintroduce the fine-tuning problem if the mass difference between stops and top is large. To illustrate this point let us calculate the 1L self-energy of H_u^0 from loops with top and stops, whose diagrams are depicted in Fig:4.1.

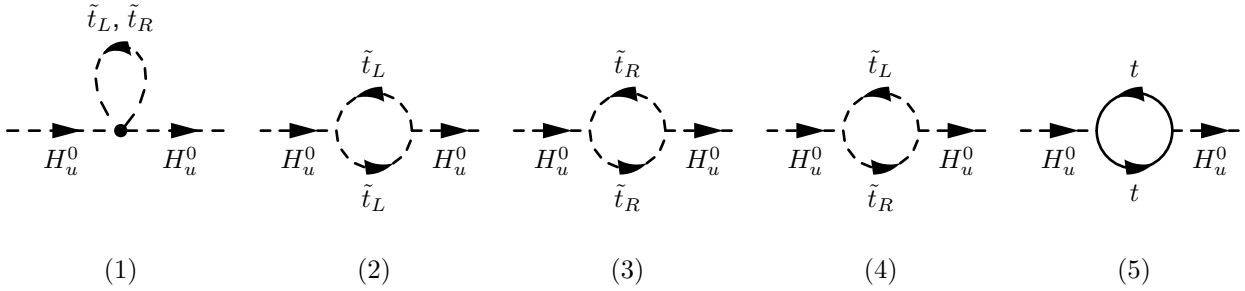

Figure 4.1: Top and stops 1L diagrams contributing to the H_u^0 complex scalar self-energy in the MSSM. Sum over the 3 QCD-colours running in each of the loops is implied.

The masses of H_u^0, LH and RH stops are given by:

$$\overline{m}_{H_u} \equiv m_{H_u}^2 + |\mu|^2\,, \quad \overline{m}_{\tilde{Q}_3}^2 \equiv m_{\tilde{Q}_3}^2 + m_t^2\,, \quad \overline{m}_{\tilde{u}_3}^2 \equiv m_{\tilde{u}_{R,3}}^2 + m_t^2\,, \tag{4.39}$$

respectively. Moreover we define for shortness $y_t \equiv y_{33}^u$. Thus, the contribution of each of the diagrams in Fig:4.1 is (in dimensional regularization $d = 4 - \epsilon$):

$$(1) = 3|y_t|^2 \left\{ I_{0,1}(\overline{m}_{\tilde{Q}_3}^2) + I_{0,1}(\overline{m}_{\tilde{u}_{R,3}^2}) \right\}\,, \tag{4.40}$$

$$(2) = 3|y_t|^2 m_t^2 \int_0^1 dx\, I_{0,2}(\Delta_1)\,, \quad \text{where} \quad \Delta_1 = p^2 x(x-1) + \overline{m}_{\tilde{Q}_3}^2\,, \tag{4.41}$$

$$(3) = 3|y_t|^2 m_t^2 \int_0^1 dx\, I_{0,2}(\Delta_2)\,, \quad \text{where} \quad \Delta_2 = p^2 x(x-1) + \overline{m}_{\tilde{u}_{R,3}}^2\,, \tag{4.42}$$

$$(4) = 3|y_t|^2|A_0|^2 \int_0^1 dx\, I_{0,2}(\Delta_3)\,, \quad \text{where} \quad \Delta_3 = p^2x(x-1) + \overline{m}^2_{\tilde{Q}_3}(1-x) + \overline{m}^2_{\tilde{u}_{R,3}}x\,, \tag{4.43}$$

$$(5) = -6|y_t|^2 \int_0^1 dx \left\{p^2x(x-1)I_{0,2}(\Delta_4) + I_{1,2}(\Delta_4)\right\}\,, \quad \text{where} \quad \Delta_4 = p^2x(x-1) + m_t^2, \tag{4.44}$$

where $I_{m,n}$ are the 1L integrals over k (we use the notation (C.10), see appendix C.2). Evaluating the divergent part of the sum $(1) + ... + (5)$, we find:

$$\frac{i3|y_t|^2}{8\pi^2\epsilon}\left[p^2 + m^2_{\tilde{Q}_3} + m^2_{\tilde{u}_{R,3}} + |A_0|^2\right]\,. \tag{4.45}$$

The mass and field counter-terms are then:

$$\delta Z_{\overline{m}^2_{H_u}} = \frac{3|y_t|^2}{8\pi^2\epsilon}\frac{1}{\overline{m}^2_{H_u}}\left[m^2_{\tilde{Q}_3} + m^2_{\tilde{u}_{R,3}} + |A_0|^2\right]\,, \quad \delta Z_{H_u} = -\frac{3}{8\pi^2\epsilon}|y_t|^2\,, \tag{4.46}$$

respectively. Hence, $\overline{Z}_{\overline{m}^2_{H_u}}\overline{m}^2_{H_u} = constant$:

$$\delta\overline{Z}_{\overline{m}^2_{H_u}} = \frac{3X_t}{8\pi^2\epsilon}\left(\frac{1}{\overline{m}^2_{H_u}}\right)\,, \quad X_t \equiv |y_t|^2\left[m^2_{\tilde{Q}_3} + m^2_{\tilde{u}_{R,3}} + |A_0|^2 + \overline{m}^2_{H_u}\right]\,. \tag{4.47}$$

Thus, the H_u soft-breaking mass squared of at the electroweak energy scale is, in the leading log approximation, given by:

$$m^2_{H_u} \approx m^{(0)2}_{H_u} + \frac{3}{4\pi^2}\ln\left(\frac{m_S}{M_{GUT}}\right)m_S^2\,, \tag{4.48}$$

where $m^{(0)2}_{H_u}$ is the soft-breaking mass squared at GUT ($M_{GUT} \approx 2\times10^{16}$ GeV, see section 4.7), m_S is an average stop mass, $m_S^2 \simeq \frac{1}{2}(m^2_{\tilde{Q}_3} + m^2_{\tilde{u}_{R,3}})$, and we have considered A_0 to be comparatively small. From (4.13) we know that $m^2_{H_u}$ should be of the order of $\frac{1}{2}M_Z^2$, thus, to avoid fine-tuning beyond 1 decimal place (see discussion about (1.60) and the definition given in footnote ([5]) on the same page) we should take $m_S \lesssim 400$ GeV.

As long as $m^{(0)2}_{H_u}$ is not too large, $m^2_{H_u}$ will run to negative values at the electroweak energy scale, favouring the EWSB condition (4.8). Therefore, on contrary to the SM EWSB, we have a way to explain, relying solely on the dynamics of the model, how EWSB is triggered. This is known as the radiatively induced EWSB.

4.7 Constrained MSSM

The strong constraints on the soft-breaking parameters at the SM energy scale suggest that whatever the breaking mechanism is it should be such as to suppress such off-diagonal terms. One of the frameworks that assures this is the supergravity unification, in particular, the minimal supergravity (mSUGRA) [54]. This is further motivated by the MSSM quasi-unification of the gauge couplings at GUT. The mSUGRA soft-breaking terms take the simple universal and flavour blind form at GUT:

$$m^2_{\tilde{L}} = m^2_{\tilde{l}_R} = m^2_{\tilde{Q}} = m^2_{\tilde{u}_R} = m^2_{\tilde{d}_R} = \mathbf{1}\,m_0^2\,, \quad m^2_{H_u} = m^2_{H_d} = m_0^2\,, \tag{4.49}$$

$$M_1 = M_2 = M_3 = m_{1/2}\,, \quad A^{u,d,l} = A_0 Y^{u,d,l}\,, \tag{4.50}$$

To explore the mSUGRA parameter space, and other minimal SUSY breaking scenarios, such as minimal AMSB (mAMSB) and minimal GMSB (mGMSB), a set of points and slopes (snowmass point

and slope or SPS) were defined by their distinctive phenomenological characteristics over the vast SUSY parameter space [55]. In Table:4.3 we show the SPS points for mSUGRA.

mSUGRA point	m_0 [GeV]	$m_{1/2}$ [GeV]	$\tan\beta$	sign(μ)	A_0 [GeV]
SPS1a'	70	250	10	+	-300
SPS1a	100	250	10	+	-100
SPS1b	200	400	30	+	0
SPS2	1450	300	10	+	0
SPS3	90	400	10	+	0
SPS4	400	300	50	+	0
SPS5	150	300	5	+	-1000

Table 4.3: mSUGRA snowmass points and slopes.

4.8 R-parity and the dark matter candidate

As we noted in section 4.2, we left out from the MSSM superpotential other 4 types of terms that could be introduced solely on the principle of renormalizability and gauge invariance. These terms are:

$$\mathcal{L}_{\Delta L=1} = \int d^2\theta \left[\lambda^l_{ijk}\widehat{L}_i i\sigma_2 \widehat{L}_j \widehat{\bar{l}}_k + \lambda^L_{ijk}\widehat{L}_i i\sigma_2 \widehat{Q}_j \widehat{\bar{d}}_k + \mu^L_i \widehat{L}_i i\sigma_2 \widehat{H}_u\right] + \text{h.c.}\,, \tag{4.51}$$

$$\mathcal{L}_{\Delta B=1} = \int d^2\theta\, \lambda^B_{ijk}\widehat{\bar{u}}_i \widehat{\bar{d}}_j \widehat{\bar{d}}_k + \text{h.c.}\,, \tag{4.52}$$

where the first three terms violate lepton number by 1 unit and the fourth term violates the baryon number by one unit (recall from section 1.2.1 that each quark (anti-quark) carries baryon number $+1/3(-1/3)$ and a lepton (anti-lepton) carries lepton number $+1(-1)$). The presence of these terms leads to B and L violating processes, such as the proton decay among many others [56], which have not been observed. Hence, these terms to be present must be extraordinarily small.

We can justify the non-inclusion of these terms by imposing a new symmetry, called R-parity, whose quantum number is multiplicatively conserved. Specifically, each particle of spin s carries a R-parity quantum number $R = (-1)^{3(B-L)+2s}$. This implies that every SM particle has $R = +1$ and the sparticles have $R = -1$.

The R-parity conservation has 3 interesting phenomenological consequences: (i) the lightest sparticle (LSP) is stable; (ii) the final product of a sparticle decay must contain an odd number of sparticles; and (iii) in accelerator experiments sparticles are pair produced as R-parity must be conserved at each vertex.

If this LSP has zero electric charge and is massive enough it may be a valid candidate for cold DM (recall the DM discussion in section 1.2.2 of the introductory chapter). Throughout the most part of the mSUGRA parameter space the LSP is the lightest neutralino which constitutes an excellent DM candidate [57].

5 MSSM extended with seesaw type-I

5.1 Implementation

In the seesaw type extensions to the MSSM (analogously to the SM) neutrino masses are generated by an effective dimension-5 operator:

$$\frac{1}{2}\epsilon_{ab}\epsilon_{cd}\left(\frac{f}{\Lambda}\right)_{ij}\int d^2\theta\left(\widehat{L}_i^a\widehat{H}_u^b\right)\left(\widehat{L}_j^c\widehat{H}_u^d\right)+\text{h.c.}\,, \tag{5.1}$$

which arises after integrating out the heavy degrees of freedom that are active at some high energy scale $\Lambda \gg M_Z$. We have defined the total antisymmetric tensor $\epsilon_{ab} = (i\sigma_2)_{ab} \Rightarrow \epsilon_{12} = -\epsilon_{21} = 1$. After electroweak symmetry breaking (EWSB) the neutrino mass term arises from the H_u^0 VEV[1]:

$$\frac{1}{2}v_u^2\left(\frac{f}{\Lambda}\right)_{ij}\bar{\nu}_j P_L\nu_i+\text{h.c.} \tag{5.2}$$

and the effective low energy neutrino mass matrix reads:

$$M_{ij}^{\nu} = -v_u^2\left(\frac{f}{\Lambda}\right)_{ij}. \tag{5.3}$$

In seesaw type-I we add, to the ordinary MSSM particle content, three gauge singlets of chiral superfields which we label as the heavy right-handed (RH) neutrinos, $\widehat{N}_i$. The super-renormalizable terms that we can add are then:

$$\mathcal{L}_{\text{susy}} = \int d^2\theta\left[\frac{1}{2}\mathcal{M}_{ii}\widehat{N}_i\widehat{N}_i+\epsilon_{ab}Y_{ij}^{\nu}\widehat{N}_j\widehat{L}_i^a\widehat{H}_u^b\right]+\text{h.c.}+F_{N_i}^{\dagger}F_{N_i}\,, \tag{5.4}$$

where we have used the freedom of both diagonalizing the RH neutrino mass matrix and the charged lepton Yukawa couplings so that the (s)lepton mixings are encoded solely in the dimensionless couplings Y_{ij}^{ν}.

It is easy to identify that this corresponds to the particular choice

$$\left(\frac{f}{\Lambda}\right)_{il} = Y_{ij}^{\nu}\mathcal{M}_{jk}^{-1}Y_{kl}^{\nu T} \tag{5.5}$$

for the dimension-5 operator of equation (5.1), with the tree-level neutrino mass matrix:

$$M^{\nu} = -v_u^2 Y^{\nu}\mathcal{M}^{-1}Y^{\nu T}\,. \tag{5.6}$$

Moreover, in the spirit of the soft SUSY breaking we add the correspondent RH sneutrino soft-breaking terms:

$$\mathcal{L}_{\text{soft}} = -\tilde{\mathcal{M}}_{ii}^2\tilde{N}_i^{\dagger}\tilde{N}_i-\left[\epsilon_{ab}A_{ij}^{\nu}\tilde{N}_j\tilde{L}_i^a H_u^b+\text{h.c.}\right]. \tag{5.7}$$

We have discarded an additional allowed soft-breaking term, $\left\{(\mathcal{M}B_M)_{ij}\tilde{N}_i\tilde{N}_j+\text{h.c.}\right\}$, whose phenomenological consequences have been studied in [58].

Expanding (5.4) in terms of ordinary fields and replacing the auxiliary fields by their equations of motion, we have the following mass terms and the trilinear terms involving the slepton doublets $\tilde{L}_i$:

$$\mathcal{L}_{bilinear} = -\left(\mathcal{M}^2+\tilde{\mathcal{M}}^2\right)_{ii}\tilde{N}_i^{\dagger}\tilde{N}_i-\frac{1}{2}\mathcal{M}_{ii}\bar{N}_i N_i\,, \tag{5.8}$$

$$\begin{aligned}\mathcal{L}_{trilinear} = &-\left[\epsilon_{ab}Y_{ij}^{\nu}\tilde{L}_i^a\bar{N}_j P_L\tilde{H}_u^b+\text{h.c.}\right]-\delta_{ab}Y_{ik}^{\nu\dagger}Y_{lj}^{\nu}\tilde{L}_k^{b\dagger}\tilde{L}_l^a\tilde{N}_i^{\dagger}\tilde{N}_j-\delta_{ab}\delta_{cd}\left(Y^{\nu}Y^{\nu\dagger}\right)_{ij}\tilde{L}_j^{a\dagger}\tilde{L}_i^c H_u^{b\dagger}H_u^d\\ &-\left[\epsilon_{ab}\mathcal{M}_{ii}Y_{ji}^{\nu\dagger}\tilde{L}_i^{a\dagger}\tilde{N}_j H_u^b+\text{h.c.}\right]-\left[\epsilon_{ab}A_{ij}^{\nu}\tilde{N}_j\tilde{L}_i^a H_u^b+\text{h.c.}\right]+\ldots\,.\end{aligned} \tag{5.9}$$

[1] In this notation, ν_i is implicitly a 4-component majorana spinor.

5.2 Slepton flavour mixing in the SUSY seesaw type-I (RGE induced)

It has been shown [59, 60] that in the seesaw type-I extension to the MSSM, even assuming flavour blind unification for the soft-breaking terms[2] , the presence of the couplings Y^ν radiatively generates flavour violating mass terms in the slepton mass matrix, which is communicated to the low energy theory by the RGE running.

At leading order there are two sources for this: one from the renormalization of the propagators of the LH sleptons and the other from the renormalization of the charged slepton soft-breaking Yukawa couplings, A^l. The low energy scale theory will then have an effective slepton mass matrix with flavour violating mass terms which come:

1. Directly from the slepton soft-breaking mass, $\propto \Delta m^2_{\tilde{L}}$;
2. Indirectly from charged slepton soft-breaking Yukawa couplings after EWSB, $\propto v_d\, \Delta A^l$.

To be more concrete we write the flavour violating part of the charged slepton mass matrix

$$(\Delta m^2_{\tilde{l},LL})_{ij} = (\Delta m^2_{\tilde{L}})_{ij}\,, \quad (\Delta m^2_{\tilde{l},RL})_{ij} = \left(\Delta m^2_{\tilde{l},LR}\right)^*_{ji} = v_d\,(\Delta A^l)_{ji}\,, \tag{5.10}$$

for $i \neq j$, and of the LH sneutrino mass matrix (we assume that the RH sneutrinos decouple from the low energy theory [58]):

$$(\Delta m^2_{\tilde{\nu}})_{ij} = (\Delta m^2_{\tilde{L}})_{ij} \quad \text{for } i \neq j, \tag{5.11}$$

after EWSB.

From (5.9) one sees that there are four types (characterized by the loop structure) of LO diagrams contributing to the propagators of the slepton doublets involving the Yukawa couplings Y^ν and the trilinear soft-breaking couplings A^ν. These are depicted below in Fig:5.1.

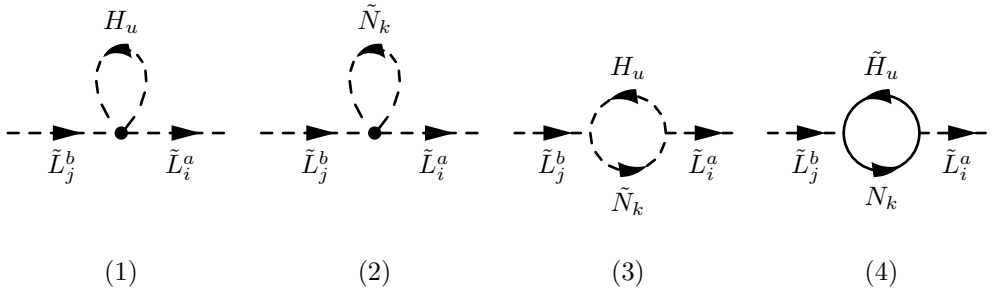

Figure 5.1: Dominant 1L diagrams contributing to the flavour mixed slepton self-energy in the MSSM extended with seesaw type-I.

Using the Feynman's parametrization (C.7)-(C.9) and 1L integrals $I_{r,m}(\Delta)$ (expressions (C.10) given in the appendix C) one finds for the contribution of each diagram (in dimensional regularization $d = 4-\epsilon$):

$$(1) = \delta_{ab}\left(Y^\nu Y^{\nu\dagger}\right)_{ji} I_{0,1}\left(m^2_{H_u} + |\mu|^2\right)\,, \quad (2) = \delta_{ab}\left[Y^\nu_{jk} I_{0,1}\left(\mathcal{M}^2_{kk} + \tilde{\mathcal{M}}^2_{kk}\right) Y^{\nu\dagger}_{ki}\right]\,, \tag{5.12}$$

$$(3) = \delta_{ab}\left[Y^\nu_{jk}\left(\mathcal{M}^2_{kk} + |\mu|^2\right) Y^{\nu\dagger}_{ki} + A^\nu_{jk} A^{\nu\dagger}_{ki}\right] \int_0^1 dx\; I_{0,2}\left(\Delta^{(k)}_1\right)\,, \tag{5.13}$$

[2]Mandatory to avoid sizable flavour changing processes - recall the discussion in section 4.6 of chapter 4.

$$(4) = -2\delta_{ab}\left[Y^{\nu}_{jk}Y^{\nu\dagger}_{ki}\right]\int_0^1 dx\left[p^2x(x-1)I_{0,2}\left(\Delta_2^{(k)}\right) + I_{1,2}\left(\Delta_2^{(k)}\right)\right], \tag{5.14}$$

where we have introduced the definition of the generalized 1L mass squared:

$$\Delta_1^{(k)} = p^2x(x-1) + \left(\mathcal{M}^2 + \tilde{\mathcal{M}}^2\right)_{kk}(1-x) + \left(m^2_{H_u} + |\mu|^2\right)x\,, \tag{5.15}$$

$$\Delta_2^{(k)} = p^2x(x-1) + \mathcal{M}^2_{kk}(1-x) + |\mu|^2x\,. \tag{5.16}$$

As we want to determine the RGE running of the slepton mass matrix (in particular, we want to determine $\gamma_{m^2_{\tilde{L}_{ij}}}$), we work as usual in the MS scheme and from (5.12)-(5.14) we get for the divergent parts $(1/\epsilon)$ of each diagram (using (C.20), (C.21) and (C.24)):

$$(\tilde{1}) = \delta_{ab}\left(Y^{\nu}Y^{\nu\dagger}\right)_{ji}\left[m^2_{H_u} + |\mu|^2\right]\left(\frac{i}{8\pi^2\epsilon}\right), \quad (\tilde{2}) = \delta_{ab}\left[Y^{\nu}_{jk}\left(\mathcal{M}^2_{kk} + \tilde{\mathcal{M}}^2_{kk}\right)Y^{\nu\dagger}_{ki}\right]\left(\frac{i}{8\pi^2\epsilon}\right), \tag{5.17}$$

$$(\tilde{3}) = \delta_{ab}\left[Y^{\nu}_{jk}\left(\mathcal{M}^2_{kk} + |\mu|^2\right)Y^{\nu\dagger}_{ki} + A^{\nu}_{jk}A^{\nu\dagger}_{ki}\right]\left(\frac{i}{8\pi^2\epsilon}\right), \tag{5.18}$$

$$(\tilde{4}) = \delta_{ab}\left[Y^{\nu}_{jk}Y^{\nu\dagger}_{ki}\right]\left(p^2 - 2\mathcal{M}^2_{kk} - 2|\mu|^2\right)\left(\frac{i}{8\pi^2\epsilon}\right), \tag{5.19}$$

from where we find the mass and field counter-terms (the slepton mass matrix is diagonal, $m^2_{\tilde{L}} = m^2_0$, at this stage)[3]:

$$\delta Z^{(ab)}_{m^2_{\tilde{L}_{ij}}} = \delta_{ab}\frac{1}{8\pi^2m^2_0\epsilon}\left[Y^{\nu}_{jk}\left(m^2_{H_u} + \tilde{\mathcal{M}}^2_{kk}\right)Y^{\nu\dagger}_{ki} + A^{\nu}_{jk}A^{\nu\dagger}_{ki}\right], \quad \delta Z^{(ab)}_{p_{ij}} = -\delta_{ab}\frac{1}{8\pi^2\epsilon}\left[Y^{\nu}_{jk}Y^{\nu\dagger}_{ki}\right]. \tag{5.20}$$

Then, $\overline{Z}^{(ab)}_{m^2_{\tilde{L}_{ij}}}\, m^2_{\tilde{L}_{ij}} = constant$:

$$\begin{aligned}\delta\overline{Z}^{(ab)}_{m^2_{\tilde{L}_{ij}}} &= \delta_{ab}\frac{1}{8\pi^2m^2_0\epsilon}\left[Y^{\nu}_{jk}\left(m^2_0 + m^2_{H_u} + \tilde{\mathcal{M}}^2_{kk}\right)Y^{\nu\dagger}_{ki} + A^{\nu}_{jk}A^{\nu\dagger}_{ki}\right] \\ &\Rightarrow \gamma_{m^2_{\tilde{L}_{ij}}} = \frac{1}{8\pi^2m^2_0}\left[Y^{\nu}_{jk}\left(m^2_0 + m^2_{H_u} + \tilde{\mathcal{M}}^2_{kk}\right)Y^{\nu\dagger}_{ki} + A^{\nu}_{jk}A^{\nu\dagger}_{ki}\right].\end{aligned} \tag{5.21}$$

Considering universal scalar masses at GUT, $m^2_{H_u} = \tilde{\mathcal{M}}^2_{kk} = m^2_0$, and moreover $A^{\nu} = A_0Y^{\nu}$, one finds at leading log approximation (LLA):

$$m^2_{\tilde{L}_{ij}} \simeq \delta_{ij}m^2_0 + \frac{1}{8\pi^2}\left(3m^2_0 + A^2_0\right)Y^{\nu}_{jk}t_kY^{\nu\dagger}_{ki}, \quad t_k \equiv \ln\left(\frac{\mathcal{M}_{kk}}{M_{GUT}}\right). \tag{5.22}$$

For the charged slepton trilinear soft-breaking couplings one would also find (in here we assume $A^l = A_0Y^l$, and notice that we are working in a basis with diagonal charged lepton Yukawa couplings):

$$A^l_{ij} \simeq \delta_{ij}A_0Y^l_{ii} + \frac{3}{16\pi^2}A_0Y^l_{ii}Y^{\nu}_{ik}t_kY^{\nu\dagger}_{kj}\,. \tag{5.23}$$

Assuming that the charged slepton left-right mixing is negligible, moreover, that the slepton soft-breaking mass matrix is diagonally dominant with non-degenerate entries, the LH charged slepton mass matrix is, to a good approximation[4], diagonalized by the rotation matrix (following [61]):

$$R^{\tilde{l}} \simeq \begin{pmatrix} 1 & \delta_{12} & \delta_{13} \\ -\delta_{12} & 1 & \delta_{23} \\ -\delta_{13} & -\delta_{23} & 1 \end{pmatrix}, \quad \delta_{ij} = \frac{\Delta m^2_{\tilde{L}(ij)}}{m^2_{\tilde{L}(ii)} - m^2_{\tilde{L}(jj)}}, \tag{5.24}$$

and likewise for the LH sneutrino mass matrix.

[3] We notice in here that if there were no soft-breaking terms we would have $\delta Z^{(ab)}_{m^2_{\tilde{L}_{ij}}} = 0$, as one expects for unbroken SUSY.

[4] Strongly dependent on the amount of degeneracy between the diagonal entries.

5.3 Consequences for low energy phenomenology: LFV and EDM

The RGE induced mixing in the slepton mass matrix leads to two low energy phenomena which depend on the quantity $Y^\nu T Y^{\nu\dagger}$ (with $T_{kk'} = \delta_{kk'} t_{k'}$):

1. Lepton Flavour Violation

Since Y^ν may be of order[5] $\mathcal{O}(1)$, the slepton rotation matrix off-diagonal entries, (5.24), can be significant and, as a consequence, the lepton flavour violating processes, as the LFV radiative decay $\mu \to e\,\gamma$, can get important contributions from loops with LH sleptons, changing abruptly the panorama of what one would expect from the simple seesaw-type realisations of the SM. See chapter 6.

2. Electric Dipole Moment of leptons

The electric dipole moment (EDM) of the charged lepton i is the coefficient d_{l_i} of the effective dimension-5 operator:

$$\mathcal{L}_{EDM} = -\frac{i}{2} d_{l_i} \bar{\psi}_{l_i} \sigma_{\mu\nu} \gamma_5 \psi_{l_i} F^{\mu\nu}\,, \tag{5.25}$$

where $F^{\mu\nu}$ is the electromagnetic energy-momentum tensor.

Decomposing the EDM into contributions of chargino and neutralino loops, $d_{l_i} = d_{l_i}^{\tilde{C}} + d_{l_i}^{\tilde{\chi}^0}$, we find at LO:

$$d_{l_i}^{\tilde{\chi}^0} = -\frac{e}{16\pi^2 m_{\tilde{l}_X}^2} m_{\tilde{\chi}_A^0}\, \mathrm{Im}\left[n_{XA}^{RL(ii)}\right] f_2(A,X)\,, \tag{5.26}$$

$$d_{l_i}^{\tilde{C}} = -\frac{e}{16\pi^2 m_{\tilde{\nu}_X}^2} m_{\tilde{C}_A}\, \mathrm{Im}\left[c_{XA}^{RL(ii)}\right] g_2(A,X)\,, \tag{5.27}$$

where the form factor functions f_2 and g_2 are given in (E.52) and (E.54), respectively, of the appendix E.1.3. The coeficients $n_{XA}^{RL(ij)}$ and $c_{XA}^{RL(ij)}$ are defined in (E.45) of the same appendix.

Assuming mSUGRA boundary conditions, the CPV phases will only appear in the off-diagonal elements of the slepton mass matrix, via $Y^\nu T Y^{\nu\dagger}$. Therefore, in this scenario, lepton EDMs are related to LFV rates and are typically bounded by the experimental upper bounds on LFV radiative decays $l_i \to l_j\,\gamma$.

Indeed, in the work developed in this thesis we have found EDMs in the following range[6]:

$$\begin{cases} -1.9\times10^{-34} < \left[\frac{d_e}{\text{e cm}}\right] < 8.4\times10^{-34}\,, \\ -1.6\times10^{-30} < \left[\frac{d_\mu}{\text{e cm}}\right] < 3.8\times10^{-30}\,, \\ -5.1\times10^{-29} < \left[\frac{d_\tau}{\text{e cm}}\right] < 3.4\times10^{-30}\,, \end{cases} \tag{5.28}$$

by applying the bounds on LFV radiative decays $BR(l_i \to l_j\,\gamma)$ shown in Table:6.1. As expected, these values were well within the present experimental bounds [1]:

$$|d_e^{(\text{exp})}| < 1.4\times10^{-27}\ \text{e cm}\,,\quad |d_\mu^{(\text{exp})}| < (3.7\pm3.4)\times10^{-19}\ \text{e cm}\,,\quad -2.2\times10^{-17} < \left[\frac{d_\tau^{(\text{exp})}}{\text{e cm}}\right] < 4.5\times10^{-17}\,.$$

[5] As long as the RH neutrino mass scale is sufficiently high to generate the small neutrino masses.

[6] These extremes occurred for SPS1a', TBM mixing angles except s_{13}^0 and δ^0, SNH light neutrinos, hierarchical RH neutrinos (with $M_R = 10^{12}$ GeV and $M_1 = M_2 = 10^{10}$ GeV) and a general R-matrix - see section 6.7.2 of chapter 6. As noted in [62], the case of non-degenerate RH neutrinos enhances significantly the EDMs. For degenerate RH neutrinos we have found $|d_e| \lesssim 10^{-35}$ e cm, $|d_\mu| \lesssim 10^{-35}$ e cm and $|d_\tau| \lesssim 10^{-36}$ e cm.

6 Lepton Flavour Violation

6.1 Introduction

It is well known that lepton flavour violating processes in the minimal version of the Standard Model - that is, vanishing neutrino masses - are completely absent. However, as we have referred in chapter 3 there are well established evidences that neutrinos are massive. In what concerns the SM, and from the strict point of view of the low energy phenomenology, whether we implement the trivial extension or a seesaw type extension (see 3.4.1) is irrelevant as long as we consider a seesaw with $Y^\nu \sim \mathcal{O}(1)$, i.e., following its primary motivation[1].

It turns out that LFV processes embodied in this extension of the SM are almost negligible and certainly beyond experimental reach when taking into account the smallness of neutrino masses. A complete deduction of the leading order (LO) decay width of a general flavour changing process fermion$_i \rightarrow$ fermion$_j + \gamma$ is made in the appendix E.1. In there we explicitly show that the decay width for this type of process is proportional to $\left(\frac{m_f^2}{m_b^2}\right)^2$, where m_f and m_b are the masses of the fermions and bosons that run in the loops. In particular, for this simple extension of the SM one arrives at the expression (E.39):

$$BR(\mu \rightarrow e\,\gamma) = \frac{3\alpha}{32\pi M_W^4}\left|\sum_k \lambda_k^{\mu e} m_k^2\right|^2 < 10^{-53}, \tag{6.1}$$

where $\lambda_k^{\mu e} \equiv (U_{PMNS})^*_{\mu k}(U_{PMNS})_{ek}$ and m_k is the neutrino mass of the eigenstate k. Hence, a LFV signal would univocally mean "new physics beyond the SM and/or the νMSM", justifying the present and future efforts devoted to experimental work in this field.

In Table:6.1 we summarize the current upper bounds on selected flavour violating processes: $l_i \rightarrow l_j\,\gamma$ (radiative decays) and $l_i \rightarrow l_j\,\bar{l}_j\,l_j$ (3-body decays).

Decay mode	Branching ratio (at 90% CL)	Decay mode	Branching ratio (at 90% CL)
$\mu \rightarrow e\,\gamma$	$< 1.2 \times 10^{-11}$	$\mu \rightarrow e\,\bar{e}\,e$	$< 1.0 \times 10^{-12}$
$\tau \rightarrow e\,\gamma$	$< 1.1 \times 10^{-7}$	$\tau \rightarrow e\,\bar{e}\,e$	$< 3.6 \times 10^{-8}$
$\tau \rightarrow \mu\,\gamma$	$< 4.5 \times 10^{-8}$	$\tau \rightarrow \mu\,\bar{\mu}\,\mu$	$< 3.2 \times 10^{-8}$

Table 6.1: Experimental upper bounds on LFV radiative decays $l_i \rightarrow l_j\,\gamma$ and 3-body decays $l_i \rightarrow l_j\,\bar{l}_j\,l_j$. Values taken from [1].

We have seen that in the MSSM with a general soft-breaking sector the amount of LFV rates largely exceeded the experimental upper bounds for a slepton mass spectrum not unnaturally heavy. This motivated us to consider that, whatever the SUSY-breaking mechanism is, the soft-breaking terms are communicated from the hidden sector to the visible sector as flavour conserving terms and, in a stronger version, as universal flavour blind terms. On the other hand we saw in chapter 5 that seesaw mediating particles, such as the RH Majorana neutrinos for type-I seesaw, radiatively generate flavour violating entries in the soft-breaking sector, giving rise to LFV processes whose rates further depend on the

[1] In situations where Y^ν is small and, consequently, the RH neutrino masses are of $\mathcal{O}(TeV)$ one can get important contributions from the seesaw dimension-6 operator [63], distinguishing the low energy phenomenology from that of the trivial extension.

seesaw realisation and its parameters. In turn, the seesaw parameters are related to the low energy neutrino parameters: masses and mixing angles. Thus, seesaw realisations of the MSSM provide a promising window into the high energy model from low energy observables.

In here we will study the correlations between the seesaw parameters and the LFV radiative decays $l_i \to l_j\,\gamma$ ($i \neq j$), 3-body decays $l_i \to l_j\,\bar{l}_j\,l_j$ ($i \neq j$), and the tree-level LFV decays of the heaviest stau $\tilde{\tau}_2 \to l_i\,\tilde{\chi}_1^0$ ($l_i \neq \tau$) in context of the seesaw type-I extended MSSM with mSUGRA boundary conditions. An explicit calculation for the widths of the LFV radiative decays and heaviest stau decays is given in the appendices E.1.3 and E.2.1.

The SUSY diagrams contributing to the radiative LFV decay processes at LO are depicted in Fig:6.1.

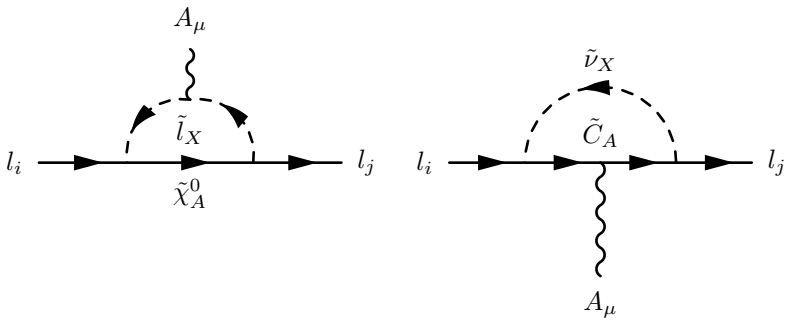

Figure 6.1: Leading order diagrams for the radiative LFV decays $l_i \to l_j\,\gamma$ from neutralino$_A$ (left) and chargino$_A$ (right) channels.

Moreover, one can show that in most part of the constrained MSSM parameter space, and even in the case of Higgs coupling enhancement through large $\tan\beta$, [64], one has:

$$BR(l_i \to l_j\,\bar{l}_j\,l_j) \simeq \frac{\alpha}{3\pi}\left(\ln\frac{m_i^2}{m_j^2} - \frac{11}{4}\right) BR(l_i \to l_j\,\gamma)\,, \tag{6.2}$$

due to the dominance of the photon-penguin diagrams over the Z and H penguins, and the dominance of the penguin diagrams over the box diagrams.

The motivation for studying LFV decays of staus has to do with the search for trilepton signatures at colliders, [65]. For instance, in hadron colliders sparticles are predominantly produced by an s-channel intermediate electroweak gauge boson (γ, Z, $W^\pm$). In typical models, such as the mSUGRA, the sparticle production cross-section will be greater for $\tilde{\chi}_2^0$ and $\tilde{\chi}_1^\pm$ because they are predominantly composed of SU(2)$_L$ gauginos. More specifically, one finds for a p-$\bar{p}$ collision that the dominant processes for sparticle production are indeed $q\bar{q} \to \tilde{\chi}_1^+\tilde{\chi}_1^-$ and $u\bar{d} \to \tilde{\chi}_2^0\tilde{\chi}_1^+$. The chargino-1 $\tilde{\chi}_1^+$ will subsequently decay into a final state with $\tilde{\chi}_1^0$ (the LSP) plus $\bar{l}_i$+$\bar{\nu}_j$ via an intermediate mass eigenstate sneutrino$_X$. In turn, the neutralino-2 $\tilde{\chi}_2^0$ will decay into a final state with $\tilde{\chi}_1^0$ plus $\bar{l}_{i'}$+$l_{j'}$ via an intermediate mass eigenstate charged-slepton$_{X'}$. Hence, this process constitutes an interesting signature to look for, as it has missing energy (both the LSPs plus the neutrino) and 3 leptons in the final state. Moreover, the neutralino-2 will preferably decay into final states with taus due to the enhanced stau mixing (which typically causes the lighter slepton to be mostly composed of RH stau).

In section 6.2 we summarize the MSSM scenario we will work on, discuss its parameters and set the regions of the parameter space to be analysed.

6.2 Model setup: overview

We consider the MSSM extended with RH Majorana neutrinos (seesaw type-I), as presented in chapter 5, and impose universal flavour conserving boundary conditions, as motivated for in chapter 4. In particular, we consider the minimal supergravity (mSUGRA) unification scenario where the soft SUSY-breaking scalar masses, gaugino masses and trilinear couplings are universal and flavour diagonal,

$$m_{\tilde{L}}^2 = m_{\tilde{l}_R}^2 = m_{\tilde{Q}}^2 = m_{\tilde{u}_R}^2 = m_{\tilde{d}_R}^2 = \tilde{\mathcal{M}}^2 = \mathbf{1}\, m_0^2\,, \quad m_{H_u}^2 = m_{H_d}^2 = m_0^2\,, \tag{6.3}$$

$$M_1 = M_2 = M_3 = m_{1/2}\,, \quad A^{u,d,l,\nu} = A_0 Y^{u,d,l,\nu}\,, \tag{6.4}$$

at some SUSY-breaking energy scale. Being this scale unknown, we follow the "unification hint" and take it as the GUT energy scale $M_{GUT} \approx 2 \times 10^{16}$ GeV, where gauge couplings unify.

With the additional input of the two parameters: sign(μ) and $\tan\beta$, one completely sets up the pure MSSM part of the theory. Moreover, in the most part of this work, and when not referred otherwise, we will set the mSUGRA parameters to SPS1a' (see section 4.7).

The seesaw type-I parameters are the neutrino Yukawa couplings Y^ν (a general 3×3 complex matrix) and the 3 RH neutrino masses. We follow the Y^ν parametrization introduced in (3.28) (with the replacement $v \to v_u$). It is determined by $(3\times2)_R+(3+3)_{PMNS}+3_{m_\nu}+3_{\mathcal{M}} = 18$ continuous parameters. Next we will discuss about the assumptions one can make to constrain this parameter space.

6.2.1 Assumptions on $3_{\mathcal{M}} + (3+3)_R$ parameters

Some assumptions can be made on the RH neutrinos by requiring successful BAU via thermal leptogenesis as discussed in [66–68]. In this scenario the baryon asymmetry is generated from the lepton asymmetry by the action of sphalerons which conserve $B - L$. The lepton asymmetry is created by the out of equilibrium decay of the RH neutrinos ($N \to l\,\phi$ and $\bar{N} \to \bar{l}\,\phi^\dagger$) in the early universe and, in the preferable case of hierarchical RH neutrinos, strongly depends on the last RH neutrino to decouple: the lightest. From this, a typical lower bound of roughly 10^{10} GeV is predicted for the RH neutrino masses.

The degenerate (or quasi-degenerated) RH neutrinos scenario is also viable, as reported in [68].

In here we will focus on scenarios which are phenomenologically more interesting by (i) providing a potential explanation for the BAU via thermal leptogenesis and (ii) having observable LFV branching ratios at near future experimental sensitivities, namely, at a level of $BR(\mu \to e\,\gamma) \gtrsim 10^{-13}$, [69].

Thus, for the $3_{\mathcal{M}}$ parameters we will transform them into $1(+1)$ continuous parameter(s)[2] plus 1 hierarchy type as shown in Table:6.2 and assume the RH neutrino masses in the range:

$$10^{10}\ \text{GeV} \leq M_i \leq 10^{15}\ \text{GeV}\,. \tag{6.5}$$

[2] In general only the heavier will have a relevant role.

Hierarchy type	Mass spectrum
DEG	$M_R \equiv M_1 = M_2 = M_3$
HIE	$M_R \equiv M_3 \gg M \equiv M_2 = M_1$

Table 6.2: Right-handed neutrino hierarchy types and mass spectra. The acronyms are formed by: DEG = Degenerated, HIE = Hierarchical.

Note: The labelling of the RH neutrino mass matrix assumes the normal ordering $\mathcal{M}_1 \leq \mathcal{M}_2 \leq \mathcal{M}_3$, which can always be implemented by redefining the basis of the RH neutrinos which, in turn, redefines the R-matrix (see (3.28)). Hence, we work with a R-matrix parametrization in a basis where, by definition, the RH neutrinos mass matrix is normal ordered.

In addition to what was noted previously, the successful BAU via thermal leptogenesis requires an imaginary R-matrix, [64]. Hence, by requiring that Y^ν stays perturbative and inspired by the BAU via leptogenesis, we take the R-matrix angles in the following range:

$$0 \leq |\theta_i| \leq 3\,, \quad |\arg\theta_i| \leq \pi\,. \tag{6.6}$$

6.2.2 Assumptions on $(3+3)_{PMNS} + 3_{m_\nu}$ parameters

In this work we will set the U_{PMNS} angles at GUT to TBM with the exception of the reactor angle, θ_{13}, which remains free within the previously quoted experimental bounds of $0 \leq s^2_{13} < (s^2_{13})^{max} = 0.05$. Moreover, we will set the neutrino mass matrix eigenvalues at high energy scale (hereafter called neutrino masses at GUT, for brevity) so that we reproduce the correct low energy mass splittings. For this we choose the best fitting point values (b.f.p.) [70]:

$$\text{b.f.p.}: \quad \Delta m^2_{sol} = 7.6 \times 10^{-5}\ \text{eV}^2\,, \quad \Delta m^2_{atm} = 2.4 \times 10^{-3}\ \text{eV}^2\,. \tag{6.7}$$

The ansatz for the high scale mixing angles must be taken with care because the experimental values for the mixing angles are, by definition, measured at low scale. As a support for this top-down approach we note that it is well known [71] that neutrino mixing angles run very little and the effect is only manifest in the solar angle, θ_{12}, and especially for the QD-type light neutrino hierarchies.

We have checked the low energy U_{PMNS} angles, Fig:6.2, and how they evolve from the high energy scale ansatz. Notoriously, the solar angle is the most sensitive especially for QD LH neutrinos. In the inverted hierarchy the experimental bound on the solar angle is broken for both small and high values of s^0_{13}, in all the lightest neutrino mass scale region. Inspired by [71], we note that the running effect is proportional to the inverse of the mass difference Δm_{21}. Being Δm_{21} always smaller in the inverted hierarchy than in the normal one, and decreasing as we go up in the lightest neutrino mass scale, this justifies why the deviation from TBM is more significant for (i) the high mass scale region and for (ii) the inverted hierarchy.

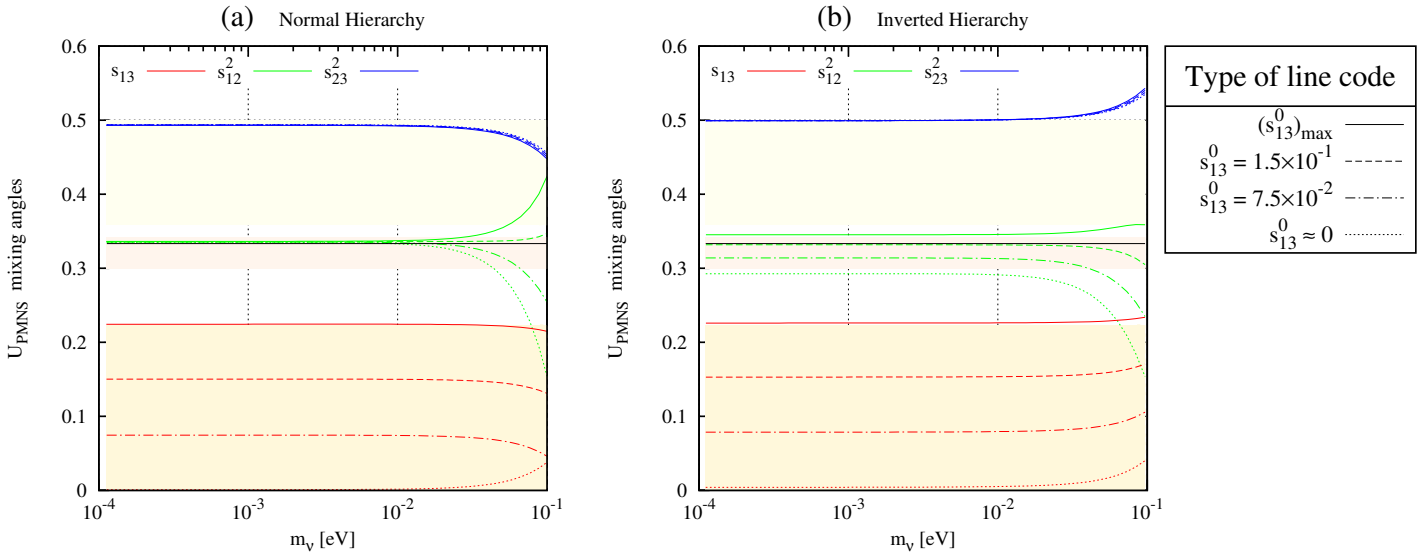

Figure 6.2: The U_{PMNS} mixing angles at low energy scale as a function of the lightest neutrino mass scale for (a) normal and (b) inverted light neutrino hierarchies and for several values of s^0_{13}. The horizontal lines enclosing an area are the experimental bounds on each of the 3 parameters. The black line is set to $1/3$ ($= s^2_{12}$ in TBM). The type of line code, identifying each value of s^0_{13}, is shown in the table at right. Parameters were set to: SPS1a', TBM mixing angles except s^0_{13} ($\delta^0 = 0$), degenerate RH neutrinos with $M_R = 10^{12}$ GeV and $R = 1$.

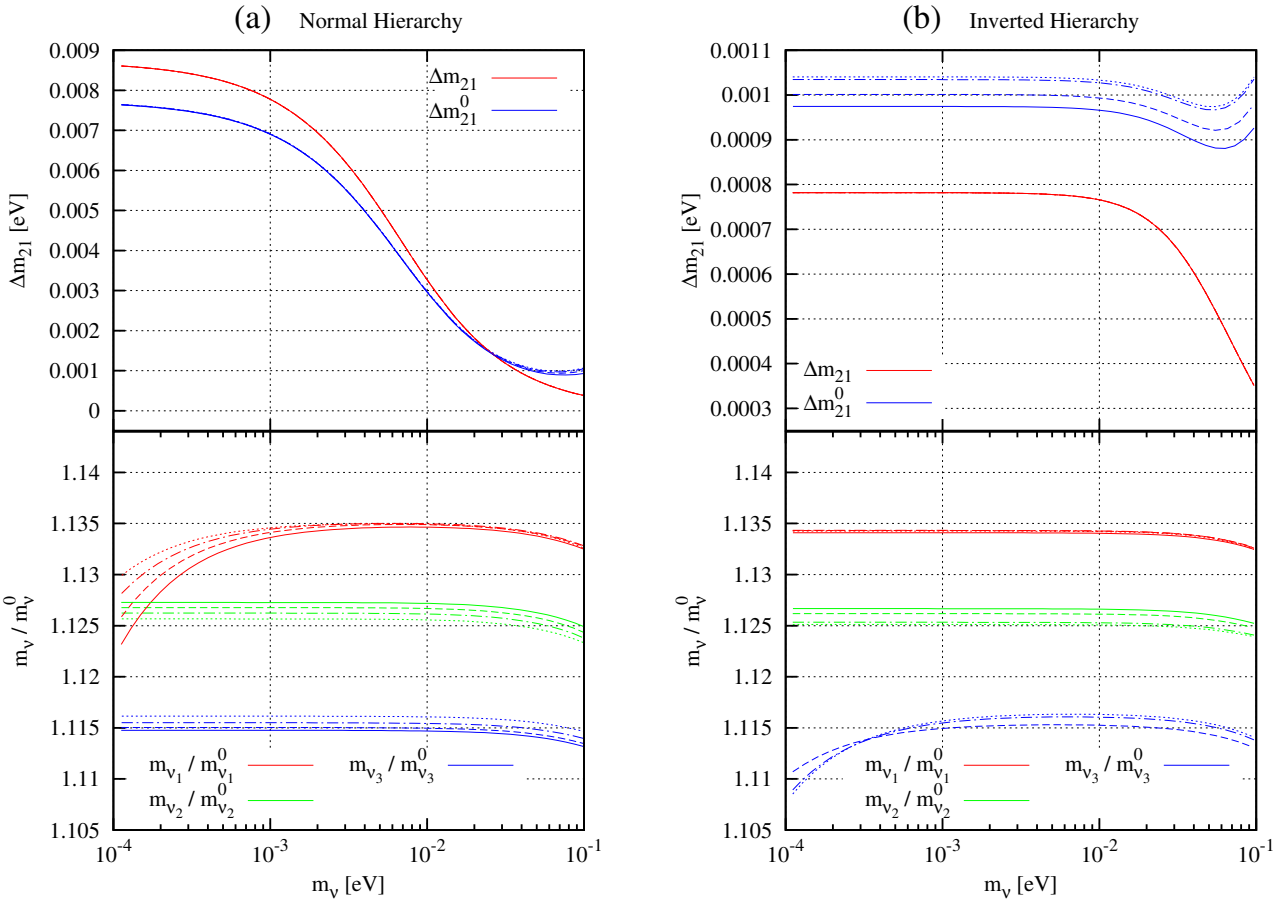

Figure 6.3: High energy scale and low energy scale mass differences for (a - top) normal and (b - top) inverted light neutrino hierarchies. Similarly, at bottom panels the ratio between high energy scale and low energy scale neutrino masses. Every plot is shown as a function of the lightest neutrino mass scale, m_ν, and for several values of s^0_{13}. The type of line code is the same as in Fig:6.2. Parameters were set as in Fig:6.2.

In the bottom panels of Fig:6.3 we show the relation between the neutrino masses at GUT, m_i^0, and the neutrino masses m_i versus the lightest neutrino mass, that is, from a strict hierarchical regime ($m_\nu \approx 10^{-4}$ eV) to a quasi-degenerated regime ($m_\nu \approx 10^{-1}$ eV). In top panels we show the mass differences. We observe that the running effects are such that to obtain the neutrino splittings, having fixed the TBM ansatz at GUT, the mass differences at GUT do not monotonically decrease from the strict hierarchical regime to the quasi-degenerated regime, as one would expect. As we will see ahead, in some particular cases the LFV observables are highly sensitive to these mass differences, whose role is communicated to the soft-breaking sector as flavour violating terms near the GUT energy scale.

For CPV Majorana and the Dirac phases no experimental information is available. The presence of Majorana phases is greatly diluted throughout the 6-dimensional parameter space of the R-matrix, since they do not appear as global phases in none of the f_{ij} and g_{ij} introduced in (6.26)-(6.28). In this analysis we will discard the Majorana phases and include the Dirac phase.

The Dirac phase is also set at GUT. We have checked that the running effects of the Dirac phase are negligible throughout the parameter space explored in this thesis.

We end this section recalling that all the U_{PMNS} parameters, whose values are taken at GUT, are shown with a superscript ^{0}.

6.3 Numerical procedure

All the numerical results presented in this thesis were made using the public code SPHENO [72]. On top of SPHENO we used a program that iteratively varied the two higher neutrino masses at GUT, that were then fed into the neutrino Yukawa couplings (parametrized as in (3.28) and sent as an input to SPHENO to obtain the low energy neutrino masses) to obtain the b.f.p. values for the neutrino mass squared differences (6.7). For this we used a quick minimization algorithm complemented with MINUIT [73]. Note that the lightest neutrino mass was kept free.

To discriminate among different hierarchy types we determined the mass eigenstates X and Y (which were ordered $m_1 < m_2 < m_3$) with maximal and minimal content of ν_e, respectively. If $X = 1 \wedge Y = 3$ we were in the normal hierarchy and if $X = 2 \wedge Y = 1$ we were in the inverted hierarchy. This was especially important for fitting QD-type hierarchies because the fitting procedure would easily scan values which changed the hierarchy type at low energy scale.

For the fitting procedure initial values we determined the two higher eigenvalues from applying the solar and atmospheric splittings together with the input of the lightest eigenvalue. One fitting run was composed of three steps. For the normal hierarchy we took the reasonable assumption of $m^2_{\nu_3} - m^2_{\nu_2}$ stability under $m^0_{\nu_2}$ variations. In turn, for the inverted hierarchy we assumed the stability of $m^2_{\nu_2} - m^2_{\nu_3}$ under $m^0_{\nu_1}$ variations. The fitting steps are summarized in Table:6.3.

When one fitting run failed we returned to the first step and used MINUIT for convergence. With MINUIT we realised a multi-dimensional fitting in each of the steps.

The use of MINUIT was mandatory to obtain convergence in the following situations: (i) strict inverted hierarchies; (ii) QD-type hierarchies; and (iii) strict hierarchies with a general complex R-matrix.

FITTING STEPS

Step	Normal hierarchy		Inverted hierarchy	
	Variation of	Fitting	Variation of	Fitting
#1	$m^0_{\nu_2}$	Δm^2_{sol}	$m^0_{\nu_1}$	Δm^2_{sol}
#2	$m^0_{\nu_3}$	Δm^2_{atm}	$m^0_{\nu_2}$	Δm^2_{atm}
#3	$m^0_{\nu_2}$	Δm^2_{sol}	$m^0_{\nu_1}$	Δm^2_{sol}

Table 6.3: Fitting steps of the solar and atmospheric splittings for normal and inverted light neutrino hierarchies.

6.4 LFV in leading log approximation and the mSUGRA parameters influence

A rough estimate for the LFV decay widths is made in the context of the mass insertion approximation (MIA) [74], where the leading order amplitude is proportional to $|\delta_{ji}|^2$ ($i \neq j$, recall equation (5.24) of the small angle approximation) which comes from the lepton-(LH slepton) flavour transition $i \to j$.

For the radiative LFV decays $l_i \to l_j\,\gamma$, with an on-shell photon, the initial and final leptons have opposite chiralities, therefore, the transition amplitudes are proportional to the masses of the fermions which flip chirality: (i) m_i, (ii) m_j and (iii) $m_{\text{neutralino or chargino}}$. Moreover, and referring to the leading log approximation (LLA), the amplitude dominant contribution comes from loops with LH sleptons, consequently, is described by: an incoming RH (LH) lepton will couple to a LH slepton through Yukawa-type (gaugino-type) coupling and the outgoing LH (RH) lepton will couple to the LH slepton through gaugino-type (Yukawa-type) coupling, while the neutralino or chargino flips chirality. Moreover, as $\hat{y}^l_{ii} > \hat{y}^l_{jj}$, the dominant process is indeed: an incoming RH lepton will couple to a LH slepton through Yukawa-type coupling and the outgoing LH lepton will couple to the LH slepton through gaugino-type coupling, while the neutralino or chargino flips chirality.

Let us implement this description in determining an approximate formula for the LFV radiative decay branching ratios and how they depend on mSUGRA parameters: scalar masses, gaugino masses, sign(μ), $\tan\beta$ and A_0.

Consider a LH slepton mass eigenstate X composed by flavour i sleptons,

$$\tilde{L}_X = \sum_{i=e,\mu,\tau} a_{Xi}\tilde{L}_i\,, \tag{6.8}$$

whose coefficients satisfy the following relations

$$a_{1e} \simeq a_{2\mu}\,, \quad a_{1\mu} \simeq -a_{2e}\,, \quad a_{1\tau} \simeq -a_{3e}\,, \tag{6.9}$$

in the small angle approximation. The diagonal entries of the slepton mass matrix will evolve from GUT scale to the low energy scale according to[3]:

$$m^2_{\tilde{L}(11)} \simeq m^2_{\tilde{L}(22)} \equiv \overline{m}^2_{\tilde{L}}\,, \quad m^2_{\tilde{L}(33)} \simeq \overline{m}^2_{\tilde{L}} - \frac{1}{c^2_\beta}|\overline{X}_\tau|^2\,, \quad \overline{m}^2_{\tilde{L}} \simeq m_0^2 + 0.5\,m^2_{1/2}\,, \tag{6.10}$$

where $\frac{1}{c^2_\beta}|\overline{X}_\tau|^2 \approx \frac{|y_\tau|^2}{8\pi^2}(m^2_{H_d} + m^2_{\tilde{L}_3} + m^2_{l_{R,3}} + |A^2_0|)\ln\frac{M_{GUT}}{M_{SUSY}}$ (compare to (4.47) with the replacement $y_t \to y_\tau$, $m^2_{H_u} \to m^2_{H_d}$, $m^2_{\tilde{Q}_3} \to m^2_{\tilde{L}_3}$, $m^2_{\tilde{u}_{R,3}} \to m^2_{l_{R,3}}$ and dropping out the QCD colour coefficient 3)

[3]For $m^2_{\tilde{L}(33)}$ see equation (5.66) of [20]. For the LH slepton masses dependence on m_0 and $m_{1/2}$ see equations (7.59) and (7.65) of the same reference.

translates the effective Yukawa coupling contribution in the running. We neglected the electron and muon Yukawa coupling contribution as they are comparatively very small.

For simplicity let us take $a_{1\tau} \simeq 0$ and consider the $\tau \to \mu\,\gamma$ process. Defining the $\Delta_{ij} \equiv s_\beta^2 \Delta m^2_{\tilde{L}(ij)}$ ($i \neq j$) and using the small angle approximation formula (5.24), we find:

$$a_{3\mu} \simeq -\frac{\Delta_{23}}{|\overline{X}_\tau|^2 t_\beta^2}\,, \quad a_{3\tau} \simeq 1 - \frac{1}{2} a_{3\mu}^2\,, \tag{6.11}$$

$$a_{2\mu} = a_{3\tau}\,, \quad a_{2\tau} = -a_{3\mu}\,. \tag{6.12}$$

Thus, summing over the contribution of the slepton eigenstates 3 and 2, one has that the transition amplitude for a radiative τ-to-μ transition behaves as,

$$y_\tau \left(\frac{a_{3\mu} a_{3\tau}}{m^2_{\tilde{L}(33)}} + \frac{a_{2\mu} a_{2\tau}}{m^2_{\tilde{L}(22)}} \right) \simeq y_\tau \frac{a_{3\mu} a_{3\tau}}{\overline{m}^2_{\tilde{L}}} \frac{|\overline{X}_\tau|^2}{\overline{m}^2_{\tilde{L}} c_\beta^2} \simeq -y_\tau \frac{\Delta_{23}}{\overline{m}^4_{\tilde{L}} s_\beta^2}\,. \tag{6.13}$$

Moreover, we have to multiply by a chargino/neutralino effective quantity which puts together the contributions of: (i) the mass m_A, (ii) the higgsino content and (iii) the gaugino content. In the neutralino channel the contribution comes from the $\tilde{H}_d^0$ and $\tilde{B}$ / $\tilde{W}^0$ content and in the chargino channel it comes from the $\tilde{H}_d^-$ and $\tilde{W}^+$ content. The neutralino and chargino contributions have opposite signs as can be seen from the form factor functions f_2 and g_2 in (E.52) and (E.54), respectively. We take the effective quantity as a numerical mean and find:

$$(NC)_{eff} \approx 30 \tag{6.14}$$

where the dominant contributions come from $N_{22}N_{23}$ ($\tilde{W}^0$ and $\tilde{H}_d^0$) and $V_{21}U_{22}$ ($\tilde{W}^+$ and $\tilde{H}_d^-$).

Putting all together with the general decay width (E.5), the generalized form of the sum over internal LH sleptons (6.13), considering the loop factor $\frac{1}{16\pi^2}$ of (E.42) and the coefficients of the vertices in (D.42), (D.43), (D.46) and (D.47), we find for a general $l_i \to l_j\,\gamma$ branching ratio:

$$\begin{aligned} BR(l_i \to l_j\,\gamma) &\approx \frac{\alpha^3 m_{l_i}^5}{256\pi^2 M_W^2 \Gamma_{l_i} s_w^4 v^4} \left(\frac{1}{c_\beta^2 s_\beta^4}\right) \left(\frac{m_0^4}{\overline{m}^8_{\tilde{L}}}\right) \left(\frac{v_u^2}{m_0^2} |\Delta m^2_{ji}|\right)^2 (NC)^2_{eff}\,, \\ &\approx \frac{225\alpha^3 m_{l_i}^5}{4096\pi^6 M_W^2 \Gamma_{l_i} s_w^4 v^4} \left(\frac{1}{c_\beta^2 s_\beta^4}\right) \left(\frac{3m_0^2 + |A_0|^2}{\overline{m}^4_{\tilde{L}}}\right)^2 |\delta'_{ji}|^2\,, \quad \delta'_{ji} \equiv v_u^2 \left[Y^\nu T Y^{\nu\dagger}\right]_{ij} \qquad (6.15) \\ &\approx \left(\frac{1}{c_\beta^2 s_\beta^4}\right) \left(\frac{3m_0^2 + A_0^2}{\overline{m}^4_{\tilde{L}}}\right)^2 |\delta'_{ji}|^2 \begin{cases} 6.36 \times 10^{-10}\,, & \text{for } i = \tau \\ 3.58 \times 10^{-9}\,, & \text{for } i = \mu \end{cases}\,. \qquad (6.16) \end{aligned}$$

We have checked explicitly that this approximation is always within less than an order of magnitude from the values of a full numerical evaluation as long as we have moderate $|A_0| \lesssim 500$ GeV and $\tan\beta \gtrsim 3$. In the low $\tan\beta \lesssim 3$ and high $|A_0| \gtrsim 1$ TeV regime the deviation can amount to 2 orders of magnitude.

The branching ratios dependence has been conveniently separated into three types of contributions: (i) seesaw parameters $|\delta'_{ji}|^2$, (ii) dimensionless mSUGRA parameters $c_\beta^{-2} s_\beta^{-4}$ and (iii) dimensionful mSUGRA parameters $\left(\frac{3m_0^2+|A_0|^2}{\overline{m}^4_{\tilde{L}}}\right)^2$, with $\overline{m}^2_{\tilde{L}}$ given by (6.10).

The $c_\beta^{-2} s_\beta^{-4}$ dependence is confirmed in the left panel of Fig:6.4. We also see that $|A_0|$ contributes to increase the rate of the LFV observables, as expected, and that the sign of μ has a small influence. The sign(μ) role is mainly felt in $(NC)_{eff}$, specifically through the diagonalization of the neutralino and

chargino mass matrices. On the other hand, the sign of A_0 is felt in the diagonalization of the full 6×6 charged slepton mass matrix through the left-right mixing.

Moreover, the branching ratios for the LFV radiative decays decrease with an increasing gaugino mass at GUT. The reason for this is contained in (6.16) together with the fact that scalar masses are fed by $m_{1/2}$ in the running from the GUT scale to the EWSB scale, (6.10). On the other hand, m_0 contributes both to enhance the flavour mixing in the slepton mass matrix and to suppress the radiative LFV decays, therefore, its influence is similar to that of $m_{1/2}$ but more moderate. This is shown in the top panel of Fig:6.5.

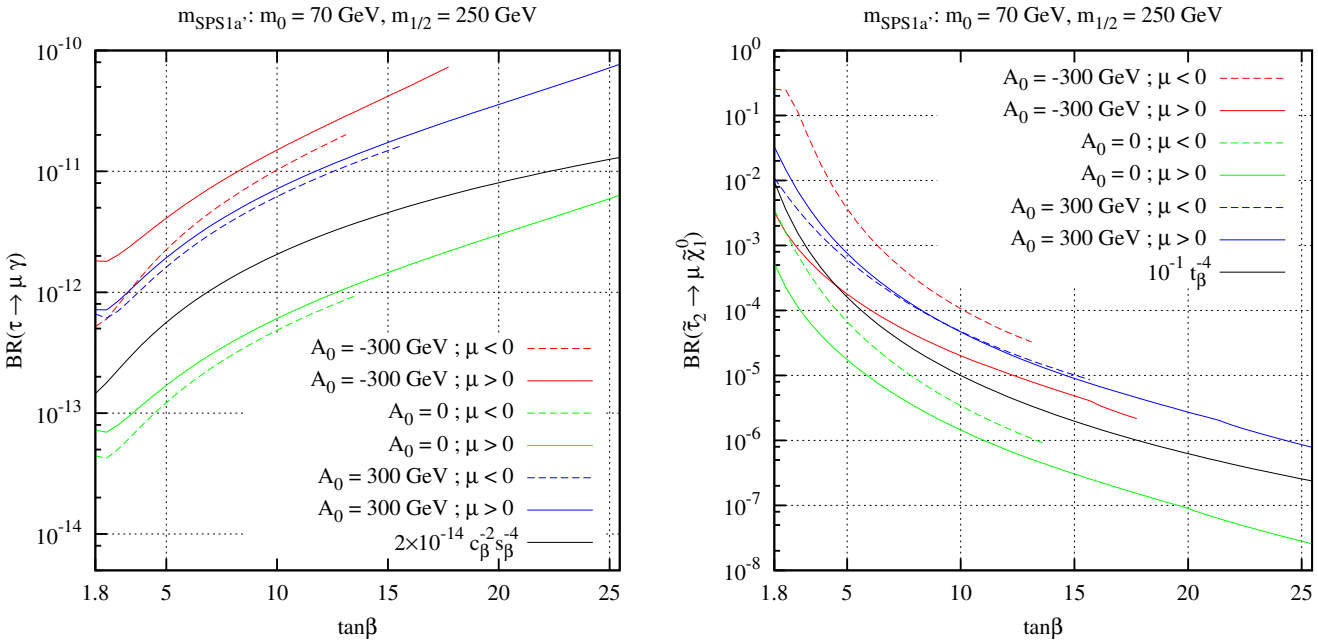

Figure 6.4: Branching ratios of the LFV radiative decay $\tau \to \mu\,\gamma$ (left panel) and tree-level decay $\tilde{\tau}_2 \to \mu\,\tilde{\chi}_1^0$ (right panel) as a function of $\tan\beta$ for paired values of $\{A_0, \text{sign}(\mu)\}$ (see legend). In both panels we show (in black) the approximate dependence on $\tan\beta$ (see text). mSUGRA mass parameters were set to SPS1a'. Remaining parameters were set to: TBM mixing angles, SNH light neutrinos with $m_\nu \approx 10^{-6}$ eV, degenerate RH neutrinos with $M_R = 10^{12}$ GeV and $R = 1$. Note: some choices of $\{A_0, \text{sign}(\mu)\}$ parameters are not extended throughout the entire $\tan\beta$ range considered because no EWSB solution was found.

We now turn to the heaviest stau decay dependence on $\tan\beta$. For this, note that δ_{i3} ($i \neq 3$), as defined in (5.24), will be approximately given by:

$$\delta_{i3} = \frac{c_\beta^2}{|\overline{X}_\tau|^2}\Delta m^2_{\tilde{L}(i3)} \propto \frac{1}{t_\beta^2}\,, \tag{6.17}$$

where we used $\Delta m^2_{\tilde{L}(i3)} \propto (Y^\nu T Y^{\nu\dagger})_{3i} \propto \frac{1}{v_u^2} \propto \frac{1}{s_\beta^2}$. Hence, $|\delta_{i3}|$ decreases with the square of $\tan\beta$ and, as such, the tree-level LFV stau$_2$ decay branching ratio,

$$BR(\tilde{\tau}_2 \to l_i\,\tilde{\chi}_1^0) \propto \left(\frac{1}{\tan\beta}\right)^4\,, \tag{6.18}$$

where $l_i \neq \tau$. This behaviour is confirmed through a full numerical analysis whose results are shown in the right panel of Fig:6.4.

In Fig:6.6 we observe that the branching ratios for the LFV stau decays increase with both mass parameters until it reaches a straight band where it has a peak. Increasing m_0 and/or $m_{1/2}$ above the peak

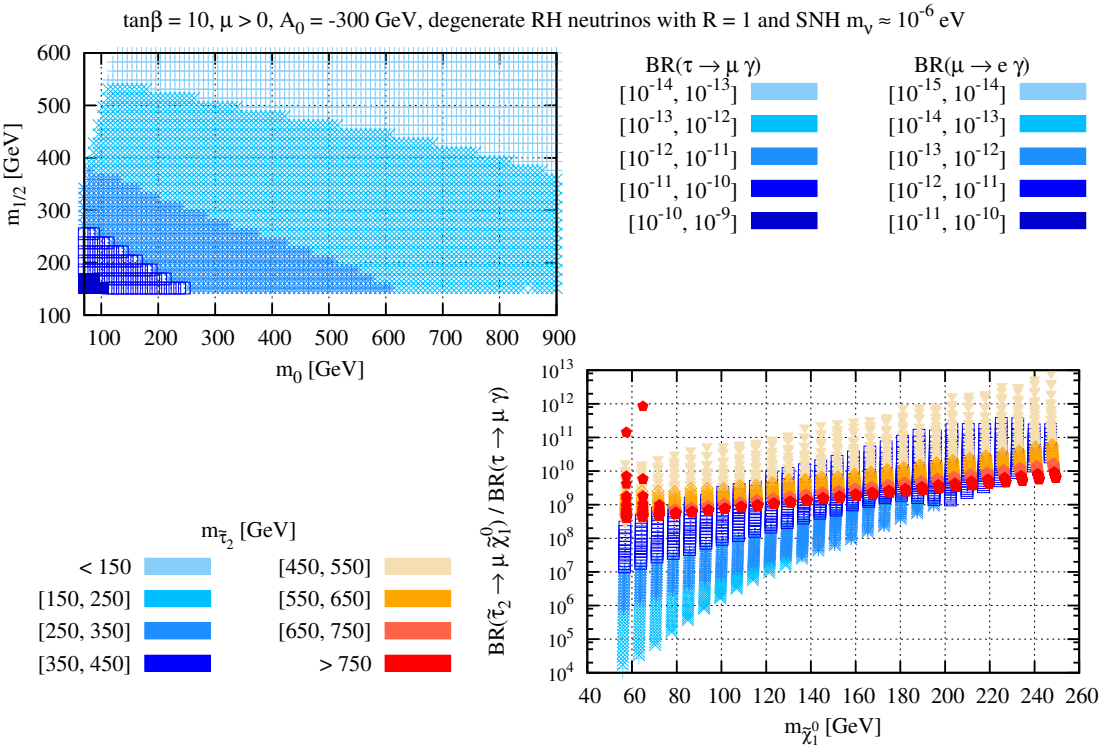

Figure 6.5: At top: contour regions for the branching ratios of the LFV radiative decays $\tau \to \mu\,\gamma$ and $\mu \to e\,\gamma$ as a function of mSUGRA mass parameters m_0 and $m_{1/2}$. At bottom: contour regions of the mass of the heaviest stau for $\frac{BR(\tilde{\tau}_2 \to \mu\,\tilde{\chi}_1^0)}{BR(\tau \to \mu\,\gamma)}$ as a function of the LSP mass. Remaining parameters were set to: $\tan\beta = 10$, $A_0 = -300$ GeV, TBM mixing angles, SNH light neutrinos with $m_\nu \approx 10^{-6}$ eV, degenerate RH neutrinos with $M_R = 10^{12}$ GeV and $R = 1$. In top plot, the removed (blank) regions at the up-left corner comprehends a disfavoured DM candidate: the LSP is the lightest stau. Similarly, the removed (blank) regions at the bottom correspond to scenarios where the LEP2 mass bounds are violated, in particular the lightest chargino lower bound $m_{\tilde{\chi}_1^\pm} \geq 94$ GeV.

the branching ratios will continuously decrease until a stable region, where the mass parameters have little influence, is reached. We argue that the mass parameters influence over the LFV stau decays are due to a resonance in the small angle approximation, concretely, in the dynamics of the slepton mass matrix diagonalization and stau$_2$ identification. For sufficiently low m_0 and $m_{1/2}$ the stau$_2$ is the heaviest slepton due to enhanced left-right mixing and in spite of the $-\frac{1}{c_\beta^2}|\overline{X}_\tau|^2$ contribution. As the mSUGRA mass parameters increase the $\tilde{\tau}_L$-content of the heaviest slepton decreases, while its $\tilde{\mu}_L$- and $\tilde{e}_L$-content increases. Thus, $BR(\tilde{\tau}_2 \to \mu\,\tilde{\chi}_1^0)$ gets higher. However, there is a line ζ in the mSUGRA mass parameter space where the amount of $\tilde{\tau}_L$-content of the next-to-lightest LH slepton (slepton$_5 \approx \tilde{\mu}_L$) and lightest LH slepton (slepton$_4 \approx \tilde{e}_L$) will get closer to the $\tilde{\tau}_L$-content of the heaviest LH slepton, and all the LH slepton mass eigenstates will have approximately the same mass. In this region $BR(\tilde{\tau}_2 \to \mu\,\tilde{\chi}_1^0)$ gets saturated as $|R^{\tilde{l}}_{\tilde{\tau}_2\mu}| \approx 0.7$. When the mass parameters go beyond the line ζ, the $\tilde{\tau}_2$ will switch from being the heaviest slepton and become the lightest LH slepton, while its $\tilde{\tau}_L$-content will commence to decrease. Therefore, $BR(\tilde{\tau}_2 \to \mu\,\tilde{\chi}_1^0)$ decreases as the mass parameters go beyond ζ. The same reasoning applies to $BR(\tilde{\tau}_2 \to e\,\tilde{\chi}_1^0)$.

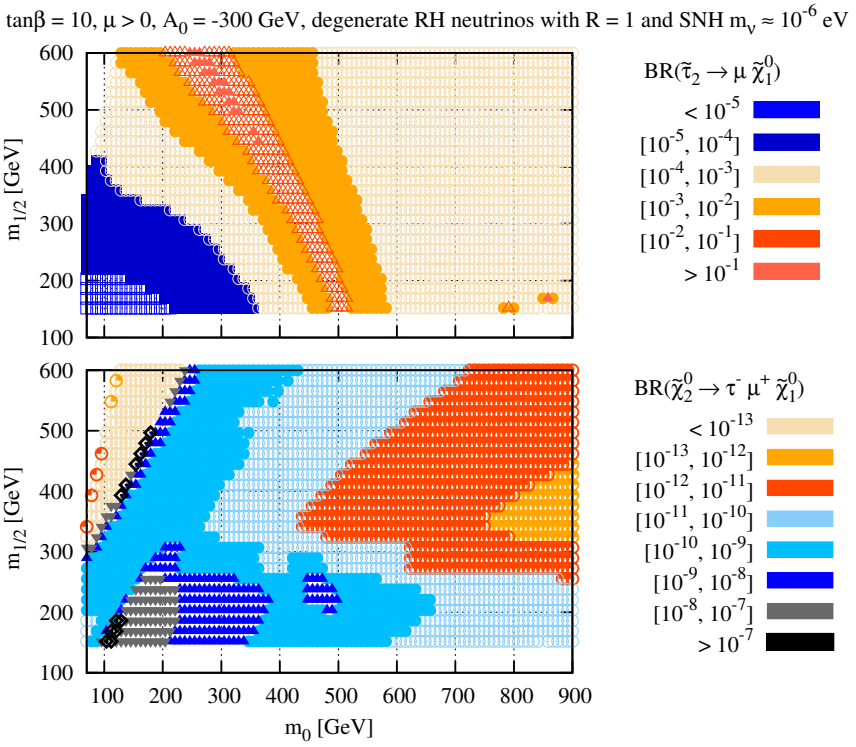

Figure 6.6: At top: contour regions for the branching ratio of the LFV heaviest stau decay $\tilde{\tau}_2 \to \mu\,\tilde{\chi}_1^0$ as a function of mSUGRA mass parameters m_0 and $m_{1/2}$. At bottom: the same for the LFV dilepton neutralino-2 decay $\tilde{\chi}_2^0 \to \tau\,\bar{\mu}\,\tilde{\chi}_1^0$. Parameters and cuts were set as in Fig:6.5.

Nevertheless, note that in the $BR(\tilde{\tau}_2 \to l_i\,\tilde{\chi}_1^0)$ enhancement region, where $|R_{\tilde{\tau}_2\mu_L}| \approx 0.7$, we will have $R_{\tilde{\mu}_L\mu_L} \approx -R_{\tilde{\tau}_2\mu_L}$, thus, together with the quasi-degeneracy of the LH slepton masses (especially in the enhancement region), this resonances will be washed out when summing over internal sleptons, as it happens in the radiative LFV decays and, for example, $\tilde{\chi}_2^0 \to \tau\,\bar{\mu}\,\tilde{\chi}_1^0$ (see bottom panel of Fig:6.6). This justifies why we did not have to account for the diagonalization dynamics to obtain the reasonable estimate (6.16).

The $BR(\tilde{\chi}_2^0 \to \tau\,\bar{\mu}\,\tilde{\chi}_1^0)$ rich pattern shown in the m_0-$m_{1/2}$ plane is preponderantly set by the total decay width of $\tilde{\chi}_2^0$ and not by the partial decay width channel[4] $\tilde{\chi}_2^0 \to \tau\,\bar{\mu}\,\tilde{\chi}_1^0$. Indeed, the suppression region at high $m_{1/2}$ and low m_0 is due to the kinematical open of the decay channel $\tilde{\chi}_2^0 \to l_L\,\tilde{l}_L^\dagger$ which is particularly important due to the SU(2)$_L$-gaugino nature of $\tilde{\chi}_2^0$. One can parametrize the region where this channel is closed by [5]

$$m_{\tilde{\chi}_2^0} \lesssim m_{\tilde{L}} \Rightarrow 0.882\,m_{12} \lessapprox \sqrt{m_0^2 + 0.5375\,m_{1/2}^2 + M_Z^2\,(-1/2 + s_w^2)\cos 2\beta}\,, \tag{6.19}$$

where in addition to (6.10) we have considered the $\tilde{B}$ running contribution for the slepton masses $\simeq \frac{0.15}{4} m_{1/2}$ and the EWSB contribution $\Delta_{\tilde{L}}$ introduced first in (4.23). A more reliable estimate must account for the left-right mixing in the slepton mass matrix. Moreover, the enhancement region for both

[4] The partial decay width evolves as $\Gamma(\tilde{\chi}_2^0 \to \tau\,\bar{\mu}\,\tilde{\chi}_1^0) \propto \frac{m_{1/2}^5}{(m_0^2 + 0.5\,m_{1/2}^2)^2}$.

[5] Recall the scale independent ratios $M_1/\alpha_1 = M_2/\alpha_2 = M_3/\alpha_3 = m_{1/2}/\alpha_{GUT}$, where g_1 is the GUT hypercharge with $\alpha_1 = \frac{5\alpha}{3c_w^2}$, $\alpha_2 = \frac{\alpha}{s_w^2}$ and $\alpha_3 = \alpha_s$. Moreover, numerically one finds $\alpha_{GUT}^{-1} \simeq 24.3$, hence, the LSP mass is approximately given by $m_{\tilde{\chi}_1^0} \approx M_1 \simeq 0.411\,m_{1/2}$ and the neutralino-2 mass by $m_{\tilde{\chi}_2^0} \approx M_2 \simeq 0.882\,m_{1/2}$.

low m_0 and $m_{1/2}$ (roughly $100 \lesssim \frac{m_0}{\text{GeV}} \lesssim 200$ and $150 \lesssim \frac{m_{12}}{\text{GeV}} \lesssim 250$) is due to the channel $\tilde{\chi}_2^0 \to l_R \tilde{l}_R^\dagger$ being kinematically closed, together with the decrease of the $\tilde{B}$-content of $\tilde{\chi}_2^0$ for higher $m_{1/2}$.

Concluding remarks

The LFV branching ratios depend strongly on three mSUGRA parameters: m_0, $m_{1/2}$ and $|A_0|$; and slightly on the sign of both μ and A_0. Moreover, this dependence is transversal among flavours and specific of the dynamical structure of the process. Concretely, one can take to an excellent approximation that the ratios,

$$\frac{BR(\tilde{\tau}_2 \to l_i\, \tilde{\chi}_1^0)}{BR(\tau \to l_i\, \gamma)} \simeq f(m_0, m_{1/2}, A_0, \tan\beta, \text{sign}(\mu))\,, \quad \text{for } l_i \neq \tau, \tag{6.20}$$

$$\frac{BR(\tilde{\tau}_2 \to l_i\, \tilde{\chi}_1^0)}{BR(\tilde{\chi}_2^0 \to \tau\, \bar{l}_i\, \tilde{\chi}_1^0)} \simeq g(m_0, m_{1/2}, A_0, \tan\beta, \text{sign}(\mu))\,, \quad \text{for } l_i \neq \tau, \tag{6.21}$$

depend uniquely on the mSUGRA point and are seesaw independent. For SPS1'a ($m_{\tilde{\chi}_1^0} \simeq 97$ GeV, $m_{\tilde{\tau}_2} \simeq 194$ GeV), we find:

$$f(\text{SPS1a'}) \simeq 1.3 \times 10^6\,, \quad g(\text{SPS1a'}) \approx 8 \times 10^4\,, \tag{6.22}$$

being, as expected, reasonably accurate throughout the seesaw parameters explored in this thesis.

A joint measure of two LFV decays with the same flavour transition can shed some light on the mSUGRA dimensionful parameters and also $\tan\beta$. In the bottom panel of Fig:6.5 we show the contour regions of the mass of the heaviest stau for $\frac{BR(\tilde{\tau}_2 \to \mu\, \tilde{\chi}_1^0)}{BR(\tau \to \mu\, \gamma)}$ as a function of the LSP mass - recall the preceding footnote ([5]).

In turn, the seesaw parameters influence will set the relative size between branching ratios with the same dynamical structure. Specifically, the ratios

$$\frac{BR(\tilde{\tau}_2 \to l_i\, \tilde{\chi}_1^0)}{BR(\tilde{\tau}_2 \to l_j\, \tilde{\chi}_1^0)} \simeq \frac{|\delta'_{i3}|^2}{|\delta'_{j3}|^2}\,, \quad \text{for } l_i, l_j \neq \tau\,, \tag{6.23}$$

are, to an excellent approximation, mSUGRA independent. Thus, to determine the LFV rates of the model one needs to study the quantities f, g (and alike mSUGRA functions) and δ'_{ji}.

To end this section we note the approximate relations among the radiative LFV decays:

$$\frac{BR(\mu \to e\,\gamma)}{BR(\tau \to e\,\gamma)} \simeq \frac{\Gamma_\tau}{\Gamma_\mu}\left(\frac{m_\mu}{m_\tau}\right)^5 \frac{|\delta'_{12}|^2}{|\delta'_{13}|^2} \simeq 5.63 \times \frac{|\delta'_{12}|^2}{|\delta'_{13}|^2}\,, \quad \frac{BR(\tau \to e\,\gamma)}{BR(\tau \to \mu\,\gamma)} \simeq \frac{|\delta'_{13}|^2}{|\delta'_{23}|^2}\,, \tag{6.24}$$

where Γ_μ and Γ_τ are the total decay widths of the μ and τ, respectively, and experimental values were taken on both of them. We verified numerically that the proportionality factor between $\mu \to e\,\gamma$ and $\tau \to e\,\gamma$ branching ratios was more accurately given by

$$\frac{BR(\mu \to e\,\gamma)}{BR(\tau \to e\,\gamma)} \simeq 4.69 \times \frac{|\delta'_{12}|^2}{|\delta'_{13}|^2}\,. \tag{6.25}$$

6.5 Seesaw parameters impact on LFV processes: a preliminary view

In here we will adopt the leading log approximation to assess qualitatively the seesaw parameters influence upon the LFV radiative decays $l_i \to l_j\,\gamma$ ($l_i \neq l_j$) and the LFV decays of the heaviest stau $\tilde{\tau}_2 \to l_i\, \tilde{\chi}_1^0$ ($l_i \neq \tau$), while comparing with a full numerical evaluation.

From δ'_{ji} given in (6.15) we define the quantities[6] $\bar{\delta}_{ij}$ - factoring the RH neutrino mass scale contribution $\tilde{M}_R \equiv M_R \ln \frac{M_R}{M_{GUT}}$ - to guide the study of the seesaw parameters impact on LFV processes[7]:

$$\tilde{M}_R\bar{\delta}_{21} \equiv v_u^2 \left[Y^\nu T Y^{\nu\dagger}\right]_{12} = m_3 f_{33} + \sqrt{m_3 m_2} f_{32} + m_2 f_{22} + \sqrt{m_3 m_1} f_{31} + \sqrt{m_2 m_1} f_{21} - m_1 f_{11}\,, \tag{6.26}$$

$$\tilde{M}_R\bar{\delta}_{31} \equiv v_u^2 \left[Y^\nu T Y^{\nu\dagger}\right]_{13} = m_3 f_{33} + \{\sqrt{m_3 m_2} f_{32} - m_2 f_{22} + \sqrt{m_3 m_1} f_{31} - \sqrt{m_2 m_1} f_{21} + m_1 f_{11}\}_{\delta\to\delta+\pi}\,, \tag{6.27}$$

$$\tilde{M}_R\bar{\delta}_{32} \equiv v_u^2 \left[Y^\nu T Y^{\nu\dagger}\right]_{23} = m_3 g_{33} + \sqrt{m_3 m_2} g_{32} - m_2 g_{22} + \sqrt{m_3 m_1} g_{31} + \sqrt{m_2 m_1} g_{21} - m_1 g_{11}\,, \tag{6.28}$$

where $T_{kk'} \equiv \delta_{kk'} \ln \frac{M_{k'}}{M_{GUT}}$. The decomposition of $\left[Y^\nu T Y^{\nu\dagger}\right]$ into sum-terms of light neutrino masses, as depicted above, is convenient to easily identify the main sources of LFV enhancement generated by the R-matrix in specific scenarios for the hierarchy of the light neutrinos. Moreover, the f_{ij} and g_{ij} functions, which depend on 4 undetermined U_{PMNS} parameters (three CPV phases and the reactor angle) plus the 6 R-matrix parameters, can be further scrutinized when considering a particular case for the RH neutrino mass spectrum. These functions, arranged in $\tilde{M}_k \equiv T_{kk'} M_{k'}$ sum-terms, are given by:

$$f_{33} = \frac{c_{13}s_{13}}{\sqrt{2}} e^{i\delta} \left\{ \tilde{M}_3 |c_1 c_2|^2 + \tilde{M}_2 |s_1 c_3 + c_1 s_2 s_3|^2 + \left(\tilde{M}_2 \to \tilde{M}_1 \wedge \theta_3 \to \theta_3 \pm \frac{\pi}{2}\right) \right\}, \tag{6.29}$$

$$\begin{aligned} f_{32} = \frac{1}{2\sqrt{3}} \Big\{ & \tilde{M}_3 \left(\sqrt{2} e^{\frac{i}{2}\phi_2} c_1^* s_1 + 2 s_{13} e^{-i\left(\frac{\phi_2}{2} - \delta\right)} c_1 s_1^* - 2\sqrt{2} s_{13}^2 e^{i\delta} \mathsf{Re}\left[e^{i\left(\frac{\phi_2}{2} - \delta\right)} c_1^* s_1 \right] \right) |c_2|^2 \\ & + \tilde{M}_2 \Big(-\sqrt{2} e^{\frac{i}{2}\phi_2} \left(c_1 c_3 - s_1 s_2 s_3\right) \left(s_1 c_3 + c_1 s_2 s_3\right)^* - 2 s_{13} e^{-i\left(\frac{\phi_2}{2} - \delta\right)} \left(c_1 c_3 - s_1 s_2 s_3\right)^* \left(s_1 c_3 + c_1 s_2 s_3\right) \\ & \quad + 2\sqrt{2} s_{13}^2 e^{i\delta} \mathsf{Re}\left[e^{-i\left(\frac{\phi_2}{2} - \delta\right)} \left(c_1 c_3 - s_1 s_2 s_3\right)^* \left(s_1 c_3 + c_1 s_2 s_3\right) \right] \Big) \\ & + \left(\tilde{M}_2 \to \tilde{M}_1 \wedge \theta_3 \to \theta_3 \pm \frac{\pi}{2}\right) \Big\}, \end{aligned} \tag{6.30}$$

$$f_{22} = \frac{c_{13}\left(2 - \sqrt{2} s_{13} e^{i\delta}\right)}{6} \left\{ \tilde{M}_3 |s_1 c_2|^2 + \tilde{M}_2 |c_1 c_3 - s_1 s_2 s_3|^2 + \left(\tilde{M}_2 \to \tilde{M}_1 \wedge \theta_3 \to \theta_3 \pm \frac{\pi}{2}\right) \right\}, \tag{6.31}$$

$$\begin{aligned} f_{31} = \frac{1}{2\sqrt{3}} \Big\{ & \tilde{M}_3 \left(2 e^{\frac{i}{2}\phi_1} c_1^* c_2^* s_2 - \sqrt{2} s_{13} e^{-i\left(\frac{\phi_1}{2} - \delta\right)} c_1 c_2 s_2^* - 4 s_{13}^2 e^{i\delta} \mathsf{Re}\left[e^{i\left(\frac{\phi_1}{2} - \delta\right)} c_1^* c_2^* s_2 \right] \right) \\ & + \tilde{M}_2 \Big(-2 e^{\frac{i}{2}\phi_1} c_2 s_3 \left(s_1 c_3 + c_1 s_2 s_3\right)^* + \sqrt{2} s_{13} e^{-i\left(\frac{\phi_1}{2} - \delta\right)} c_2^* s_3^* \left(s_1 c_3 + c_1 s_2 s_3\right) \\ & \quad + 4 s_{13}^2 e^{i\delta} \mathsf{Re}\left[e^{i\left(\frac{\phi_1}{2} - \delta\right)} c_2 s_3 \left(s_1 c_3 + c_1 s_2 s_3\right)^* \right] \Big) \\ & + \left(\tilde{M}_2 \to \tilde{M}_1 \wedge \theta_3 \to \theta_3 \pm \frac{\pi}{2}\right) \Big\}, \end{aligned} \tag{6.32}$$

$$\begin{aligned} f_{21} = \frac{c_{13}}{6} \Big\{ & \tilde{M}_3 \left(2\sqrt{2} e^{\frac{i}{2}(\phi_1 - \phi_2)} s_1^* c_2^* s_2 - \sqrt{2} e^{-\frac{i}{2}(\phi_1 - \phi_2)} s_1 c_2 s_2^* - 4 s_{13} e^{i\delta} \mathsf{Re}\left[e^{\frac{i}{2}(\phi_1 - \phi_2)} s_1^* c_2^* s_2 \right] \right) \\ & + \tilde{M}_2 \Big(2\sqrt{2} e^{\frac{i}{2}(\phi_1 - \phi_2)} c_2 s_3 \left(c_1 c_3 - s_1 s_2 s_3\right)^* - \sqrt{2} e^{-\frac{i}{2}(\phi_1 - \phi_2)} c_2^* s_3^* \left(c_1 c_3 - s_1 s_2 s_3\right) \\ & \quad - 4 s_{13} e^{i\delta} \mathsf{Re}\left[e^{\frac{i}{2}(\phi_1 - \phi_2)} c_2 s_3 \left(c_1 c_3 - s_1 s_2 s_3\right)^* \right] \Big) \\ & + \left(\tilde{M}_2 \to \tilde{M}_1 \wedge \theta_3 \to \theta_3 \pm \frac{\pi}{2}\right) \Big\}, \end{aligned} \tag{6.33}$$

$$f_{11} = \frac{c_{13}\left(1 + \sqrt{2} s_{13} e^{i\delta}\right)}{3} \left\{ \tilde{M}_3 |s_2|^2 + \tilde{M}_2 |c_2 s_3|^2 + \left(\tilde{M}_2 \to \tilde{M}_1 \wedge \theta_3 \to \theta_3 \pm \frac{\pi}{2}\right) \right\}, \tag{6.34}$$

and

$$g_{33} = \left(\frac{c_{13}}{\sqrt{2} s_{13}}\right) f_{33}|_{\delta=0}\,, \quad g_{22} = \left(1 + i\sqrt{2} s_{13} \sin\delta - \frac{1}{2} s_{13}^2\right) f_{22}|_{\theta_{13}=0}\,, \tag{6.35}$$

$$g_{11} = \left(\frac{1}{2} - i\sqrt{2} s_{13} \sin\delta - s_{13}^2\right) f_{11}|_{\theta_{13}=0}\,, \tag{6.36}$$

[6] In here we work with δ'_{ij} as opposed to δ'_{ji}. These quantities are equivalent since $\left[Y^\nu T Y^{\nu\dagger}\right]$ is hermitian and we are interested in the absolute values.

[7] For brevity we drop the superscript ^{0} in m_i^0, s_{13}^0 and δ^0 - the last two on f_{ij} and g_{ij}.

which have been decomposed in such a manner that s_{13} can be seen as a perturbative parameter in f_{ij} and g_{ij} for $i \neq j$. Note that $f_{33} \propto s_{13}$, which does not happen for any other f_{ij} nor does it happen for g_{ij}. For brevity we don't show the expressions for g_{ij} ($i \neq j$).

We note that the R-matrix parametrization, as in (3.27), and its appearance in $\left[Y^{\nu} T Y^{\nu\dagger}\right]$ is closely related to the order chosen to label the RH neutrino mass matrix. Clearly, the M_3 terms are independent of θ_3. Moreover, if one performs the permutation $1 \leftrightarrow 2$ in the RH neutrinos labelling, it is easy to see that by rotating around z an angle $\pi/2$, $\theta_3 \to \theta_3 \pm \pi/2$, everything is left unchanged. Specifically:

$$R^{\dagger}\mathcal{M}\,R = R^{\dagger}P_z^{-1}P_z\mathcal{M}\,P_z^{-1}P_z\,R\,, \quad P_z \equiv \pm\pi/2 \text{ rotation around z}\,. \tag{6.37}$$

This justifies why in the expressions for f_{ij} and g_{ij} the $\tilde{M}_1$ terms can be simply obtained from the $\tilde{M}_2$ terms, or vice-versa, by just performing the operation $\tilde{M}_2 \to \tilde{M}_1 \wedge \theta_3 \to \theta_3 \pm \pi/2$.

The dominant RH neutrino mass parameter, M_R, has the role of scaling LFV branching ratios proportionally[8], in particular, one can extract heuristically that for every 1 order of magnitude increment in M_R the LFV branching ratios grow 2 orders of magnitude. This can be seen from the dependence:

$$|\delta'_{ij}| \propto M_R \ln\frac{M_R}{M_{GUT}} \Rightarrow \left|\frac{\delta'_{ij}(M_R = 10^x)}{\delta'_{ij}(M_R = 10^y)}\right| = 10^{x-y}\left(\frac{x-m}{y-m}\right) \sim 10^{x-y}\,, \tag{6.38}$$

where $m \equiv \log(M_{GUT})$ (base-10 logarithm) and, obviously, $m > x, y$. A complete numerical analysis, see Fig:6.7 and Fig:6.8, clearly shows this scaling behaviour for both SNH and SIH light neutrinos.

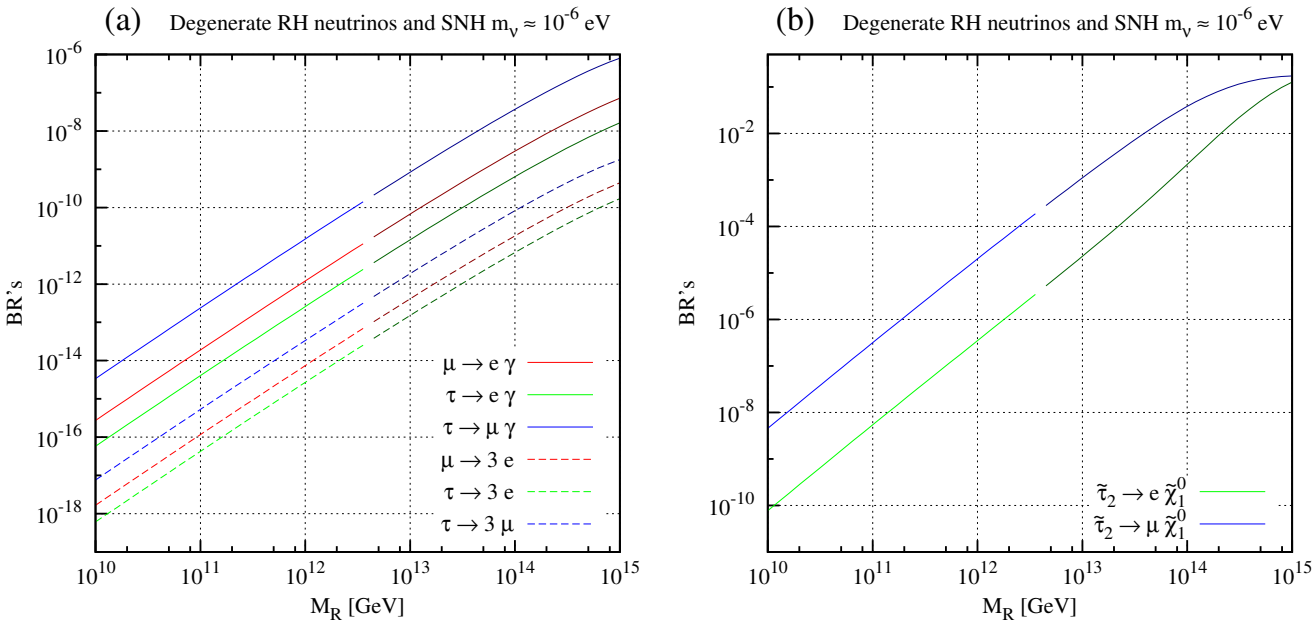

Figure 6.7: Branching ratios of the LFV radiative decays $l_i \to l_j\,\gamma$ (a) and heaviest stau decays (b) for SNH light neutrinos as a function of the RH neutrino mass scale. Parameters were set to: SPS1a', TBM mixing angles, degenerate RH neutrinos and $R = 1$. Shown in darker colours are the experimental excluded regions.

[8]This is not completely true in the case of dominant RH neutrinos, because not all the LFV branching ratios depend upon the dominant mass scale, M_R.

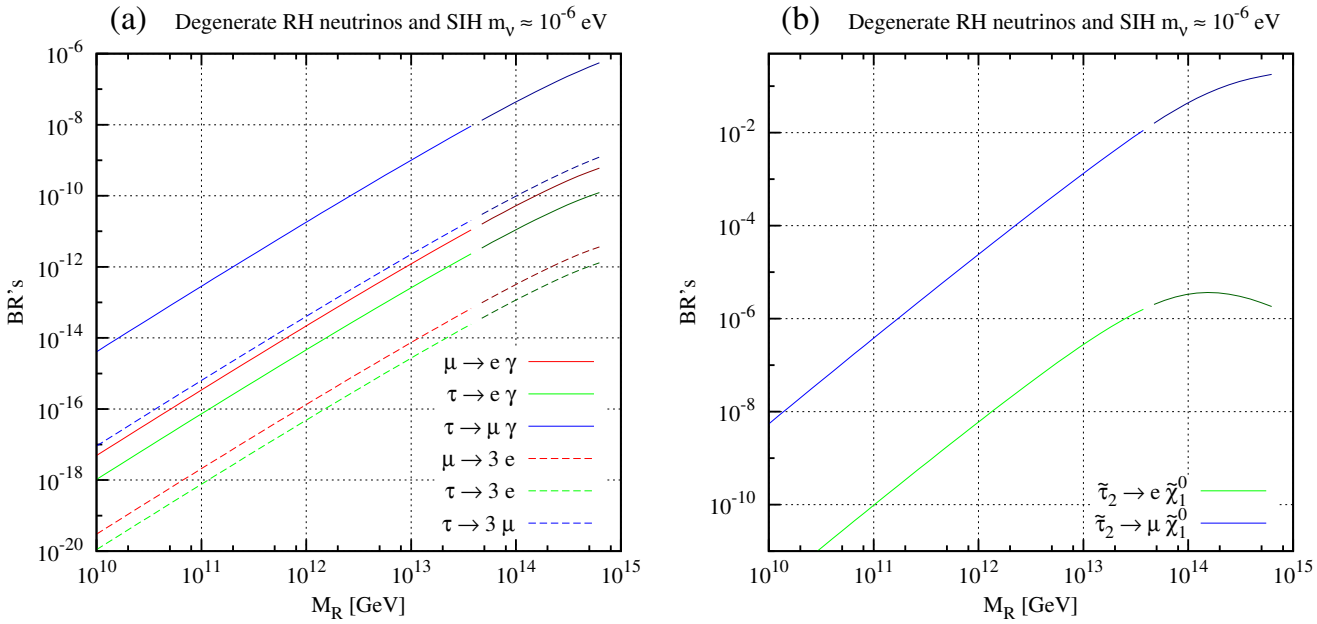

Figure 6.8: Same as in Fig:6.7 but for SIH light neutrinos.

However, for larger values of M_R this scaling behaviour is altered since one has sizable flavour violating terms in the slepton mass matrix. Thus, the small angle approximation fails and the fully diagonalization procedure must be accounted for.

Furthermore, we see that $BR(\tilde{\tau}_2 \to \mu\,\tilde{\chi}_1^0)$ can reach $\sim 10^{-4}$ for SNH and 10^{-2} for SIH. The reason for this distinction has to do with the lower $\mu \to e\,\gamma$ branching ratio for SIH light neutrinos (compare the left panels of Fig:6.7 and Fig:6.8) with the same settlement of parameters. We will return to this in section 6.6.1. Finally, we confirm that the ratio between $BR(l_i \to l_j\,\gamma)$ and $BR(l_i \to l_j\,\bar{l}_j\,l_j)$ is constant as in (6.2), a correlation that was verified throughout the parameter space explored in this work.

6.5.1 On the impact of subdominant RH neutrino masses

We have argued in the previous section that the LFV processes depend largely on the heaviest RH neutrino and very little on the other RH neutrino masses. However, this is not entirely true for some characteristical choices of parameters. Indeed, the smallness of the reactor angle can be an important suppression factor in the case of hierarchical RH neutrinos. This suppression could be further enhanced in the case of strictly hierarchical light neutrinos. This is shown in Fig:6.9, where for the SIH light neutrinos (right panel) the M_R parameter is doubly suppressed by $m^0_{\nu_3}$ and s^0_{13}. For SNH light neutrinos (left panel) the suppression is only set by the reactor angle because $m^0_{\nu_3}$ is the heaviest LH neutrino. One can understand what is happening by looking at (6.49).

In Fig:6.10 we show the LFV branching ratios dependence on the subdominant RH neutrino masses for SIH light neutrinos. It is clear that there is a direction $M_1 = M_2$ in the subdominant mass space where a significant increase in $BR(\tau \to \mu\,\gamma)$ can be achieved while keeping $BR(\mu \to e\,\gamma)$ low. This situation is analogous to the case of degenerate RH neutrinos, a subject to be discussed in section 6.6.1.

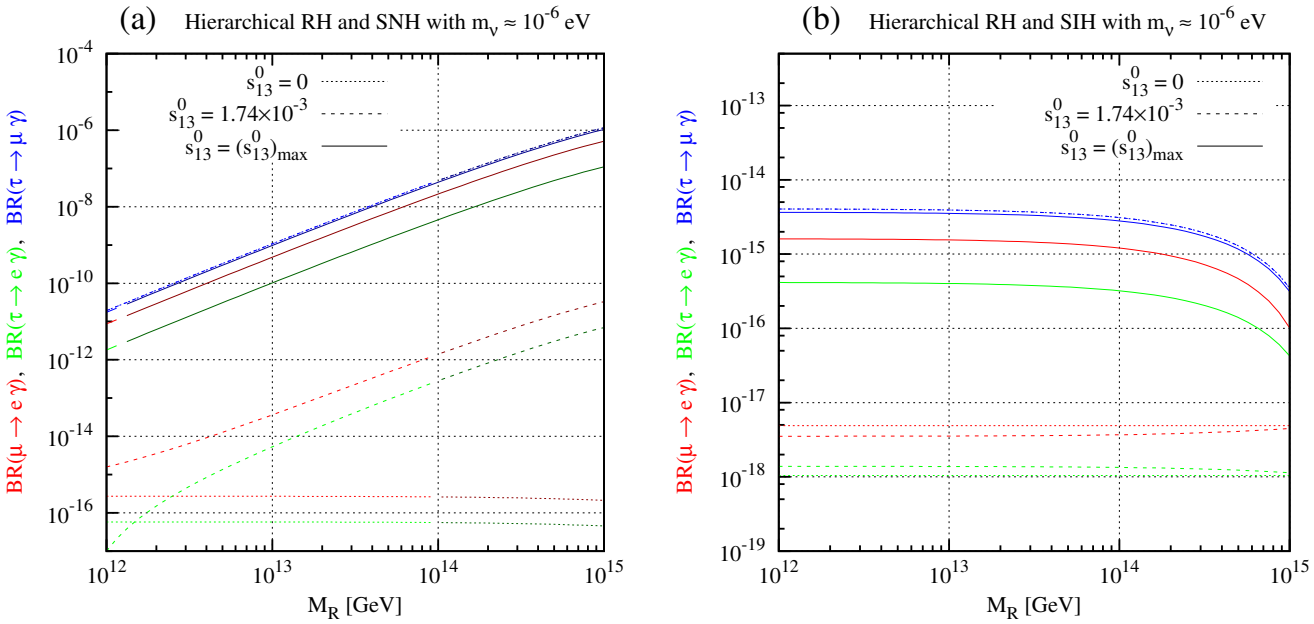

Figure 6.9: Branching ratios of the LFV radiative decays $l_i \to l_j\,\gamma$ for SNH (a) and SIH (b) light neutrino hierarchies as a function of the RH neutrino mass scale. Parameters were set to: SPS1a', TBM mixing angles, hierarchical RH neutrinos with $M \equiv M_1 = M_2 = 10^{10}$ GeV and $R = 1$. Shown in darker colours are the experimental excluded regions.

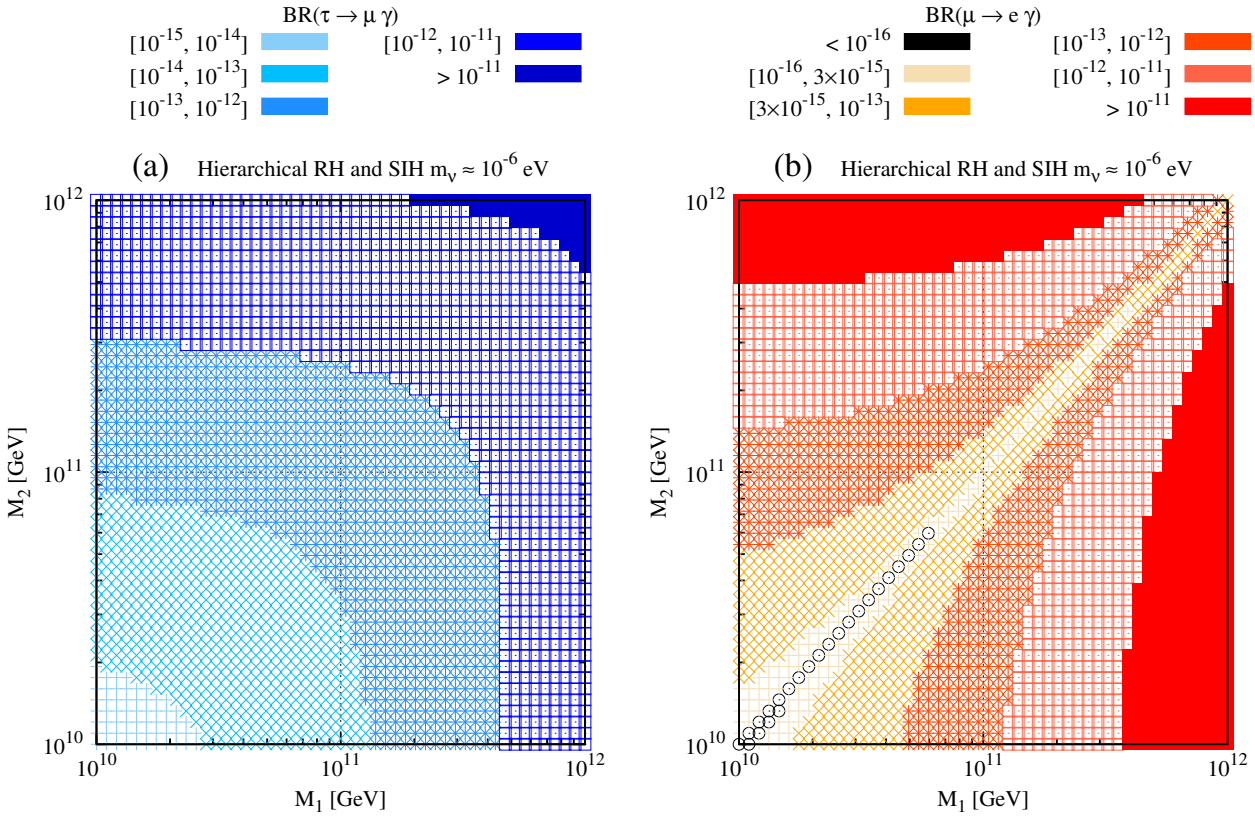

Figure 6.10: Contour regions for the branching ratios of the LFV radiative decays $\tau \to \mu\,\gamma$ (a) and $\mu \to e\,\gamma$ (b) for SIH light neutrinos as a function of the subdominant RH neutrino masses with $M_R = 10^{12}$ GeV. Remaining parameters were set as in Fig:6.9. Darker colours represent larger values (see colour legend).

Another subdominant situation comes from shifting M_3 with M_1 - achieved by a R-matrix of the form of (6.50) which we call $R = \text{dominant}_1$ - for SNH light neutrinos. In this case, the dominant mass scale will be suppressed by the lightest neutrino mass $m^0_{\nu_1}$ and the dominant RH masses will be M_1 for τ-μ transitions and M_2 for τ-e and μ-e transitions.

Concluding remarks

For hierarchical RH neutrinos the reactor angle suppression can only discriminate among LFV branching ratios - and be distinguishable from the case of absent M_R - in the following cases for the light neutrino hierarchies: SNH, QDNH and QDIH.

Moreover, the scenario of strong hierarchical RH neutrinos ($M_R \gg M_2 \simeq M_1$) can resemble the case of degenerate RH neutrinos if and only if we have strictly hierarchical light neutrinos. This occurs "naturally" ($R = 1$) for SIH light neutrinos and can also occur for SNH with $R = \text{dominant}_1$.

6.5.2 Organizing note

Solely from lifetime arguments $\Gamma_\tau^{-1} < \Gamma_\mu^{-1}$ and the mass of the decaying particles, $m_\tau > m_\mu$, one would expect that the relative size of the branching ratios of the LFV radiative decays obeys

$$BR(\mu \to e\,\gamma) > BR(\tau \to e\,\gamma) \simeq BR(\tau \to \mu\,\gamma)\,, \tag{6.39}$$

corresponding to $|\delta'_{ji}|$ quantities of roughly the same size - this is the natural scenario. However, the flavour information carried by s^0_{13} (the square root of the amount of electron-muon in the neutrino$_3$ mass eigenstate) can change the panorama and distinguish flavour transitions involving the electron-flavour from those of no electron-flavour. This is what we have come to see in the two preceding sections, with τ-μ flavour transitions dominating both τ-e and μ-e transitions, being related to the discriminative role of s^0_{13} suppression for $s^0_{13} \sim 0$ and as long as no double suppression occurs from the $m^0_{\nu_3}$ mass. Note that we are restricting ourselves to cases where $f_{ij} = g_{ij} = 0$ for $i \neq j$, see (6.26)-(6.28) and subsequent expressions.

In the previous section we have identified the situations where this discriminative s^0_{13} suppression can occur. We will see below that with degenerate RH neutrinos the reactor angle can also change the natural order (6.39), and this includes the degenerate-like hierarchical cases: SIH light neutrinos with $R = 1$ and SNH with $R = \text{dominant}_1$.

Moreover, from (6.26) and (6.27) it is clear that τ-e and μ-e flavour transitions have roughly the same size being any distinction among them played simultaneously by the reactor angle and the Dirac phase, $s^0_{13}e^{-i\delta^0}$. This is even valid for an arbitrary R-matrix. Thus, the relative size

$$BR(\mu \to e\,\gamma) > BR(\tau \to e\,\gamma)\,, \tag{6.40}$$

is a strong natural scenario.

In the following sections we will discuss the case of degenerate RH neutrinos with $R = 1$ (which, for the low energy LFV processes, is equivalent to real R) and hierarchical RH neutrinos with $R = 1$. Then, we will consider cases with $R \neq 1$ but still real (we will talk about R-matrices set to dominant$_1$ and

dominant$_2$) and end with the case of a completely general complex R-matrix. We will care to analyse the impact of (i) the reactor angle, (ii) the light neutrino hierarchies and (iii) the Dirac phase on the relative size of the LFV branching ratios.

6.6 Reference case: $R = 1$

The $R = 1$ case belongs to a broader class of R-matrices which guarantee that the mixed light neutrino mass terms in (6.26)-(6.28) vanish, i.e., $f_{ij} = g_{ij} = 0$ for $i \neq j$. In this class of R-matrices the dependence on Majorana phases drops out and the LFV seesaw parameters are reduced to 6 continuous parameters: s^0_{13}, δ^0, M_i and m_ν (the lightest neutrino mass); plus the hierarchy of the light neutrinos.

R-matrices of this class display a more pronounced sensitiveness to the light neutrino hierarchies and the reactor angle. We postpone to section 6.7.1 the discussion about this class.

6.6.1 Degenerate right-handed neutrinos

In spite of not being the preferable scenario for a successful BAU via thermal leptogenesis, one can establish a correspondence between hierarchical scenarios that display a degenerate-like behaviour. As noted previously, this can happen as long as the light neutrinos are strictly hierarchical. For instance, with SNH light neutrinos the case of degenerate RH neutrinos is similar to the $R = 1$ hierarchical case of $M_1 \ll M_2 \simeq M_3$ due to m_{ν_1} suppression. Similarly for SIH light neutrinos with $R =$ dominant$_1$, see (6.50), due to m_{ν_3} suppression.

From (6.26)-(6.28) with (6.29)-(6.36) one finds:

$$\bar{\delta}_{21} = \frac{s_{13}c_{13}}{\sqrt{2}} e^{i\delta} \left(\Delta m_{32} + \frac{2}{3}\Delta m_{21} \right) + \frac{c_{13}}{3}\Delta m_{21} \,, \tag{6.41}$$

$$\bar{\delta}_{31} = \frac{s_{13}c_{13}}{\sqrt{2}} e^{i\delta} \left(\Delta m_{32} + \frac{2}{3}\Delta m_{21} \right) - \frac{c_{13}}{3}\Delta m_{21} \,, \tag{6.42}$$

$$\bar{\delta}_{32} = \frac{c^2_{13}}{2} \left(\Delta m_{32} + \frac{2}{3}\Delta m_{21} \right) - \frac{1}{3} \left(\frac{1}{2} + i\sqrt{2} s_{13} \sin\delta \right) \Delta m_{21} \,, \tag{6.43}$$

where $\Delta m_{ij} \equiv m_i - m_j$. An effective GIM-like cancellation mechanism clearly appears for degenerate RH neutrinos, since in the limit of high degeneracy between light neutrino masses one expects rather low values for $|\bar{\delta}_{21}|$, $|\bar{\delta}_{31}|$ and $|\bar{\delta}_{32}|$, hence, for the LFV observables involving μ-e, τ-e and τ-μ flavour transitions. If one drops the degeneracy condition, the cancellation mechanism disappears, as it happens for hierarchical RH neutrinos (excluding degenerate-like hierarchical cases), and the LFV branching ratios will grow proportionally with the lightest neutrino mass, that is, with neutrino degeneracy.

The matrix element for the τ-μ flavour transition, $|\bar{\delta}_{32}|$, is always the larger of the off-diagonal elements. Moreover, the δ-oscillatory term gives rise to an enhancement that is negligible in face of the $\frac{\sqrt{2}}{3} s_{13}\Delta m_{21}$ suppression compared to the δ-constant term: $\frac{c^2_{13}}{2}\Delta m_{32}$ (recall that $|\Delta m_{32}| \gg \Delta m_{21}$, especially for SIH light neutrinos). So, the rates involving τ-μ flavour transitions are, to an excellent approximation, δ-independent and of the same size for both NH and IH light neutrino hierarchies.

Turning to μ-e and τ-e flavour transitions, note the obvious symmetry in the above expressions: $|\bar{\delta}_{21}| = |\bar{\delta}_{31}|_{\delta\to\delta+\pi} = |\bar{\delta}_{31}|_{s_{13}\to -s_{13}}$. Moreover, we know that for NH(IH) light neutrinos one has $\Delta m_{32} >$

$0 (< 0)$. Thus, one concludes categorically that:

$$\begin{cases} |\bar{\delta}_{32}| > |\bar{\delta}_{21}| = |\bar{\delta}_{31}| \,, & \text{for } |\delta| = \pi/2 \,; \\ |\bar{\delta}_{32}| > |\bar{\delta}_{21}| > |\bar{\delta}_{31}| \,, & \text{for } (\, |\delta| < \pi/2 \wedge (\text{SNH} \vee \text{QDNH}) \,) \vee (\, \pi/2 < |\delta| \leq \pi \wedge (\text{SIH} \vee \text{QDIH}) \,) \,; \\ |\bar{\delta}_{21}| < |\bar{\delta}_{31}| < |\bar{\delta}_{32}| \,, & \text{for } (\, |\delta| < \pi/2 \wedge (\text{SIH} \vee \text{QDIH}) \,) \vee (\, \pi/2 < |\delta| \leq \pi \wedge (\text{SNH} \vee \text{QDNH}) \,) \,. \end{cases}$$

The matrix elements $|\bar{\delta}_{21}|$ and $|\bar{\delta}_{31}|$ will, in general, be higher for SNH than for SIH light neutrinos due to the size of the mass difference Δm_{21}.

The role of the δ-constant term depends crucially on the size of the mass difference Δm_{21} compared to $|\Delta m_{32}|$, which controls the δ-oscillatory term. Since $|\Delta m_{32}|$ is always higher than Δm_{21}, the mean oscillatory value of both $|\bar{\delta}_{21}|$ and $|\bar{\delta}_{31}|$ for $s_{13} \neq 0$ will be greater than the corresponding values in the $s_{13} = 0$ limit. For SIH and QD-type light neutrinos the mass difference Δm_{21} is always very small compared to $|\Delta m_{32}|$, making the $s_{13} \neq 0$ case be greatly enhanced relative to the $s_{13} = 0$ case. This enhancement is more moderate for SNH light neutrinos, since Δm_{32} and Δm_{21} are roughly of the same order of magnitude. This is confirmed in Fig:6.11.

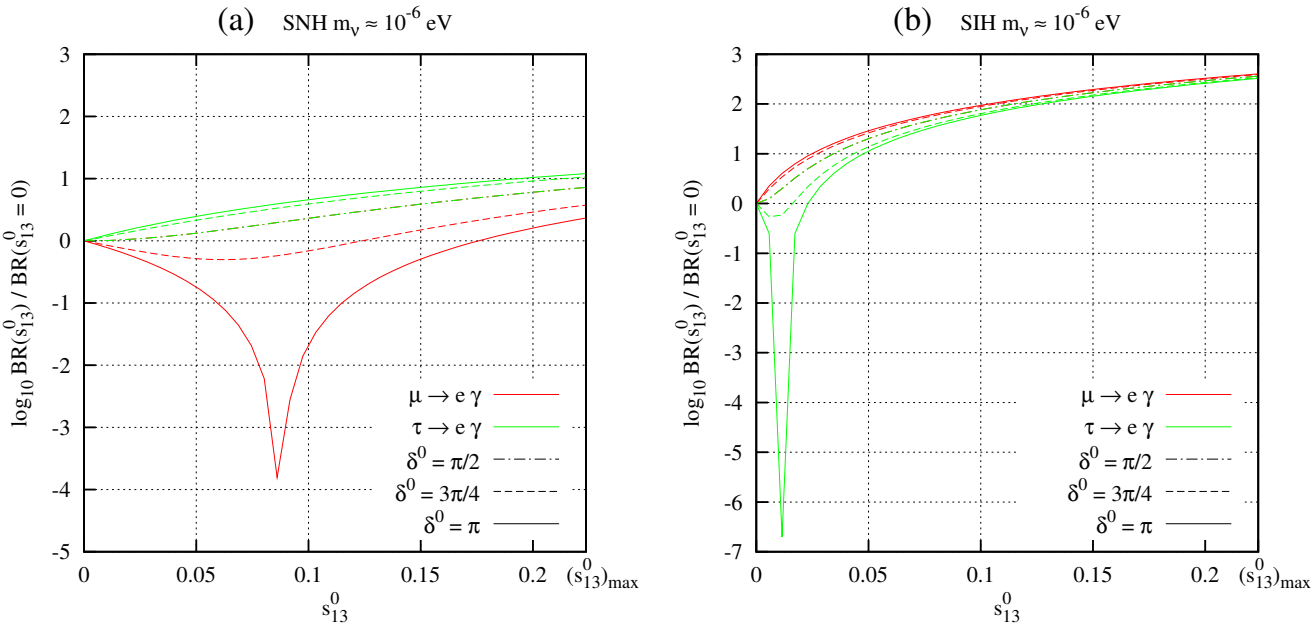

Figure 6.11: s^0_{13} influence over the branching ratios of the LFV radiative decays $\mu \to e\,\gamma$ and $\tau \to e\,\gamma$ for SNH (a), SIH (b) light neutrino hierarchies. Parameters were set to: SPS1a', TBM mixing angles except s^0_{13} and δ^0, degenerate RH neutrinos with $M_R = 10^{12}$ GeV and $R = 1$.

In the parameter space of the flavour transitions involving the electron-flavour there is an unnatural[9] cancellation region between the δ-oscillatory term and the δ-constant term. This occurs when θ_{13} is set such that with $|\delta| = 0$ or π we have $|\bar{\delta}_{21}|$ or $|\bar{\delta}_{31}|$, but not both, vanishing. Concretely:

$$s_{13} = \frac{\sqrt{2}}{|3a + 2|} \,, \quad a \equiv \frac{\Delta m_{32}}{\Delta m_{21}} \,, \tag{6.44}$$

[9]Unnatural in the sense that, to occur, two unrelated quantities must be simultaneously tuned.

and, due to s_{13} experimental bounds, this may happen as long as

$$\left|\frac{\Delta m_{32}}{\Delta m_{21}}\right| \geq \frac{\sqrt{2}}{3 s_{13}^{max}} + \frac{2}{3} \simeq 2.77\,, \tag{6.45}$$

being always satisfied. For SNH one can have a region of unnatural cancellation for s_{13} relatively high (~ 0.09) while for SIH this happens with $s_{13} \sim 0.008$, see Fig:6.11. For QD-type hierarchies we would expect $s_{13} \sim 0.015$ but due to running effects on Δm_{21}, as we have discussed earlier, this region occurs for $s_{13} \sim 0.05$.

Moreover, the Dirac phase acts as a shifter of the relative size between μ-e and τ-e flavour transitions, as can be seen in Fig:6.11. The δ^0 and s_{13}^0 role in the strong representative scenario chosen for the QD-type hierarchies is roughly the same for QDIH and QDNH, however in the QDNH one can achieve a comparatively small but higher enhancement. In the case of strictly hierarchical light neutrinos this difference is more pronounced: for SIH one can achieve a ~ 2.5 orders of magnitude enhancement compared to ~ 1 in the SNH case. In contrast, the unnatural cancellation region is wider for the latter, as it is the difference between μ-e and τ-e flavour transitions.

We turn now to the study of the relative size of the LFV branching ratios, setting M_R such that the experimental bounds on $BR(\mu \to e\,\gamma)$ and $BR(\tau \to \mu\,\gamma)$ are saturated - Fig:6.12. We see that for SIH light neutrinos one expects larger values for $BR(\tau \to \mu\,\gamma)$, i.e., for rates involving τ-μ flavour transitions. This is justified by smaller rates on $BR(\mu \to e\,\gamma)$ due to the smaller values of $|\bar{\delta}_{21}|$ in the case of SIH light neutrinos compared to the SNH case. The QD-type hierarchies are once more very similar and one expects that $BR(\tau \to \mu\,\gamma)$, in the low s_{13} regime, ~ 1 order magnitude higher than in the case of SNH light neutrinos.

We have also checked that the branching ratios drop with increasing lightest neutrino mass scale, see Fig:6.13. The exceptions are the previously referred cancellation regions (left panel $s_{13}^0 = 7.5 \times 10^{-2}$ and right panel $s_{13}^0 = 1 \times 10^{-2}$). Moreover, there is a noticeable exception in the inverted hierarchy for $s_{13}^0 \approx 0$, which is simply justified by the fact that Δm_{21}^0, which dominates $|\bar{\delta}_{21}|$ and $|\bar{\delta}_{31}|$ in this regime, changes very little in the inverted hierarchy. Nevertheless, at large m_ν one would still expect a significant drop in the branching ratios, since Δm_{21}^0 would decrease considerably. This departure from analytical considerations in the region of large lightest neutrino mass, $m_\nu \approx 6.5 \times 10^{-2}$ eV, comes from the RGE running effects involved in the fitting procedure of the low energy mass splittings, see Fig:6.3 and related discussion.

Concluding remarks

For degenerate RH neutrinos with $R = 1$ the relative size of the LFV branching ratios is highly sensitive to paired variations arranged in the following two cases:

1. the light neutrino hierarchies vs s_{13}^0: setting the relative size of τ-μ vs μ-e flavour transitions;
2. s_{13}^0 vs δ^0 for SNH light neutrinos: setting the relative size of μ-e vs τ-e flavour transitions.

The reactor angle affects significantly the LFV branching ratios involving μ-e and τ-e flavour transitions and is completely negligible for τ-μ. The Dirac phase can shift the s_{13}^0 role, a shift whose amount is set by the size of $|a|^{-1}$, defined in (6.44).

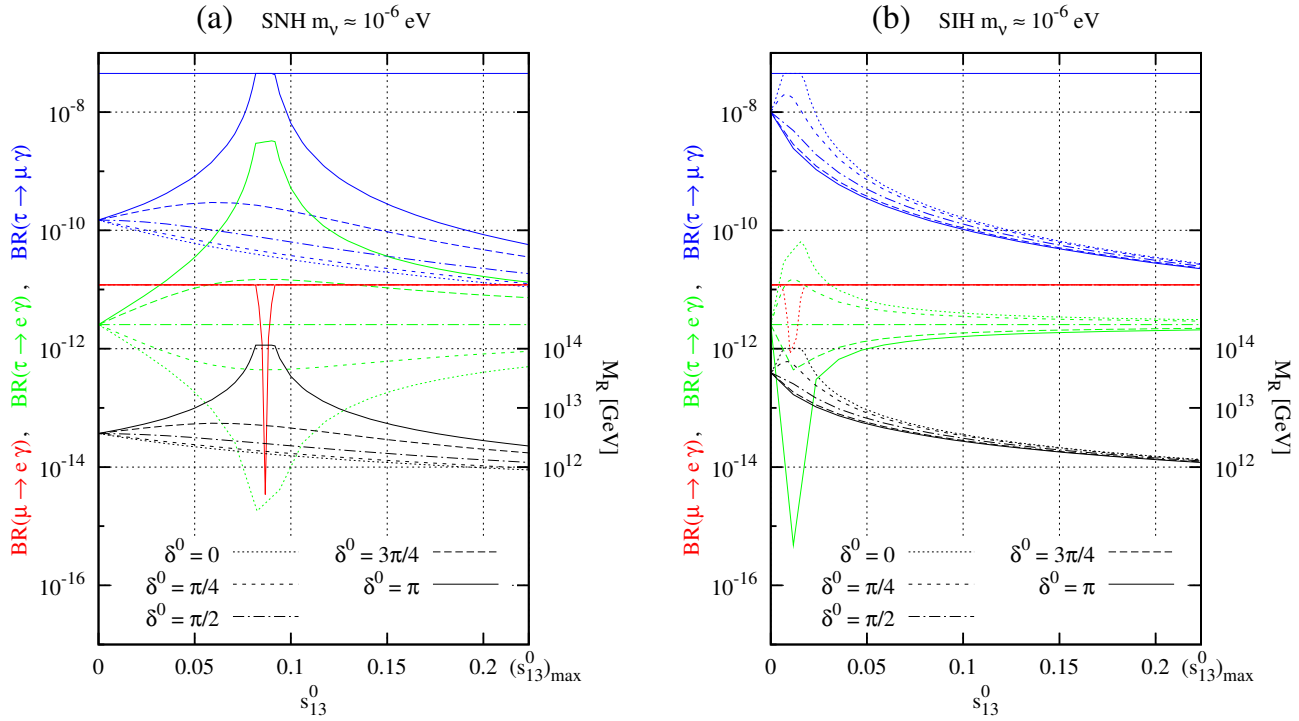

Figure 6.12: Branching ratios of the LFV radiative decays $l_i \to l_j\,\gamma$ for SNH (a) and SIH (b) light neutrino hierarchies as a function of s^0_{13}. The RH neutrino mass scale (black colour) was set to saturate the experimental bounds on $BR(l_i \to l_j\,\gamma)$. In most part of the s^0_{13} parameter space the limitative role was played by $BR(\mu \to e\,\gamma)$ and in the narrow "unnatural cancellation region" by $BR(\tau \to \mu\,\gamma)$ (see text). Remaining parameters were set as in Fig:6.11.

The ordering of the branching ratios of the LFV radiative decays differ from the natural ordering of (6.39), specifically:

$$BR(\tau \to \mu\,\gamma) > BR(\mu \to e\,\gamma) > BR(\tau \to e\,\gamma)\,, \tag{6.46}$$

a consequence of the s^0_{13} discriminative role. When $|a|^{-1}$ is sizable, as it happens for SNH and QD-type light neutrinos, the ordering of (6.39) can be further altered when the Dirac phase is large, $|\delta| > 3\pi/4$,

$$BR(\mu \to e\,\gamma) < BR(\tau \to e\,\gamma)\,, \tag{6.47}$$

for moderate s^0_{13} (for e.g. $0.025 \lesssim s^0_{13} \lesssim 0.15$ for QD-type and $0.075 \lesssim s^0_{13} \lesssim (s^0_{13})_{max}$ for SIH light neutrinos, with $|\delta| = \pi$). Moreover, in the limit of high s^0_{13} and very large $|a|^{-1}$, as in SNH light neutrinos, one can get

$$BR(\tau \to \mu\,\gamma) \approx BR(\mu \to e\,\gamma)\,, \tag{6.48}$$

for $|\delta| < \pi/4$. The following case is excluded: $BR(\tau \to e\,\gamma) \gtrsim BR(\tau \to \mu\,\gamma)$.

Independently of determining the mSUGRA point one can say that if the rate of a μ-e flavour transition is larger than that of a τ-μ flavour transition for the same type of process, then high δ^0 is favoured and SIH light neutrinos is disfavoured. If additionally one determines the neutrino mass scale and the hierarchy type then we would set a favoured range for s^0_{13}, or the other way around: from determining s^0_{13} and guessing the hierarchy type or even the neutrino mass scale.

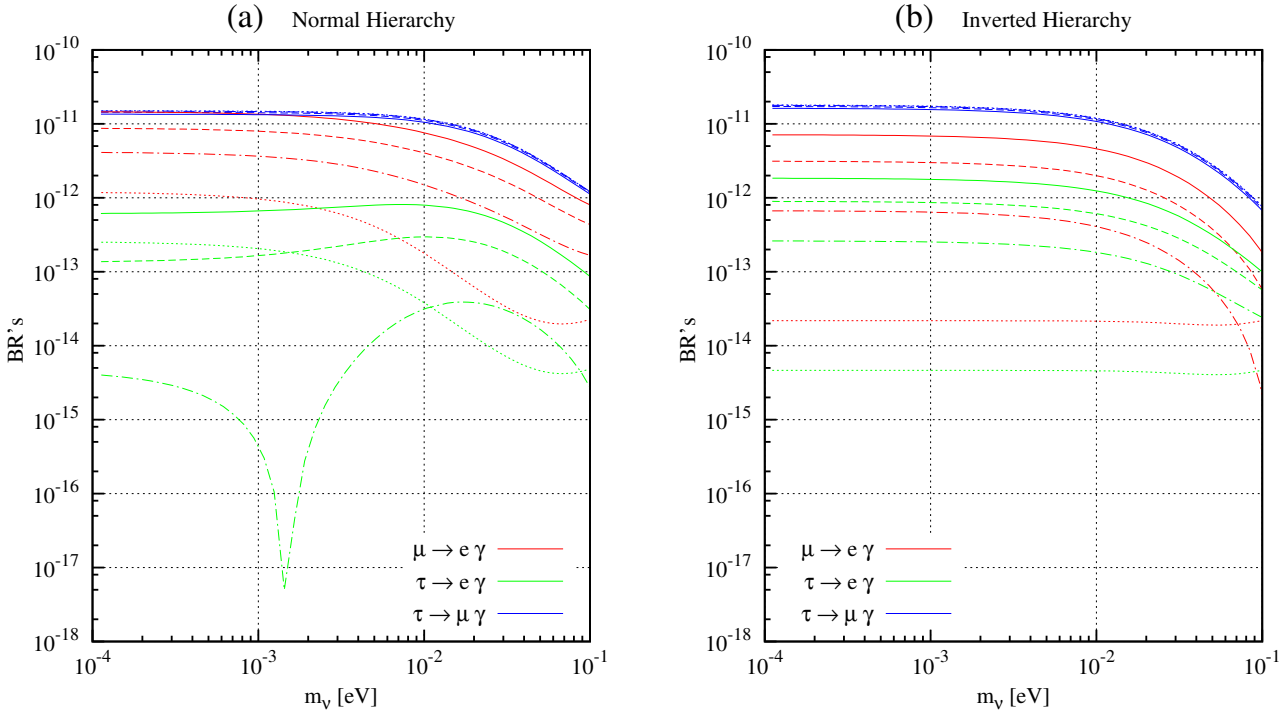

Figure 6.13: Branching ratios of the LFV radiative decays $l_i \to l_j\,\gamma$ as a function of the lightest neutrino mass scale m_ν, for both normal (a) and inverted (b) light neutrino hierarchies. Parameters were set to: SPS1a', TBM mixing angles except for s^0_{13} ($\delta^0 = 0$), degenerate RH neutrinos and $R = 1$. The type of line code is the same as in Fig:6.2.

If the mSUGRA point is known and it has a light mass spectrum (as SPS1a') then the RH neutrino mass scale is already constrained from above by the experimental bounds on radiative LFV decays. If one is able to measure $BR(\mu \to e\,\gamma)$ and other process involving a τ-μ flavour transition, a hint on both the light neutrino hierarchy and the mSUGRA point can be determined.

6.6.2 Hierarchical right-handed neutrinos

In the case of hierarchical RH neutrinos the s^0_{13} role in distinguishing τ-μ from τ, μ-e is even more striking and the δ^0 influence is lost as the mass degeneracy is lifted. Indeed, in the limit of not very small m_3 one has:

$$\bar{\delta}_{21} \simeq m_3 \frac{c_{13}s_{13}}{\sqrt{2}} e^{i\delta}\,, \quad \bar{\delta}_{31} \simeq m_3 \frac{c_{13}s_{13}}{\sqrt{2}} e^{i\delta}\,, \quad \bar{\delta}_{32} \simeq m_3 \frac{c^2_{13}}{2}\,, \tag{6.49}$$

which is always satisfied for QD-type and SNH hierarchies. For the SIH we are in an analogous situation to that of degenerate RH neutrinos with M_R being irrelevant - see panel (b) of Fig:6.14.

In the case of SNH light neutrinos - panel (a) of Fig:6.14 - one can achieve a ~ 4 orders of magnitude separation between τ-μ and μ-e flavour transitions for $s^0_{13} \sim 0$. This separation is reduced for increasing s^0_{13} and for $s^0_{13} > 0.1$ we are in a situation very similar to that of degenerate RH neutrinos with SIH light neutrinos. In the vanishing s^0_{13} limit the experimental bound on $BR(\tau \to \mu\,\gamma)$ already points towards $BR(\mu \to e\,\gamma) \lesssim 10^{-12}$, while bounding the RH neutrino mass scale $M_R \lesssim 10^{14}$ GeV. Moreover, the ordering of (6.46) is assured.

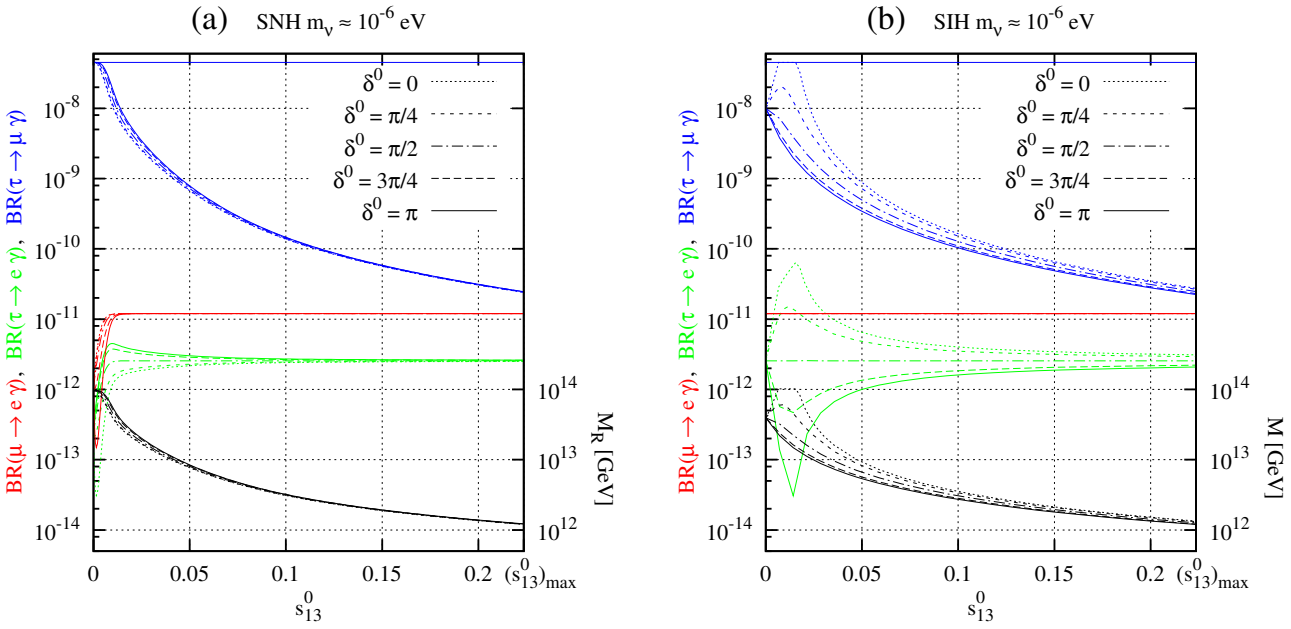

Figure 6.14: Branching ratios of the LFV radiative decays $l_i \to l_j\,\gamma$ for SNH (a) and SIH (b) light neutrino hierarchies as a function of s^0_{13}. In (a) the RH neutrino mass scale M_R (black colour) was set to saturate the experimental bounds on $BR(l_i \to l_j\,\gamma)$, while $M \equiv M_1 = M_2 = 10^{-2} M_R$. Similarly in (b) for $M \equiv M_1 = M_2$ mass (black colour), while M_R is arbitrary. In most part of the s^0_{13} parameter space the limitative role was played by $BR(\mu \to e\,\gamma)$. In the narrow low s^0_{13} region the limitative role was played by $BR(\tau \to \mu\,\gamma)$. Remaining parameters were set to: SPS1a', TBM mixing angles except s^0_{13} and δ^0, $R = 1$.

6.7 R-matrix analysis

In this section we will analyse the impact of a general complex R-matrix upon the LFV rates and establish a comparison to the phenomenology of the specific R-matrix scenarios we have been discussing. Due to the complex nature of the R-matrix angles one can generally say that a deviation from identity can be characterized by three types of impacts on the $|\delta'_{ij}|$ $(i \neq j)$ matrix elements:

1. Moderate sinusoidal influence when all the phases or the absolute values are small;
2. Large enhancement proportional to $\cosh^2|\theta|$, which can represent a maximum shift of about ~ 3 orders of magnitude for $|\theta| \sim 3$;
3. Large reduction due to the cancellation between terms.

We will explore the case 1 in the limit of a real R-matrix and for the case 2 we will consider the most general form of a complex R-matrix. We will discard the third case because the cancellations are unstable under small variations of parameters, such as the light neutrino masses.

6.7.1 Case 1: real R

The study of an arbitrary real R-matrix is more easily done by selecting limiting cases, such that any arbitrary real R-matrix can be envisioned as a qualitative linear combination of these limiting cases. Thus, we chose for these limiting cases the class of real R-matrices which guarantee that the product

$R^T \mathcal{M} R^*$ is diagonal[10]. One of such cases has already being studied, $R = 1$. The remaining cases are the permutations of elements of the diagonal matrix $\mathcal{M}$.

Two of these permutations are $M_1 \leftrightarrow M_3$ (dominant$_1$) and $M_2 \leftrightarrow M_3$ (dominant$_2$), concretely:

$$\text{dominant}_1\text{:} \quad \theta_2 = \tfrac{\pi}{2}\,, \quad \theta_1 = 0\,, \quad \theta_3 = 0\,, \tag{6.50}$$

$$\text{dominant}_2\text{:} \quad \theta_1 = \tfrac{\pi}{2}\,, \quad \theta_2 = 0\,, \quad \theta_3 = 0\,. \tag{6.51}$$

The permutation involving the subdominant RH neutrino masses, $M_1 \leftrightarrow M_2$, and R-matrices formed by a composition of permutations, can be reduced to the cases we have considered.

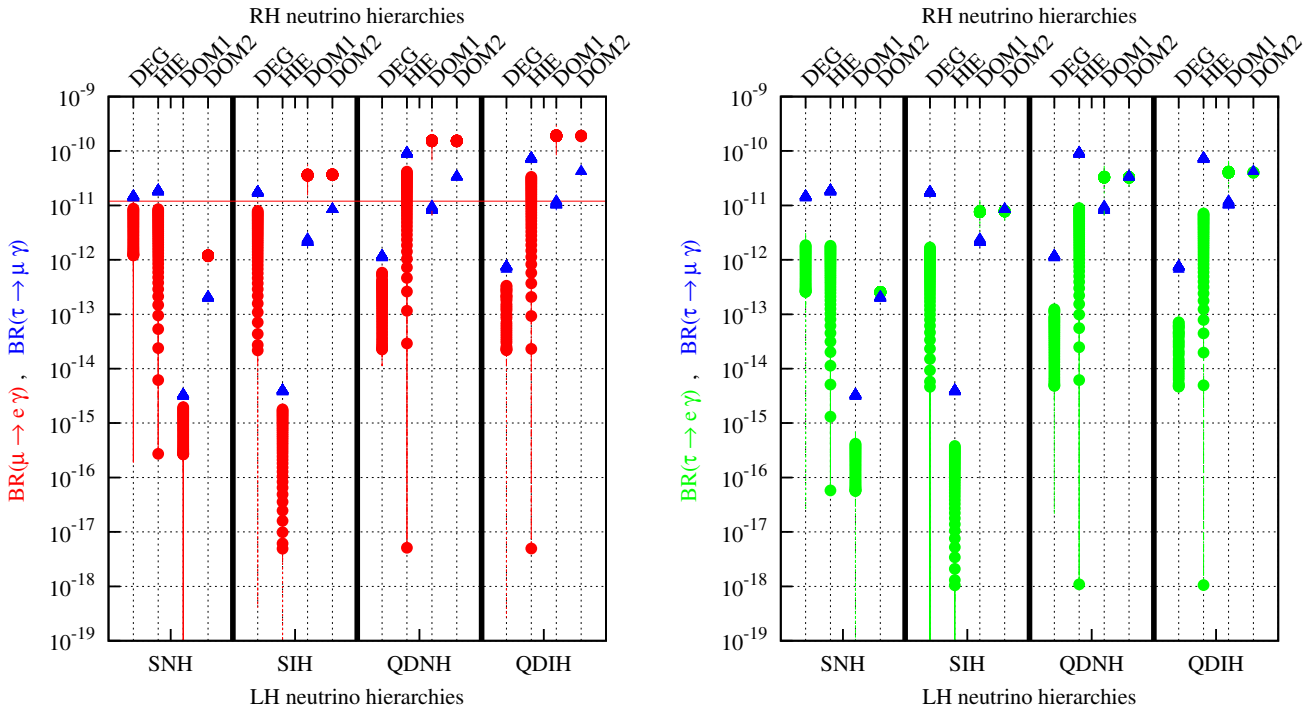

Figure 6.15: Branching ratios of the LFV radiative decays for LH neutrino hierarchies (SNH, SIH, QDNH and QDIH) and RH neutrino hierarchies (DEG, HIE, DOM1 and DOM2 - see text). The branching ratio range shown for each pair {LH hierarchy, RH hierarchy} comprehends a variation of $0 \leq s^0_{13} \leq (s^0_{13})_{max}$ for 4 different values of $\delta^0 = 0, \pi/4, \pi/2, \pi$. Points with $\delta^0 = \pi/2$ are shown as blue triangles, red circles and green circles. Parameters were set to: SPS1a', TBM mixing angles except s^0_{13} and δ^0, RH neutrino masses $M_R = 10^{12}$ GeV and $M = 10^{10}$ GeV. The horizontal red line in the left panel is the experimental upper bound on $BR(\mu \to e\,\gamma)$.

With the exception of SNH light neutrinos for $R = \text{dominant}_1$, we have:

$$\text{dominant}_1 \begin{cases} \bar{\delta}_{21} \simeq -\frac{m_1 c_{13}}{3}\left(1 + \sqrt{2} s_{13} e^{i\delta}\right)\,, \quad \bar{\delta}_{31} \simeq \frac{m_1 c_{13}}{3}\left(1 - \sqrt{2} s_{13} e^{i\delta}\right)\,, \\ \bar{\delta}_{32} \simeq -\frac{m_1}{6}\left(1 - 2i\sqrt{2} s_{13} \sin\delta - 2 s^2_{13}\right)\,, \end{cases} \tag{6.52}$$

$$\text{dominant}_2 \begin{cases} \bar{\delta}_{21} \simeq \frac{m_2 c_{13}}{6}\left(2 - \sqrt{2} s_{13} e^{i\delta}\right)\,, \quad \bar{\delta}_{31} \simeq -\frac{m_2 c_{13}}{6}\left(2 + \sqrt{2} s_{13} e^{i\delta}\right)\,, \\ \bar{\delta}_{32} \simeq -\frac{m_2}{6}\left(2 + 2i\sqrt{2} s_{13} \sin\delta - s^2_{13}\right)\,. \end{cases} \tag{6.53}$$

None of these matrix elements show the type of discriminative suppression as in the $R = 1$ hierarchical

[10]Note that the interesting case is that of hierarchical RH neutrinos, otherwise any real R-matrix is equivalent to any other since R is orthogonal

case. Therefore, we expect the branching ratios to follow the natural ordering of (6.39), with a very small influence of the reactor angle and the Dirac phase.

In Fig:6.15 we show a compilation of the branching ratios of the LFV radiative decays for each RH neutrino scenario we have been discussing, arranged into four groups of light neutrino hierarchies. We see that (i) in non degenerate-like RH neutrinos the branching ratios grow with the light neutrino degeneracy, (ii) with hierarchical RH neutrinos and QD-type light neutrinos we can have a separation of ~ 6 orders of magnitude between τ-μ and τ-e flavour transitions, (iii) QD-type hierarchies are similar. Moreover, the remarks made in the preceding paragraph are confirmed.

6.7.2 Case 2: general R

The influence of a general complex R-matrix can only be isolated from the heavy mass parameter M_R if the enhancement - in comparison to the $R = 1$ case - is not universal, i.e., if the contribution to the matrix elements $\bar{\delta}_{32}$, $\bar{\delta}_{32}$ and $\bar{\delta}_{32}$ distinguishes them. This can easily be seen by, for instance, considering that we work with a certain R-matrix form which enhances all the mass matrix elements in the same manner, thus, from (6.38) we see that this is equivalent to setting $R = 1$ and augment M_R. Therefore, we define the relevant quantities for studying the R-matrix impact on the LFV observables:

$$\tilde{\mathcal{R}}_{32} = \frac{BR(\tau \to \mu\,\gamma)}{BR(\mu \to e\,\gamma)}\,, \quad \tilde{\mathcal{R}}_{31} = \frac{BR(\tau \to e\,\gamma)}{BR(\mu \to e\,\gamma)}\,, \quad \tilde{\mathcal{R}}_{21} = \frac{BR(\mu \to e\,\gamma)}{BR(\mu \to e\,\gamma)|_{R=1}}\,, \tag{6.54}$$

and

$$\mathcal{R}_{ijmn} \equiv \frac{\tilde{\mathcal{R}}_{ij}}{\tilde{\mathcal{R}}_{mn}\Big|_{R=1}}\,. \tag{6.55}$$

The choice of $BR(\mu \to e\,\gamma)$ for the comparison element is motivated by its stringent experimental upper bound. For instance, if one concludes that a particular choice for the R-matrix results in $\mathcal{R}_{3232} = 10^a$, then, even if that choice increases both $|\bar{\delta}_{32}|$ and $|\bar{\delta}_{21}|$ we can always set M_R so that we lower $|\bar{\delta}_{21}|$ (and likewise $|\bar{\delta}_{32}|$) to respect the experimental bound on $BR(\mu \to e\,\gamma)$. Then, we can claim that the R-matrix presence allows a separation between τ-μ and μ-e flavour transitions that is approximately a orders of magnitude higher than that of $R = 1$.

In a first step we studied, via the LFV radiative decays, correlations between τ-μ, μ-e and τ-e flavour transitions, by spawning randomly the 6-dimensional R-matrix parameter space within the bounds referred in (6.6). Some representative results are shown in Fig:6.16, for SNH light neutrinos with both hierarchical and degenerate RH neutrinos.

We observed that the correlation between μ-e and τ-e flavour transitions is strong, since (i) the mean value of $BR(\mu \to e\,\gamma)/BR(\tau \to e\,\gamma)$ is stable under s^0_{13} variations and (ii) the spread around the mean value is small in comparison to $BR(\tau \to \mu\,\gamma)/BR(\mu \to e\,\gamma)$ and $BR(\tau \to \mu\,\gamma)/BR(\tau \to e\,\gamma)$. Indeed, the ratio follows closely the natural ordering $BR(\mu \to e\,\gamma)/BR(\tau \to e\,\gamma) \sim 4.69$, see expression (6.25).

In Table:6.4 we list the mean values and the extremes corresponding to 1σ deviations, above and below the mean, for 3 values of s^0_{13} and limiting cases of δ^0.

Moreover, the correlations for the case of hierarchical RH neutrinos are very similar to that of degenerate RH neutrinos. The only distinction between them is the higher spread of the former in the limit of

		slope $\left\langle \frac{BR(\tau\to\mu\,\gamma)}{BR(\mu\to e\,\gamma)} \right\rangle$		slope $\left\langle \frac{BR(\mu\to e\,\gamma)}{BR(\tau\to e\,\gamma)} \right\rangle$		slope $\left\langle \frac{BR(\tau\to\mu\,\gamma)}{BR(\tau\to e\,\gamma)} \right\rangle$	
s^0_{13}	δ^0	DEG	HIE	DEG	HIE	DEG	HIE
1.74×10^{-3}	0	$2.86^{+6.18}_{-1.96}$	$3.17^{+12.03}_{-2.51}$	$4.70^{+5.68}_{-2.57}$	$4.76^{+5.31}_{-2.51}$	$13.46^{+29.90}_{-9.28}$	$15.07^{+57.23}_{-11.93}$
3×10^{-2}	0	$2.75^{+5.65}_{-1.85}$	$2.93^{+9.39}_{-2.23}$	$5.04^{+6.16}_{-2.77}$	$4.86^{+6.39}_{-2.76}$	$13.85^{+31.07}_{-9.58}$	$14.25^{+43.86}_{-10.75}$
	π	$2.90^{+6.38}_{-1.99}$	$3.09^{+9.69}_{-2.34}$	$4.50^{+5.44}_{-2.46}$	$4.55^{+4.91}_{-2.36}$	$13.05^{+28.32}_{-8.93}$	$14.07^{+45.57}_{-10.75}$
$(s^0_{13})_{max}$	0	$1.09^{+1.44}_{-0.62}$	$1.18^{+2.00}_{-0.74}$	$5.36^{+5.48}_{-2.71}$	$4.67^{+5.11}_{-2.44}$	$5.84^{+5.25}_{-2.77}$	$5.51^{+5.37}_{-2.72}$
	π	$1.25^{+1.19}_{-0.61}$	$1.19^{+1.15}_{-0.58}$	$4.21^{+4.54}_{-2.18}$	$4.65^{+4.74}_{-2.35}$	$5.26^{+7.26}_{-3.05}$	$5.54^{+9.20}_{-3.46}$

Table 6.4: Average slopes taken from datasets with 3000 random points in the R-matrix parameter space ($|\theta_i| \leq 3$ and $|\arg\theta_i| \leq \pi$). 1σ deviation extremes, above and below the mean, are shown. Each dataset corresponds to a choice of $\{s^0_{13}, \delta^0,$ RH hierarchy$\}$. Parameters were set to: SPS1a', TBM mixing angles except s^0_{13} and δ^0, SNH light neutrinos with $m_\nu \approx 10^{-6}$ eV and RH neutrino masses $M_R = 10^{12}$ GeV and $M \equiv M_1 = M_2 = 10^{10}$ GeV.

very small s^0_{13}. This is related to what we have seen previously: the higher separation between τ-μ and μ-e flavour transitions is achieved in scenarios with hierarchical RH neutrinos and $R = 1$, especially for small s^0_{13}.

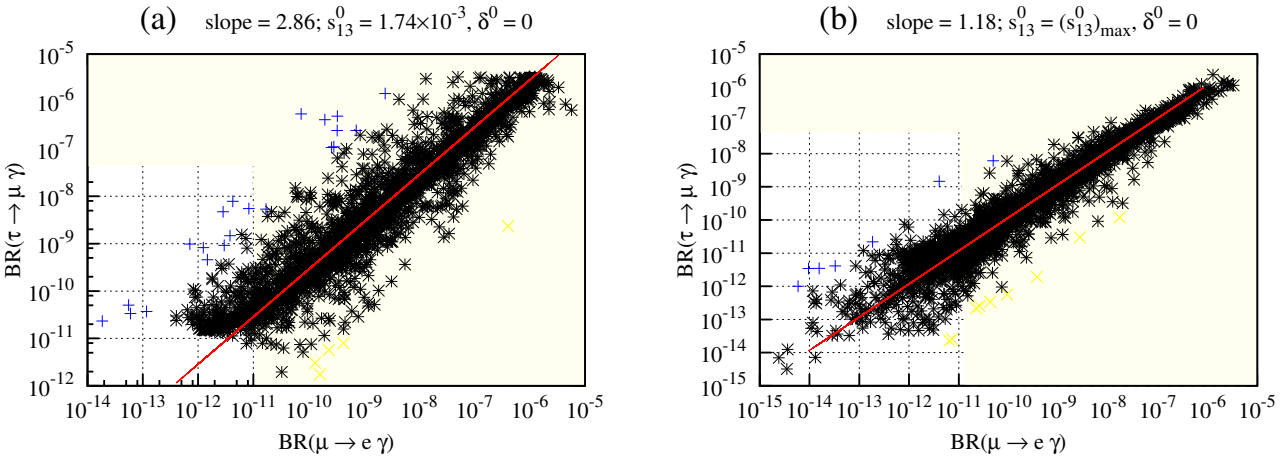

Figure 6.16: Panel (a): $BR(\tau \to \mu\,\gamma)$ vs $BR(\mu \to e\,\gamma)$ for $s^0_{13} = 1.74 \times 10^{-3}$, degenerate RH neutrinos and 3000 random points in the R-matrix parameter space ($|\theta_i| \leq 3$ and $|\arg\theta_i| \leq \pi$). Similarly, panel (b) for $s^0_{13} = (s^0_{13})_{max}$ and hierarchical RH neutrinos. Red lines are the average slopes. Blue and yellow points are $\geq 10^2$ and $\leq 10^{-2}$ departures from the average slope, respectively. Parameters were set to: SPS1a', TBM mixing angles except s^0_{13} ($\delta^0 = 0$), SNH light neutrinos with $m_\nu \approx 10^{-6}$ eV, $M_R = 10^{12}$ GeV and $M \equiv M_1 = M_2 = 10^{10}$ GeV.

For small s^0_{13} the preferred ordering of branching ratios is that of (6.46), concretely, $BR(\tau \to \mu\,\gamma) \sim 3\,BR(\mu \to e\,\gamma)$ and $BR(\tau \to \mu\,\gamma) \sim 14\,BR(\tau \to e\,\gamma)$. This separation between τ-μ vs μ-e flavour transitions is lowered for larger s^0_{13}. When the reactor angle is close to the experimental bound we have

$$BR(\tau \to \mu\,\gamma) \simeq BR(\mu \to e\,\gamma)\,. \tag{6.56}$$

Recall that we have been analysing the case with SNH light neutrinos. For SIH light neutrinos the panorama changes since the s^0_{13} discriminative role is removed due to the suppression by the lightest neutrino mass m_{ν_3}. Concretely, taking 300 random points in the R-matrix parameter space and setting $s^0_{13} = 1.74 \times 10^{-3}$ we found

$$\left\langle \frac{BR(\tau \to \mu\,\gamma)}{BR(\mu \to e\,\gamma)} \right\rangle = 0.22^{+0.47}_{-0.15}\,, \quad \left\langle \frac{BR(\mu \to e\,\gamma)}{BR(\tau \to e\,\gamma)} \right\rangle = 4.69^{+0.13}_{-0.13}\,, \quad \left\langle \frac{BR(\tau \to \mu\,\gamma)}{BR(\tau \to e\,\gamma)} \right\rangle = 1.03^{+2.18}_{-0.70}\,, \tag{6.57}$$

for degenerate RH neutrinos and SIH light neutrinos. This agrees with the natural ordering (6.39) with all the quantities $|\bar{\delta}_{ij}|$ ($i \neq j$) roughly of the same size. Similar results were obtained for hierarchical RH neutrinos. Moreover, we verified that these correlations are stable under s^0_{13} variations.

In a second step we determined the set of parameters that lead to extreme cases of separation between the LFV rates. For this we used MINUIT to look for these extremes while requiring that no unnatural cancellation is at work. The implemented criterion to avoid unnatural cancellations was $BR(l_i \to l_j\,\gamma) \gtrsim BR(l_i \to l_j\,\gamma)|_{R=1}$. We found that the extreme cases occurred for variable real θ_1, high $|\theta_2|$ with $\arg\theta_2 = \pi/2$ and $\arg\theta_1 = \theta_3 = 0$.

In the left panels of Fig:A.1 we show, in the $(\theta_1, |\theta_2|)$ plane, these enhanced separations between $BR(\tau \to \mu\,\gamma)$ and $BR(\mu \to e\,\gamma)$ (normalized to the $R = 1$ case) via the quantity R_{3232} defined in (6.55). We observe that a greater separation is achieved for larger $|\theta_2|$ while the value of θ_1 controls the "sign" of the separation, that is, whether $BR(\tau \to \mu\,\gamma)/BR(\mu \to e\,\gamma)$ will increase or decrease in comparison to the $R = 1$ case. In the right panels of the same figure we confirm that (i) the separations increase with increasing $|\theta_2|$ and (ii) no unstable cancellation is at work. For a separation of $\gtrsim 1$ magnitude one must have $|\theta_2| \gtrsim 0.6$. Moreover, the Dirac phase has no role in the very small s^0_{13} regime, as expected, and for high s^0_{13} the Dirac phase acts as shifter of the R_{3232} peaks in the θ_1 space. This is manifestly evident in the comparison between the (a) and (b) panels of Fig:6.18.

In Fig:6.17 and Fig:6.18 we show the branching ratios of the LFV radiative decays, with M_R set to saturate the experimental bounds, as a function of θ_1 with $|\theta_2| = 3$. We observe that in the region of maximum τ-e flavour transitions one has:

$$BR(\tau \to e\,\gamma) \gg BR(\tau \to \mu\,\gamma) \simeq BR(\mu \to e\,\gamma)\,, \tag{6.58}$$

occurring for $\theta_1 \sim 5\pi/8$ and being stable under s^0_{13} and δ^0 variations. The same stability under both s^0_{13} and δ^0 variations occurs for the region where $BR(\mu \to e\,\gamma)$ is the higher branching ratio,

$$BR(\mu \to e\,\gamma) \gg BR(\tau \to \mu\,\gamma) \simeq BR(\tau \to e\,\gamma)\,, \tag{6.59}$$

for $\theta_1 \sim 3\pi/8$. The size of the τ-μ flavour transition is the most sensible to s^0_{13} and δ^0 variations. In the low s^0_{13} regime $BR(\tau \to \mu\,\gamma)$ is maximum for $\theta_1 = 0$, while for $s^0_{13} = (s^0_{13})_{max}$ its maximum is shifted to $\theta_1 \simeq 3\pi/4$ for $\delta^0 = 0$ and $\theta_1 \simeq \pi/4$ for $\delta^0 = \pi$.

Concluding remarks

We have seen that, even for a completely general complex R-matrix, there is a fundamental distinction between SNH and SIH light neutrinos in the relative size of the LFV rates. Specifically, for the latter the natural ordering (6.39) is favoured while for the former the favoured ordering follows (6.46). Very small s^0_{13} and SNH light neutrinos is clearly favoured to achieve higher separations between τ-μ and τ, μ-e flavour transitions. On the other hand, no fundamental distinction exists between degenerate RH neutrinos and hierarchical RH neutrinos for a completely general R-matrix, that is, with $f_{ij}, g_{ij} \neq 0$ for $i \neq j$. Moreover, the size of μ-e and τ-e flavour transitions are highly correlated for any of the light neutrino hierarchies.

We have also established that there is always a wide region where the relative size between any two of the three types of flavour transitions is at least of ± 1 order of magnitude. Nevertheless, the following two cases for the ordering of the relative sizes are disfavoured (and absent in Fig:6.17 and Fig:6.18):

$$BR(\tau \to e\,\gamma) \gg BR(\mu \to e\,\gamma) > BR(\tau \to \mu\,\gamma)\,, \quad BR(\mu \to e\,\gamma) \gg BR(\tau \to e\,\gamma) > BR(\tau \to \mu\,\gamma)\,, \tag{6.60}$$

where $\gg$ and $>$ apply to > 1 and $\gtrsim 0.5$ orders of magnitude, respectively.

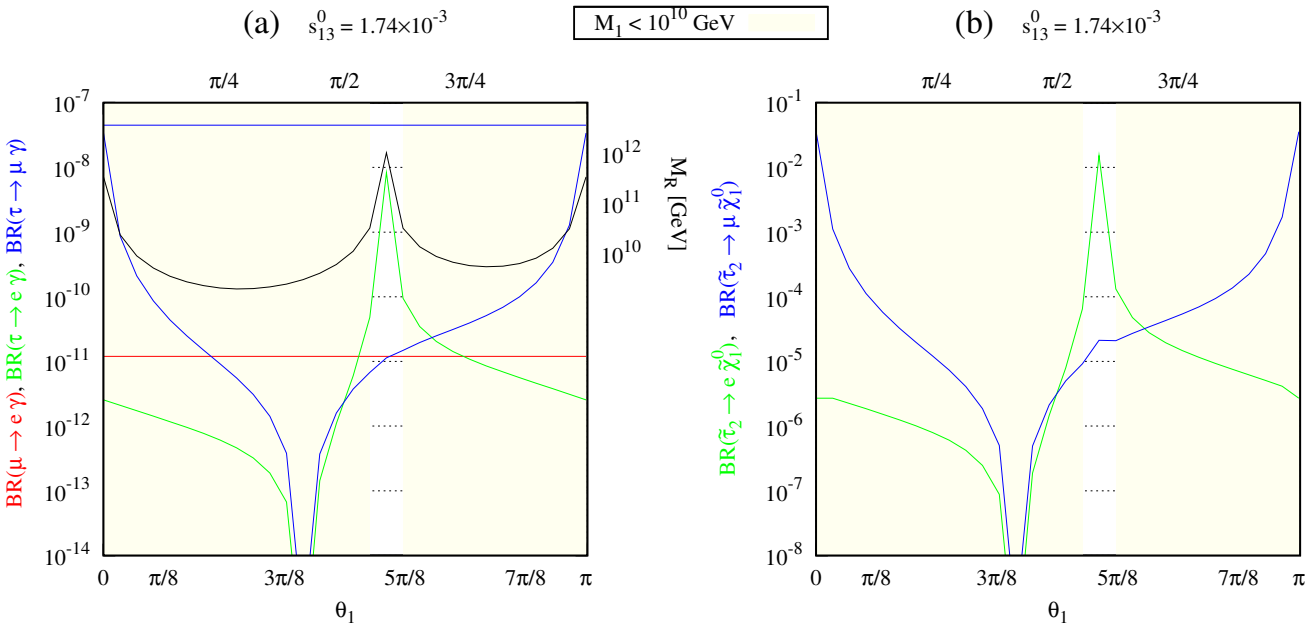

Figure 6.17: $BR(l_i \to l_j\,\gamma)$ (a) and $BR(\tilde{\tau}_2 \to l_i\,\tilde{\chi}^0_1)$ (b) as a function of θ_1 for $s^0_{13} = 1.74 \times 10^{-3}$ and $\arg\theta_1 = \theta_3 = 0$, $\theta_2 = 3\exp\{i\pi/2\}$. The RH neutrino mass scale (black colour) was set to saturate the experimental bounds on $BR(l_i \to l_j\,\gamma)$. The limitative role was played by $BR(\mu \to e\,\gamma)$. Parameters were set to: SPS1a', TBM mixing angles except s^0_{13} ($\delta^0 = 0$), SNH light neutrinos and hierarchical RH neutrinos with $M \equiv M_1 = M_2 = 10^{-2} M_R$.

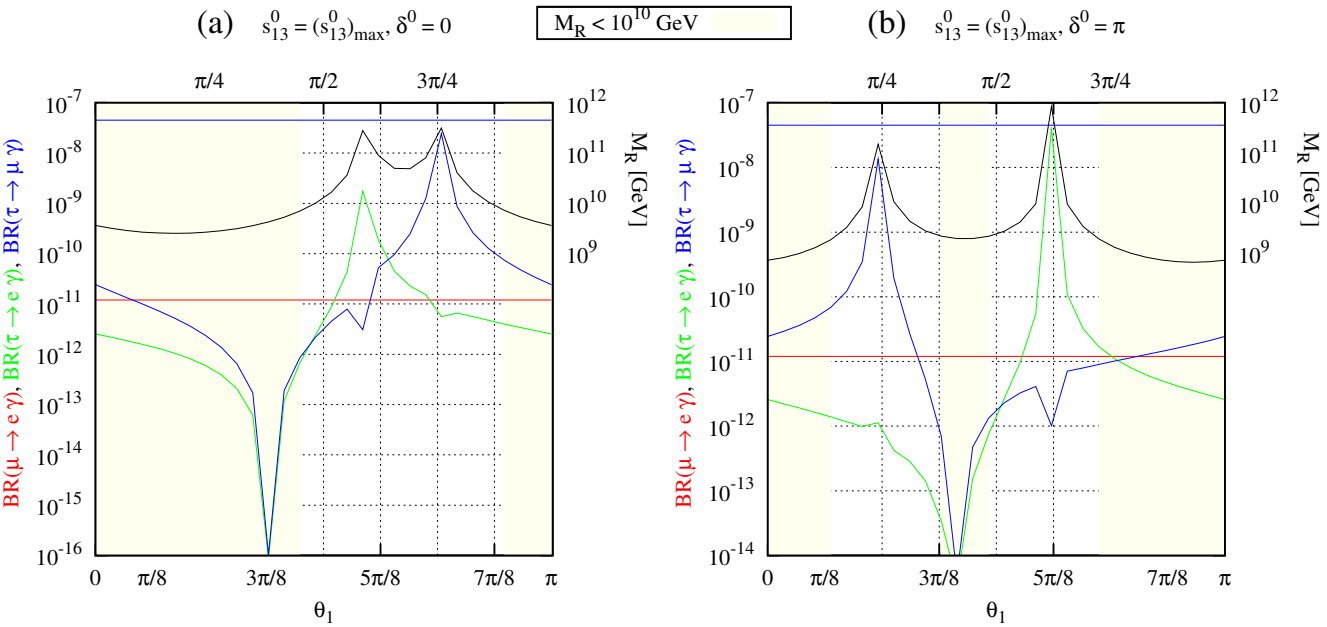

Figure 6.18: $BR(l_i \to l_j\,\gamma)$ as a function of θ_1 for $\delta^0 = 0$ (a) and $\delta^0 = \pi$ (b) with $s^0_{13} = (s^0_{13})_{max}$, $\theta_2 = 3\exp\{i\pi/2\}$, $\arg\theta_1 = \theta_3 = 0$ and degenerate RH neutrinos. Remaining parameters were set as in Fig:6.17.

7 Conclusions

We have seen how lepton flavour violation arises in the MSSM extended with right-handed Majorana neutrinos and how it depends on two subsets of parameters: (i) the pure MSSM and (ii) the seesaw. Concerning the MSSM part we have taken the opportunely motivated simplified assumption of mSUGRA boundary conditions, while for the seesaw parameters we applied the currently available constraints from neutrino physics.

In this context we have shown that it is possible, to an excellent approximation, to factorize the LFV rates into a mSUGRA function and a seesaw function, studying in particular the case of LFV radiative decays $l_i \to l_j \gamma$. We concluded that the LFV rates depend strongly on the mSUGRA parameters, a dependence which is roughly the same for the same type of process and does not distinguish the flavour being violated.

We argued that, while a low mSUGRA mass spectrum could easily push the LFV radiative decays to its current experimental upper bounds, the interesting feature of this mSUGRA dependence was to relate different types of LFV processes, namely, both those involving known particles (as for the LFV radiative decays) and those involving sparticles. This is further motivated because the LFV rates largely depend upon the RH neutrino masses, which can only be directly constrained by the LFV rates. Thus, specific knowledge of the LFV branching ratios would ultimately set the RH neutrino mass scale.

On the other hand, the seesaw functions distinguish the type of flavour being violated while being the same for every type of process. Thus, apart from the RH neutrino mass scale, the interesting way to probe the seesaw sector is to study the relative size of the different flavour transitions. We have taken this approach in the second half of the preceding chapter.

General conclusions can be drawn which do not rely on specific R-matrix assumptions: (i) a larger separation between τ-μ and μ, τ-e flavour transitions is favoured in scenarios of SNH and QD-type light neutrinos with a very small reactor angle; (ii) the case of SIH light neutrinos favours the natural ordering (all flavour transitions are roughly of the same size).

Moreover, we established two types of ordering for the branching ratios of the LFV radiative decays, $BR(\mu \to e\,\gamma) > BR(\tau \to e\,\gamma) \simeq BR(\tau \to \mu\,\gamma)$ (natural) and $BR(\tau \to \mu\,\gamma) > BR(\mu \to e\,\gamma) > BR(\tau \to e\,\gamma)$, that were the most common situations obtained with a real R-matrix. We then showed that these could be manifestly changed if one allows the R-matrix to be complex, and determined a region in the R-matrix parameter space that strongly displayed these different types of ordering: real variable θ_1, large $|\theta_2|$ with $\arg\theta_2 = \pi/2$ and $\arg\theta_1 = \theta_3 = 0$.

Bibliography

[1] C. Amster et al. Review of Particle Physics. *Phys. Lett. B*, 667(1), 2008.

[2] The LEP Collaborations: ALEPH Collaboration, DELPHI Collaboration, L3 Collaboration, OPAL Collaboration, the LEP Electroweak Working Group, the SLD Electroweak and Heavy Flavour Groups. A Combination of Preliminary Electroweak Measurements and Constraints on the Standard Model. *arXiv*, hep-ex/0312023, 7 Dec. 2003.

[3] Guido Altarelli and Martin W. Grünewald. Precision Electroweak Tests of the Standard Model. *arXiv*, hep-ph/0404165v1, 20 Apr. 2004.

[4] The ALEPH Collaboration, the DELPHI Collaboration, the L3 Collaboration, the OPAL Collaboration and the LEP Working Group for Higgs Boson Searches. Search for the Standard Model Higgs Boson at LEP. *arXiv*, hep-ex/0306033, 16 Jun. 2003.

[5] E. Tournefier. Electroweak Results from LEP and SLC and Tests of the Standard Model. *arXiv*, hep-ex/0105091v1, 31 May 2001.

[6] Jaan Einasto. Dark matter. *arXiv*, 0901.0632, 6 Jan. 2009.

[7] G. Hinshaw et al. Five-Year Wilkinson Microwave Anisotropy Probe (WMAP) Observations: Cosmological Interpretation. *arXiv*, 0803.0547, 4 Mar. 2008.

[8] Vimal Simha and Gary Steigman. Constraining The Early-Universe Baryon Density And Expansion Rate. *arXiv*, 0803.3465v3, 25 Mar. 2008.

[9] Andrew R Liddle. An introduction to cosmological inflation. *arXiv*, astro-ph/9901124, 11 Jan. 1999.

[10] A. D. Sakharov. Violation of CP invariance, C asymmetry, and baryon asymmetry of the universe. *Soviet Physics Journal of Experimental and Theoretical Physics (JETP)*, 5:24–27, 1967.

[11] Mark Trodden. Electroweak Baryogenesis. *arXiv*, hep-ph/9803479, 27 Mar. 1998.

[12] M. B. Gavela, P. Hernández, and O. Pène J. Orloff. Standard Model CP-violation and Baryon asymmetry. *arXiv*, hep-ph/9312215, 2 Dec. 1993.

[13] Patrick Huet and Eric Sather. Electroweak Baryogenesis and Standard Model CP Violation. *arXiv*, hep-ph/9404302, 20 Apr. 1994.

[14] M. B. Gavela, P. Hernández, J. Orloff, O. Pène, and C. Quimbay. Standard Model CP-violation and Baryon asymmetry Part II: Finite Temperature. *arXiv*, 11 Jun. 1994.

[15] I. J. R. Aitchison and A. J. G. Hey. *Gauge Theories in Particle Physics*, volume I: *From Relativistic Quantum Mechanics to QED*. Bristol and Philadelphia: IoP Publishing, 2003.

[16] Thomas Hambye and Kurt Riesselmann. Matching conditions and Higgs mass upper bounds revisited. *arXiv*, hep-ph/9610272v1, 7 Oct. 1996.

[17] G. 't-Hooft. Naturalness, chiral symmetry and spontaneous chiral symmetry breaking. *Recent developments in gauge theories (NATO ASI Series B: Physics)*, 59:135–157, 1979.

[18] Ian Aitchinson. *Supersymmetry in Particle Physics*. Cambridge University Press, 2007.

[19] D. Balin and A. Love. *Supersymmetric Gauge Field Theory and String Theory*. Tayler & Francis, 1994.

[20] Stephen P. Martin. A Supersymmetry Primer. *arXiv*, hep-ph/9709356, 10 Dec. 2008.

[21] D. J. H. Chung, L. L. Everett, G. L. Kane, J. Lykken S. F. King, and Lian-Tao Wang. The Soft Supersymmetry-Breaking Lagrangian: Theory and Applications. *arXiv*, hep-ph/0312378, 30 Dec. 2003.

[22] L. O'Raifeartaigh. *Nucl. Phys. B*, 96(331-52), 1975.

[23] P. Fayet and J. Iliopoulos. *Phys. Lett. B*, 51(461-4), 1974.

[24] Don S. Harmer Raymond Davis, Jr. and Kenneth C. Hoffman. Search for Neutrinos from the Sun. *Phys. Rev. Lett.*, 20:1205–1209, 1968.

[25] Kamiokande-II Collaboration. Observation of a small atmospheric ν_μ/ν_e ratio in Kamiokande. *Phys. Lett. B*, 280(146), Apr. 1992.

[26] SNO Collaboration. Direct Evidence for Neutrino Flavor Transformation from Neutral-Current Interactions in the Sudbury Neutrino Observatory. *arXiv*, nucl-ex/0204008, 21 Apr. 2002.

[27] M. Apollonio et al. Search for neutrino oscillations on a long base-line at the CHOOZ nuclear power station. *arXiv*, hep-ex/0301017, 13 Jan. 2003.

[28] J. Bonn et al. Final Results from phase II of the Mainz Neutrino Mass Search in Tritium β Decay. *arXiv*, hep-ex/0412056, 20 Dec. 2004.

[29] A. I. Beleseva et al. Results of the troitsk experiment on the search for the electron antineutrino rest mass in tritium beta-decay. *Phys. Lett. B*, 350(263), May 1995.

[30] D. N. Spergel et al. Wilkinson Microwave Anisotropy Probe (WMAP) Three Year Results: Implications for Cosmology. *arXiv*, astro-ph/0603449v2, 19 Mar. 2006.

[31] Mikhail Shaposhnikov. The nuMSM, leptonic asymmetries, and properties of singlet fermions. *arXiv*, 0804.4542, 29 Apr. 2008.

[32] J. W. F. Valle. Neutrino physics overview. *arXiv*, hep-ph/0608101, 9 Aug. 2006.

[33] Ernest Ma. Pathways to Naturally Small Neutrino Masses. *arXiv*, hep-ph/9805219, 4 May 1998.

[34] A. Broncano, M. B. Gavela, and E. Jenkins. The Effective Lagrangian for the Seesaw Model of Neutrino Mass and Leptogenesis. *arXiv*, hep-ph/0210271v2, 21 Oct. 2002.

[35] Evgeny Kh. Akhmedov and Michele Frigerio. Interplay of type I and type II seesaw contributions to neutrino mass. *arXiv*, hep-ph/0609046, 5 Sep. 2006.

[36] J.A. Casas and A. Ibarra. Oscillating neutrinos and $\mu \to e\,\gamma$. *arXiv*, hep-ph/0103065v2, 7 Nov. 2001.

[37] B. C. Allanach et al. SUSY Les Houches Accord: Interfacing SUSY Spectrum Calculators, Decay Packages, and Event Generators. *arXiv*, hep-ph/0311123v3, 14 Sep. 2007.

[38] B. C. Allanach et al. SUSY Les Houches Accord 2. *arXiv*, 0801.0045v2, 29 Dec. 2007.

[39] L. Girardello and M. T. Grisaru. *Nucl. Phys. B*, 194(65), 1982.

[40] J.A. Casas and C. Munoz. A Natural Solution to the MU Problem. *arXiv*, hep-ph/9302227, 5 Feb. 1993.

[41] G. Dvali, G.F. Giudice, and A. Pomarol. The μ-Problem in Theories with Gauge-Mediated Supersymmetry Breaking. *arXiv*, hep-ph/9603238, 6 Mar. 1996.

[42] Ulrich Ellwanger. The constrained NMSSM: mSUGRA and GMSB. *arXiv*, 0809.0779, 4 Sep. 2008.

[43] Savas Dimopoulos and Dave Sutter. The Supersymmetric Flavor Problem. *arXiv*, hep-ph/9504415v1, 28 Apr. 1995.

[44] R. Barbieri and L. Hall, A. Strumia. Violations of lepton flavour and CP in supersymmetric unified theories. *arXiv*, hep-ph/9501334, 18 Jan. 1995.

[45] Mikolaj Misiak, Stefan Pokorski, and Janusz Rosiek. Supersymmetry and FCNC effects. *arXiv*, hep-ph/970344, 27 Mar. 1997.

[46] R. Barbieri and G.F. Giudice. $b \to s\gamma$ Decay and Supersymmetry. *arXiv*, hep-ph/9303270, 17 Mar. 1993.

[47] F. Gabbiani, E. Gabrielli, A. Masiero, and L. Silvestrini. A complete analysis of FCNC and CP constraints in general SUSY extensions of the standard model. *arXiv*, hep-ph/9604387, 23 Apr. 1996.

[48] JoAnne L. Hewett and James D. Wells. Searching for supersymmetry in rare B decays. *arXiv*, hep-ph/9610323, 10 Oct. 1996.

[49] S. Pokorski, J. Rosiek, and C. A. Savoy. Constraints on Phases of Supersymmetric Flavour Conserving Coupling. *arXiv*, hep-ph/9906206, 1 Jun. 1999.

[50] S. Abel, S. Khalil, and O. Lebedev. EDM Constraints in Supersymmetric Theories. *arXiv*, hep-ph/0103320, 29 Mar. 2001.

[51] M. Ciuchini et al. ΔM_K and ϵ_K in SUSY at the Next-to-Leading order. *arXiv*, hep-ph/9808328, 14 Aug. 1998.

[52] S. Pokorski, J. Rosiek, and C. A. Savoy. Constraints on Phases of Supersymmetric Flavour Conserving Couplings. *arXiv*, hep-ph/9906206, 1 Jun. 1999.

[53] S. Abel, S. Khalil, and O. Lebedev. EDM Constraints in Supersymmetric Theories. *arXiv*, hep-ph/0103320, 29 Mar. 2001.

[54] A. H. Chamseddine, R. Arnowitt, and P. Nath. *Phys. Rev. Lett.*, 49:970–4, 1982.

[55] J.A. Aguilar-Saavedra et al. Supersymmetry Parameter Analysis: SPA Convention and Project. *arXiv*, hep-ph/0511344, 30 Nov. 2005.

[56] R. Barbier et la. R-parity violating supersymmetry. *arXiv*, hep-ph/0406039, 3 Jun. 2004.

[57] G. Jungman, M. Kamionkowski, and K. Griest. Supersymmetric Dark Matter. *arXiv*, hep-ph/9506380, 22 Jun. 1995.

[58] Yuval Grossman and Howard E. Haber. Sneutrino Mixing Phenomena. *arXiv*, hep-ph/9702421, 6 Mar. 1997.

[59] F. Borzumati and A. Masiero. Large Muon and electron Number Violations in Supergravity Theories. *Phys. Rev. Lett.*, 57(961), 1986.

[60] J. Hisano, T. Moroi, K. Tobe, and M. Yamaguchi. Lepton-Flavor Violation via Right-Handed Neutrino Yukawa Couplings in Supersymmetric Standard Model. *arXiv*, hep-ph/9510309, 16 Oct. 1995.

[61] M. Hirsch, W. Porod, J. C. Romão, J. W. F. Valle, and A. Villanova del Moral. Probing minimal supergravity in the type-I seesaw mechanism with lepton flavour violation at the CERN LHC. *arXiv*, hep-ph/0804.4072v2, 20 Oct. 2008.

[62] John Ellis, Junji Hisano, Martti Raidal, and Yasuhiro Shimizu. Lepton Electric Dipole Moments in Non-Degenerate Supersymmetric Seesaw Models. *arXiv*, hep-ph/0111324v2, 26 Nov. 2001.

[63] A. Abada, C. Biggio, F. Bonnet, M. B. Gavela, and T. Hambye. Low energy effects of neutrino masses. *arXiv*, 0707.4058v3, 27 Jul. 2007.

[64] S. Antusch, E. Arganda, M. J. Herrero, and A. M. Teixeira. Impact of θ_{13} on Lepton Flavour Violating processes within SUSY Seesaw. *arXiv*, hep-ph/0607263, 6 Nov. 2006.

[65] Howard Baer, Chung Kao, and Xerxes Tata. Aspects of Chargino-Neutralino Production at the Tevatron Collider. *arXiv*, hep-ph/9307347, 27 Jul. 1993.

[66] W. Buchmüller and M. Plümacher. Neutrino masses and the baryon asymmetry. *arXiv*, hep-ph/0007176, 17 Jul. 2000.

[67] G.F. Giudice, A. Notari, M. Raidal, A. Riotto, and A. Strumia. Towards a complete theory of thermal leptogenesis in the SM and MSSM. *arXiv*, hep-ph/0310123, 12 Feb. 2004.

[68] W. Buchmüller, P. Di Bari, and M. Plümacher. The Neutrino Mass Window for Baryogenesis. *arXiv*, hep-ph/0302092, 12 Feb. 2003.

[69] J. Hisano, M. Nagai, P. Paradisi, and Y. Shimizu. Waiting for $\mu \to e\,\gamma$ from the MEG experiment. *arXiv*, 0904.2080, 14 Apr. 2009.

[70] M. Maltoni, T. Schwetz, M. A. Tortola, and J. W. F. Valle. Status of global fits to neutrino oscillations. *arXiv*, hep-ph/0405172v6, 18 May 2004.

[71] M. Hirsch, Ernest Ma, J. C. Romão, J. W. F. Valle, and A. Villanova del Moral. Minimal supergravity radiative effects on the tri-bimaximal neutrino mixing pattern. *arXiv*, hep-ph/0606082v3, 27 Apr. 2007.

[72] Werner Porod. SPHENO, a program for calculating supersymmetric spectra, SUSY particle decays and SUSY particle production at e+ e- colliders. *arXiv*, hep-ph/0301101, 15 Jan. 2003.

[73] CERN Program Library. MINUIT. 2006.

[74] J. Hisano and Daisuke Nomura. Solar and Atmospheric Neutrino Oscillations and Lepton Flavor Violation in Supersymmetric Models with Right-handed Neutrinos. *arXiv*, hep-ph/9810479v2, 26 Oct. 1998.

[75] Boudewijn F. Roukema and Gary A. Mamon. Tangential Large Scale Structure as a Standard Ruler: Curvature Parameters from Quasars. *arXiv*, astro-ph/9911413, 18 Apr. 2008.

[76] Ta-Pei Cheng and Ling-Fong Li. *Gauge theory of elementary particle physics*. Oxford University Press, 1984.

[77] L. Lavoura. General formulae for $f_1 \to f_2\,\gamma$. *arXiv*, hep-ph/0302221v1, 25 Feb. 2003.

[78] FEYNCALC. http://www.feyncalc.org/.

A Backup figures

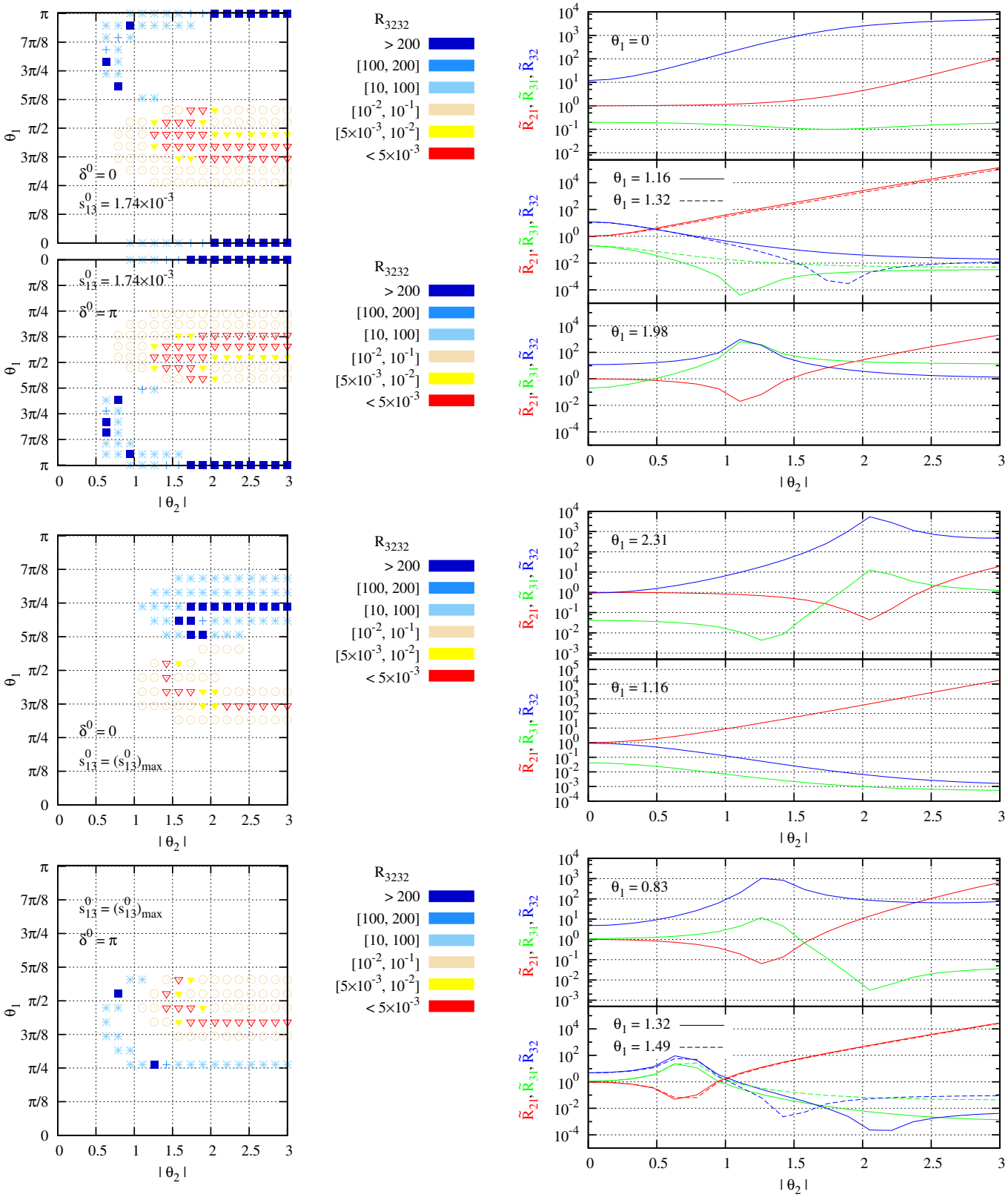

Figure A.1: Impact of θ_1 vs θ_2 upon the relative size of LFV radiative decays for several values of s^0_{13} and δ^0, with degenerate RH neutrinos $M_R = 10^{12}$ GeV, SNH light neutrinos, TBM except s^0_{13} and δ^0, $\arg\theta_2 = \pi/2$ and $\arg\theta_1 = \theta_3 = 0$. The definitions of $\tilde{R}_{ij}$ and R_{3232} are given in (6.54) and (6.55). At right: the first three panels are for $s^0_{13} = 1.74 \times 10^{-3}$, the next two are for $s^0_{13} = (s^0_{13})_{max} \wedge \delta^0 = 0$ and the final two for $s^0_{13} = (s^0_{13})_{max} \wedge \delta^0 = \pi$.

B Cosmology basics

From the FLRW metric one can deduce, through the Einstein field equations, the Friedmann equation:

$$H^2 \equiv \frac{\dot{R}^2}{R^2} = \frac{8\pi G_N \rho}{3} + \Lambda - \frac{k}{R^2}\,, \tag{B.1}$$

where ρ is the total energy density of the universe, k is the curvature constant ($k = 0$ for a flat universe, $k = \pm 1$ for a closed universe and unbounded universe, respectively), Λ is the cosmological constant[1] and H is called the Hubble parameter. It is customary to introduce the reduced Hubble parameter, h, through:

$$H = 100h \text{ km s}^{-1} \text{ Mpc}^{-1}. \tag{B.2}$$

At the present the combined results of of WMAP (5 years) + BAO (Baryonic Acoustic Oscillations) + SN (SuperNovae) give $h^{(0)} = 0.701 \pm 0.0013$, from table D1 of [7]. Another usual definition is that of the critical density ρ_c and the density parameter Ω_X (of an energy type X):

$$\rho_c \equiv \frac{3H^2}{8\pi G_N} \Rightarrow \rho_c^{(0)} = 1.8787 \times 10^{-26} h^{(0)2} \text{ kg m}^{-3} \quad \text{and} \quad \Omega_X \equiv \frac{\rho_x}{\rho_c}, \tag{B.3}$$

respectively. **Note 1:** when a quantity x is to be taken at the present time we write it as $x^{(0)}$. **Note 2:** all the quantities are expressed with $c = 1$. The c factors are restored by dimensional analysis only when we intend to evaluate a quantity numerically.

The critical density is the turning point between an open universe ($\Omega_{total} < 1$) and a closed universe ($\Omega_{total} > 1$). Experimental evidences[2] have suggested that the universe is flat ($\Omega_{total} \approx 1$) with a non-vanishing cosmological constant. The energy of the universe is divided into 4 types of contributions:

$$\Omega_{total} = \Omega_M + \Omega_R + \Omega_\Lambda + \Omega_k\,, \quad \Omega_M = \Omega_B + \Omega_{DM}\,, \tag{B.4}$$

where Ω_M, Ω_R, Ω_Λ and Ω_k (≈ 0) are the matter, the radiation, the dark energy and the curvature contributions, respectively. Moreover, Ω_B and Ω_{DM} are the components of the matter present in the universe, namely, baryonic matter and dark matter, respectively.

To end this brief exposition we note that from energy-momentum conservation one can deduce:

$$\dot{\rho} = -3H\,(p + \rho)\,. \tag{B.5}$$

B.1 Equilibrium thermodynamics: n, ρ and p

For species in kinetic equilibrium the number density, energy density and pressure are given by[3]:

$$n = \frac{g}{(2\pi\hbar)^3}\int d^3p\, f(\vec{p})\,, \quad \rho = \frac{g}{(2\pi\hbar)^3}\int d^3p\, E f(\vec{p}) \quad \text{and} \quad p = \frac{g}{(2\pi\hbar)^3}\int d^3p\, \frac{|\vec{p}|^2}{3E} f(\vec{p})\,, \tag{B.6}$$

[1] Also called dark energy. It is interpreted as the energy density of the vacuum of all the quantum fields (particles) of the universe.

[2] One of the methods used to determine the curvature of the universe without relying on many model-dependent assumptions is by comparing "bubbles" of large scale structure in the universe (the large scale structure formation follows from the universe expansion and is little influenced by local details) with the structure of the local universe (the standard ruler). See [75].

[3] Discarding the chemical potential.

respectively. In here: $f(\vec{p})$ is the distribution function $f(\vec{p}) = (\exp\{E/(k_BT)\} \pm 1)^{-1}$ for fermions $(+)$ and bosons $(-)$, respectively; and g is the number of d.o.f. of the type of particle that characterizes the specie (for instance, $g = 1$ for LH neutrinos and Majorana fermions, $g = 2$ for Dirac fermions and massless vector bosons and $g = 3$ for massive vector bosons).

In the relativistic limit ($k_BT \gg m$) we can integrate the previous equations to obtain:

$$n = \left(\frac{3}{4}\right)_F \frac{\zeta(3)}{\pi^2} g \left(\frac{k_BT}{\hbar}\right)^3, \quad \rho = \left(\frac{7}{8}\right)_F \frac{1}{2} g a_R T^4 \quad \text{and} \quad p = \frac{\rho}{3}, \tag{B.7}$$

where the factors within $(..)_F$ are to be taken if we are dealing with a fermion, ζ is the well known Riemann zeta function, a_R is the radiation constant,

$$a_R \equiv \frac{4\,\sigma_{SB}}{c} = \frac{\pi^2 k_B^4}{15 c^3 \hbar^3} \simeq 7.55 \times 10^{-16}\ \text{J m}^{-3}\ \text{K}^{-4}, \tag{B.8}$$

and σ_{SB} is the Stefan-Boltzmann constant. In the non-relativistic limit ($k_BT \ll m$) we have:

$$\rho = m\,n, \quad n = g\left(\frac{m k_B T}{2\pi\hbar^2}\right)^{\frac{3}{2}} \exp\left\{-\frac{m}{k_BT}\right\} \quad \text{and} \quad p = 0. \tag{B.9}$$

Additionally, from (B.5) one has:

$$\text{Radiation or relativistic matter: } p = \frac{1}{3}\rho \Rightarrow \rho_{\text{radiation}} \propto R^{-4}, \tag{B.10}$$

$$\text{Non-relativistic matter: } p = 0 \Rightarrow \rho_{\text{non-relativistic matter}} \propto R^{-3}. \tag{B.11}$$

B.2 Universe evolution: $R \propto T^{-1}$

By universe entropy conservation, $dS = 0$, one has that the entropy in a covolume, sR^3, remains constant. Furthermore, from the equation of state one can deduce:

$$T\,dS = dE + p\,dV \Rightarrow s \equiv \frac{S}{V} = \frac{\rho + p}{T}, \tag{B.12}$$

where s is called the reduced entropy. Knowing from (B.7) that $\rho_{\text{relativistic}} \propto T^4$ and comparing to (B.9) for $\rho_{\text{non-relativistic matter}} \propto T^{3/2}\exp\left\{-\frac{1}{T}\right\}$ it is clear that the universe entropy is dominated by relativistic particles for T sufficiently high. Hence, from (B.12) and $dS = d(sR^3) = 0$ one concludes that $TR =$ constant, because $\rho_{\text{relativistic}} \propto R^{-4}$ - from (B.10). Being the entropy dominated by relativistic particles of different species one can write the reduced entropy as (using (B.12) with (B.7)):

$$s = \frac{2}{3} g_s a_R T^3, \quad g_s = \sum_{\text{boson}_i} g_i \left(\frac{T_i}{T}\right)^3 + \frac{7}{8} \sum_{\text{fermion}_i} g_i \left(\frac{T_i}{T}\right)^3. \tag{B.13}$$

B.3 Hubble parameter evolution with T

From (B.7), we can write the energy density of all the species of relativistic particles as:

$$\rho_R = \frac{1}{2} g_* a_R T^4, \quad g_* = \sum_{\text{boson}_i} g_i \left(\frac{T_i}{T}\right)^4 + \frac{7}{8} \sum_{\text{fermion}_i} g_i \left(\frac{T_i}{T}\right)^4. \tag{B.14}$$

Hence, assuming that ρ_R dominates over any other type of energy density present in the universe (this is certainly true for sufficiently high T), one has from (B.1):

$$H = \frac{\pi}{3\hbar}\sqrt{\frac{1}{10}}\sqrt{g_*}\frac{k_B^2 T^2}{M_P}, \quad M_P \equiv \sqrt{\frac{\hbar c}{8\pi G_N}}. \tag{B.15}$$

C One-loop calculations

C.1 Feynman's parametrizations

$$\Pi_{i=1}^{n}\frac{1}{a_i} = \Gamma(n)\int_0^1 dx_1\int_0^1 dx_2\ ...\int_0^1 dx_{n-1}\frac{1}{\left[a_n+\sum_{i=1}^{n-1}(a_i-a_{i+1})\,x_i\right]^n} \tag{C.1}$$

$$= \Gamma(n)\int_0^1 dx_1\int_0^{1-x_1} dx_2\ ...\int_0^{1-\sum_{i=1}^{n-2}x_i} dx_{n-1}\frac{1}{\left[\left(1-\sum_{i=1}^{n-1}x_i\right)a_n+\sum_{i=1}^{n-1}a_i x_i\right]^n} \tag{C.2}$$

C.1.1 Useful results

In an one-loop (1L) diagram, the denominator of the propagator i can be written as:

$$D_i \equiv (k-r_i)^2 - m_i^2\,, \tag{C.3}$$

where $(k-r_i)$ is the 4-momentum carried by the virtual particle i, k is the integrating 4-momentum and m_i is the mass of the virtual particle i.

Thus, using Feynman's parametrization, the loop structure of an 1L diagram with 3 propagators can be rewritten as:

$$D^{(3)}(k;r_i,m_i) \equiv \frac{1}{D_0D_1D_2} = \Gamma(3)\int_0^1 dx\int_0^{1-x} dy\frac{1}{\left[(k-P_3)^2-\Delta_3\right]^3}\,, \tag{C.4}$$

with the generalized 1L momentum and mass squared

$$\begin{cases} P_3 \equiv r_0x + r_1y + r_2(1-x-y) \\ \Delta_3 \equiv (m_0^2-r_0^2-m_2^2+r_2^2)x + (m_1^2-r_1^2-m_2^2+r_2^2)y + m_2^2-r_2^2+P_3^2 \end{cases} \tag{C.5}$$

respectively. Applying a change of variables $k \to k+P_3$ we get the k-even function:

$$D^{(3)}(k+P_3;r_i,m_i) = 2\int_0^1 dx\int_0^{1-x} dy\frac{1}{\left[k^2-\Delta_3\right]^3}\,. \tag{C.6}$$

Applying the same procedure to the loop structure of an 1L diagram with 2 propagators, renders:

$$D^{(2)}(k;r_i,m_i) \equiv \frac{1}{D_0D_1} = \int_0^1 dx\frac{1}{\left[(k-P_2)^2-\Delta_2\right]^2}\,, \tag{C.7}$$

with 1L momentum and mass squared

$$\begin{cases} P_2 \equiv r_0x + r_1(1-x) \\ \Delta_2 \equiv \left(m_0^2-r_0^2-m_1^2+r_1^2\right)x + m_1^2-r_1^2+P_2^2 \end{cases} \tag{C.8}$$

and k-even function

$$D^{(2)}(k+P_2;r_i,m_i) = \int_0^1 dx\ \frac{1}{\left[k^2-\Delta_2\right]^2}\,. \tag{C.9}$$

C.2 One-loop integrals in dimensional regularization

The 1L integral in dimensional regularization, $d = 4 - \epsilon$ ($\epsilon \to 0$),

$$I_{m,n}(\Delta) \equiv \mu^\epsilon \int \frac{d^d k}{(2\pi)^d} \frac{k^{2m}}{[k^2 - \Delta]^n} \,, \tag{C.10}$$

is integrated to

$$I_{m,n}(\Delta) = i(-1)^{n-m} \frac{(2\sqrt{\pi}\mu)^\epsilon}{16\pi^2} \Delta^{d/2+m-n} \frac{\Gamma(m+2)}{\Gamma(n)} \Gamma(n - m - d/2) \,, \tag{C.11}$$

having poles through $\Gamma(z)$ whenever $z \leq 0$ and integer. Evaluating $\Gamma(z)$ near the poles, we have:

$$\Gamma(z \to -m) = \frac{(-1)^m}{m!} \left[\frac{1}{m+z} + \psi(m+1) \right] \,, \quad \psi(m+1) \equiv \left. \frac{d\Gamma(z)}{dz} \right|_{z=m+1} \tag{C.12}$$

$$\psi(m+1) = \psi(m) + \frac{1}{m} \,, \quad \psi(1) = -\gamma \tag{C.13}$$

$$\Rightarrow \Gamma(-m + \epsilon/2) = \frac{(-1)^m}{m!} \left[\frac{2}{\epsilon} - \gamma + H_m \right] \,, \quad H_m \equiv \sum_{k=1}^{m} \frac{1}{k} \,, \tag{C.14}$$

where H_m is the m'th partial sum of the harmonic series, also called the m'th harmonic number, and $\gamma = 0.5772156649015329...$ is known as the Euler-Mascheroni constant and does not have any particular physical meaning.

Therefore, $I_{m,n}$ is divergent whenever $n - m \leq 2$, being this divergence parametrized by $\lim_{\epsilon \to 0} \frac{2}{\epsilon}$. Expanding $(2\sqrt{\pi}\mu)^\epsilon$ and $\Delta^{-\epsilon/2}$, multiplying both by $2/\epsilon$ and then taking the limit $\epsilon \to 0$, one finds:

$$\begin{cases} (2\sqrt{\pi}\mu)^\epsilon = \exp\{\epsilon \ln(2\sqrt{\pi}\mu)\} = 1 + \epsilon \ln(2\sqrt{\pi}\mu) + \mathcal{O}(\epsilon^2) \Rightarrow \frac{2}{\epsilon}(2\sqrt{\pi}\mu)^\epsilon = \frac{2}{\epsilon} + \ln(4\pi\mu^2) + \mathcal{O}(\epsilon) \,, \\ \Delta^{-\epsilon/2} = \exp\{-\epsilon \ln(\Delta)/2\} = 1 - \frac{\epsilon}{2} \ln(\Delta) + \mathcal{O}(\epsilon^2) \Rightarrow \frac{2}{\epsilon}\Delta^{-\epsilon/2} = \frac{2}{\epsilon} - \ln(\Delta) + \mathcal{O}(\epsilon) \,. \end{cases} \tag{C.15}$$

For future convenience we define

$$\Delta_\epsilon \equiv \lim_{\epsilon \to 0} \frac{2}{\epsilon} - \gamma + \ln(4\pi) \,. \tag{C.16}$$

C.2.1 Useful results

From equation (C.14) we get for $m = 0, 1, 2$:

$$\lim_{\epsilon \to 0} \Gamma(z \to \epsilon/2) = \lim_{\epsilon \to 0} \frac{2}{\epsilon} - \gamma \,, \tag{C.17}$$

$$\lim_{\epsilon \to 0} \Gamma(z \to -1 + \epsilon/2) = -\left[\lim_{\epsilon \to 0} \frac{2}{\epsilon} - \gamma + 1 \right] \,, \tag{C.18}$$

$$\lim_{\epsilon \to 0} \Gamma(z \to -2 + \epsilon/2) = \frac{1}{2} \left[\lim_{\epsilon \to 0} \frac{2}{\epsilon} - \gamma + \frac{3}{2} \right] \,. \tag{C.19}$$

Hence, together with (C.15), we find:

$$I_{0,1}(\Delta) = \frac{i}{16\pi^2} \Delta \left[\Delta_\epsilon + 1 - \ln\left(\frac{\Delta}{\mu^2}\right) \right] \,, \tag{C.20}$$

$$I_{0,2}(\Delta) = \frac{i}{16\pi^2} \left[\Delta_\epsilon - \ln\left(\frac{\Delta}{\mu^2}\right) \right] \,, \tag{C.21}$$

$$I_{0,3}(\Delta) = -\frac{i}{32\pi^2 \Delta} \,, \tag{C.22}$$

$$I_{1,1}(\Delta) = \frac{i}{32\pi^2} \Delta^2 \left[2\Delta_\epsilon + 3 - 2\ln\left(\frac{\Delta}{\mu^2}\right) \right] \,, \tag{C.23}$$

$$I_{1,2}(\Delta) = \frac{i}{8\pi^2} \Delta \left[\Delta_\epsilon + 1 - \ln\left(\frac{\Delta}{\mu^2}\right) \right] \,. \tag{C.24}$$

D Vertices and propagators

D.1 Notation

A "dagger" (†) put in an operator is always to be taken as the hermitian conjugate (h.c.) in the quantum sense but also as the complex transpose of an ordinary vector space (like Dirac space or internal symmetry space) in which the operator may live in.

We write a Dirac fermion particle p as ψ_p. In the chiral representation, $\gamma_5 = diagonal(1,1,-1,-1)$, we can write ψ_p as:

$$\psi_p = \begin{pmatrix} \overline{\psi}^{\dot{a}} \\ \chi_a \end{pmatrix}, \tag{D.1}$$

in which $a = 1,2$ are the components of the 2-component Weyl spinors $\overline{\psi}^{\dot{a}}$ and χ_a. By definition, under Lorentz transformations $\overline{\psi}^{\dot{a}}$ transforms as the RH component of a Dirac spinor and χ_a transforms as the LH component. This distinction is only for the boosts. Moreover, one can show that:

$$\overline{\chi}^{\dot{b}} \equiv i(\sigma_2)_{ab}\chi_b^\dagger\,, \tag{D.2}$$

transforms as a RH component. If we introduce the anti-particle spinor $\psi_{\bar{p}}$ we have by charge conjugation that $\psi_{\bar{p}} \equiv C\bar{\psi}_p^T$, where $C \equiv diagonal(i\sigma_2, -i\sigma_2)$ in the chiral representation. Hence, we chose to write the Dirac fermion as:

$$\psi_p = \begin{pmatrix} (\overline{\chi}_{\bar{p}})^{\dot{a}} \\ (\chi_p)_a \end{pmatrix}, \tag{D.3}$$

that is, only referring to LH components of the Dirac particle, namely, the LH anti-particle $\chi_{\bar{p}}$ and the LH particle χ_p. Thus, for shortness, we fix the convention that when we write p relative to a Dirac particle p, we are talking about the LH component of the particle - χ_p - and when we write $\bar{p}$ we are talking about the LH component of the anti-particle - $\chi_{\bar{p}}$.

When in doubt, the Dirac space contraction of Weyl spinors is inferred by requiring Lorentz invariance. For instance, we use interchangeably the definitions:

$$(p\cdot p) = p^a p_a = p_a\left\{-i(\sigma_2)_{ab}\right\}p_b \equiv p\,p\,, \quad (\bar{p}\cdot p) \equiv \bar{p}\,p\,, \tag{D.4}$$

for Majorana and Dirac bilinear terms, respectively.

Additionally, we define:

$$\begin{pmatrix} \sigma^\mu & 0 \\ 0 & \bar{\sigma}^\mu \end{pmatrix} = \gamma^0\gamma^\mu\,, \tag{D.5}$$

where γ^0 and γ^μ are in the chiral representation and $\sigma^\mu \equiv (1,\vec{\sigma})$, $\bar{\sigma}^\mu \equiv (1,-\vec{\sigma})$. Moreover, concerning the dotted-undotted notation, the indices appear as $(\sigma^\mu)_{a\dot{b}}$ and $(\bar{\sigma}^\mu)^{\dot{a}b}$.

D.2 Generalities

The fermion f and the complex scalar ϕ "covariantized" kinetic terms are:

$$\mathcal{L}^f_{kin} = if^\dagger\bar{\sigma}^\mu D_\mu f + \text{h.c.} \quad \text{and} \quad \mathcal{L}^\phi_{kin} = (D^\mu\phi)^\dagger D_\mu\phi\,, \tag{D.6}$$

respectively. The generalized kinetic term of the gauge bosons can be constructed in complete analogy to the energy density of the electromagnetic field as:

$$\mathcal{L}_{kin}^{W} = -\frac{1}{4} F_{\mu\nu}^{\alpha} F^{\alpha;\mu\nu}, \tag{D.7}$$

where F_{μ}^{α} is the generalized energy-momentum tensor for non-abelian gauge bosons; μ and ν are Lorentz indices and α is the index denoting each gauge boson of the multiplet of gauge bosons. The energy-momentum tensor is inferred from the commutator of the covariant derivative:

$$[D_\mu, D_\nu] = igF_{\mu\nu}^{\alpha} T_\alpha \quad \text{with } D_\mu \equiv \partial_\mu + igT_\alpha W_\mu^\alpha \,,$$

from which we have:

$$\begin{aligned} T_\alpha F_{\mu\nu}^{\alpha} &= \left(\partial_\mu W_\nu^\alpha - \partial_\nu W_\mu^\alpha\right) T_\alpha + ig\left[T_\alpha, T_\beta\right] W_\mu^\alpha W_\nu^\beta = \left(\partial_\mu W^\alpha - \partial_\nu W_\mu^\alpha\right) T_\alpha - g T_\alpha f^{\beta\gamma\alpha} W_\mu^\beta W_\nu^\gamma \\ \Rightarrow F_{\mu\nu}^{\alpha} &= \partial_\mu W_\nu^\alpha - \partial_\nu W_\mu^\alpha - g f^{\alpha\beta\gamma} W_\mu^\beta W_\nu^\gamma . \end{aligned} \tag{D.8}$$

We also consider a gauge-fixing term with gauge parameter ξ. However, in case of non-abelian gauge bosons we have to include auxiliary fields. These fields are complex scalar fields that anti-commute[1], known as the Faddeev-Popov (FP) ghosts (denoted by ω^α and the hermitian conjugate $\bar{\omega}^\alpha$, where α is the index of the ghost in the multiplet of ghosts. The ghosts are in the adjoint representation of the gauge group), which guarantee gauge-invariance with the gauge-fixing term, [76]. Finally we have:

$$\mathcal{L}_{gauge} = \mathcal{L}_{kin}^{W} - \frac{1}{2\xi}\left(\partial_\mu W^{\alpha,\mu}\right)\left(\partial_\nu W^{\alpha,\nu}\right) + \partial^\mu \bar{\omega}^\alpha [D_\mu(R=A)]^{\alpha\beta} \omega^\beta \,, \tag{D.9}$$

where $R = A$ denotes the adjoint representation.

D.3 Standard Model

We define the covariant derivative as:

$$D_\mu \equiv \partial_\mu + ig'\frac{y}{2} B_\mu + igW_\mu^\alpha T_\alpha + ig_s g_\mu^\alpha T_\alpha \,, \tag{D.10}$$

which differs from the choice of some authors. In here B_μ, W_μ^α ($\alpha = 1,2,3$) and g_μ^α ($\alpha = 1,..,8$) are the U(1)$_y$, SU(2)$_\mathsf{L}$ and SU(3)$_c$ gauge bosons, respectively; T_α is the α generator of the respective gauge group and is given in the representation of the matter multiplet to which the covariant derivative is applied.

The gauge interactions involving fermions are found to be given by:

$$\mathcal{L}_{e.m.}^{int} = -eA_\mu j_{e.m.}^\mu \,, \quad \mathcal{L}_{Z}^{int} = -\frac{g}{c_w} Z_\mu \left(j_Z^\mu - s_w^2 j_{e.m.}^\mu\right) \,, \quad \mathcal{L}_{W^\pm}^{int,q} = -gW_\mu^+ h_{W^+}^\mu + \text{h.c.} \,, \tag{D.11}$$

where the currents are ($Q \equiv T_3 + y/2$)

$$\begin{cases} j_{e.m.}^\mu = L_i^\dagger Q \bar{\sigma}^\mu L_i + Q_{(a)i}^\dagger Q \bar{\sigma}^\mu Q_{(a)i} + \bar{l}_i^\dagger Q \bar{\sigma}^\mu \bar{l}_i + \sum_{q=u,d} \bar{q}_i^\dagger Q \bar{\sigma}^\mu \bar{q}_i \,, \\ j_Z^\mu = L_i^\dagger T_3 \bar{\sigma}^\mu L_i + Q_{(a)i}^\dagger T_3 \bar{\sigma}^\mu Q_{(a)i} \,, \\ h_{W^+}^\mu = \frac{1}{\sqrt{2}} u_{(a)i}^\dagger \bar{\sigma}^\mu (V_{CKM})_{ij} d_{(a)j} \,, \quad h_{W^-}^\mu = h_{W^+}^{\mu\dagger} \,. \end{cases}$$

Finally, the SM Yukawa interactions are:

$$\mathcal{L}_Y = y_{ij}^u \bar{u}_{(a)j} \phi \, i\sigma_2 \, Q_{(a)i} - y_{ij}^d \bar{d}_{(a)j} \phi^\dagger Q_{(a)i} - y_{ij}^l \bar{l}_j \phi^\dagger L_i + \text{h.c.} \,. \tag{D.12}$$

[1] They would violate the spin-statistics theorem if they were real particles. However, they cannot appear on external lines.

D.3.1 Vertices

In here we give the vertices that are relevant for the work done in this thesis. They are extracted from the Lagrangian densities given previously. For this we cast the relevant quantities from Weyl 2-component spinors to Dirac spinors. For a complete list, but with some different conventions, see for instance [76].

$$h^{\mu}_{W^+} = \frac{1}{\sqrt{2}} \sum_{u=u,c,t} \sum_{d=d,s,b} \bar{\psi}_u \gamma^\mu P_L (V_{CKM})_{ud} \psi_d \tag{D.13}$$

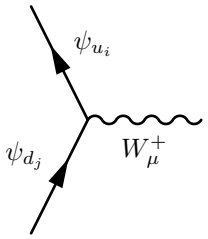

$= -i\frac{g}{\sqrt{2}}(V_{CKM})_{ij}\gamma^\mu P_L$

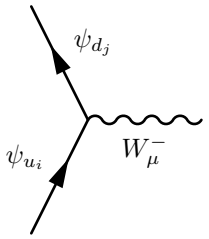

$= -i\frac{g}{\sqrt{2}}(V^*_{CKM})_{ij}\gamma^\mu P_L$

$$\begin{cases} L_Y^{int,u} &= \frac{(M_u)_{ii}}{\sqrt{2}v}\left(i\xi\bar{\psi}_{u_i}\gamma_5\psi_{u_i} - H\bar{\psi}_{u_i}\psi_{u_i}\right) + \frac{1}{v}\left[M_u V_{CKM}\right]_{mn}\phi^+\bar{\psi}_{u_m}P_L\psi_{d_n} \\ & \quad + \frac{1}{v}\left[V^\dagger_{CKM}M_u\right]_{mn}\phi^-\bar{\psi}_{d_m}P_R\psi_{u_n} \\ L_Y^{int,d} &= \frac{(M_d)_{ii}}{\sqrt{2}v}\left(-i\xi\bar{\psi}_{d_i}\gamma_5\psi_{d_i} - H\bar{\psi}_{d_i}\psi_{d_i}\right) - \frac{1}{v}\left[M_d V^\dagger_{CKM}\right]_{mn}\phi^-\bar{\psi}_{d_m}P_L\psi_{u_n} \\ & \quad - \frac{1}{v}\left[V_{CKM}M_d\right]_{mn}\phi^+\bar{\psi}_{u_m}P_R\psi_{d_n} \\ L_Y^{int,d} &= \frac{(M_l)_{ii}}{\sqrt{2}v}\left(-i\xi\bar{\psi}_{l_i}\gamma_5\psi_{l_i} - H\bar{\psi}_{l_i}\psi_{l_i}\right) - \frac{1}{v}(M_l)_{ii}\left(\phi^-\bar{\psi}_{l_i}P_L\psi_{\nu_i} + \phi^+\bar{\psi}_{\nu_i}P_R\psi_{l_i}\right) \end{cases} \tag{D.14}$$

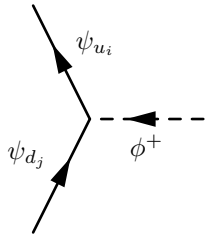

$= i\frac{g}{\sqrt{2}M_W}(V_{CKM})_{ij}\left[m_{u_i}P_L - m_{d_j}P_R\right]$

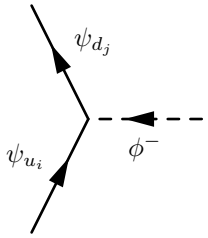

$= i\frac{g}{\sqrt{2}M_W}(V^*_{CKM})_{ij}\left[m_{u_i}P_R - m_{d_j}P_L\right]$

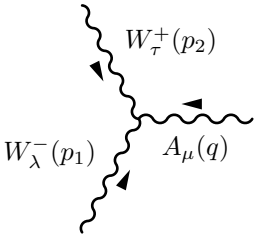

$= -ie\left[(p_1-p_2)^\mu g^{\lambda\tau} + (p_2-q)^\lambda g^{\tau\mu} + (q-p_1)^\tau g^{\mu\lambda}\right]$

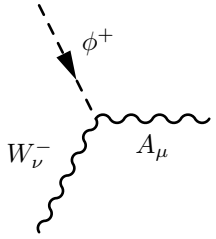

$= ieM_W g^{\mu\nu}$

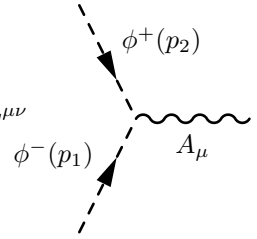

$= ie\,(p_1-p_2)^\mu$

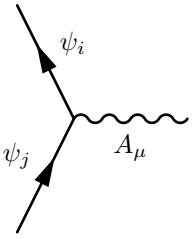

$= -ieQ_{p_i}\delta_{ij}\gamma^\mu$

D.4 The supersymmetric model

D.4.1 The MSSM superpotential

The expansion of the superpotential - expression (4.1) - in terms of elementary fields can be carried out formally. Below we give these terms, separated into two types, in the super-CKM basis - see equation (4.15) - with 4-component spinors:

1. Fermion interactions (the hat denotes a diagonal matrix):

$$-\hat{y}^u_{ij}\left\{H^0_u\bar{u}_jP_Lu_i+\tilde{u}^\dagger_{j,R}\bar{\tilde{H}}^0_uP_Lu_i+\tilde{u}_{i,L}\bar{u}_jP_L\tilde{H}^0_u\right\}+\text{h.c.} \tag{D.15}$$

$$-\hat{y}^d_{ij}\left\{H^0_d\bar{d}_jP_Ld_i+\tilde{d}^\dagger_{j,R}\bar{\tilde{H}}^0_dP_Ld_i+\tilde{d}_{i,L}\bar{d}_jP_L\tilde{H}^0_d\right\}+\text{h.c.} \tag{D.16}$$

$$+[\hat{y}^uV_{CKM}]_{ij}\left\{H^+_u\bar{u}_iP_Ld_j+\tilde{u}^\dagger_{i,R}\bar{\tilde{H}}^+_uP_Ld_j+\tilde{d}_{j,L}\bar{u}_iP_L\tilde{H}^+_u\right\}+\text{h.c.} \tag{D.17}$$

$$+[\hat{y}^dV^\dagger_{CKM}]_{ij}\left\{H^-_d\bar{d}_iP_Lu_j+\tilde{d}^\dagger_{i,R}\bar{\tilde{H}}^-_dP_Lu_j+\tilde{u}_{j,L}\bar{d}_iP_L\tilde{H}^-_d\right\}+\text{h.c.} \tag{D.18}$$

$$-\hat{y}^l_{ij}\left\{H^0_d\bar{l}_jP_Ll_i+\tilde{l}^\dagger_{j,R}\bar{\tilde{H}}^0_dP_Ll_i+\tilde{l}_{i,L}\bar{l}_jP_L\tilde{H}^0_d\right\}+\text{h.c.} \tag{D.19}$$

$$+\hat{y}^l_{ij}\left\{H^-_d\bar{l}_jP_L\nu_i+\tilde{l}^\dagger_{j,R}\bar{\tilde{H}}^-_dP_L\nu_i+\tilde{\nu}_{i,L}\bar{l}_jP_L\tilde{H}^-_d\right\}-\mu\left\{\bar{\tilde{H}}^+_uP_L\tilde{H}^-_d-\bar{\tilde{H}}^0_uP_L\tilde{H}^0_d\right\}+\text{h.c.} \tag{D.20}$$

2. Boson interactions (F-fields mediated: $F_{H^0_u}$, $F_{H^+_u}$, $F_{H^-_d}$, $F_{H^0_d}$, $F_{\bar{u}_i}$, $F_{\bar{d}_i}$, F_{u_j}, F_{d_j}, $F_{\bar{l}_i}$, F_{l_j}, F_{ν_j}):

$$\left\{\begin{array}{ll}
F_{H^0_u}\left\{\hat{y}^u_{ij}\tilde{u}^\dagger_{j,R}\tilde{u}_{i,L}-\mu H^0_d\right\}, & F_{H^0_d}\left\{\hat{y}^d_{ij}\tilde{d}^\dagger_{j,R}\tilde{d}_{i,L}+\hat{y}^l_{ij}\tilde{l}^\dagger_{j,R}\tilde{l}_{i,L}-\mu H^0_u\right\},\\
F_{H^+_u}\left\{-[\hat{y}^uV_{CKM}]_{ij}\tilde{u}^\dagger_{i,R}\tilde{d}_{j,L}+\mu H^-_d\right\}, & F_{H^-_d}\left\{-[\hat{y}^dV^\dagger_{CKM}]_{ij}\tilde{d}^\dagger_{i,R}\tilde{u}_{j,L}-\hat{y}^l_{ij}\tilde{l}^\dagger_{j,R}\tilde{\nu}_{i,L}+\mu H^+_u\right\},\\
F_{\bar{u}_i}\hat{y}^u_{ij}\left\{\tilde{u}_{j,L}H^0_u-[V_{CKM}]_{jk}\tilde{d}_{L,k}H^+_u\right\}, & F_{\bar{d}_i}\hat{y}^d_{ij}\left\{\tilde{d}_{j,L}H^0_d-[V^\dagger_{CKM}]_{jk}\tilde{u}_{L,k}H^-_d\right\},\\
F_{u_j}\left\{\hat{y}^u_{ij}H^0_u\tilde{u}^\dagger_{i,R}-[\hat{y}^dV^\dagger_{CKM}]_{ij}H^-_d\tilde{d}^\dagger_{i,R}\right\}, & F_{d_j}\left\{\hat{y}^d_{ij}H^0_d\tilde{d}^\dagger_{j,R}-[\hat{y}^uV_{CKM}]_{ij}H^+_u\tilde{u}^\dagger_{i,R}\right\},\\
F_{\bar{l}_i}\hat{y}^l_{ij}\left\{\tilde{l}_{j,L}H^0_d-\tilde{\nu}_{j,L}H^-_d\right\}, & F_{\nu_i}\left\{-\hat{y}^l_{ij}H^-_d\tilde{l}^\dagger_{j,R}\right\}+F_{l_i}\left\{\hat{y}^l_{ij}H^0_d\tilde{l}^\dagger_{j,R}\right\}.
\end{array}\right. \tag{D.21}$$

D.4.2 MSSM gaugino-matter 3-interactions

We decompose the gaugino-matter sector into three parts:

$$\mathcal{L}^{gauginos}=\mathcal{L}^{gauginos}_{\text{SU(3)}}+\mathcal{L}^{gauginos}_{\text{SU(2)}}+\mathcal{L}^{gauginos}_{\text{U(1)}}. \tag{D.22}$$

Writing the gaugino fields as Majorana 4-component spinors and casting the matter fields to Dirac 4-component spinors, we have:

$$\mathcal{L}^{gauginos}_{\text{SU(3)}} = -\sqrt{2}g_s\sum_{q=u,d,c,s,t,b}\left\{T^\alpha_{ab}\,\tilde{q}_{(b)L}\left(\bar{q}_{(a)}P_R\,\tilde{g}^\alpha\right)+T^\alpha_{ab}\,\tilde{q}_{(a)R}\left(\bar{q}_{(b)}P_L\,\tilde{g}^\alpha\right)+\text{h.c.}\right\}.$$

Defining $P_{L,R}\tilde{W}^\pm\equiv\frac{P_{L,R}\tilde{W}^1\mp iP_{L,R}\tilde{W}^2}{\sqrt{2}}$, we find in the gauge interaction basis:

$$\begin{aligned}
\mathcal{L}^{gauginos}_{\text{SU(2)}} = & -\frac{1}{\sqrt{2}}g\sum_{l=e,\mu,\tau}\left\{-\tilde{l}_L\bar{l}P_R\tilde{W}^0+\tilde{\nu}_{l,L}\bar{\nu}_lP_R\tilde{W}^0+\text{h.c.}\right\}-g\sum_{l=e,\mu,\tau}\left\{\tilde{l}_L\bar{\nu}_lP_R\tilde{W}^-+\tilde{\nu}_{l,L}\bar{l}P_R\tilde{W}^++\text{h.c.}\right\}\\
& -\frac{1}{\sqrt{2}}g\sum_{u=u,c,t}\sum_{d=d,s,b}\left\{-\tilde{d}_{(a)L}\left(\bar{d}_{(a)}P_R\tilde{W}^0\right)+\tilde{u}_{(a)L}\left(\bar{u}_{(a)}P_R\tilde{W}^0\right)+\text{h.c.}\right\}\\
& -g\sum_{u=u,c,t}\sum_{d=d,s,b}\left\{\tilde{d}_{(a)L}\left(\bar{u}_{(a)}P_R\tilde{W}^-\right)+\tilde{u}_{(a)L}\left(\bar{d}_{(a)}P_R\tilde{W}^+\right)+\text{h.c.}\right\}\\
& -\frac{1}{\sqrt{2}}g\left\{-H^0_u\bar{\tilde{H}}^0_uP_R\tilde{W}^0+H^+_u\bar{\tilde{H}}^+_uP_R\tilde{W}^0-H^-_d\bar{\tilde{H}}^-_dP_R\tilde{W}^0+H^0_d\bar{\tilde{H}}^0_dP_R\tilde{W}^0+\text{h.c.}\right\}\\
& -g\left\{H^0_u\bar{\tilde{H}}^+_uP_R\tilde{W}^-+H^+_u\bar{\tilde{H}}^0_uP_R\tilde{W}^++H^-_d\bar{\tilde{H}}^0_dP_R\tilde{W}^-+H^0_d\bar{\tilde{H}}^-_dP_R\tilde{W}^++\text{h.c.}\right\}.
\end{aligned}$$

Finally, for the U(1)$_y$ gaugino interactions:

$$\begin{aligned}\mathcal{L}^{gauginos}_{\mathsf{U(1)}} &= -\frac{1}{\sqrt{2}}g' \sum_{l=e,\mu,\tau} \left\{-\tilde{l}_L \bar{l} P_R \tilde{B} - \tilde{\nu}_{l,L}\bar{\nu}_{l,L} P_R \tilde{B} + 2\tilde{l}_R \bar{l} P_L \tilde{B} + 2\tilde{\nu}_{l,R}\bar{\nu}_l P_L \tilde{B} + \mathsf{h.c.}\right\} \\ &\quad -\frac{1}{\sqrt{2}}g' \sum_{u=u,c,t} \sum_{d=d,s,b} \left\{\frac{1}{3}\tilde{u}_{(a)L}\left(\bar{u}_{(a)} P_R \tilde{B}\right) + \frac{1}{3}\tilde{d}_{(a)L}\left(\bar{d}_{(a)} P_R \tilde{B}\right)\right. \\ &\qquad \left. -\frac{4}{3}\tilde{u}_{(a)R}\left(\bar{u}_{(a)} P_L \tilde{B}\right) + \frac{2}{3}\tilde{d}_{(a)R}\left(\bar{d}_{(a)} P_L \tilde{B}\right) + \mathsf{h.c.}\right\} \\ &\quad -\frac{1}{\sqrt{2}}g' \left\{H_u^+ \bar{\tilde{H}}_u^+ P_R \tilde{B} + H_u^0 \bar{\tilde{H}}_u^0 P_R \tilde{B} - H_d^- \bar{\tilde{H}}_d^- P_R \tilde{B} - H_d^0 \bar{\tilde{H}}_d^0 P_R \tilde{B} + \mathsf{h.c.}\right\} . \end{aligned} \tag{D.23}$$

D.4.3 MSSM mass matrices after electroweak symmetry breaking

We refer to section 4.4 of chapter 4 for the description of the MSSM EWSB. In here we list the mass matrices that arise after EWSB and refer to section 4.5 of chapter 4 for the complete MSSM mass spectrum.

D.4.3.1 Higgs states and corresponding mass matrices

Basis: $\left\{\mathsf{Im}\left[H_u^0\right], \mathsf{Im}\left[H_d^0\right]\right\}$

$$M^2_{\mathsf{Im}[H^0]} \equiv \begin{pmatrix} b\cot\beta & b \\ b & b\tan\beta \end{pmatrix} \tag{D.24}$$

Basis: $\left\{H_u^+, H_d^{-\dagger}\right\}$

$$M^2_{H\text{-charged}} = M^2_{\mathsf{Im}[H^0]} + M_W^2 \begin{pmatrix} \cos^2\beta & \frac{1}{2}\sin 2\beta \\ \frac{1}{2}\sin 2\beta & \sin^2\beta \end{pmatrix} \tag{D.25}$$

Basis: $\left\{\mathsf{Re}\left[H_u^0\right] - v_u, \mathsf{Re}\left[H_d^0\right] - v_d\right\}$

$$M^2_{\mathsf{Re}[H^0]-v} \equiv \begin{pmatrix} b\cot\beta + M_Z^2\sin^2\beta & -b - \frac{1}{2}M_Z^2\sin 2\beta \\ -b - \frac{1}{2}M_Z^2\sin 2\beta & b\tan\beta + M_Z^2\cos^2\beta \end{pmatrix} \tag{D.26}$$

D.4.3.2 Neutralino and chargino states and corresponding mass matrices

Neutralinos are linear combinations of $\tilde{G}^0 \equiv \left\{\tilde{B}, \tilde{W}^0, \tilde{H}_d^0, \tilde{H}_u^0\right\}$ with bilinear terms:

$$-\frac{1}{2}M^N_{ij}\bar{\tilde{G}}_i^0 P_L \tilde{G}_j^0 + \mathsf{h.c.}\,, \quad M^N \equiv \begin{pmatrix} M_1 & 0 & -c_\beta s_w M_Z & s_\beta s_w M_Z \\ 0 & M_2 & c_\beta c_w M_Z & -s_\beta c_w M_Z \\ -c_\beta s_w M_Z & c_\beta c_w M_Z & 0 & -\mu \\ s_\beta s_w M_Z & -s_\beta c_w M_Z & -\mu & 0 \end{pmatrix} . \tag{D.27}$$

As the neutralino mass matrix is complex symmetric, it can be diagonalized by one unitary matrix N such that:

$$\hat{M}^N = N^* M^N N^{-1}\,, \quad \tilde{\chi}_A^0 = N_{Ai}\tilde{G}_i^0\,, \tag{D.28}$$

where $\tilde{\chi}^0_A$ $(A = 1, .., 4)$ are the mass eigenstates, called neutralinos.

Charginos are linear combinations of $\tilde{G}^+ \equiv \left\{\tilde{W}^+, \tilde{H}^+_u\right\}$ and $\tilde{G}^- \equiv \left\{\tilde{W}^-, \tilde{H}^-_d\right\}$, with bilinear terms:

$$-M^C_{ij}\bar{\tilde{G}}^-_i P_L \tilde{G}^+_j + \text{h.c.}\,, \quad M^C \equiv \begin{pmatrix} M_2 & \sqrt{2}s_\beta M_W \\ \sqrt{2}c_\beta M_W & \mu \end{pmatrix}. \tag{D.29}$$

This mass matrix is most generally bidiagonalized by two unitary matrices U and V, such that:

$$\hat{M}^C = U^* M^C V^{-1}\,, \quad \tilde{\chi}^+_A = V_{Ai}\tilde{G}^+_i\,, \quad \tilde{\chi}^-_A = U_{Ai}\tilde{G}^-_i\,, \tag{D.30}$$

where $\tilde{\chi}^\pm_A$ are the mass eigenstates, called charginos.

D.4.3.3 Sfermion masses

From the superpotential F-terms we find the bilinear terms in the sfermion fields:

$$\begin{array}{lll} +v_d y^{u*}_{ij}\mu\,\tilde{u}_{j,R}\tilde{u}^\dagger_{i,L} + \text{h.c.} & +v_u y^{d*}_{ij}\mu\,\tilde{d}_{j,R}\tilde{d}^\dagger_{i,L} + \text{h.c.} & +v_u y^{l*}_{ij}\mu\,\tilde{l}_{j,R}\tilde{l}^\dagger_{L,i} + \text{h.c.} \\ -y^u_{ik}y^{u*}_{jk}v_u^2\tilde{u}_{i,L}\tilde{u}^\dagger_{j,L} & -y^d_{ik}y^{d*}_{jk}v_d^2\tilde{d}_{i,L}\tilde{d}^\dagger_{j,L} & -y^l_{ik}y^{l*}_{jk}v_d^2\tilde{l}_{i,L}\tilde{l}^\dagger_{j,L} \\ -y^u_{ki}y^{u*}_{kj}v_u^2\tilde{u}^\dagger_{i,R}\tilde{u}_{j,R} & -y^d_{ki}y^{d*}_{kj}v_d^2\tilde{d}^\dagger_{i,R}\tilde{d}_{j,R} & -y^l_{ki}y^{l*}_{kj}v_d^2\tilde{l}^\dagger_{i,R}\tilde{l}_{j,R}\,, \end{array} \tag{D.31}$$

written in the gauge interaction basis.

From the D-terms we find the following bilinear terms in the sfermion fields:

$$-\frac{(v_u^2 - v_d^2)g'^2}{4}\sum_\phi y_\phi \phi^\dagger\phi\,, \tag{D.32}$$

$$-\frac{1}{2}g^2(-v_u^2 + v_d^2)\left\{\sum_{c=x,y,z}\sum_{Q=U,C,T}\left\{\tilde{Q}^{\dagger a}_{(c)L}T^3_{ab}\tilde{Q}^b_{(c)L}\right\} + \sum_L\left\{\tilde{L}^{\dagger a}_L T^3_{ab}\tilde{L}^b_L\right\}\right\}, \tag{D.33}$$

for D_B and D^3_W, respectively.

Thus, we have a general mass term Δ_ϕ for each of the sfermion fields, ϕ, which is given by:

$$\begin{aligned} -\Delta_\phi &\equiv -\frac{v_d^2 - v_u^2}{2}\left[g^2 T^3|_\phi - g'^2\frac{y_\phi}{2}\right] = -\frac{v_d^2 - v_u^2}{2}(g^2 + g'^2)\left[T^3|_\phi - \frac{g'^2}{g^2 + g'^2}Q_\phi\right] \\ &= -M_Z^2\frac{v_d^2 - v_u^2}{v_d^2 + v_u^2}\left[T^3|_\phi - s_w^2 Q_\phi\right] = -M_Z^2\cos(2\beta)\left[T^3|_\phi - s_w^2 Q_\phi\right]. \end{aligned} \tag{D.34}$$

Putting all together and changing to the super-CKM basis, we find the sfermion $\tilde{q}$ mass matrix arising solely from the EWSB (that is, without the mass terms coming from the soft-breaking sector):

$$M^{2;\text{EWSB}}_{\tilde{q}} = \begin{pmatrix} m_q^2 + \Delta_{\tilde{q}_L} & -\mu\, m_q \begin{cases} \cot\beta, \text{ if } q = u \\ \tan\beta, \text{ if } q = d \end{cases} \\ -\mu^*\, m_q \begin{cases} \cot\beta, \text{ if } q = u \\ \tan\beta, \text{ if } q = d \end{cases} & m_q^2 + \Delta_{\tilde{q}_R} \end{pmatrix}. \tag{D.35}$$

Due to the absence of RH sneutrinos (in the pure MSSM, that is, with vanishing neutrino masses) or in the limit where the RH sneutrinos decouple from the low energy model (in the seesaw type-I extended MSSM), the sneutrino mass matrix arising solely from EWSB reads:

$$M^{2;\text{EWSB}}_{\tilde{\nu}_L} = \Delta_{\tilde{\nu}_L} = \frac{1}{2}M_Z^2\cos(2\beta)\,, \tag{D.36}$$

where we have dropped out the neutrino mass squared, m_ν^2, compared to $M_Z^2\cos(2\beta)$.

D.4.4 Vertices

We fix the convention that the coefficient of a vertex with left-chirality, name it A, is denoted by A_L when the "interesting" fermionic particle is being destroyed and A_R^* when it is being created. An "interesting" fermionic particle is the fermion which will appear on external lines for the process under analysis. In most cases for the present work, the "interesting" fermionic particles are the charged leptons and the down-type quarks or, more generally, the down-components of the SU(2)$_L$ doublets (and, obviously, extended to the corresponding anti-particles).

In here we determine the two vertices that are useful for the study carried out in this thesis: (i) (charged lepton)-(charged slepton)-neutralino and (ii) (charged lepton)-sneutrino-chargino.

Destroy a charged slepton, create a charged lepton and destroy a neutralino ($\bar{l}_i - \tilde{l}_X - \tilde{\chi}_A^0$):

$$\tilde{l}_X \bar{l}_i \left[N_{iXA}^{(L)*} P_R + N_{iXA}^{(R)*} P_L \right] . \tag{D.37}$$

The relevant terms for this vertex are contained in the U(1) and SU(2) gaugino sectors plus the superpotential sector, respectively:

$$-\frac{1}{\sqrt{2}} g' \left\{ -\tilde{l}_L \bar{l} P_R \tilde{B} + 2 \tilde{l}_R \bar{l} P_L \tilde{B} + \text{h.c.} \right\} , \quad -\frac{1}{\sqrt{2}} g \left\{ -\tilde{l}_L \bar{l} P_R \tilde{W}^0 + \text{h.c.} \right\} \tag{D.38}$$

$$\text{and} \qquad \hat{y}_{ij}^l \left\{ -\bar{\tilde{l}}_{j,R}^{\dagger} \bar{\tilde{H}}_d^0 P_L l_i - \tilde{l}_{i,L} \bar{l}_j P_L \tilde{H}_d^0 \right\} + \text{h.c.} . \tag{D.39}$$

Noting that $v_d = \frac{1}{g}\sqrt{2} M_W c_\beta$, $g' = g\, t_w$, $\hat{y}_{ij}^l = \delta_{ij} \frac{m_{l_i}}{v_d}$ and changing to the neutralino mass basis, we can rewrite them as:

$$\tilde{l}_{i,L} \bar{l}_i \left[\frac{g\, t_w}{\sqrt{2}} N_{A1} P_R + \frac{g}{\sqrt{2}} N_{A2} P_R - \frac{g\, m_{l_i}}{\sqrt{2} M_W c_\beta} N_{A3}^* P_L \right] \tilde{\chi}_A^0 , \tag{D.40}$$

$$\tilde{l}_{i,R} \bar{l} \left[-\sqrt{2} g\, t_w N_{A1}^* P_L - \frac{g\, m_{l_i}}{\sqrt{2} M_W c_\beta} N_{A3} P_R \right] \tilde{\chi}_A^0 . \tag{D.41}$$

Rotating to the charged slepton mass basis, $\tilde{l}_X = R_{Xi}^{\tilde{l}} \tilde{l}_i$, we find

$$N_{iXA}^{(L)*} \equiv -\frac{g}{\sqrt{2}} \left[-(t_w N_{A1} + N_{A2}) R_{X;i(1,2,3)}^{\tilde{l}*} + \frac{m_{l_i}}{M_W c_\beta} N_{A3} R_{X;i(4,5,6)}^{\tilde{l}*} \right] , \tag{D.42}$$

$$N_{iXA}^{(R)*} \equiv -\frac{g}{\sqrt{2}} \left[\frac{m_{l_i}}{M_W c_\beta} N_{A3}^* R_{X;i(1,2,3)}^{\tilde{l}*} + 2 t_w N_{A1}^* R_{X;i(4,5,6)}^{\tilde{l}*} \right] . \tag{D.43}$$

where $i = 1,2,3$ (LH charged sleptons) and $j = 4,5,6$ (RH charged sleptons).

Destroy a sneutrino, create a charged lepton and destroy a chargino ($\bar{l}_i - \tilde{\nu}_X - \tilde{C}_A$):

$$\tilde{\nu}_X \bar{l}_i \left[C_{iXA}^{(L)*} P_R + C_{iXA}^{(R)*} P_L \right] \tilde{C}_A , \quad \text{where} \quad \tilde{C}_A \equiv \begin{pmatrix} i\sigma_2 \tilde{\chi}_A^{+\dagger T} \\ \tilde{\chi}_A^- \end{pmatrix} . \tag{D.44}$$

The relevant terms arise from the charged SU(2) gaugino sector and the superpotential sector:

$$\tilde{\nu}_{l,L} \bar{l} \left[-g V_{A1} \right] P_R \, \tilde{\chi}_A^+ + \text{h.c.} , \quad \tilde{\nu}_{l,L} \bar{l} \left[\frac{g\, m_l}{\sqrt{2} M_W c_\beta} U_{A2}^* \right] P_L \, \tilde{\chi}_A^- + \text{h.c.} . \tag{D.45}$$

Rotating to the chargino and sneutrino mass bases, we find:

$$C_{iXA}^{(L)*} = -g V_{A1} R_{X;i(1,2,3)}^{\tilde{\nu}*} , \tag{D.46}$$

$$C_{iXA}^{(R)*} = \frac{g\, m_{l_i}}{\sqrt{2} M_W c_\beta} U_{A2}^* R_{X;i(1,2,3)}^{\tilde{\nu}*} . \tag{D.47}$$

D.5 Propagators

The propagators are defined as the vacuum amplitude for creating a particle at a space-time point y and destroying it at a space-time point x (with $t_x > t_y$ - causality) "plus" the amplitude of creating an anti-particle at a space-time point x and destroying it at a space-time point y (with $t_y > t_x$). Explicitly, we write this amplitude as:

$$\begin{cases} \text{Real scalars:} & i\Delta_{(rs)}(x-y) \equiv \langle 0|T\left(\phi(x)\phi(y)\right)|0\rangle\,, \quad \text{Complex scalars:} & i\Delta_{(cs)}(x-y) \equiv \langle 0|T\left(\phi(x)\phi^\dagger(y)\right)|0\rangle\,, \\ \text{Dirac fermions:} & iS_{\alpha\beta}(x-y) \equiv \langle 0|T\left(\psi_\alpha(x)\bar{\psi}_\beta(y)\right)|0\rangle\,, \quad \text{Gauge bosons:} & iD^{ab}_{\mu\nu}(x-y) \equiv \langle 0|T\left(W^a_\mu(x)W^b_\nu(y)\right)|0\rangle\,, \\ \text{FP Ghosts:} & i\Delta^{ab}_{(gf)}(x-y) \equiv \langle 0|T\left(\omega^a(x)\bar{\omega}^b(y)\right)|0\rangle\,, \end{cases}$$

where the field operators are in the interaction picture and so they are given in terms of free-solutions; T denotes the time ordered product: $T\left(a(t)b(t')\right) = \theta(t-t')a(t)b(t') \pm \theta(t'-t)b(t')a(t)$, where $(+)$ is for bosonic (commuting) fields and $(-)$ is for fermionic (anti-commuting) fields.

For Majorana fermions we have 3 types of bilinear combinations with non-vanishing vacuum expectation values, i.e., we have 3 types of propagators. This is because particle and anti-particle are the same entity (see, for example, [18]). Explicitly, we have:

$$\begin{cases} \langle 0|T\left(\psi^\chi_{M,\alpha}(x)\bar{\psi}^\chi_{M,\beta}(y)\right)|0\rangle = iS_{\alpha\beta}(x-y)\,, \quad \langle 0|T\left(\psi^\chi_{M,\alpha}(x)\psi^\chi_{M,\beta}(y)\right)|0\rangle = iS_{\alpha\beta'}(x-y)C^T_{\beta'\beta}\,, \\ \langle 0|T\left(\bar{\psi}^\chi_{M,\alpha}(x)\bar{\psi}^\chi_{M,\beta}(y)\right)|0\rangle = iC^T_{\alpha\alpha'}S_{\alpha'\beta}(x-y)\,, \end{cases} \tag{D.48}$$

where we used that $\psi^\chi_M = C\bar{\psi}^{\chi T}_M$, being C the charge conjugation matrix defined by $C \equiv -i\gamma^2\gamma^0$, with $C^T = C^{-1}$.

Next we list the momentum-space propagators of a general theory.

Notation: The index i specifies the multiplet and the indices a,b are used for specifying the components of that multiplet. Note that there is no bilinear mix between different fields, therefore, the propagators are diagonal in the multiplet space, justifying the δ^{ab} factors.

Scalars, Goldstone Bosons and FP Ghosts propagators

a ---- $\phi_i(p)$ ---- b $\quad = \frac{i\delta^{ab}}{p^2-m_i^2}$ | a ---- $\phi_W(p)$ ---- b $\quad = \frac{i\delta^{ab}}{p^2-\xi M_W^2}$ | a ····· $\omega(p)$ ····· b $\quad = \frac{i\delta^{ab}}{p^2}$

Dirac Fermions and Gauge Bosons propagators

a ——▶—— $\psi_i(p)$ ——▶—— b $\quad = i\delta^{ab}\left[\frac{1}{\not{p}-m_i}\right]_{\alpha\beta}$ | a,μ ~~~ $W(p)$ ~~~ b,ν $\quad = \frac{-i\delta^{ab}}{p^2-M_W^2}\left(g_{\mu\nu} - (1-\xi)\frac{p_\mu p_\nu}{p^2-\xi M_W^2}\right)$

Majorana fermions propagators $\quad iS^{(i)ab}_{\alpha\beta}(p) \equiv i\delta^{ab}\left[\frac{1}{\not{p}-m_i}\right]_{\alpha\beta}$

a,α ——▶—— $\chi_i(p)$ ——▶—— b,β $\quad = iS^{(i)ab}_{\alpha\beta}(p)$ | a,α ——▶◀—— $\chi_i(p)$ ——▶◀—— b,β $\quad = iS^{(i)ab}_{\alpha\beta'}(p)C^T_{\beta'\beta}$ | a,α ——◀▶—— $\chi_i(p)$ ——◀▶—— b,β $\quad = iC^T_{\alpha\alpha'}S^{(i)ab}_{\alpha'\beta}(p)$

E General formulae in Flavour Violating processes

E.1 FV radiative decays: fermion$_i$ $\to$ fermion$_j$ + γ

In this section a deduction for the amplitude of the process fermion$_i$ $\to$ fermion$_j$ + γ is made to leading order (LO). The conventions are fixed so that the fermion$_i$ has mass m_i and momentum p and the fermion$_j$ has mass m_j and momentum $p-q$. Then, the emitted photon has momentum q which, for now, is not taken as being necessarily on-shell.

Denoting by $\epsilon^*_\mu(q)\mathcal{M}^\mu$ the amplitude and demanding gauge invariance ($q_\mu \mathcal{M}^\mu = 0$) one can write in all generality $\mathcal{M}^\mu$ as [77]:

$$\mathcal{M}^\mu = \bar{u}_j(p-q)\left[iq_\nu\sigma^{\mu\nu}\Omega^{(ij)} + B_L^{(ij)}\Delta_L^\mu(m_i,m_j) + B_R^{(ij)}\Delta_R^\mu(m_i,m_j)\right]u_i(p)\,, \quad \text{(E.1)}$$

$$\Omega^{(ij)} \equiv A_L^{(ij)}P_L + A_R^{(ij)}P_R\,, \quad \text{(E.2)}$$

$$\Delta^\mu_{L,R}(m_i,m_j) \equiv q^\mu\left(m_i^2 - m_j^2\right)P_{L,R} - q^2\gamma^\mu\left(m_jP_{L,R} + m_iP_{R,L}\right)\,, \quad \text{(E.3)}$$

where $A^{(ij)}_{L,R}$ and $B^{(ij)}_{L,R}$ are coefficients with mass dimension $[M]^{-1}$ and $[M]^{-3}$, respectively, whose form is fixed by a particular underlying theory and not by a fundamental principle as it is gauge-invariance.

One can readily see that for an on-shell photon, $q_\mu\epsilon^{\mu*}(q) = 0$ and $q^2 = 0$, the coefficients $B^{(ij)}_{L,R}$ will not contribute to the process' amplitude. Moreover, the $A_L^{(ij)}$ and $A_R^{(ij)}$ coefficients correspond to a flip in the chirality between the incoming and outgoing fermions, namely, from left-handed to right-handed and right-handed to left-handed, respectively.

For an emitted on-shell photon the averaged amplitude squared, taking the fermion$_i$ as a massive spin-1/2 particle (thus, two allowed polarizations), is calculated as:

$$\overline{|\mathcal{M}|^2} = 4\left(|A_L^{(ij)}|^2 + |A_R^{(ij)}|^2\right)(p\cdot q)^2\,, \quad \text{(E.4)}$$

and the correspondent decay width is:

$$\Gamma = \frac{m_i^3}{16\pi}\left(1-x_{ji}\right)^3\left[|A_L^{(ij)}|^2 + |A_R^{(ij)}|^2\right]\,, \quad x_{ji} \equiv \frac{m_j^2}{m_i^2}\,. \quad \text{(E.5)}$$

For the purpose of determining the decay width by evaluating the relevant LO diagrams it is convenient to further manipulate the amplitude's expression (E.1), in particular its on-shell contribution encoded in $\Omega^{(ij)}$. One has:

$$\bar{u}_j(p-q)\left[iq_\nu\sigma^{\mu\nu}\Omega^{(ij)}\right]u_i(p) = \bar{u}_j(p-q)\left[(2p-q)^\mu\,\Omega^{(ij)} - m_i\gamma^\mu\bar{\Omega}^{(ij)} - m_j\gamma^\mu\Omega^{(ij)}\right]u_i(p)\,, \quad \text{(E.6)}$$

$$\bar{\Omega}^{(ij)} \equiv A_L^{(ij)}P_R + A_R^{(ij)}P_L\,. \quad \text{(E.7)}$$

By choosing to work only with the set of momenta $\{p,q\}$ it is notorious that the exclusively off-shell components of the amplitude, i.e., $\Delta^\mu_{L,R}$, do not depend on p^μ. Thus, from (E.6), one concludes that the coefficients $A^{(ij)}_{L,R}$ can be isolated by just looking to the contribution p^μ (or $\epsilon^*_\mu p^\mu$) of each diagram. This procedure of determining $A^{(ij)}_{L,R}$ works even if we are interested in the off-shell process.

In the next sub-sections we will show explicitly the form of the coefficients $A^{(ij)}_{L,R}$ in the context of the SM and of the MSSM.

E.1.1 FV radiative decay fermion$_i \to$ fermion$_j + \gamma$ in the SM

In the SM the LO diagrams for fermion$_i \to$ fermion$_j + \gamma$ (where i and j label two distinct flavours) arise solely from the known CKM quark-mixing. In the 't-Hooft-Feynman gauge we have to consider both the W's charged current and the Yukawa couplings with charged Goldstone bosons, $\phi^{\pm}$.

The diagrams are depicted below. As all the particles involved are charged there are three sets of diagrams which are characterized by the photon emission: in the first row the photon is emitted from a charged boson line (internal); the second row from an external fermion line; and the third from an internal fermion line.

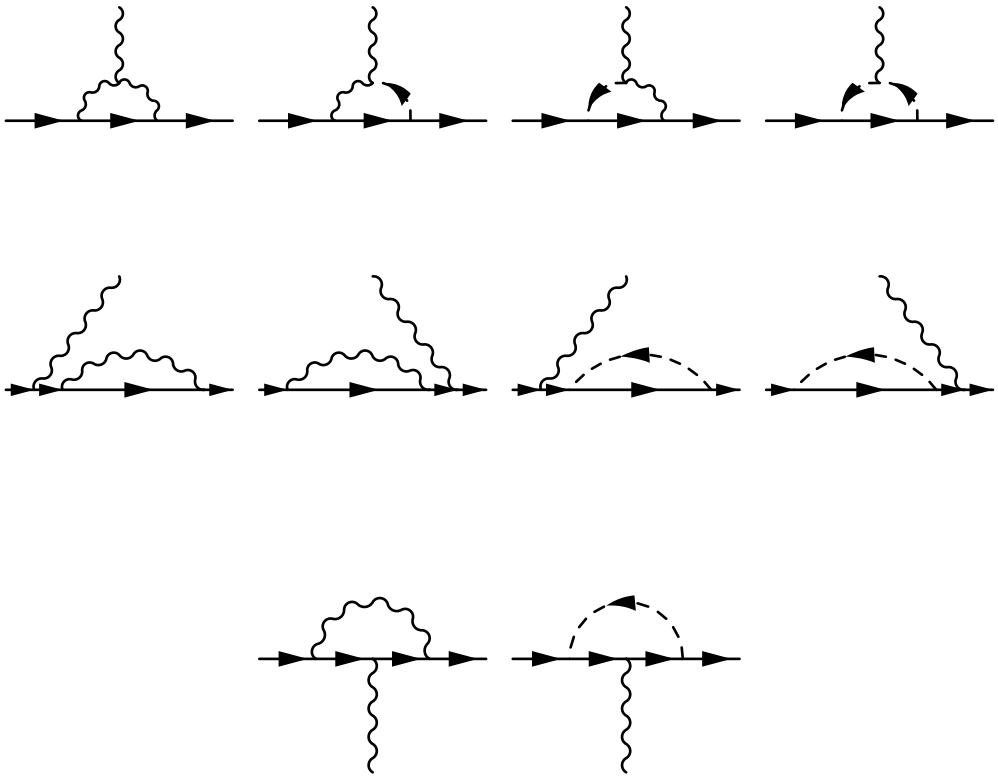

We note that this is the general case. If one is obliged to extend the SM by considering, for instance, mixing in the leptonic sector, the diagrams are the same with the exception that the third (second) row has to be discarded for a charged lepton (neutral lepton) $i \to j$ transition.

As the tree-level vertices involved in the transition couple only left-handed chiralities, in the limit where the outgoing fermion is massless its chirality is necessarily left-handed. Thus, $A_L^{(ij)}$ must be proportional to the outgoing right-handed fermion mass, vanishing when $m_j^{(R)} = 0$. Analogously, $A_R^{(ij)}$ is proportional to the incoming right-handed fermion mass, $m_i^{(R)}$. We will see this explicitly below.

From the argument given at the end of the previous sub-section, namely, that the on-shell contribution to the fermion$_i \to$ fermion$_j + \gamma$ process can be isolated by just looking at the coefficients of p^μ, we can write the on-shell amplitude as:

$$\mathcal{M}^\mu = 2p^\mu \bar{u}_j(p-q)\left(A_L^{(ij)}P_L + A_R^{(ij)}P_R\right)u_i(p)\,. \tag{E.8}$$

We readily see that the diagrams on the second row are not relevant for the on-shell process because the Lorentz index will be of the form γ^μ, originated by the photon emission on external lines. In fact, these

diagrams are only important to cancel the divergences in the vertex fermion$_i$ $-$ fermion$_j$ $-$ A_μ, rendering a finite result.

The relevant vertices will have a general coupling strength given by $eg^2/2$ and the mixing matrix element $V_{ki} \equiv (V_u^\dagger V_d)_{ki}$ (where V_u and V_d are the flavour-to-mass rotation matrices of the up and down components of the SU(2)$_L$ doublet, respectively) from W^+-$\overline{\text{fermion}}_k$-fermion$_i$ and ϕ^+-$\overline{\text{fermion}}_k$-fermion$_i$ vertices. We then factorize these terms to write:

$$A_{L,R}^{(ij)} = \left(\frac{eg^2}{2}\right) \sum_k \lambda_k^{(ij)} F_{L,R}^{(ij)}(k)\,, \quad \lambda_k^{(ij)} = V_{kj}^* V_{ki}\,, \tag{E.9}$$

where we sum the contribution of all possible internal particles denoted by k.

We note that $F_{L,R}^{ij}(k)$ has mass dimension -1 and from the argument given above, namely, that A_L^{ij} (A_R^{ij}) is proportional to m_j (m_i), we conclude that we can factorize the amplitude of each diagram so that the on-shell contribution of the loop integral over d^4k will have mass dimension -2. Then, seeing that each diagram will have 3 scalar denominators with mass dimension 2, we conclude that, by performing a change of variables over k, motivated by Feynman's parametrization (C.5), the loop integral will be proportional to $I_{0,3}$ (see (C.22)). We can then write:

$$F_L^{(ij)}(k) = 2\left(\frac{-i}{32\pi^2}\right)\frac{m_j}{M_W^2}\sum_{n=1}^{10} C_k^{(n)} f_L^{(n;ij)}(k) \equiv \left(\frac{-i}{16\pi^2}\right)\frac{m_j}{M_W^2} G_L^{(ij)}(k)\,, \tag{E.10}$$

$$F_R^{(ij)}(k) = 2\left(\frac{-i}{32\pi^2}\right)\frac{m_i}{M_W^2}\sum_{n=1}^{10} C_k^{(n)} f_R^{(n;ij)}(k) \equiv \left(\frac{-i}{16\pi^2}\right)\frac{m_i}{M_W^2} G_R^{(ij)}(k)\,, \tag{E.11}$$

where the factor 2 comes from the Feynman's parametrization for a 3-denominator integral and $\frac{-i}{32\pi^2}$ comes from the global coefficient of the $I_{0,3}$ integral. We take out an inverse of the boson mass to define the dimensionless form factor functions $f_{L,R}^{(n;ij)}$. The coefficients $C_k^{(n)}$ are related to the charge of the mediating particles, being defined as:

$$C_k^{(1)} = Q_B\,, \quad C_k^{(2)} = C_k^{(3)} = Q_B\,, \quad C_k^{(4)} = Q_B\,, \tag{E.12}$$

$$C_k^{(9)} = Q_k\,, \quad C_k^{(10)} = Q_k\,, \tag{E.13}$$

where $Q_B = -1$ for W and ϕ exchange and Q_k is the exchanged fermion charge.

We used FeynCalc [78] to calculate the coefficient p^μ of the amplitude of each diagram and perform the change variables $k \to k + P_i$ (see (C.4–C.6)) - where $i = 1, 2$ for the diagram of the first and third rows, respectively.

The first row form factor functions were calculated to be given by:

$$f_L^{(1)}(k) = M_W^2 \int_0^1 dx \int_0^{1-x} dy \left[\frac{2a_1b_1 - a_1 - b_1}{\Delta_1}\right], \quad f_R^{(1)}(k) = M_W^2 \int_0^1 dx \int_0^{1-x} dy \left[\frac{-2a_1^2 - 2b_1a_1 + b_1}{\Delta_1}\right], \tag{E.14}$$

$$f_L^{(2)}(k) = M_W^2 \int_0^1 dx \int_0^{1-x} dy \left[\frac{-a_1 - b_1}{\Delta_1}\right], \quad f_R^{(2)}(k) = 0\,, \tag{E.15}$$

$$f_L^{(3)}(k) = 0\,, \quad f_R^{(3)}(k) = M_W^2 \int_0^1 dx \int_0^{1-x} dy \left[\frac{b_1}{\Delta_1}\right], \tag{E.16}$$

$$f_L^{(4)}(k) = -\frac{1}{m_j}\int_0^1 dx \int_0^{1-x} dy \left\{ \frac{m_i(a_1-1)(a_1+b_1)n_{SM}^R + m_j b_1(1-a_1)n_{SM}^L + m_k(a_1-1)n_{SM}^{LR}}{\Delta_1} \right\}, \tag{E.17}$$

$$f_R^{(4)}(k) = \frac{m_j}{m_i}\, f_L^{(4)}(k)\Big|_{L\leftrightarrow R}, \tag{E.18}$$

where $n_{k;SM}^{L(ij)} = m_k^2\lambda_k^{(ij)}$, $n_{k;SM}^{R(ij)} = m_j m_i \lambda_k^{(ij)}$, $n_{k;SM}^{LR(ij)} = -m_j m_k \lambda_k^{(ij)}$, $n_{k;SM}^{RL(ij)} = -m_i m_k \lambda_k^{(ij)}$. The couplings replacement renders:

$$f_L^{(4)}(k) = \int_0^1 dx \int_0^{1-x} dy \left\{ \frac{(1-a_1)\left[a_1 m_i^2 - m_k^2 + b_1(m_i^2 - m_k^2)\right]}{\Delta_1} \right\}, \tag{E.19}$$

$$f_R^{(4)}(k) = \int_0^1 dx \int_0^{1-x} dy \left\{ \frac{(1-a_1)\left[(a_1-1)m_k^2 + b_1(m_k^2 - m_j^2)\right]}{\Delta_1} \right\}. \tag{E.20}$$

The diagrams of the second row vanish:

$$f_{L,R}^{(5)} = f_{L,R}^{(6)} = f_{L,R}^{(7)} = f_{L,R}^{(8)} = 0\,. \tag{E.21}$$

For the third row diagrams we have found:

$$f_L^{(9)}(k) = M_W^2 \int_0^1 dx \int_0^{1-x} dy \left[\frac{2a_2(1-b_2)}{\Delta_2}\right], \quad f_R^{(9)}(k) = M_W^2 \int_0^1 dx \int_0^{1-x} dy \left[\frac{2a_2(a_2+b_2)}{\Delta_2}\right], \tag{E.22}$$

and

$$f_L^{(10)}(k) = -\frac{1}{m_j}\int_0^1 dx \int_0^{1-x} dy \left\{ \frac{m_i a_2(1-b_2-a_2)n_{SM}^R + m_j a_2 b_2 n_{SM}^L + m_k(1-a_2)n_{SM}^{LR}}{\Delta_2} \right\}, \tag{E.23}$$

$$f_R^{(10)}(k) = \frac{m_j}{m_i}\, f_L^{(10)}(k)\Big|_{L\leftrightarrow R}, \tag{E.24}$$

rendering after n_{SM}^R, n_{SM}^L and n_{SM}^{LR} replacement:

$$f_L^{(10)}(k) = \int_0^1 dx \int_0^{1-x} dy \left\{ \frac{a_2\left[(b_2-1)m_i^2 - (b_2+1)m_k^2\right] + a_2^2 m_i^2 + m_k^2}{\Delta_2} \right\}, \tag{E.25}$$

$$f_R^{(10)}(k) = \int_0^1 dx \int_0^{1-x} dy \left\{ \frac{a_2\left[b_2(m_k^2 - m_j^2) - 2m_k^2\right] + a_2^2 m_k^2 + m_k^2}{\Delta_2} \right\}. \tag{E.26}$$

In here a_1, b_1 and a_2, b_2 come from the change of variables $k \to k + P_i = k + a_i p + b_i q$ to make the k-integral denominator even after introducing the Feynman's parametrization. We have two P_i's (or two sets of a_i,b_i) because the loop structure of the first and third row diagrams are different. Correspondingly, one has Δ_1 and Δ_2 as the generalized 1L mass squared for the diagrams of the first and third rows, respectively.

Using the convention expressed in (C.3), one can choose for the diagrams of the first row:

$$\begin{aligned} r_0 &= 0\,, & m_0 &= m_k\,, \\ r_1 &= p - q\,, & m_1 &= M_W\,, \\ r_2 &= p\,, & m_2 &= M_W, \end{aligned} \tag{E.27}$$

and by (C.5) one has:

$$\begin{aligned} P_1 &= (1-x)p + (x+y-1)q \;\Rightarrow\; a_1 = 1-x\,,\;\; b_1 = -y\,, && \text{(E.28)} \\ \Delta_1 &= m_k^2 x + M_W^2(1-x) + p^2 x(x-1) + q^2 y(y-1) + 2(p\cdot q)xy \\ &= m_k^2 x + M_W^2(1-x) + x\left(m_i^2(x+y-1) - m_j^2 y\right)\,, && \text{(E.29)} \end{aligned}$$

where on the last line we took on-shell conditions.

For the diagrams of the third row we choose:

$$\begin{aligned} r_0 &= 0\,, \qquad m_0 = m_k\,, \\ r_1 &= q\,, \qquad m_1 = m_k\,, \\ r_2 &= p\,, \qquad m_2 = M_W\,, \end{aligned} \tag{E.30}$$

with

$$\begin{aligned} P_2 &= p(1-x-y) + qy \;\Rightarrow\; a_2 = 1-x-y\,,\;\; b_2 = y\,, && \text{(E.31)} \\ \Delta_2 &= m_k^2(x+y) + M_W^2(1-x-y) + p^2(x+y-1)(x+y) + q^2 y(y-1) + 2(p\cdot q)y(1-x-y) \\ &= m_k^2(x+y) + M_W^2(1-x-y) + (m_i^2 x + m_j^2 y)(x+y-1)\,. && \text{(E.32)} \end{aligned}$$

In the limit where we neglect the external masses (m_i and m_j) compared to M_W and/or m_k, we integrate easily the $f_{L,R}^{(n)}$ expressions to obtain:

$$\begin{aligned} G_R^{(ij)}(k) &= -Q_B\left\{\frac{4t_k^3 - 45t_k^2 + 33t_k - 10}{12(t_k-1)^3} + \frac{3t_k^3 \ln t_k}{2(t_k-1)^4}\right\} + Q_k\left\{\frac{5t_k^3 - 9t_k^2 + 30t_k - 8}{12(t_k-1)^3} - \frac{3t_k^2 \ln t_k}{2(t_k-1)^4}\right\}\,, \\ &= G_L^{(ij)}(k)\,, \qquad t_k \equiv \frac{m_k^2}{M_W^2}\,, && \text{(E.33)} \\ &= -Q_B\left\{\frac{-2t_k^3 - 5t_k^2 + t_k}{4(t_k-1)^3} + \frac{3t_k^3 \ln t_k}{2(t_k-1)^4} + \frac{5}{6}\right\} + Q_k\left\{\frac{-t_k^3 + 5t_k^2 + 2t_k}{4(t_k-1)^3} - \frac{3t_k^2 \ln t_k}{2(t_k-1)^4} + \frac{2}{3}\right\}\,, && \text{(E.34)} \end{aligned}$$

where in the last line we have isolated the mass independent terms, namely, $5/6$ and $2/3$. As the mixing matrix is unitary, these mass independent terms will not contribute to the process fermion$_i \to$ fermion$_j + \gamma$ (with $i \neq j$) because $\sum_k \lambda_k^{(ij)} = 0$ for $i \neq j$.

E.1.2 LFV $\mu \to e\,\gamma$ in the minimal extended SM

The μ-lepton decay width to $e + \bar{\nu}_e + \nu_\mu$ at tree-level is very well known to be given by (at an excellent approximation, where we collapse the W propagator to a single point 4-fermion interaction and neglect m_e compared to m_μ, specifically, putting $m_e^2/m_\mu^2 = 0$):

$$\Gamma(\mu \to e\,\bar{\nu}_e \nu_\mu) = \frac{m_\mu^5 G_F^2}{192\pi^3}\,. \tag{E.35}$$

This is by far the dominant contribution to the total decay width of the μ-lepton. Thus, we take the excellent approximation $\Gamma(\mu \to \text{all}) = \Gamma(\mu \to e\,\bar{\nu}_e \nu_\mu)$.

The branching ratio, BR, for the decay of μ into $e+\gamma$ is then given by:

$$\begin{aligned} BR(\mu \to e\,\gamma) &= \frac{12\pi^2}{G_F^2 m_\mu^2}\left[|A_L^{\mu e}|^2 + |A_R^{\mu e}|^2\right] = \frac{3\alpha}{2\pi m_\mu^2}\left\{\left|m_\mu \sum_k \lambda_k^{\mu e} G_R^{(\mu e)}(k)\right|^2 + \left|m_e \sum_k \lambda_k^{\mu e} G_L^{(\mu e)}(k)\right|^2\right\} \\ &\simeq \frac{3\alpha}{2\pi}\left|\sum_k \lambda_k^{\mu e} G_R^{(\mu e)}(k)\right|^2 , \end{aligned} \tag{E.36}$$

where in the last line we have neglected m_e compared to m_μ.

Noting that $Q_{k=\nu_e,\nu_\mu,\nu_\tau} = 0$ and $Q_B = -1$, we have for $G_R^{\mu e}(k)$ given by (E.34):

$$G_R^{\mu e}(k) = \frac{-2t_k^3 - 5t_k^2 + t_k}{4(t_k-1)^3} + \frac{3t_k^3 \ln t_k}{2(t_k-1)^4} + \frac{5}{6}\,. \tag{E.37}$$

Moreover, in the limit $m_k \ll M_W$, expanding $G_R^{\mu e}(k)$ in powers of $t_k \equiv m_k^2/M_W^2$ and keeping only the first term, one finds:

$$G_R^{\mu e}(k) = \frac{5}{6} - \frac{1}{4}t_k + \ldots\,. \tag{E.38}$$

Then, in the limit $t_k \ll 1$ and noting that the mixing matrix is unitary, one has for the branching ratio:

$$BR(\mu \to e\,\gamma) = \frac{3\alpha}{32\pi M_W^4}\left|\sum_k \lambda_k^{\mu e} m_k^2\right|^2 < 10^{-53}\,, \tag{E.39}$$

where $V_{ki} = (U_{PMNS})_{ik}^* \Rightarrow \lambda_k^{\mu e} \equiv (U_{PMNS})_{\mu k}^*(U_{PMNS})_{ek}$ and m_k is the mass of the neutrino mass eigenstate k.

E.1.3 (L)FV radiative decay fermion$_i$ $\to$ fermion$_j$ $+\,\gamma$ in the MSSM

In the MSSM we have additional contributions from diagrams involving sparticles. Concerning the internal fermion mediating the process, these are of two types: (i) a neutralino and (ii) a chargino. For a transition between two SU(2)$_L$ up-type (down-type) fermions the neutralino will be accompanied by down-sfermions (up-sfermions) and the chargino by up-sfermions (down-sfermions). In here we will address directly the case of charged lepton transitions $l_i \to l_j\,\gamma$ $(i \neq j)$, whose master equations can be extended/adapted to similar flavour violating processes fermion$_i$ $\to$ fermion$_j$ $+\,\gamma$.

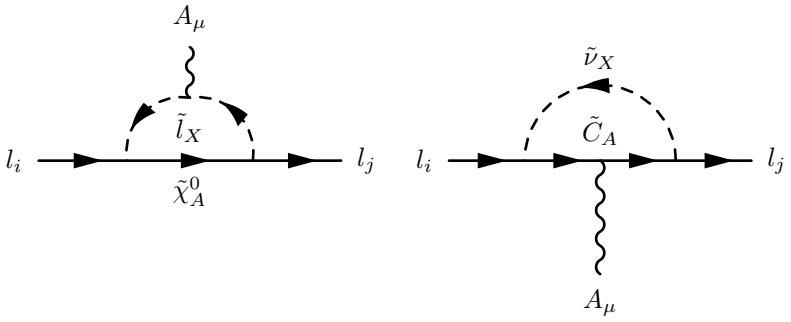

Following the same steps used previously in section E.1.1, we define:

$$A_{L,R}^{(ij)} = e\,F_{L,R}^{(ij)}\,, \tag{E.40}$$

and decompose $F_{L,R}^{(ij)}$ into a neutralino (diagram 1) and chargino (diagram 2) contribution:

$$F_L^{(ij)} = \left(\frac{-i}{16\pi^2}\right) m_j \left(\sum_{X=1}^{6} (-Q_{\tilde{l}_X}) \frac{1}{m_{\tilde{l}_X}^2} \sum_{A=1}^{4} f_L^{(1)}(A,X) + \sum_{X=1}^{3} \frac{1}{m_{\tilde{\nu}_X}^2} \sum_{A=1}^{2} (-Q_{\tilde{C}_A}) f_L^{(2)}(A,X) \right) \equiv \left(\frac{-i}{16\pi^2}\right) m_j G_L^{(ij)} \,, \tag{E.41}$$

$$F_R^{(ij)} = \left(\frac{-i}{16\pi^2}\right) m_i \left(\sum_{X=1}^{6} (-Q_{\tilde{l}_X}) \frac{1}{m_{\tilde{l}_X}^2} \sum_{A=1}^{4} f_R^{(1)}(A,X) + \sum_{X=1}^{3} \frac{1}{m_{\tilde{\nu}_X}^2} \sum_{A=1}^{2} (-Q_{\tilde{C}_A}) f_L^{(2)}(A,X) \right) \equiv \left(\frac{-i}{16\pi^2}\right) m_i G_R^{(ij)} \,, \tag{E.42}$$

where $Q_{\tilde{l}_X} = -1$ and $Q_{\tilde{C}_A} = -1$ are the charges of the charged slepton X and chargino A, respectively.

Using the couplings derived in (D.42), (D.43), (D.46) and (D.47), we define for convenience:

$$n_{XA}^{R(ij)} = N_{jXA}^{(R)*} N_{iXA}^{(R)} \,, \quad n_{XA}^{L(ij)} = N_{jXA}^{(L)*} N_{iXA}^{(L)} \,, \quad n_{XA}^{LR(ij)} = N_{jXA}^{(R)*} N_{iXA}^{(L)} \,, \tag{E.43}$$

$$c_{XA}^{R(ij)} = C_{jXA}^{(R)*} C_{iXA}^{(R)} \,, \quad c_{XA}^{L(ij)} = C_{jXA}^{(L)*} C_{iXA}^{(L)} \,, \quad c_{XA}^{LR(ij)} = C_{jXA}^{(R)*} C_{iXA}^{(L)} \,, \tag{E.44}$$

$$n_{XA}^{RL(ij)} = N_{jXA}^{(L)*} N_{iXA}^{(R)} \,, \quad c_{XA}^{RL(ij)} = C_{jXA}^{(L)*} C_{iXA}^{(R)} \,. \tag{E.45}$$

The form factor functions are calculated to be given by:

$$f_L^{(1)}(A,X) = \frac{m_{\tilde{l}_X}^2}{m_j} \int_0^1 dx \int_0^{1-x} dy \left\{ \frac{m_i(a_1-1)(a_1+b_1) n_{XA}^{R(ij)} + m_j b_1 (1-a_1) n_{XA}^{L(ij)} + m_{\tilde{\chi}_A^0}(a_1-1) n_{XA}^{LR(ij)}}{\Delta_1} \right\} , \tag{E.46}$$

$$f_L^{(2)}(A,X) = \frac{m_{\tilde{\nu}_X}^2}{m_j} \int_0^1 dx \int_0^{1-x} dy \left\{ \frac{m_i a_2 (1-b_2-a_2) c_{XA}^{R(ij)} + m_j a_2 b_2 c_{XA}^{L(ij)} + m_{\tilde{C}_A}(1-a_2) c_{XA}^{LR(ij)}}{\Delta_2} \right\} , \tag{E.47}$$

$$f_R^{(1)}(A,X) = \frac{m_j}{m_i} f_L^{(1)}(A,X)\Big|_{L\leftrightarrow R} \,, \quad f_R^{(2)}(A,X) = \frac{m_j}{m_i} f_L^{(2)}(A,X)\Big|_{L\leftrightarrow R} \,, \tag{E.48}$$

which can be easily compared to (E.17)-(E.18) and (E.23)-(E.24). In here a_1, b_1, a_2, b_2, Δ_1 and Δ_2 are analogous to the ones introduced in section E.1.1.

Integrating the form factor functions, we find:

$$f_L^{(1)}(A,X) = -\frac{m_i n_{XA}^{R(ij)} + m_j n_{XA}^{L(ij)}}{m_j} f_1(A,X) - \frac{m_{\tilde{\chi}_A^0}}{m_j} n_{XA}^{LR(ij)} f_2(A,X) \,, \tag{E.49}$$

$$f_L^{(2)}(A,X) = \frac{m_i c_{XA}^{R(ij)} + m_j c_{XA}^{L(ij)}}{m_j} g_1(A,X) - \frac{m_{\tilde{C}_A}}{m_j} c_{XA}^{LR(ij)} g_2(A,X) \,, \tag{E.50}$$

$$f_1(A,X) \equiv \frac{1 - 6t_{AX} + 3t_{AX}^2 + 2t_{AX}^3 - 6t_{AX}^2 \ln t_{AX}}{12(1-t_{AX})^4} \,, \tag{E.51}$$

$$f_2(A,X) \equiv \frac{1 - t_{AX}^2 + 2t_{AX} \ln t_{AX}}{2(1-t_{AX})^3} \,, \tag{E.52}$$

$$g_1(A,X) \equiv \frac{2 + 3r_{AX} - 6r_{AX}^2 + r_{AX}^3 + 6r_{AX} \ln r_{AX}}{12(1-r_{AX})^4} \,, \tag{E.53}$$

$$g_2(A,X) \equiv \frac{3 - 4r_{AX} + r_{AX}^2 + 2\ln r_{AX}}{2(1-r_{AX})^3} \,, \tag{E.54}$$

where

$$t_{AX} \equiv \frac{m_{\tilde{\chi}_A^0}^2}{m_{\tilde{l}_X}^2} \,, \quad r_{AX} \equiv \frac{m_{\tilde{C}_A}^2}{m_{\tilde{\nu}_X}^2} \,. \tag{E.55}$$

E.2 FV sparticle decays: sparticle$_X$ → (gaugino-higgsino)$_A$ + fermion$_i$

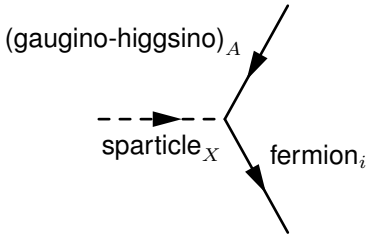

We write the transition amplitude as:

$$T_{iXA} = \bar{u}(p_i)\left[A_{iXA}^{(R)*}P_L + A_{iXA}^{(L)*}P_R\right]v(p_A)\,, \tag{E.56}$$

from where we determine the averaged amplitude squared:

$$\overline{|\mathcal{M}_{iXA}|^2} = 2\left[\left(|A_{iXA}^{(L)}|^2 + |A_{iXA}^{(R)}|^2\right)p_A\cdot p_i - \left(A_{iXA}^{(L)}A_{iXA}^{(R)*} + \text{h.c.}\right)m_A m_i\right]\,. \tag{E.57}$$

The kinematic of the process is described by $p_X = p_A + p_i$ and masses m_X, m_A, m_i. In the C.M. referential we have:

$$|\vec{p}_A| = |\vec{p}_i| = \frac{m_X}{2}\sqrt{(1-x_A-x_i)^2 - 4x_Ax_i}\,,\quad p_i\cdot p_A = m_X^2\left(\frac{1-x_A-x_i}{2}\right)\,. \tag{E.58}$$

Therefore, noting that in the C.M. the decay width per solid angle is $\frac{d\Gamma}{d\Omega} = \frac{1}{32\pi^2}\frac{|\vec{p}_{CM}|}{m_X^2}\overline{|\mathcal{M}|^2}$, we find:

$$\begin{aligned}\Gamma_{iXA} &= \frac{\overline{|\mathcal{M}_{iXA}|^2}}{16\pi m_X}\sqrt{(1-x_i-x_A)^2-4x_ix_A}\,,\quad x_i\equiv\frac{m_i^2}{m_X^2}\,,\ x_A\equiv\frac{m^2_{\tilde{\chi}^0_A}}{m_X^2}\\ &= \frac{m_X}{16\pi}\left\{\left(|A_{iXA}^{(L)}|^2+|A_{iXA}^{(R)}|^2\right)[1-x_i-x_A] - 4\text{Re}\left[A_{iXA}^{(L)}A_{iXA}^{(R)*}\right]\sqrt{x_ix_A}\right\}\sqrt{(1-x_i-x_A)^2-4x_ix_A}\,.\end{aligned} \tag{E.59}$$

E.2.1 LFV charged slepton decays: $\tilde{l}_X \to \tilde{\chi}^0_A + l_i$

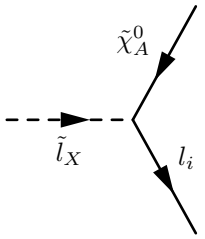

The couplings of the amplitude written in equation (E.56) are identified as:

$$A_{iXA}^{(L)} = N_{iXA}^{(L)}\,,\quad A_{iXA}^{(R)} = N_{iXA}^{(R)}\,. \tag{E.60}$$

where $N_{iXA}^{(L)}$ and $N_{iXA}^{(R)}$ are defined in (D.42) and (D.43), respectively.

Noticing that $m_i \ll m_X$, we can approximate the decay width of (E.59) to:

$$\Gamma_{iXA} \simeq \frac{m_X}{16\pi}(1-x_A)^2\left\{|A_{iXA}^{(L)}|^2 + |A_{iXA}^{(R)}|^2\right\}\,. \tag{E.61}$$

Being the lepton flavour violation dominant in the LH slepton sector ($R^{\tilde{l}}_{X;i(1,2,3)} > R^{\tilde{l}}_{X;i(4,5,6)}$) we find, for the decay to the lightest neutralino $\tilde{\chi}^0_1$ (usually the LSP) in mSUGRA scenarios $\tilde{\chi}^0_1 \approx \tilde{B}$ ($N_{11}\simeq 1 > N_{13} > N_{12} \gg N_{14}$),

$$\Gamma(\tilde{l}_X \to l_i\,\tilde{\chi}^0_1) \approx \frac{\alpha\, m_X}{8c_w^2}(1-x_A)^2\left\{\left|N_{11}+\frac{1}{t_w}N_{12}\right|^2|R^{\tilde{l}}_{X;i(1,2,3)}|^2 + 4|N_{11}|^2|R^{\tilde{l}}_{X;i(4,5,6)}|^2\right\}\,. \tag{E.62}$$